



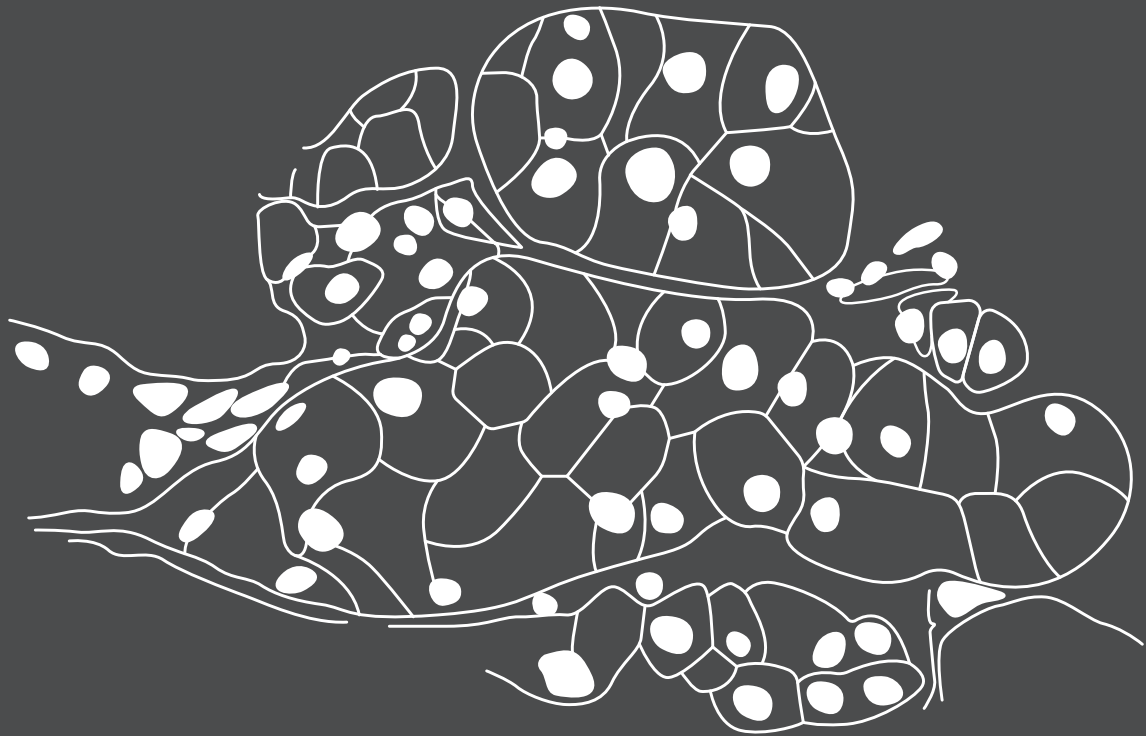


Universitat Autònoma de Barcelona

ADVERTIMENT. L'accés als continguts d'aquesta tesi queda condicionat a l'acceptació de les condicions d'ús establertes per la següent llicència Creative Commons:  http://cat.creativecommons.org/?page_id=184

ADVERTENCIA. El acceso a los contenidos de esta tesis queda condicionado a la aceptación de las condiciones de uso establecidas por la siguiente licencia Creative Commons:  <http://es.creativecommons.org/blog/licencias/>

WARNING. The access to the contents of this doctoral thesis it is limited to the acceptance of the use conditions set by the following Creative Commons license:  <https://creativecommons.org/licenses/?lang=en>



**THE ROLE OF STAT3 PHOSPHORYLATION STATE
IN CLEAR CELL RENAL CELL CARCINOMA (ccRCC)**

Jazmine Paola Arévalo Bautista

PhD Thesis, 2019

THE ROLE OF STAT3 PHOSPHORYLATION STATE IN CLEAR CELL RENAL CELL CARCINOMA (ccRCC)

By

JAZMINE PAOLA ARÉVALO BAUTISTA

To obtain the title of

PhD

in Biochemistry, Molecular Biology and Biomedicine,
of the **Universitat Autònoma de Barcelona (UAB)**

This thesis was performed in the
Kidney Physiopathology (CIBBIM-Nanomedicine) group,
at the **Vall d'Hebron Institut de Recerca (VHIR)**

November, 2019



Director and Tutor

Anna Meseguer Navarro, PhD.



PhD Candidate

Jazmine Paola Arévalo Bautista

A Carlos, por iluminarme la vida.

LIST OF CONTENTS

ABSTRACT	10
INTRODUCTION	12
1. The Kidney	13
1.1. Functions	13
1.2. Anatomy	13
1.3. The nephron.....	14
2. Renal Cell Carcinoma	17
2.1. Histologic subtypes.....	17
2.2. Epidemiology.....	19
2.3. Diagnosis	19
2.4. Treatment	21
3. Clear Cell Renal Cell Carcinoma.....	23
3.1. Etiology.....	23
3.2. Disease models	28
3.3. Treatment	28
3.4. Biomarkers	30
4. Signal Transducer and Activator of Transcription 3	33
4.1. Structure.....	33
4.2. Isoforms.....	33
4.3. Post-translational modifications	34
4.4. Canonical STAT3 activation and function	36
4.5. Non-canonical STAT3 activation and functions.....	37
4.6. Cancer (the paradox)	40
RATIONALE	46
OBJECTIVES	48
METHODOLOGY	50
1. Cell Culture	51
1.1. Cell lines	51
1.2. Authentication	51
1.3. Culture.....	52
1.4. Trypsinization	52
1.5. Counting	53
1.6. Cryopreservation	53
1.7. Thawing	53
1.8. Treatments.....	53
2. Gene Silencing.....	54
2.1. Short hairpin RNA (shRNA)-mediated silencing	54

3.	Mutants Generation	56
3.1.	Primers design.....	56
3.2.	Site-directed mutagenesis.....	59
4.	Bacterial Manipulation	61
4.1.	Bacterial transformation.....	61
4.2.	Bacterial growth	61
4.3.	Bacterial storage	62
5.	Nucleic Acids Manipulation	63
5.1.	Plasmid DNA isolation	63
5.2.	RNA isolation	63
5.3.	Nucleic acids quantification.....	64
5.4.	Agarose-gel electrophoresis	64
5.5.	Sequencing	64
5.6.	RT-PCR.....	65
5.7.	RT-qPCR	65
6.	Transient Transfection.....	68
7.	Generation of Stable Transduced Cell Lines.....	69
7.1.	Transient co-transfection for lentivirus production.....	69
7.2.	Lentiviral transduction.....	70
8.	Protein Manipulation.....	72
8.1.	Protein purification.....	72
8.2.	Protein quantification	72
8.3.	Western blot	73
8.4.	Immunocytochemistry	75
8.5.	Immunohistochemistry	76
9.	Functional Assays	78
9.1.	Cell proliferation (XTT assay).....	78
9.2.	Cell aggregation	78
9.3.	Adhesion assay.....	78
9.4.	Clonogenic assay	79
9.5.	Migration (wound-healing assay).....	79
9.6.	Transwell invasion assay.....	80
9.7.	Anchorage-independent growth (soft agar assay)	81
9.8.	Tumorspheres formation assay.....	81
10.	LUCIFERASE-REPORTER ASSAY	83
10.1.	Transient co-transfection of luciferase-reporter constructs	84
10.2.	Quantitative determination of gene expression	84
11.	Tissue Microarray (TMA).....	86
11.1.	Case selection.....	86
11.2.	TMA construction.....	86

11.3.	TMA immunohistochemistry	87
11.4.	TMA analysis	87
12.	Microarray	88
12.1.	Experimental design.....	88
12.2.	Sample preparation and hybridization.....	89
12.3.	Quality control.....	89
12.4.	Preprocessing: normalization and filtering.....	89
12.5.	Selection of differentially expressed genes	90
12.6.	Multiple comparisons	90
12.7.	Analysis of biological significance.....	91
	RESULTS.....	92
1.	pSer727-STAT3 expression levels in ccRCC patients (validation)	93
2.	Generation and characterization of STAT3 phosphomutants	96
2.1.	STAT3 silencing	96
2.2.	Generation of STAT3 phosphomutants	97
2.3.	Overexpression and characterization of STAT3 phosphomutants.....	99
3.	Functional characterization of STAT3 phosphomutants.....	102
3.1.	Phosphorylation at Ser727-STAT3 induces proliferation	102
3.2.	Phosphorylation at Ser727-STAT3 promotes migration	104
3.3.	Phosphorylation at Ser727-STAT3 favors colony formation.....	105
3.4.	Phosphorylation at Ser727-STAT3 increases anchorage-independent growth.....	106
3.5.	Phosphorylation at Ser727-STAT3 promotes cell aggregation	107
3.6.	None of the STAT3 phosphomutants induces cell adhesion	108
3.7.	The absence of phosphorylation at Ser727-STAT3 promotes invasion	109
3.8.	All STAT3 phosphomutants form tumorspheres	110
4.	Validation of Gene expression profiles from microarray.....	111
5.	Transcriptional activity of STAT3 phosphomutants	114
5.1.	Endogenous STAT3 regulates the expression of 818 genes	114
5.2.	STAT3 WT overexpression recovers the expression of 249 genes	118
5.3.	Phosphorylation of Tyr705-STAT3 (SA mutant) induces the expression of 132 genes.	121
5.4.	Complete STAT3 phosphorylation (SD mutant) regulates the expression of 455 genes.	123
5.5.	Unphosphorylated STAT3 (YF/SA mutant) induced the expression of 144 genes.....	126
5.6.	Phosphorylation of Ser727-STAT3 (YF/SD mutant) regulates 342 genes.....	129
6.	YF and YF/SD mutants represent the same STAT3 phosphorylation state	132
7.	STAT3 WT expresses genes associated with different phosphorylation states.....	134
8.	The STAT3 expression pattern changes as Tyr705 and Ser727 become phosphorylated	135
9.	STAT3 regulates the expression of 265 genes regardless of its phosphorylation state.....	136
10.	Phosphorylation of Ser727 acts by a different pathway from canonical STAT3 activation	138
11.	Phosphorylation of Ser727-STAT3 specifically regulates the expression of 132 genes	139
12.	Identification of putative and novel biomarkers for ccRCC	143

DISCUSSION.....144

1. Nuclear and cytosolic pSer727-STAT3 expression levels in ccRCC patients145
2. STAT3 phosphomutants (experimental design)146
3. STAT3 localizes at nucleus and cytosol regardless its phosphorylation state147
4. Phosphorylation at Ser727-STAT3 promotes a pro-tumoral phenotype *in vitro*147
5. The effect of endogenous STAT3 activation in ccRCC.....151
6. The effect of STAT3 phosphorylation state in ccRCC.....152
7. Phosphorylation of Ser727 acts by a different activation signaling pathway from canonical154
8. The subset of pSer727-dependent genes as potential therapeutic targets for ccRCC treatment 155
9. Putative and novel prognostic biomarkers for ccRCC (future validation).....156

CONCLUSIONS.....158

BIBLIOGRAPHY160

ABBREVIATIONS

ADH	Antidiuretic hormone
ALDH	Aldehyde dehydrogenase
AML	Acute myelogenous leukemia
AT1	Angiotensin II
bFGF	Basic fibroblast growth factor
bp	Base pairs
CAC	Colitis-associated cancer
CCD	Coiled-coil domain
ccRCC	Clear cell renal cell carcinoma
CD	Collecting duct
cDNA	Complementary DNA
cdRCC	Collecting duct renal cell carcinoma
CDS	Coding sequence
chCRR	Chromophobe renal cell carcinoma
CIN	Cervical intraepithelial neoplasia
CSCs	Cancer stem cells
CT	Computed tomography
CTLA4	Cytotoxic T lymphocyte-associated protein 4
CypA	Cyclophilin A
DBD	DNA-binding domain
DCT	Distal convoluted tube
dsDNA	Double-stranded DNA
dsRNA	Double-stranded RNA
ECM	Extracellular matrix
ECT	Electron transport chain
EGF	Epidermal growth factor
EMT	Epithelial to mesenchymal transition
ER	Endoplasmic reticulum
ESCC	Esophageal squamous cell carcinoma
ETC	Electron transport chain
EZH2	Enhancer of zeste homolog 2
FAK	Focal adhesion kinase
FGF	Fibroblast growth factor
GAS	Gamma interferon activation site
GICs	Glioma-initiating cells
GO	Gene ontology
GPCR	G-protein coupled receptor
GSCs	Glioma stem cells
GSK3b	Glycogen synthase kinase 3b
GWAS	Genome-wide association studies
HCC	Hepatocellular carcinoma
HDAC	Histone deacetylase
HEK293	Human embryonic kidney 293

HGF	Hepatocyte growth factor
hHAVCR1	Human hepatitis A virus cellular receptor 1
HIF	Hypoxia-inducible factor
HRP	Horseradish peroxidase
ICC	Immunocytochemistry
IFN	Interferon
IGF1	Insulin-like growth factor 1
IGFBP7	Insulin-like growth factor-binding protein 7
IHC	Immunohistochemistry
IL6	Interleukin 6
IP3	Inositol 1,4,5-triphosphate
JAK	Janus kinase
JGA	Juxtaglomerular apparatus
KIM1	Kidney injury molecule 1
LD	Linker domain
LIF	Leukemia inhibitory factor
LTR	Long terminal repeat
MAMs	Mitochondria-associated membranes
MAP	Mitogen-activated protein
miRNA	Micro RNA
MMP	Matrix metalloproteinases
MPTP	Mitochondrial permeability transition pore
MRCA	Most recent common ancestor
mRCC	Medullary renal cell carcinoma
MRI	Magnetic resonance imaging
mRNA	Messenger RNA
mtDNA	Mitochondrial DNA
mTOR	Mechanistic target of rapamycin
NBT	Nitro blue tetrazolium chloride
nccRCC	Non-clear-cell renal cell carcinomas
NFkB	Nuclear factor kappa B
NSCLC	Non-small cell lung cancer
NTD	N-terminal domain
PAMPs	Pathogen-associated molecular patterns
PCa	Prostate cancer
PCA	Principal components analysis
PCR	Polymerase chain reaction
PCT	Proximal convoluted tube
PD1	Programmed cell death 1
PDGF	Platelet-derived growth factor
PDL1	Programmed cell death ligand 1
PEI	Polyethyleneimine
PI3K	Phosphoinositide 3-kinase
PIAS	Protein inhibitors of activated STATs
PIC	Protease inhibitor cocktail
PKC	Protein kinase C
PKCε	Protein kinase C epsilon

pRCC	Papillary renal cell carcinoma
PTases	Protein tyrosine phosphatases
PTC	Papillary thyroid carcinoma
PTH	Parathyroid hormone
PTMs	Post-transcriptional modifications
PVDF	Polyvinylidene difluoride
QC	Quality control
RAPD-PCR	RNA-based arbitrary primed polymerase chain reaction
RAS	Renin-angiotensin system
RCC	Renal cell carcinoma
RIPA	Radioimmunoprecipitation assay
RISC	RNA-induced silencing complex
RLU	Relative light units
RMA	Robust microarray analysis
RNAi	RNA interference
RNases	Ribonuclease enzymes
ROS	Reactive oxygen species
RSM	Ribose sugar metabolism
RT	Room temperature
RTKs	Receptor tyrosine kinases
RT-PCR	Reverse transcription-PCR
RT-qPCR	Reverse transcription-qPCR
S1P	Sphingosine-1-phosphate
SDS	Sodium dodecyl sulfate
SDS-PAGE	Sodium dodecyl sulfate-polyacrylamide gel electrophoresis
SH2	Src homology 2
shRNA	Short hairpin RNA
siRNA	Small interfering RNA
SNAI	Snail-1
SOCS	Suppressors of cytokine signaling
STAT3	Signal transducer and activator of transcription 3
STR	Short tandem repeats
SV40	Simian virus 40
TAD	Transcription activation domain
TBP	Tata box protein
TCA	Tricarboxylic acid
TFAM	Transcription factor A, mitochondrial
TGF α	Transforming growth factor- α
TLR	Toll-like receptors
TMA	Tissue microarray
TRE	Transcriptional response element
uRCC	Unclassified renal cell carcinoma
VEGF	Vascular endothelial growth factor
VHL	Von Hippel-Lindau
VSV-G	Vesicular stomatitis virus G
WT	Wildtype

ABSTRACT

The *signal transducer and activator of transcription 3* (STAT3) is a latent transcription factor that regulates downstream genes involved in essential biological processes such as cell differentiation, proliferation, migration, apoptosis inhibition, and survival. The aberrant activation of STAT3 has been related to the development of near 50% of all human cancers including *clear cell renal cell carcinoma* (ccRCC). To date, the oncogenic properties of STAT3 are attributed to the phosphorylation of its Tyr705, however, the phosphorylation of its Ser727 has recently emerged as a residue that enhances STAT3 transcriptional activity, in addition to non-genomic activities that promote cancer development. Our group was one of the pioneers in bringing the Ser727 phosphorylation to light by demonstrating that nuclear pSer727 expression levels, in tissue samples of ccRCC patients, correlated with poor prognosis and low overall survival. Since ccRCC is the most prevalent and lethal histological subtype of *renal cell carcinoma* (RCC) and the molecular mechanisms behind its tumorigenesis remain unclear, we aimed to elucidate the role of STAT3 phosphorylation state in ccRCC development, and especially the contribution of pSer727 to tumor progression. For that purpose, we generated simple and double STAT3 phosphomutants (Tyr705Phe, Ser727Ala, Ser727Asp, Tyr705Phe/Ser727Ala, and Tyr705Phe/Ser727Asp) transduced in human-derived ccRCC cell lines (769-P and 786-O), and we evaluated their functional behavior as well as their differential gene expression through microarray analysis. Our data demonstrates that STAT3 mutants carrying a phosphomimetic substitution for Ser727 (Ser727Asp) promote a pro-tumoral phenotype *in vitro* in a Tyr705-independent manner. Moreover, we describe that the overall STAT3 phosphorylation state determines the expression of different subsets of target genes associated with distinct biological processes, being pSer727-dependent genes the most related to cellular hallmarks of cancer development. In summary, the present study constitutes the first analysis on the role of overall STAT3 phosphorylation state in ccRCC and demonstrates that pSer727 activates STAT3 signaling through transcription of a specific subset of target genes that are clinically relevant as potential therapeutic targets and novel biomarkers for ccRCC.

INTRODUCTION

1. THE KIDNEY

1.1. Functions

The kidney is a multifunction organ that performs a wide range of functions within the body, most of which are essential for life. It is usual to consider that the fundamental task of the kidney is the excretion of waste, although this is certainly a major function, it carries out other important tasks as regulation of blood volume, regulation of total body salt and water composition, excretion of metabolic waste and bioactive substances (hormones and drugs), maintenance of acid-base balance, regulation of red blood cell and vitamin D production, gluconeogenesis and assuring bone integrity¹. Furthermore, the kidney cooperates tightly with many other organs to maintain homeostasis using a coordinated array of cellular mechanisms.

The overall functioning of the kidney involves transporting water and solutes between the blood through the lumina of tubules (nephrons and collecting tubules that comprise the working mass of the kidney), thus any substance that is not transported back into the blood is eventually excreted in the urine.

The kidney is a highly structured organ in which every part develops specific tasks, therefore, to understand the function it is necessary to know its anatomy.

1.2. Anatomy

External anatomy: The two kidneys in the human body lie outside the peritoneal cavity close to the posterior abdominal wall, one on each side of the vertebral column and directly covered by a fibrous capsule that helps to hold their bean-like shape and protect them (see Figure 1). The capsule is covered by adipose tissue which in turn is encompassed by a tough renal fascia. The fascia and the overlying peritoneum serve to firmly anchor the kidneys in the retroperitoneal position. The rounded, outer convex surface of each kidney faces the side of the body, and the indented surface, called the hilum, is medial^{1,2}.

Internal anatomy: The hilum represents the entrance and exit to the inner part of the kidneys and is penetrated by a renal artery, renal vein, nerves, and ureter, which carries urine out of the kidney to the bladder. Each ureter is formed from funnel-like structures called major calyces, which, in turn, are formed from minor calyces. The minor calyces project into papilla underlying a cone-shaped renal tissue called pyramids. The calyces act as collecting cups for the urine formed in the pyramids. The pyramids are arranged radially around the hilum, and their broad bases facing the outside, top, and bottom of the kidney¹. The internal anatomy of the kidneys can be divided into an outer region called the renal cortex, formed by renal columns that radiate down to the inner region, which in turn is called the medulla and constituted by the pyramids. The renal columns and the pyramids comprise the kidney lobes that provide a supportive framework for vessels that enter and exit the cortex² (see Figure 1).

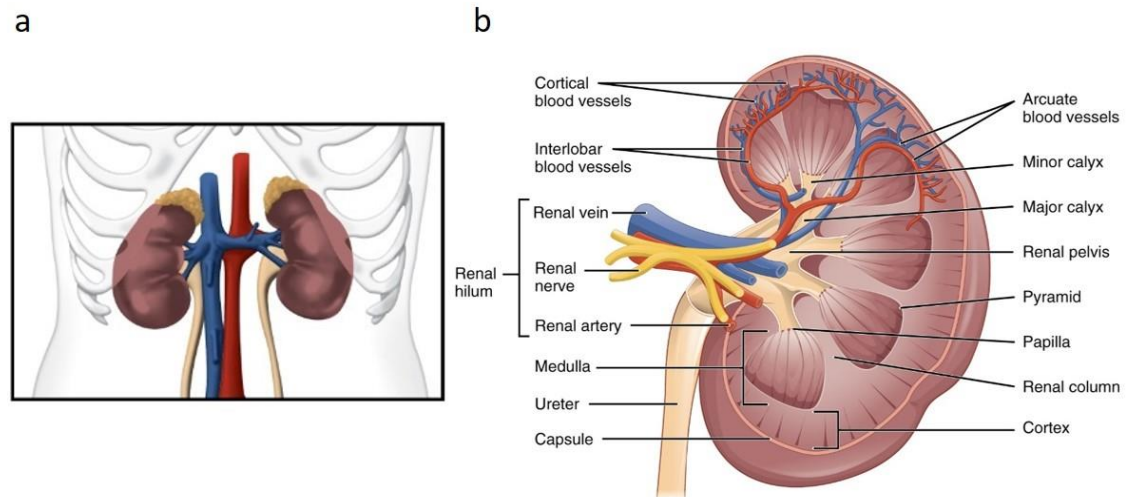


Figure 1. External and internal anatomy of the kidney. a) External anatomy and the situation of both kidneys within the human body. b) Sagittal plane of the kidney's internal anatomy showing the structures forming the renal cortex and the medulla.²

The working tissue mass of both the cortex and medulla is constructed almost entirely of tubules (nephrons and collecting tubules) and blood vessels (capillaries and capillary-like vessels). Between the tubules and blood vessels lies an interstitium, which comprises less than 10% of the renal volume. The cortex and medulla have very different properties both structurally and functionally that reflect the arrangement of the tubules and blood vessels¹.

1.3. The nephron

The nephron is the functional unit of the kidney in which three main mechanisms take place: filtration and reabsorption of substances in the blood, and secretion of residual products by the urine. Each kidney contains approximately 1 million nephrons consisting of a spherical filtering component, called the renal corpuscle, and a renal tubule.

The renal corpuscle consists of a glomerulus (interconnected capillary loops) surrounded by a Bowman's capsule and functions as the primary filtration unit¹ (see Figure 2). The filtration occurring in these structures is dependent on the intracapillary blood pressure, therefore it is a passive process. About 20% of total plasma is filtered as the blood passes through the glomerular capillaries and 99% of water is reabsorbed. Normally, the only components of the blood that are not filtered in the glomerulus are proteins of high molecular weight².

The renal tubule is a sophisticated structure extending from the Bowman's capsule and has five anatomically and functionally different segments: the *proximal convoluted tube* (PCT), the descending loop of Henle, the ascending loop of Henle, the *distal convoluted tube* (DCT) and the *collecting duct* (CD) (see Figure 2). Reabsorption occurs in the renal tubule and is either passive (by diffusion) or active (by pumping against a concentration gradient). Secretion also occurs in the tubule as an active process.

Proximal convoluted tubule: Is the first immediate segment from the renal corpuscle, in which around 60% of salt and water are reabsorbed and organics solutes (primarily glucose and amino acids) are filtered. The cells comprising this segment are densely packed with mitochondria, which are needed to supply the energy for active transport. The high metabolic demand and activity of the proximal convoluted tubule, makes it prone to damage that result in several renal diseases originating from it.

Descending loop of Henle: This segment extends from the proximal tubule and is permeable to water and considerably less permeable to salt, however, as the filtrate descends deeper, water begins to flows freely out of the tubule by osmosis until the tonicity of the filtrate and the interstitium equilibrate.

Ascending loop of Henle: Unlike the descending loop of Henle, this segment is impermeable to water, a critical feature of the countercurrent exchange mechanism employed by the loop. The ascending loop actively pumps salt out the filtrate, generating a hypertonic interstitium. As filtrate ascends through the limb, the filtrate grows hypotonic since salt has been lost.

Therefore, the main role of the loop of Henle is to concentrate salt in the interstitium.

Distal convoluted tubule: This segment receives the hypotonic filtrate from the loop of Henle. Moreover, most of the active transport takes place in this segment regulated by the endocrine system. For example, in hypovolemia, aldosterone is secreted inducing reabsorption of salt and secretion of potassium, otherwise, the atrial natriuretic peptide causes secretion of salt.

Collecting duct: This is the final segment of the tubule and connected with the distal convoluted tubule through the connecting tubule. Though the collecting duct is usually impermeable to water, it becomes permeable in the presence of the *antidiuretic hormone* (ADH) in response to dehydration. The ADH affects the functions of aquaporins (promoting their membranous expression), resulting in the reabsorption of water, therefore determining whether urine will be concentrated or diluted. Finally, urine travels down into the urinary bladder via the ureter².

There is another specialized region associated with the nephron, but separate from it, the *juxtaglomerular apparatus* (JGA). The JGA is located between the ascending loop of Henle and the afferent arteriole and contains three components: the macula densa, the juxtaglomerular cells, and the extraglomerular mesangial cells. This region produces and secretes the enzyme renin into the circulation, which activates the *renin-angiotensin system* (RAS). The activation of this system responds to hypovolemic conditions and is a mechanism for reabsorption of water¹.

The functioning of the nephron is a highly regulated process, in which every segment carries out specific functions of electrolyte filtration and reabsorption, however, as this goes beyond our scope, we will remain with the basic concepts.

Due to the high complexity of the nephron and the functions it performs, there is a wide range of kidney-related diseases. Kidney disease is defined as a heterogeneous group of disorders affecting kidney structure and function and it is recognized that even mild abnormalities in measures of kidney structure and function are associated with increased risk for developing complications in other organ systems as well as mortality². Among the

many kidney diseases described so far, the renal cell carcinoma is one of the most lethal worldwide.

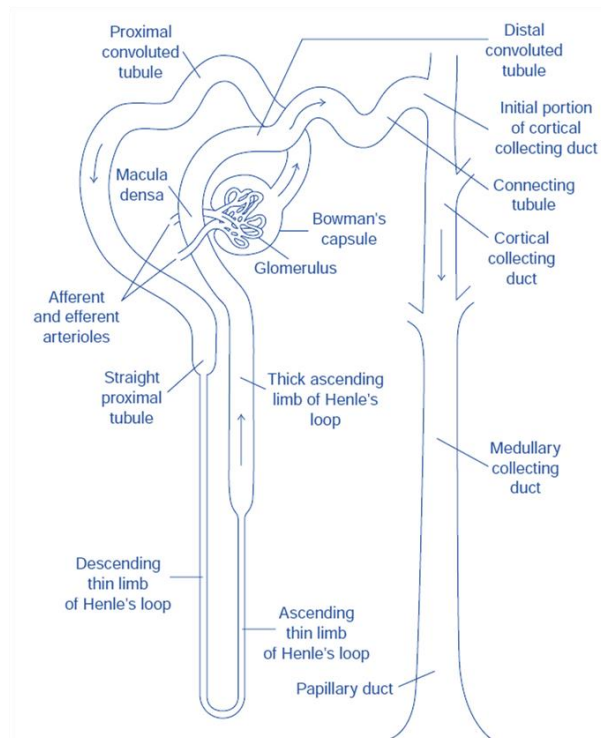


Figure 2. The nephron. The combination of the glomerulus and the Bowman's capsule formed the renal corpuscle. The different segments of the renal tubule are represented in an uncoiled manner for clarity.¹

2. RENAL CELL CARCINOMA

Different types of tumors have been described in the kidney. Arising from the tubular epithelial cells, *renal cell carcinoma* (RCC) is a common and deadly disease representing over 90% of the primary tumors in adult kidneys and accounting for ~2% of all cancer diagnosis and cancer deaths worldwide³. The understanding of this disease has evolved from initially considering it as a single, uniform entity to recognizing that RCC comprises a group of heterogeneous diseases with divergent clinical, pathological, and molecular characteristics.

2.1. Histologic subtypes

The major RCC histologic subtypes with $\geq 5\%$ incidence are *clear cell RCC* (ccRCC), *papillary RCC* (pRCC) and *chromophobe RCC* (chCRR). The remaining subtypes are very rare (each with $\geq 1\%$ total incidence) such as *collecting duct RCC* (cdRCC) and *medullary RCC* (mRCC). In cases in which the tumor does not fit any subtype in the diagnostic criteria, it is designated as *unclassified RCC* (uRCC; ~4% total incidence)^{4,5} (see Figure 3). Each different histological subtypes have distinctive genetic and molecular alterations, differing clinical courses and response to therapies⁴.

Clear cell type RCC: This subtype is the most common of the major RCC subtypes accounting for 60-70% of all RCCs. It predominantly affects male patients, with a peak incidence in the adulthood⁶. The majority of ccRCC arises sporadically with $< 5\%$ of the cases presenting as part of the inherited cancer syndromes, including von-Hippel-Lindau syndrome, and constitutional chromosomal 3 translocation syndrome⁷. Most ccRCC presents as a solitary and well-demarcated mass. Hemorrhage, necrosis, cystic degeneration, and calcification are frequently found, especially in large tumors. It is characteristically golden yellow due to the rich lipid content of the tumor cells⁵. Microscopically, several architectural patterns, including solid, alveolar, and acinar, and occasionally cystic, tubular or pseudopapillary can be found in ccRCC, and more than one pattern can be seen in one tumor. The tumor cells have clear cytoplasm due to the loss of cytoplasmic lipid and glycogen⁸. It contains a regular network of thin-walled blood vessels, a distinct and consistent feature. High-grade ccRCC often lose cytoplasm clarity and acquires more eosinophilic and granular cytoplasm⁵.

Papillary type RCC: This subtype accounts for 10-15% of RCCs and normally has a 5-year survival approaching 90% in some cases. However, high-grade variants can behave in a highly aggressive-manner⁶. Grossly, pRCC presents as a well-circumscribed mass with a pseudo capsule. Hemorrhage and necrosis are frequently seen, and some tumor appears entirely necrotic. Bilateral and multifocal tumors are more common in pRCC than in other subtypes. Microscopically, pRCC has variable proportions of papillae, characteristically containing delicate fibrovascular cores. Necrosis, hemorrhage, hemosiderin deposition, macrophages, stromal cells, and calcification are common⁵.

Two types of pRCC are recognized based on the histology⁹. pRCC type I accounts for about 60% of pRCCs and contains papillae that are lined with a single layer of tumor cells with scant pale cytoplasm and low-grade nuclei. In contrast, pRCC type II have abundant

eosinophilic cytoplasm and large pseudostratified nuclei with prominent nucleoli. Patients with pRCC type I have a better prognosis than those with type II tumor⁵.

Chromophobe type RCC: This subtype is the less common of the major RCC subtypes accounting for ~5% of RCCs and a mortality rate < 10%⁶. The chRCC is usually solitary and forms a circumscribed and nonencapsulated mass with a homogenous light brown cut surface. The tumor cells are large and polygonal and have finely reticulated cytoplasm due to numerous cytoplasmic microvesicles, prominent cell border, and irregular, often wrinkled nuclei with perinuclear clearing⁵.

Collecting duct type RCC: This subtype is a rare (< 1% of renal tumors) and poorly defined entity between RCCs. Typically, it is centrally located and forms a firm gray mass with infiltrative borders. The highly pleomorphic tumor cells form irregular tubules that infiltrate in a desmoplastic stroma⁵. The diagnosis of cdRCC is one of exclusion due to morphological resemble with other poorly differentiated RCCs and very limited genetic data¹⁰. Recent studies affirmed that cdRCC is a highly aggressive disease with grave outcomes^{11,12}. It usually presents at an advanced stage, with a high rate of metastasis at the time of diagnosis. However, cdRCC is no more lethal than ccRCC, with similar cancer-specific survival in nephrectomized patients¹¹.

Medullary type RCC: This subtype is an extremely rare and highly aggressive subtype of RCC¹³. The tumor comprises high-grade tumor cells arranged in solid sheets or more commonly in a reticular pattern with microcystic areas. The stroma is desmoplastic and resembles cdRCC histologically. mRCC also shares similarities with high-grade urothelial carcinoma, given its central location, infiltrative pattern, and high-grade cytology¹⁴. Most mRCC do not respond to chemotherapy or radiation therapy, thus prognosis is poor⁵.

Unclassified type RCC: This subtype corresponds more to a diagnostic category, rather than a true biologic entity. It represents a heterogeneous group of tumors with little in common in terms of clinical, morphologic, or genetic features⁵.

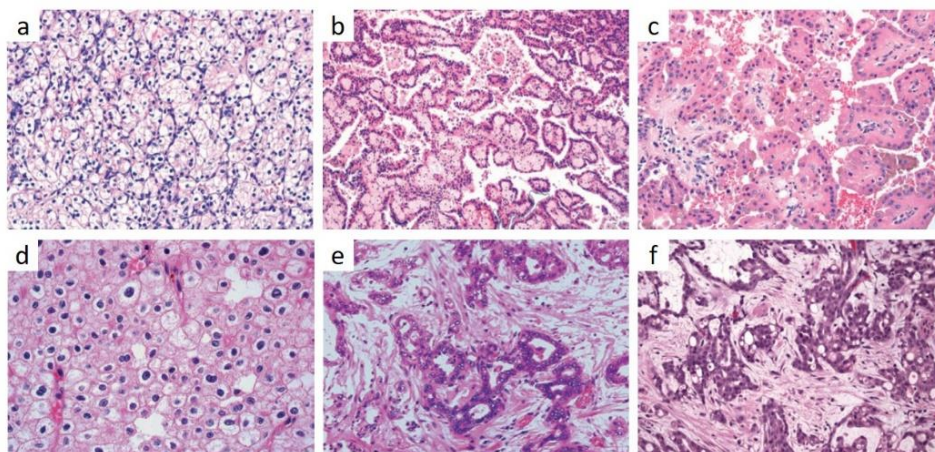


Figure 3. RCC histologic subtypes. a) ccRCC is composed of compact nests of tumor cells with clear cytoplasm separated by delicate arborizing vasculature. b) pRCC type I tumors are composed of papillae covered by a single layer of tumor cells with scant cytoplasm. c) pRCC type II tumor cells have abundant eosinophilic cytoplasm and large pseudostratified nuclei with prominent nucleoli. d) chRCC has large and polygonal tumor cells and finely reticulated cytoplasm, prominent cell border, and irregular nuclei with perinuclear clearing. e) cdRCC consists of high-grade tumor cells forming a complex and angulated tubules embedded in a remarkably desmoplastic stroma. f) mRCC comprises high-grade tumor cells arranged in irregular nests with microcystic formation and desmoplastic stroma. Modified from ¹.

2.2. Epidemiology

Incidence and mortality: Kidney cancer represents ~400,000 new cases (2018) and ~175,000 deaths annually^{5,4}, and in general, men are more affected than women (ratio 2:1)¹⁵. The median age of patients with RCC is 64 years-old with a near-normal distribution¹⁶. Accordingly, when RCC is diagnosed at younger ages (≤ 46 years old), the possibility of an underlying hereditary kidney cancer syndrome, which accounts for 3-5% of all RCCs, is considered. Overall, incidence rates have been increasing in the last years in most populations, but mortality rates have leveled off or have been decreasing. This divergent pattern is particularly evident due to the increasingly frequent incidental detection of small renal masses¹⁷. The global incidence and the prevalence of obesity, an established RCC risk factor, might also play a role in increasing RCC incidence, as well as in influencing clinical outcome¹⁵.

Risk factors: The major established risk factor for RCC include an excess of body weight, hypertension, and cigarette smoking. Other medical conditions that have been associated with RCC in epidemiological studies include chronic kidney disease, hemodialysis, kidney transplantation, acquired kidney cystic disease, a previous RCC diagnosis and, possibly, diabetes mellitus¹⁸.

Many lifestyle, dietary, occupational and environmental factors are associated with RCC with different levels of evidence. For example, red meat and moderate alcohol consumption have been contradictorily related to risk for RCC¹⁸.

Genetic factors also contribute to RCC risk, as evidenced by individuals with a family history of renal cancer having an approximately 2-fold increased risk¹⁹. Investigations into familial RCC have uncovered mutations in at least 11 genes (BAP1, FLCN, FH, MET, PTEN, SDHB, SDHC, SDHD, TSC1, TSC2, and VHL), some of which have also been implicated in sporadic RCC development²⁰. A notable example is the mutated gene VHL underlying von Hippel-Lindau disease, which is characterized by a high risk of developing ccRCC²¹. Inactivation of *Vhl* leads to the unregulated expression of oncogenic *hypoxia-inducible factor 1* (HIF1) and HIF2, which represents also a hallmark of sporadic ccRCC tumors^{20,21}. *Genome-wide association studies* (GWAS) of RCC have identified six susceptibility loci on chromosomes regions 2p21, 2q22.3, 8q24.21, 11q13.3, 12p11.23 and 12q24.31¹⁵.

2.3. Diagnosis

Historically, patients were diagnosed with RCC after presenting flank pain, gross hematuria, and a palpable abdominal mass. Currently, the majority of diagnoses result from incidental findings. This shift is a consequence of the widespread use of non-invasive techniques, performed for another reason. Paraneoplastic syndromes, which are symptoms caused by hormones or cytokines excreted by tumor cells or by an immune response against the tumor, are not uncommon in RCC and include hypercalcemia, fever, and erythrocytosis. Most of these symptoms are usually reversed after tumor resection. Diagnosis is usually strongly suspected by imaging studies; although RCCs can show variable radiographic appearances¹⁵.

Staging: The stage of RCC reflects the tumor size, the extent of invasion outside of the kidney, the involvement of lymph nodes and whether the tumor has metastasized (see

Figure 4). *Computed tomography* (CT) imaging with contrast enhancement of the chest, abdominal cavity and pelvis is required for optimal staging. Such imaging enables the assessment of the primary tumor (such as size and whether the tumor is organ-confined or extends to perinephric fat or the renal hilum), regional spread (lymph node involvement) and distant metastases (including lung, bone and distant lymph nodes). *Magnetic resonance imaging* (MRI) can also provide additional information, especially to determine whether the tumor extends into the vasculature. Prognostic assessment will require further laboratory testing including hemoglobin levels, leukocyte, and platelet counts, serum-corrected calcium levels and lactate dehydrogenase levels²².

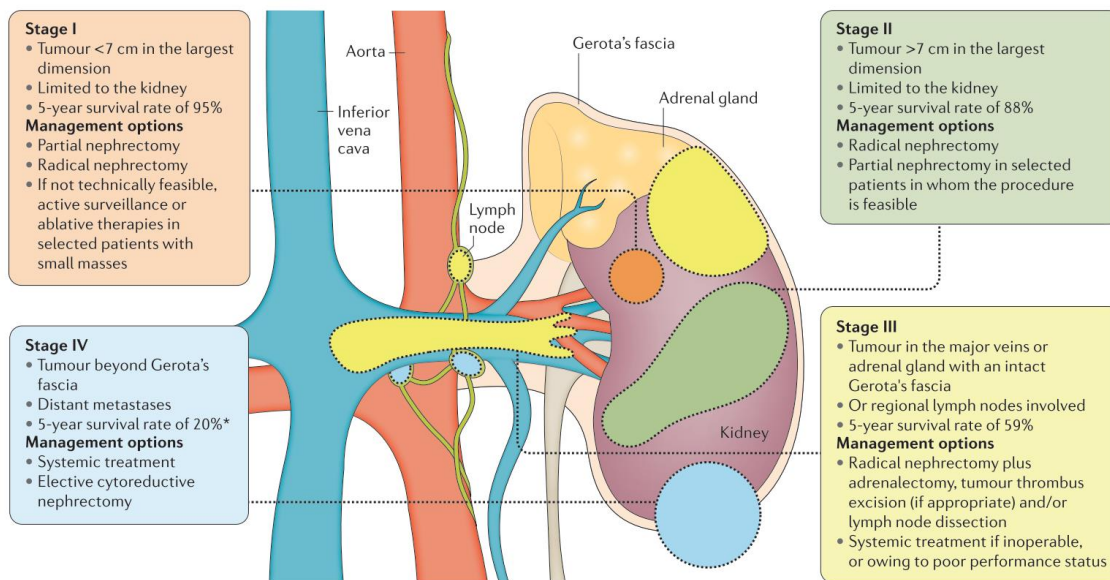


Figure 4. Stages of RCC and recommended treatments. Staging of RCC is based on size, position and lymph node involvement. For example, a stage I or stage II tumor is enclosed wholly in the kidney. Stage III tumors can extend into major veins or adrenal glands within Gerota's fascia (the layer of connective tissue encapsulating the kidneys and adrenal glands) or can involve one regional lymph node. Stage IV tumors can invade beyond Gerota's fascia and/or have distant metastases. Treatment is largely guided by stage¹⁵.

Histopathological confirmation: Histopathological confirmation of malignancy is obtained either with renal core biopsy or on the partial or radical nephrectomy specimen. An initial biopsy is recommended before ablative therapy is undertaken or before initiating system therapy¹⁵. Although most RCCs can be easily classified on the basis of histological criteria, some tumors pose a diagnostic problem because they show a combination of features that are characteristic of different subtypes. For instance, the presence of clear cells is not unique to ccRCC but can be observed in pRCC or chRCC²³. Similarly, papillary structures, which are characteristic of pRCC, can be present in other RCC subtypes. In challenging cases, careful evaluation of cytological features, growth patterns, immunophenotype, and genetic alterations usually enables the proper diagnosis¹⁵. However, a subset of RCCs (~4%) cannot be assigned to any specific category because they either present with combined morphologies or show unusual features and are, therefore, designated uRCC.

The most widely used grading system for RCC is the Fuhrman grading system, which defines four nuclear grades (1-4) in order of increasing nuclear size, irregularity, and nucleolar prominence²⁴. The Fuhrman grade has prognostic value in RCC.

2.4. Treatment

For patients with surgically resectable RCC, the standard of care is surgical excision by either partial or radical nephrectomy. By contrast, those with inoperable or metastatic RCC typically undergo systemic treatment with targeted agents and/or immune checkpoint inhibitors. Deciding on which treatment to undertake has been largely guided by tumor stage (see Figure 4) or several nomograms that in general recommend the length and frequency of clinical follow-up and the selection of high-risk patients for adjuvant studies²⁵. Similarly, key prognostic factors have been identified, validated and adopted to guide and stratify patients with metastatic RCC for systemic treatment. These factors include performance status, time from diagnosis to systemic treatment, hemoglobin, calcium, and lactate dehydrogenase levels and neutrophil and platelet counts in the blood²⁶.

Surgery: Surgical treatment of RCC is related to the clinical stage of the disease and to the general condition of the patient (see Figure 4). Although typically reserved for localized disease, both partial and radical nephrectomy can also be used with cytoreductive intent in patients with metastatic disease. However, cytoreductive nephrectomy is offered only if there is a substantial disease volume at the primary site but a low burden of metastatic disease²⁷.

Radical nephrectomy consists of the removal of the entire kidney, perirenal fat tissue, adrenal gland, and regional lymph nodes. In cases with multiple small renal tumors or tumor extending into the vasculature, radical nephrectomy is also considered and can be laparoscopic or open procedure. In patients with stage I and stage II tumors, nephrectomy is usually performed using a laparoscopic approach, while in more complex cases, the open approach remains the gold standard treatment²⁸.

Partial nephrectomy consists of completely remove the primary tumor while preserving the largest possible amount of healthy renal tissue. This treatment is often indicated for patients with a small mass (tumor ≤ 7 cm) and a normal contralateral kidney. Moreover, partial nephrectomy is imperative in RCC patients who have only one kidney (anatomically or functionally). Indeed, partial nephrectomy offers lower renal function impairment and equivalent oncological survival outcomes compared with radical nephrectomy in those with small tumoral masses²⁹. However, the favorable effect of partial nephrectomy on overall survival is more controversial in terms of oncological outcome, because the removal of the whole kidney seems a better option. In this context, surgical feasibility remains the main factor that influences the final decision.

Ablative therapies: Active surveillance in combination with ablative techniques, such as cryotherapy or radiofrequency, are alternative strategies for patients (frequently, elderly) unsuitable for surgery due to health risks and limited life expectancy¹⁵.

Active surveillance should be performed through ultrasonography imaging, CT or MRI at regular intervals and intervention should be considered when the tumor grows >0.4 – 0.5

cm per year³⁰. Ablative technology must be able to completely destroy all viable tumor tissue. A meta-analysis of case series showed 89% and 90% of efficacy for cryoablation and radiofrequency ablation, respectively³¹; however, some studies suggest a higher local recurrence rate for ablative therapies than for partial nephrectomy³⁰.

Target therapies and immunotherapy (limitations): Over the past 10 years, the study of RCC has been focused primarily on understanding the etiology of ccRCC, the most aggressive and lethal subtype, and certainly, trials of targeted therapies and immunotherapy agents have excluded the study of *non-clear-cell renal cell carcinomas* (nccRCC). Therefore, tumors with non-clear-cell histology rarely have a specific adjuvant treatment. The limited data available for medical management of nccRCC leads to some patients being treated with target agents approved for metastatic ccRCC, such as sunitinib¹⁵. Unfortunately, most patients with nccRCC succumb to their disease within 18 months despite systemic treatment³², and to date, there is no evidence base for treatment of nccRCC with immune checkpoints inhibitors.

3. CLEAR CELL RENAL CELL CARCINOMA

3.1. Etiology

Genes and molecular pathways: ccRCC originate from the PCT in nephrons and the most frequent mutation is *Von Hippel-Lindau* (VHL) tumor suppressor gene. The complete loss of VHL gene through genetic and/or epigenetic mechanisms constitutes the earliest oncogenic driving event²¹. VHL is the substrate recognition component of an E3 ligase complex that ubiquitylates HIF1 α and HIF2 α via proteasome degradation²¹. Thus, loss of VHL leads to aberrant accumulation of HIF proteins despite an adequately oxygenated microenvironment, resulting in uncontrolled activation of HIF target genes that regulate angiogenesis (such as *vascular endothelial growth factor*, VEGF), glycolysis and apoptosis¹⁵. Accordingly, ccRCC tumors are rich in lipids and glycogens and are highly vascularized⁸, hence, inhibitors of VEGF and its receptor (VEGFR) are effective treatments for metastatic ccRCC (see Figure 5). However, VHL loss alone is insufficient to induce ccRCC, as evidenced by the long latency (< 30 years) in individuals who harbor VHL germline mutations²¹ and by the observation that *Vhl* loss in mice is unable to induce ccRCC³³. Moreover, low-frequency mutations in TCEB1 and CUL2 genes, which are components of the VHL E3 ubiquitin ligase complex, were found in ccRCC cells that did not have VHL alterations but had a phenotype mimicking VHL loss^{34,35}. These observations suggest that additional genetic and/or epigenetic events are probably needed for ccRCC development.

To identify these events, large-scale cancer genomics projects have revealed several novel prevalent mutations in ccRCC, including AR1D1A, SMARCA4, PBRM1 (29-41% of tumor samples), MLL3, SETD2 (8-12%), ASXL1, BAP1 (6-10%), KDM5C (4-7%) and MTOR (5-6%). Interestingly, PBRM1, SETD2, and BAP1 encode chromatin-regulating and histone-regulating proteins (located at 3p21) that function as tumor suppressors^{4,35}. As VHL resides at 3p25, a single-copy loss of the short arm of chromosome 3 (3p) results in the haploinsufficiency of these four tumor suppressor genes, corroborating that 3p loss is a key event in ccRCC³⁶. By contrast, *phosphoinositide 3-kinase* (PI3K)–AKT–*mechanistic target of rapamycin* (mTOR) pathway mutations (PTEN, MTOR, and PIK3CA) also found in ccRCC are generally missense and functionally activating³⁵, which explain why mTOR pathway inhibitors are effective³⁷. Loss of CDKN2A and TP53 mutations are also frequent in ccRCC (16.2% and 2.6%, respectively)³⁴. In addition to chromosome arm 3p loss, gain of chromosome arm 5q (67%), which includes SQSTM1 oncogene, and loss of chromosome arm 14q (45%), which includes HIF1 α , have been also confirmed in ccRCC³⁸. The gain of chromosome arm 5q and loss of chromosome arm 3p can occur simultaneously³⁹ (see Figure 6).

As inactivation of VHL is the founding event of ccRCC, its mutation status has no effect on clinical outcome, whereas mutations involved in disease progression, such as PBRM1, CDKN2A, TP53, SETD2, and BAP1, as well as KDM5C, are associated with aggressive phenotypes and poorer survival^{40–42}. Interestingly, mutations in BAP1 and PBRM1 or KDM5C seem to occur mutually exclusively, offering a molecular subclassification of ccRCC¹⁵. Furthermore, mutations in KDM5C, which is located at Xp.11.22, are predominantly detected in male patients and correlated with long-term therapeutic benefit⁴³. Mutations in SET2D are associated with reduced relapse-free survival⁴⁴

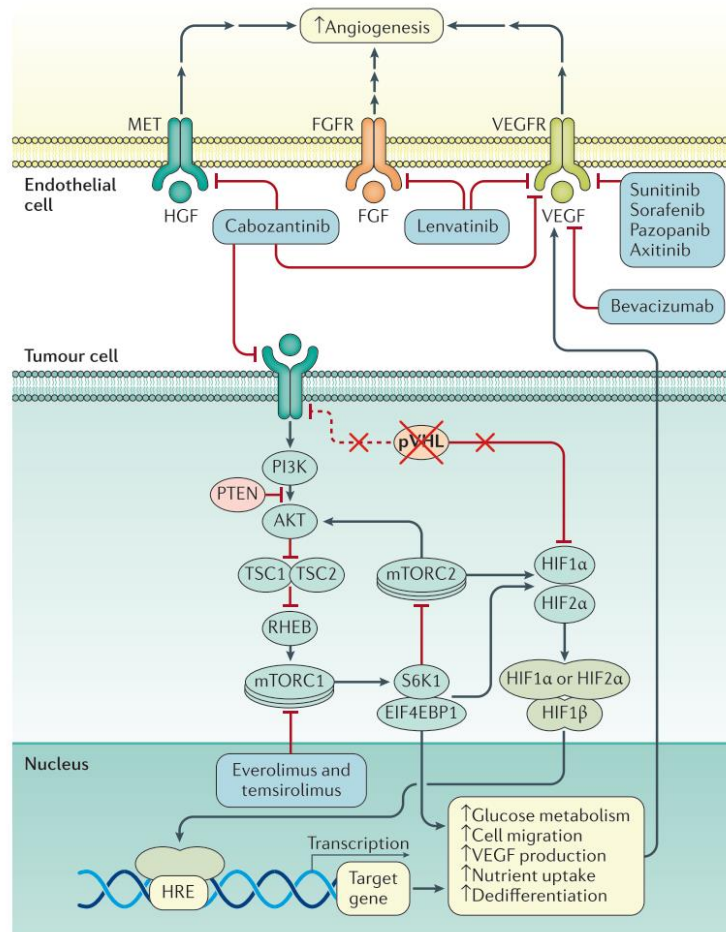


Figure 5. VHL inactivation in ccRCC and its implication in target therapy. Loss of VHL (which encodes pVHL) is the most frequent genetic feature of ccRCC. Its loss relieves the cell of negative regulation of the hypoxia-inducible factors (HIFs), which results in increased HIF target gene expression and the consequent changes in cellular metabolism and signaling that enhances cell survival. For example, increased VEGF expression increases angiogenesis along with increased growth factor signaling in endothelial cells in the tumor microenvironment, including *fibroblast growth factor* (FGF) and *hepatocyte growth factor* (HGF). Collectively, these changes provide the targets for therapeutic agents to impede tumor growth¹⁵.

It is still unknown, how individual mutations and their interactions contribute to the pathogenesis of ccRCC. Moreover, their values as prognostic or predictive biomarkers have yet to be elucidated.

Intratumoral heterogeneity: It has been widely described that genetic diversity within tumors enables their adaptation to a variety of micro-environmental pressures and metabolic demands during the natural history of cancer. Such genetic diversity has been extensively studied in ccRCC. A multi-region genetic analysis performed with four ccRCC patients carrying multiple tumors, found VHL mutation and loss of 3p as ubiquitous events across all regions sampled. By contrast, common events, such as SETD2, PBRM1, MTOR, PIK3CA, PTEN, and KDM5C mutations were present heterogeneously within the primary tumor and metastatic sites⁴⁵. Such genetic divergence allowed the construction of tumor phylogenies, whereby the ‘trunk’ of the evolutionary tree depicts mutations found in the *most recent common ancestor* (MRCA) that are also present in every tumor cell (VHL mutation and 3p loss). ‘Branched’ mutations (SETD2, PBRM1, MTOR, PIK3CA,

PTEN, and KDM5C) were found in some subclones but not others. These mutations may be regionally distributed across the tumor, either occupying distinct regional niches within the primary tumor or different niches between the primary and the metastatic sites of disease¹⁵ (see Figure 7).

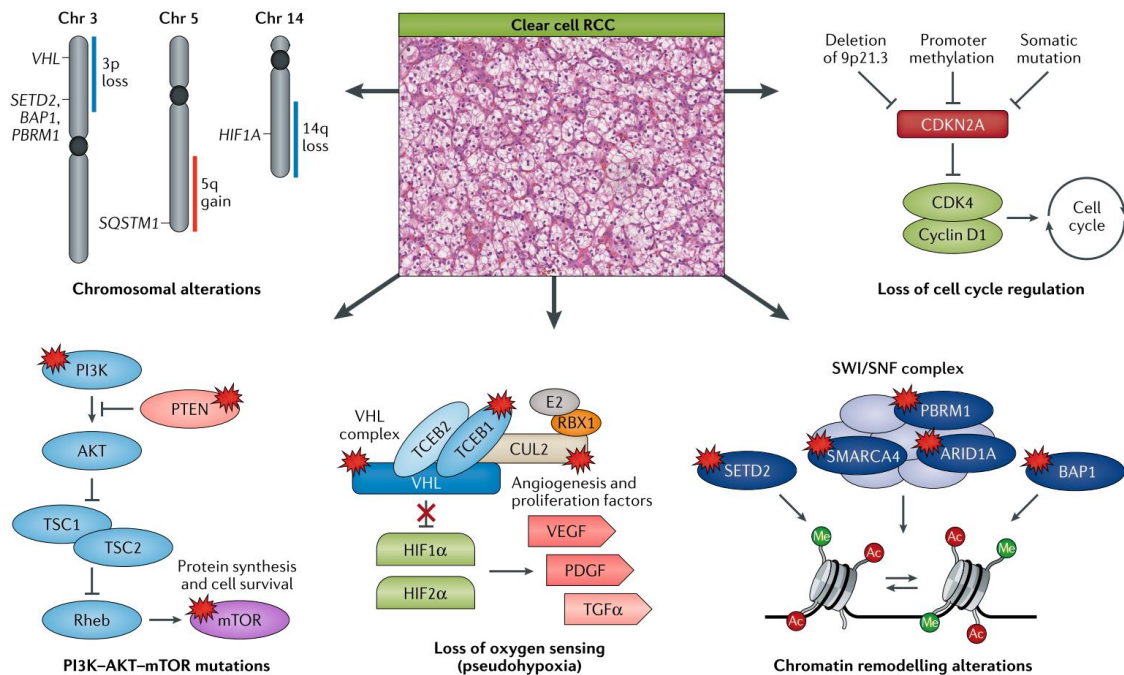


Figure 6. Main alterations in ccRCC identified by large-scale cancer genomic analyses. Most ccRCC tumors had loss of the von Hippel-Lindau (VHL) E3 ubiquitin ligase complex (VHL complex), which results from VHL mutation, hypermethylation or deletion in combination with chromosome arm 3p loss. In some tumors that lacked VHL mutations, genes encoding other VHL complex members, such as TCEB1 and CUL2, were found mutated. Loss of the VHL complex leads to stabilization of HIF1 α and HIF2 α , creating a state of pseudohypoxia in which expression of several angiogenesis and proliferation factors (such as VEGF, *platelet-derived growth factor* (PDGF) and *transforming growth factor- α* (TGF α)) is upregulated. ccRCC had specific chromosomal alterations, including nearly universal chromosome arm 3p loss, frequent chromosome arm 5q gain, and chromosome arm 14q loss. Mutation of genes in the PI3K-AKT-mTOR pathway, such as PTEN and mTOR, result in the activation of this pathway, which promotes protein synthesis and cell survival, were frequent in ccRCC. Mutation of chromatin-remodeling genes was common in ccRCC, including PBRM1, SETD2, and BAP1, which are present in the commonly lost region of chromosome arm 3p, and PBRM1, ARID1A and SMARCA4, which encode components of the SWI/SNF complex. Mutation of these genes is proposed to alter gene transcription. Loss of CDKN2A in ccRCC predominantly resulted from the deletion of a small region in chromosome band 9p21.3 or from promoter hypermethylation, whereas point mutation of CDKN2A was rare. CDKN2A encodes p16, which has an inhibitory effect on CDK4 and cyclin D1, and loss of CDKN2A results in increased activation of the cell cycle⁴.

Moreover, parallel evolution has been observed, whereby recurrent branch alterations in subclones affect the same gene, the signal transduction pathway or the protein complex. In some cases, such recurrent but distinct alterations can be readily explained as the second-hit event in the evolution of the tumor. In other cases, parallel evolutions suggest considerable selection pressures for disruption of the same signaling pathway or protein complex. In addition, a convergence of genetic characteristics has been noted in several studies of ccRCC, whereby mutations in genes occur at different time points but result in similar overall genomic and phenotypic profiles⁴³. Regardless of the modality, a

follow-up study of ccRCC samples from eight patients demonstrated evidence for branched evolution, in which 73-75% of driver alterations were found to be subclonal⁴⁶.

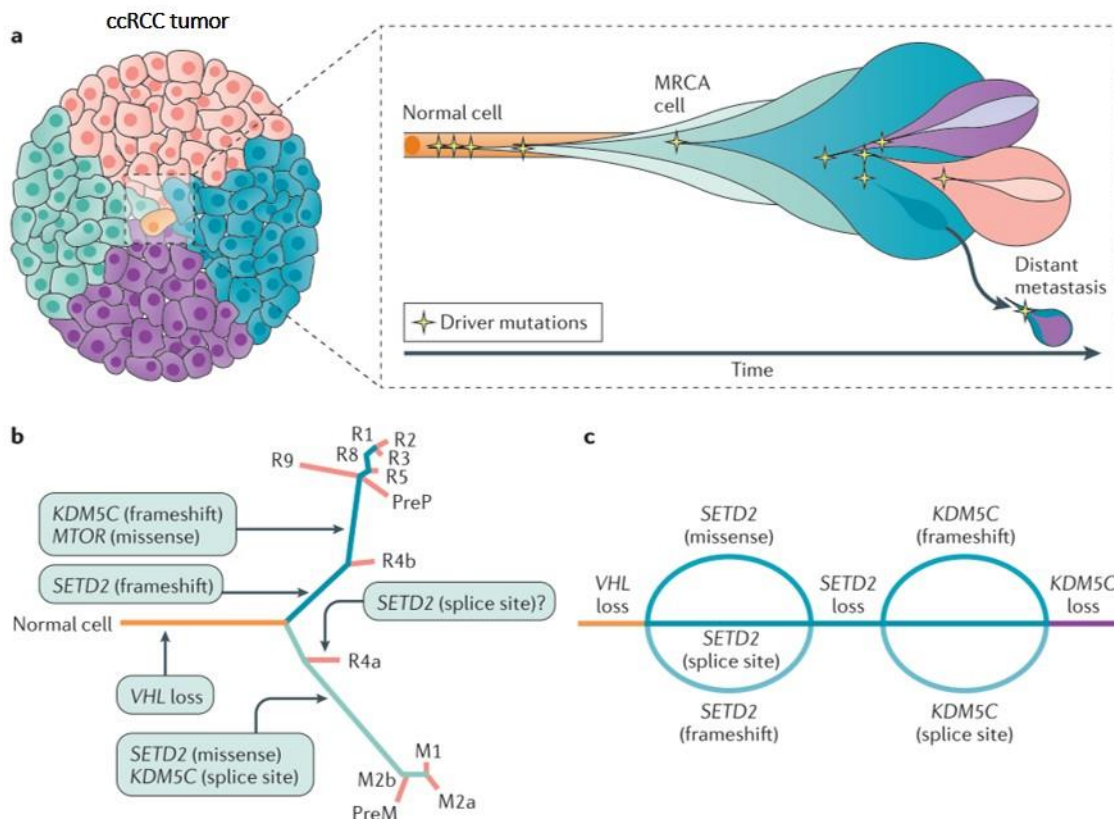


Figure 7. Cancer evolution and tumor heterogeneity in ccRCC. Although VHL mutation and 3p loss are early events that are evident in all ccRCC cells regardless of the region of the tumor sampled, common driver mutations (for example, SETD2, MTOR, and KDM5C mutations) are present heterogeneously suggesting subclonal evolution of the tumor. a) Cancer subclones originate from the MRCA cell, in which a normal cell acquires all functional capacities to become a cancer cell. b) Genomic heterogeneity can result from the sequential, parallel accumulation of mutations, contributing to the heterogeneity and the evolution of ccRCC. In this example, ‘R’ represents the genomic characteristics of the primary tumor and ‘M’ represents the genomic characteristics of the metastatic sites, numbered accordingly. The major genetic lesions acquired after VHL mutation feature in different samples are indicated on the branches. c) However, some evidence suggests that tumors can converge by way of parallel evolution. Here, a hypothetical braided river model depicts the sequential convergence of SETD2 and KDM5C mutations through different spatiotemporally distinct genetic events. Modified from ³⁵.

Multiregion tumor analyses suggest the possibility that evolutionary trajectories within ccRCC tumors are remarkably constrained, representing predictable evolutionary routes and, therefore therapeutically tractable. For example, it has been shown that patients who responded well to mTOR inhibition harbored recurrent but separated aberrations in components of the mTOR pathway³⁷. Furthermore, some subclonal alterations might be involved in the initiation and maintenance of cell-to-cell variations that are necessary for clonal selection. These events, dispersed in distinct regional niches within the tumor, could represent plausible genomic biomarkers in ccRCC⁴⁷.

Metabolic pathways: Dysregulated metabolism is a hallmark of cancer whereby tumors reorganize their metabolism to produce sufficient energy and biosynthetic building blocks, such as nucleotides, lipids, and amino acids, for malignant cellular proliferation. It has been proposed that tumor cells shift to aerobic glycolysis followed by lactic acid fermentation as the predominant form of energy production rather than oxidative phosphorylation even in the presence of normoxia (Warburg effect)⁴⁸. Although this is not true for all cancers, ccRCC is considered driven by metabolic change owing to the high frequency of mutation in genes that control aspects of metabolism, such as mutation of VHL in the hypoxia pathway, mutation of PI3K–AKT–mTOR pathway genes that dysregulates the control of growth in response to nutrient levels, and mutation of genes encoding essential components of the Krebs cycle (FH and SDHB)⁴⁹.

To date, many studies have focused on the study of ccRCC metabolism using transcriptomics data and relating gene expression changes with particular metabolic pathways and clinical aggressiveness. For instance, it has been demonstrated that expression levels of the gene signatures for the Krebs cycle and the *electron transport chain* (ECT) were low in ccRCC, while genes related to glycolysis pathways were highly expressed³⁴. This observation is consistent with the Warburg effect of aerobic glycolysis and suppression of oxidative phosphorylation⁵⁰. Furthermore, ccRCC tumors in stage III and stage IV had higher expression of the *ribose sugar metabolism* (RSM) than stage I and stage II tumors, and correlating with poorer survival⁴.

As mentioned earlier, ccRCC cells are lipid- and glycogen-loaded, implicating altered fatty acid and glucose metabolism. Accordingly, it has been described that ccRCC presents upregulation of the pentose phosphate pathway and fatty acid synthesis pathway genes, and downregulation of the *tricarboxylic acid* (TCA) cycle genes¹⁵.

A metabolic profiling study of ccRCC, including 138 ccRCC tumor/normal pairs of different Fuhrman grades, identified 319 metabolites (170 higher and 149 lower) that display differential abundance between tumor and normal tissue samples. Interestingly, most of the pathways overrepresented in tumor samples were involved in carbohydrate metabolism, whereas most of the decreased pathways were involved in amino acid metabolism (except for cysteine, glutamate, and glutamine). The same study also showed that the highest percentage (56%) of early-stage tumors was characterized by low abundance of dipeptides and that late-stage tumors displayed exceptionally high levels of glutathione-related metabolites and the highest abundance of dipeptides. The presence of dipeptides may be produced through protein degradation processes, such as lysosomal degradation, phagocytosis, endocytosis, pinocytosis, and autophagy. Regarding ccRCC progression, there were increases in metabolite levels of fatty acid biosynthesis and decreases in oxidative phosphorylation at pathogenesis and opposite patterns during progression⁵¹.

Immune infiltration and tumor microenvironment: Besides genetic alterations, gene expression, metabolomic and immunological analysis of ccRCC have also yielded important mechanistic and clinical insights. Of these, the immune infiltration characteristics of ccRCC are highly interesting. ccRCC tumors demonstrate immunohistochemical staining for tumor-infiltrating immune cells and strong expression of the immune signatures. Notably, among 19 cancer types examined by The Cancer Genome Atlas research program, ccRCC has the highest T cell infiltration score. Tumors

that are heavily infiltrated with immune cells could be destroyed by the immune response but are often suppressing immune responses by expressing immune checkpoints regulators, such as *programmed cell death ligand 1* (PDL1), which interacts with *programmed cell death 1* (PD1) on immune cells to inhibit these responses. Among the immune cell gene-specific signatures found in ccRCC are dendritic cells, B cells, T cells, regulatory T cells, cytotoxic cells and type 2 T helper cells³⁴. Furthermore, higher nuclear grade and stage in ccRCC were correlated with an increase in type 2 T helper cells and regulatory T cell infiltration⁵².

3.2. Disease models

Although human-derived ccRCC cell lines have been used for mechanistic studies, ccRCC tumors in patients are highly vascular, a feature that cannot be recapitulated with *in vitro* studies. Furthermore, such cell lines can acquire additional genetic and/or epigenetic changes during passages such that *in vitro* drug screening does not produce specific, translatable insights. Nevertheless, when these cell lines are injected subcutaneously into laboratory animals, xenografted tumors indeed respond to anti-VEGF therapy and can be used to investigate resistance mechanisms⁵³. Regardless of the evident limitations of cell lines use, they still represent a valid and reliable tool to study the mechanisms underlying ccRCC, such as differential gene expression analysis.

More recently, patient-derived xenograft models have been established and shown to recapitulate the patients' documented clinical response to target therapies, which could be used in preclinical drug trials⁵⁴. Furthermore, efforts to develop mouse models that truly reflect human ccRCC genomics and morphology have been hampered by the fact that homozygous inactivation of *Vhl* in mice does not result in ccRCC³³. However, the identification of additional recurrent, prevalent mutations in human ccRCC has renewed the will to generate such models. For example, a mouse model carrying homozygous deletion of *Vhl* and *Pbrm 1* resulted in multifocal, lipid-rich, glycogen-rich, transplantable ccRCC¹⁵. Interestingly, homozygous deletion of *Vhl* and *Bap1* in another mouse model resulted in early lethality (< 1 month), and some mice carrying homozygous deletion of *Vhl* and heterozygous deletion of *Bap1* developed tumor micronodules with unknown tumor incidence and molecular characteristics⁵⁵. Overall, animal models of ccRCC are currently limited but readily being pursued.

3.3. Treatment

Targeted therapies: In the past 10 years, several targeted therapeutic agents for the treatment of metastatic ccRCC have been approved. The inhibition of VEGF represents the primary therapeutic target due to the universal VHL loss in all ccRCC tumors, whereas secondary targets can include mTORC1, MET and IL8¹⁵.

Given the highly vascular nature of the ccRCC, several targeted therapies available exploit this feature. Currently, the approved tyrosine kinase inhibitors targeting the VEGF signaling axis are sorafenib, sunitinib, pazopanib, axitinib, lenvatinib, and cabozantinib¹⁵. All these therapies have been approved as single agents, apart from the combination of lenvatinib with everolimus. In addition, bevacizumab (an anti-VEGF monoclonal antibody)

was approved for use with interferon- α ⁵⁶. As first-line treatments, sunitinib, pazopanib and the combination of bevacizumab with interferon- α are approved, whereas axitinib and cabozantinib are approved as second-line options. The mTOR inhibitors everolimus and temsirolimus are approved as single agents as second-line treatment in patients with poor risk²⁶. At present, sunitinib is the standard of care due to its superiority in terms of response rate, progression-free survival and overall survival (see Figure 5 and 8).

Model systems have shown that treatment of ccRCC with multiple drugs is superior to single-agent, however, such approach tends to produce more toxicity. For example, the combination of sunitinib with everolimus leads to severe on-target and off-target toxicity⁵⁷. Thus, the immediate challenge is to design the most effective combination of drugs to treat ccRCC patients and also to prevent resistance.

Immunotherapy: Before the introduction of sunitinib, cytokines such as interferon- α and IL2 that enhance the antitumor immune activity, were standards of care. However, both drugs are effective in a small subset of patients and associated with significant toxicity. Many studies are currently searching for immunotherapy agents to establish T cell immune checkpoint inhibitors. Among them, antibodies against PDL1 (avelumab and atezolizumab), and antibodies against PD1 (nivolumab and pembrolizumab). PD1 negatively regulates T cell function and its ligand PDL1 is highly expressed by cancer cells, therefore, blockade of the PD1–PDL1 axis promotes T cell activation and immune killing of cancer cells¹⁵. Regardless of the current studies, nivolumab is the only immunotherapy agent actually approved for the treatment of metastatic ccRCC. Nivolumab is well tolerated, however, its response rate is only 25% and most patients treated did not experience significant tumor reduction⁵⁸ (see Figure 8).

Several promising new drugs with novel mechanisms of action are under study. For instance, ipilimumab, an inhibitor of the T cell checkpoint *cytotoxic T lymphocyte-associated protein 4* (CTLA4). CTLA4 downregulates T cell function, hence its inhibition promotes T cell activation¹⁵. The combination of nivolumab with ipilimumab has shown a remarkable response rate of ~40%.

As immune checkpoint inhibitors function independently of specific oncogenic pathways, the combination of these drugs with targeted therapies is under extensive study. For example, the efficacy of autologous dendritic cell-based immunotherapy, which consists of expanding the patient's own dendritic cell numbers *in vitro* followed by the introduction of tumor RNA before re-infusion back into the patient, in combination with sunitinib has been examined and seems promising⁵⁹. Other inhibitors specifically targeting HIF2 have been developed⁶⁰. Aberrant glycolysis (with aberrant glutamine and tryptophan metabolism) is another feature of ccRCC, therefore, the use of the glutaminase inhibitor CB-839 and the indoleamine-2,3-dioxygenase inhibitor INCB024360 could yield additional benefits when added to existing therapies¹⁵.

Further understanding of the intricate relationship between ccRCC and its respective immune microenvironment, would be crucial for the future success in designing novel therapeutic agents that modulate the anticancer response in patients.

Unfortunately, to date, there are no clinically usable markers to select patients for particular therapies, but the increasing understanding of tumor biology and the increasing number of treatment options will solve this issue in the near future.

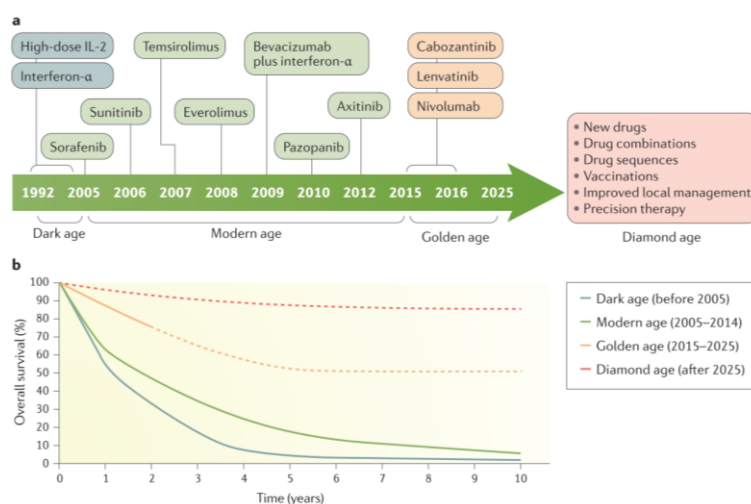


Figure 8. Therapeutic evolution and survival outcome of metastatic ccRCC. a) Before 2005, two drugs were available to treat ccRCC (with a median survival of ~15 months) and was called the dark age of treatments. By the modern age (2005–2014), seven additional agents were approved (increasing the median survival to ~30 months). Currently, the golden age has introduced three new drugs, with more to come over the next decade. b) It is expected that the advance in drug discovery to be translated to a significant number of patients (~50%), achieving durable remissions by 2025 with a median survival of ~5 years. The ultimate goal of the future diamond age of drug approvals is >80% of patients with metastatic ccRCC achieving long-term survival. Dashed lines represent predicted survival¹⁵.

3.4. Biomarkers

The perfect biomarker should be characterized by high sensitivity, specificity, and reproducibility, as well as obtained in a relatively non-invasive manner. Henceforth, plasma, serum, and urine have been thought of as potential sources of promising biomarkers. These fluids contain a wide range of proteins, minerals, nucleic acids, and hormones and can be analyzed by proteomics and molecular approaches for the identification of disease-specific markers. The analysis of urine becomes more appealing to renal diseases because urine content may reflect the pathological state directly from the kidney. Moreover, the use of urine as source of biomarkers results advantageous due to the greater availability of sample and the complete non-invasiveness of the procedure.

Regarding ccRCC, the most promising biomarkers are associated with treatment outcome and range from clinical parameters (such as blood pressure) and endogenous substances (such as plasma proteins) to pathobiological features specific to individual tumors (such as mutations). For instance, hypertension (≥ 140 mmHg) is considered a clinical biomarker since it has been associated with improved progression-free survival and overall survival in patients receiving VEGF inhibitors⁵³. As circulating biomarkers, high levels of IL6, IL8, hepatocyte growth factor, and osteopontin have been associated with shorter progression-free survival in patients receiving pazopanib and sunitinib⁶¹, whereas high levels of lactate dehydrogenase have been associated with better overall survival in those receiving temsirolimus but not interferon- α ⁶². For genetic biomarkers, a large randomized trial with 471 metastatic patients demonstrated that BAP1 mutation was associated with a better response to sunitinib (progression-free survival of 8.1 months)

versus everolimus (progression-free survival of 5.5 months). By contrast, PBRM1 mutation showed no correlation. Moreover, patients with KDM5C mutations were associated with a much longer progression-free survival with sunitinib (20.6 months) than with everolimus (9.8 months)⁴³. Although these biomarkers can be useful to predict clinical outcomes, early ccRCC-specific diagnostic and disease progression biomarkers are not available.

In 2004, our group identified for the first time, the overexpression of the *human hepatitis A virus cellular receptor 1* (hHAVCR1), also known as *kidney injury molecule 1* (KIM1), in 60% of surgical samples from localized ccRCC tumors by *RNA-based arbitrary primed polymerase chain reaction* (RAPD-PCR) and confirmed by Northern and Western blot⁶³. The expression of KIM1 was completely absent in benign oncocytomas. KIM1 is a type 1 transmembrane glycoprotein that sheds its ectodomain into the extracellular space⁶⁴. A subsequent study analyzed the expression of KIM1 in a *tissue microarray* (TMA) of 98 tumors ccRCC founding that KIM1 was expressed not only in ccRCC tumors but also in normal parenchyma of ccRCC patients suggesting that KIM1 could play a role in tumor ccRCC development and progression (see Figure 9). Moreover, the same study demonstrated that shedding of KIM1 (detected in the urine) correlated with a more aggressive ccRCC phenotype⁶⁵. Altogether, these results suggested KIM1 either as a diagnostic and prognostic urinary biomarker for ccRCC.

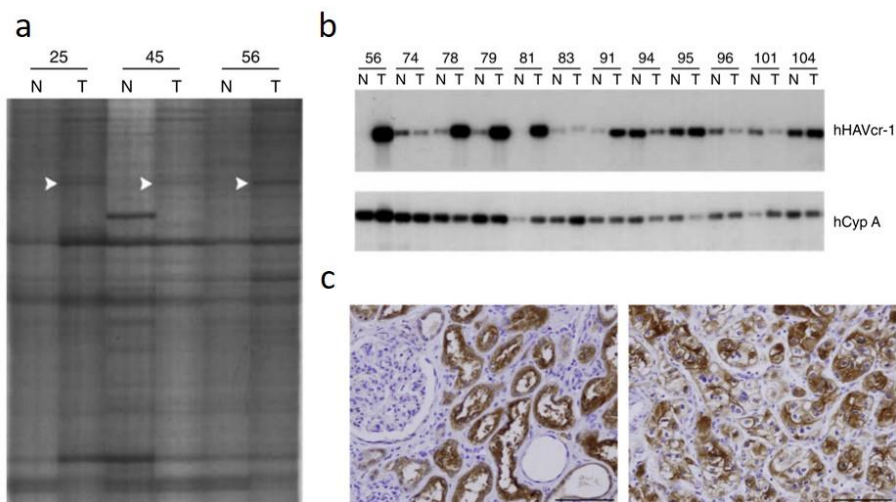


Figure 9. hHAVCR1/KIM1 expression in ccRCC. a) Representative results of RAP-PCR analysis in normal (N) and tumor (T) kidney tissues from three different ccRCC patients. Arrowheads indicate the differential product corresponding to hHAVCR1/KIM1. b) RT-PCR/Southern blot analysis depicting the expression of hHAVCR1/KIM1 and *cyclophilin A* (CypA), as an internal control. Total RNA was extracted from normal (N) and tumoral (T) tissues from the same ccRCC patient, indicated on top of each pair of lanes. c) Representative immunohistochemical evaluation of hHAVCR1/KIM1 in tissue samples of ccRCC patients. Regular histologic sections of normal parenchyma (left) and tumor (right). Modified from ^{63,65}.

To explore the effects of KIM1 on ccRCC, our group analyzed the differential gene expression between KIM1 overexpression and silencing in the human-derived ccRCC cell line 769-P, identifying cell death and survival, cell proliferation, cell development, and cell cycle as the most significant molecular and cellular functions related with KIM1

expression levels. From this study, a high expression of IL6, induced by KIM1 overexpression, was identified⁶⁶. IL6 was selected for further study because its role in tumorigenesis has been widely described and also because the majority of patients with metastatic ccRCC and poor survival rates exhibit increased IL6 serum levels⁶⁷. Furthermore, the mechanism by which KIM1 induced IL6 expression and activates the IL6/STAT3 signaling pathway was related to KIM1 shedding. By using KIM1 mutants with constitutive or impaired shedding, our group demonstrated that IL6 expression levels increased when shedding was constitutively induced, whereas shedding-defective KIM1 mutant was unable to induce IL6 expression⁶⁶. IL6 exerts its biological effects through binding to its ligand-receptor gp80 which leads to phosphorylation of tyrosine residues of the transducing receptor gp130, allowing for the docking and activation (phosphorylation of Tyr705) of STAT3⁶⁸. Besides IL6, high expression levels of gp130, STAT3, and HIF1 α were found when KIM1 was overexpressed, thus supporting the concept of IL6/STAT3 pathway activation⁶⁶. HIF1 α is a target gene of STAT3 and a master regulator of cellular homeostatic response to hypoxia and a driving event for ccRCC development, as has been discussed earlier²¹. Moreover, the knocking-down of IL6 expression demonstrated that HIF1 α upregulation was dependent on IL6-induced STAT3 activation⁶⁶ (see Figure 10).

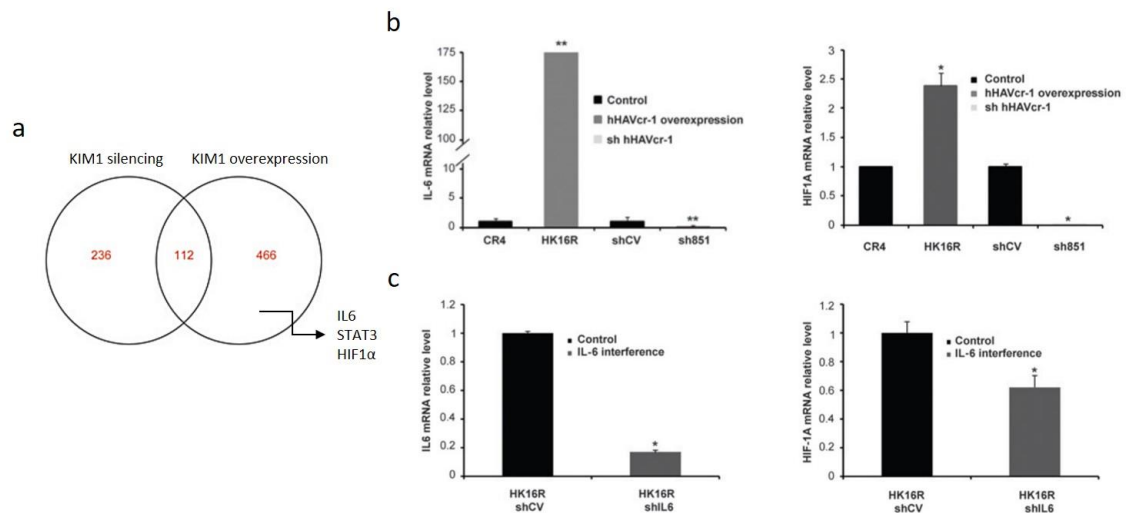


Figure 10. KIM1 induces IL6, STAT3, and HIF1 α expression. a) Venn diagram showing the number of genes up- or downregulated by KIM1 overexpression or silencing. Genes modified in both situations are placed in the intersection. b) RT-qPCRs showing that KIM1 overexpression (HK16R) increases IL-6 and HIF1 α mRNA expression levels compared with KIM1 silencing (sh851). CR4 and shCV are shown as control cell lines, respectively. c) RT-qPCR of IL6 silencing on KIM1 overexpressing cell lines (HK16R/shIL6) (left graph) and RT-qPCR showing that HIF1 α expression depends on IL6 levels (right graph). Modified from ⁶⁶.

4. SIGNAL TRANSDUCER AND ACTIVATOR OF TRANSCRIPTION 3

The *signal transducer and activator of transcription 3* (STAT3) is a key signaling protein who regulates diverse biological processes including cell growth, differentiation, and survival⁶⁹. STAT3 is a transcription factor that mediates the functions of cytokines, growth factors, and oncogenes under both physiological and pathological conditions. Moreover, augmented STAT3 activity is strongly implicated in cellular transformation and oncogenesis, reported in as many as 50% of all human tumors⁶⁹.

STAT3 belongs to a family of transcription factors called STATs, which consists of seven members (STAT1, STAT2, STAT3, STAT4, STAT5a, STAT5b, and STAT6), each of them responding to a distinct cohort of extracellular stimuli and controlling different cellular processes. The complete loss of STAT3 is incompatible with life, demonstrated by death in embryogenesis of STAT3 knockout mice, and even partial loss of function mutations lead to diverse pathologies⁷⁰.

The dogma of STAT3 activity relies on the phosphorylation of its Tyr705 which modulates the expression of hundreds of genes in the nucleus. However, the regulation and biological outcomes of STAT3 activation are far more complex. In addition to Tyr705 phosphorylation, STAT3 suffers a plethora of *post-transcriptional modifications* (PTMs), which regulate the nuclear function of STAT3 in addition to other non-genomic activities. Moreover, recent studies have revealed that STAT3 is either oncogenic or a tumor suppressor, suggesting that its activity is strongly context-specific.

4.1. Structure

STAT3 possesses a highly conserved structure consisting of 6 domains: *N-terminal domain* (NTD), *coiled-coil domain* (CCD), *DNA-binding domain* (DBD), *linker domain* (LD), *Src homology 2* (SH2) domain and *transcription activation domain* (TAD)⁷¹ (see Figure 11). The NTD allows STAT3 dimerization and nuclear import, whereas the helical CCD interacts with other proteins involved in nuclear import and export. The DBD, as the name suggests, is required for binding to specific palindromic sequences in promoters of target genes and the SH2 domain is required for the recognition of tyrosine phosphorylation on receptor subunits and stabilizes the association between STAT3 monomers via reciprocal phosphotyrosine-SH2 interactions. Lastly, the C-terminal TAD contains Tyr705 and Ser727 phosphorylation sites, essential for maximal transcriptional activation of STAT3-regulated genes.

4.2. Isoforms

STAT3 exists in two alternatively isoforms, the full-length STAT3 α , and the truncated STAT3 β , which possess both specific and overlapping transcriptional activities. The main difference between both isoforms is that STAT3 β lacks part of the TAD including the Ser727 residue, thus STAT3 β can be phosphorylated at the Tyr705, dimerize and binds to DNA⁷². However, several works have established that STAT3 β plays unique functions, activating sets of specific target genes. Interestingly, this isoform can sustain embryonal development but is lethal after the birth of mice lacking the α isoform⁷³.

Several reports indicate that STAT3 α and STAT3 β apparently play opposite functions in tumorigenesis⁷⁴. While STAT3 α appears to be responsible for most, if not all, the pro-oncogenic activities ascribed to STAT3, STAT3 β opposes and acts as a dominant-negative form⁷². However, it has been reported that STAT3 β can behave as an oncogene as well, inducing T cell leukemia development when overexpressed in transplanted bone marrow cells⁷⁵. Other studies have suggested that STAT3 β suppresses systemic inflammation. Indeed, STAT3 β null mice are extremely sensitive to endotoxic shock and developed exacerbated atherosclerosis⁷⁶. Consistent with these observations, mice lacking STAT3 β undergo exacerbated acute inflammatory responses to irritants, resulting in accelerated skin and intestinal tumorigenesis. Despite this, inhibition of STAT3 β has no effect on tumor development compared to WT mice, suggesting that STAT3 β indeed is important in maintaining tissue homeostasis through its anti-oncogenic role in inflammation-driven cancer⁷⁷. Hence, the balance between these two isoforms may determine tumor transformation and progression under specific signals. Unfortunately, there is no available information on the presence of PTMs in STAT3 β , as they have been described in STAT3 α .

4.3. Post-translational modifications

The main PTM described in STAT3 is the phosphorylation of its Tyr705, and recently, the phosphorylation of Ser727. However, STAT3 PTMs are not restricted only to phosphorylation, STAT3 can be also acetylated, methylated, ubiquitinated, and oxidized and glutathionylated⁶⁹ (see Figure 11). Each of them is implicated in STAT3 transcriptional activity, dimerization, nuclear translocation, complex formation with nuclear coactivators, and degradation.

Tyr705 phosphorylation: The phosphorylation of this residue constitutes the canonical activation of STAT3 and determines the ability to form dimers, to concentrate in the nucleus, and to bind DNA. Tyr705 phosphorylation occurs downstream of many activator signals such as cytokines, growth factors, and oncogenes^{73,78}, and its deactivation is controlled by negative regulators that lead to STAT3 dephosphorylation. In addition to its main nuclear localization, pTyr705-STAT3 has also been observed to localize in focal adhesions of ovarian cancer cells, where it interacts with phosphorylated paxillin and *focal adhesion kinase* (FAK), thus regulating cell migration⁷⁹.

Ser727 phosphorylation: In addition to pTyr705, STAT3 can be also phosphorylated at Ser727. Ser727 residue is located within a CDK/MAPK consensus motif and can undergo phosphorylation by a variety of serine kinases, such as MAP kinases, PKC ϵ , and mTOR, downstream of both classical STAT3 activating cytokines and growth factors, of the PI3 kinases and of Ras proteins⁸⁰. It has been described that pSer727 is required for the optimal transcriptional induction of a subset of target genes, and it can also modify STAT3 activation dynamics by inhibiting subsequent pTyr705^{80,81}. Recently, it became clear that pSer727 can confer specific activities to STAT3 independently of pTyr705, and not involving either nuclear localization or transcriptional activity. In particular, pSer727-STAT3 drives important functions in the mitochondria. It is presumed, but not certain, that Ser727 phosphorylation occurs in the cytosol prior to import into the mitochondria⁸².

Besides pTyr705 and pSer727, STAT3 undergoes phosphorylation at Thr714, which is located adjacent to Ser727. Moreover, Thr714 and Ser727 can be phosphorylated simultaneously showing an augmented STAT3 transcriptional activity⁸³. However, no further studies on pThr714 have been carried out to understand its role in the overall activation and functioning of STAT3.

Acetylation: Upon cytokine treatment, STAT3 can be acetylated on the lysine 685 (K685) by the histone acetyltransferase p300. As K685 locates in the SH2 domain, it is unsurprising that this PTM promotes STAT3 dimerization, thus DNA binding and gene transcription⁸⁴. STAT3 is also acetylated at the lysine 49 and 87 (K49 and K87) by p300 in response to *interleukin 6* (IL6), whereas deacetylation of these residues is mediated by *histone deacetylase* (HDAC). K49 and K87 deacetylation reduce the binding affinity between STAT3 and p300, thus acting as a mechanism to control IL6-dependent gene expression⁸⁵. In contrast, K87 acetylation after insulin stimulation promotes STAT3 mitochondrial translocation and functions⁸⁶.

Methylation: Methylation and demethylation of lysine 140 (K140) in the CCD of STAT3 has also been reported to alter its ability to bind DNA. Methylation on K140 by the histone methyltransferase SET9 blocks the binding of STAT3 to DNA, whereas inhibition of methylation (by K140A or K140R mutations) significantly enhances STAT3-mediated gene expression of a subset of genes and it has been linked to the pro-tumorigenic activity of STAT3⁸⁷. STAT3 is also methylated at lysine 180 (K180) by *enhancer of zeste homolog 2* (EZH2). K180A mutation blocks methylation and resulted in a loss of the STAT3 ability to be phosphorylated at Tyr705, which in turn suppressed STAT3-mediated gene expression on glioblastoma stem-like cells and prostate cancer⁸⁸.

Ubiquitination: STAT3 also undergoes poly-ubiquitination and proteasomal degradation by the 26S proteasome to abolish its transcriptional activity⁸⁹. Although STAT3 poly-ubiquitination is linked to its degradation, mono-ubiquitination has been linked with signaling. Lysine 97 (K97) has been identified as the major mono-ubiquitin conjugation site on STAT3. Ectopic expression of STAT3 mono-ubiquitinated led to an increase in the STAT3-BRD4 complex. The STAT3-BRD4 complex has been described as an anti-apoptotic and pro-proliferative mechanism through increased expression of BCL2, BCL2L1, APEX1, SOD2, CCND1 and MYC genes⁹⁰.

Oxidation and glutathionylation: STAT3 is also regulated by changes in cellular redox balance and can become oxidized and glutathionylated on cysteine residues, impairing its transcriptional activity, either under conditions of oxidative stress or by IL6 signaling, which can raise *reactive oxygen species* (ROS) levels^{91,92}. In an oxidative environment, STAT3 is S-gluthionylated at cysteine 328 and 542 (C328 and C542) in the DBD and LD, impairing the STAT3 ability to be phosphorylated on Tyr705⁹³. In contrast, mild ROS production, induced by stimulation with *insulin-like growth factor 1* (IGF1) or *epidermal growth factor* (EGF), activates JAK kinases and enhance pTyr705-STAT3 nuclear activity⁷³. These observations suggest that STAT3 is part of a mechanism controlling redox homeostasis. Indeed, the expression of a redox-insensitive cysteine mutant STAT3 leads to increased STAT3 activity and cell growth rates. Therefore, this cross-talk between oxidative and non-oxidative STAT3 modifications can affect the activities of pTyr705-STAT3 as well as cell proliferation and survival⁷³.

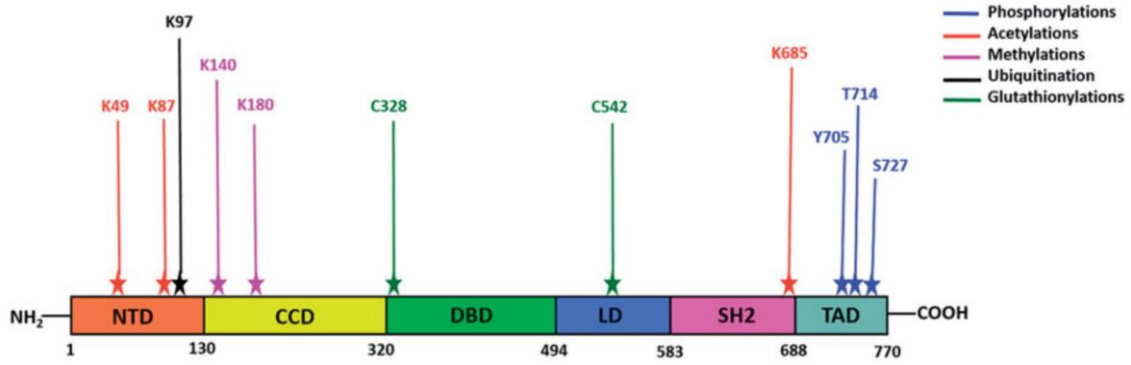


Figure 11. The structure of STAT3 and its major post-translational modifications. The image represents the six domains that constitute STAT3 and the sites where major PTMs occur are indicated. The NTD, TAD, and CCD provide niches for most of the PTMs. The key phosphorylation sites (Y705 and S727) of STAT3 are localized in the TAD. Modified from ⁶⁹.

These observations show an impressive number of PTMs, all of which have been identified on STAT3 isolated from total cell lysates and the functional significance of these modifications has been studied only in the context of canonical STAT3 activity. However, to date, we lack detailed knowledge of compartment-specific modifications and/or combinations of PTMs and how they influence STAT3 signaling and biology.

4.4. Canonical STAT3 activation and function

The accepted mechanism for STAT3 signaling consists in the presence of STAT3 as a latent monomer in the cytosol until an autocrine or paracrine stimulus bind to their corresponding cell surface receptors initiating a cascade of signaling events. STAT3 is canonically activated by a wide variety of cytokines (IL6, leptin, IL12, IL17, IL10, interferons), growth factors (G-CSF, EGF, PDGF), and oncogenes (Scr, Abl, Sis, Fps, Ros, Met, ErbB2)^{73,78}. STAT3 is also activated by *G-protein coupled receptors* (GPCRs) and *Toll-like receptors* (TLRs)^{94,95}. Regarding receptor lacking intrinsic tyrosine kinase activity, such as IL6 or *interferon* (IFN) family receptors, multimerization of the receptor brings *Janus kinase* (JAK) family kinases into close proximity allowing transphosphorylation of each other on their cytoplasmic tail. These phosphorylated tyrosine residues create docking sites for STAT3 recruitment by its SH2 domain. Once recruited, STAT3 is phosphorylated on Tyr705, facilitating homodimerization, nuclear translocation, DNA binding on the canonical *gamma interferon activation site* (GAS) sequences (TTCCN₂₋₄GGAA), and initiation of transcription⁹⁶. Besides STAT3 homodimers, STAT3 can form heterodimers with other STAT family members, including STAT1 and STAT3⁹⁷. Once the JAK/STAT3 pathway is activated, it is rapidly shut off by negative regulators which mainly belong to three groups: *protein tyrosine phosphatases* (PTases), *suppressors of cytokine signaling* (SOCS), and *protein inhibitors of activated STATs* (PIAS), or via ubiquitin-proteasome degradation⁶⁹ (see Figure 12).

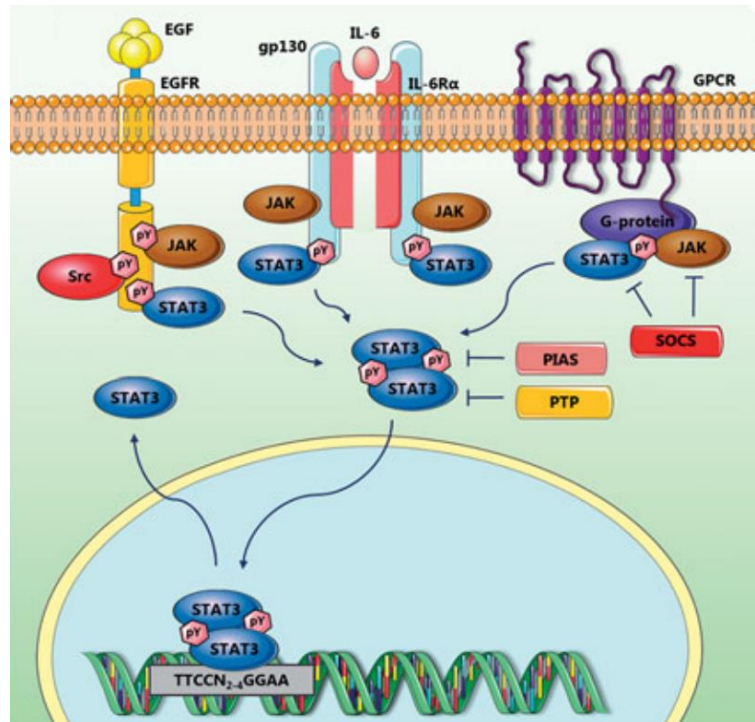


Figure 12. Canonical STAT3 signaling. A stimulus activates cell surface receptors and non-receptor tyrosine kinases. For EGFR and cytokine receptors lacking intrinsic tyrosine kinase activity, JAKs are recruited upon ligand-receptor aggregation. Phosphorylation of the receptors by JAKs provides docking sites for STAT3 recruitment. Once phosphorylated on the Tyr705 residue, STAT3 dimers translocate into the nucleus and bind to specific DNA motif to regulate the expression of target genes. Once activated, the JAK/STAT3 pathway is turned off by negative regulators⁶⁹.

4.5. Non-canonical STAT3 activation and functions

Whilst the classic model of STAT3 signaling is largely correct, it has to be revised to reflect recent findings. For instance, the idea of STAT3 existing solely as a monomer in the absence of stimuli is incorrect, moreover, monomeric STAT3 is undetectable in the cytoplasm in the absence of cytokine stimulation, rather, it is present as a dimer or as a higher molecular mass called “statosome”. This statosome is a complex categorized in two main molecular sizes: 200-400 kDa (statosome I) and 1-2 MDa (statosome II)⁹⁸. Furthermore, it has been reported that STAT3 self-association is independent of IL6 stimulation, thus existing as preformed complexes in the absence of phosphorylation⁹⁹. Cytokine stimulation has also been proven to be unnecessary for nuclear translocation¹⁰⁰. Certainly, STAT3 continuously shuttle between the cytosol and the nucleus independent of pTyr705. Nevertheless, pTyr705 alters the presence of STAT3 in the nucleus due to STAT3 binding to DNA¹⁰¹.

The *unphosphorylated STAT3* (U-STAT3), which refers to a STAT3 non-phosphorylated at Tyr705, can also regulate gene transcription of a subclass of STAT3 target genes, including RANTES, IL6, IL8, MET and MRAS. It has been demonstrated that U-STAT3 forms a novel transcription factor complex with the *nuclear factor kappa B* (NFκB), which is a potent inflammatory transcription factor related to the activation of B cells^{102,103}. Therefore, U-STAT3-mediated gene transcription can be carried out by direct or indirect binding to DNA on sites distinct from the GAS sequences^{103,104}. Accordingly, high nuclear levels of U-STAT3 correlate with poor prognosis in glioblastoma¹⁰⁵.

In addition to non-canonical nuclear activities, several non-genomic functions of STAT3 have been reported in the past few years. STAT3, as well as other STAT proteins, associate with a variety of cytosolic structures including focal adhesions, microtubules, mitotic spindle and membranous structures, such as plasma membrane rafts, endo-lysosomes, mitochondria, and endoplasmic reticulum⁶⁹. The first evidence of STAT3 association with non-genomic structures arises from the observation that STAT3 was present in cytosolic, sedimentable membrane fractions from both untreated and cytokine-stimulated cells^{106,107}. More recently, the extranuclear functions of STAT3, especially in the mitochondria, have been identified by several groups⁶⁹.

Mitochondria: STAT3 has been identified in the mitochondria of all tissues and cell lines assayed^{82,108,109}. Biochemical fractioning of mitochondria suggests that, despite the lack of a classical N-terminal mitochondrial targeting sequence, STAT3 is associated with the inner mitochondrial membrane and the mitochondrial matrix. In contrast to nuclear STAT3 activity, which is strongly influenced by pTyr705, the activity of *mitochondrial* STAT3 (mSTAT3) is dependent on pSer727¹¹⁰ (see Figure 13). Therefore, when referred to mSTAT3 it really means pSer727-STAT3. Although pSer727 is vital for mitochondrial activity, mouse knock-in models suggest that it remains dispensable for most normal activities of STAT3 in all tissues¹¹¹.

STAT3 loss significantly reduced the activity of the *electron transport chain* (ETC) complexes I, II and V, and it is restored by the introduction of a mSTAT3 form in the cells^{82,109}. Subsequent studies have confirmed these findings and additionally shown that mSTAT3 also regulates the activity of complexes III and IV⁶⁹. It has been described that mSTAT3 co-immunoprecipitates with the integral complex I component *gene associated with retinoic and interferon-induced mortality 19* (GRIM19), suggesting that mSTAT3 is physically associated with the ETC¹¹⁰. However, a study using isobaric labeling and mass-spectrometry to measure the relative expression of mSTAT3 to ETC proteins, estimated only 0,00001% of mSTAT3 expression, which makes the putative physical interaction unlikely to be necessary for the modulation of complex I activity¹¹².

mSTAT3 function, are in line with its pro-oncogenic activities, contributing to cell survival under specific stress conditions such as downstream of Ras-mediated transformation⁸². Specifically, mSTAT3 was shown to preserve optimal ETC activity, increasing membrane polarization and ATP production, and enhancing the activity of lactate dehydrogenase. Consequently, aerobic glycolysis is induced and ROS production decreased^{110,113,114}. In addition to these actions, which contribute to the maintenance of energy balance under stress, protection from apoptosis could also be triggered by the inhibition of the *mitochondrial permeability transition pore* (MPTP) opening, which in turn may be explained by its ability to interact with cyclophilin D¹¹⁵.

In normal conditions, the ETC complexes I, II and III shuttle electrons to complex IV to complete the reduction of oxygen to water. Electron leakage occurring in this process leads to the production of *reactive oxygen species* (ROS)¹¹⁶. It has been observed that mSTAT3 levels correlate with altered concentrations of ROS, however, its role in the production of ROS is controversial. Elevated ROS concentrations were observed in STAT3-deficient murine bone marrow cells and astrocytes leading to cell death^{117,118}, whereas IL-6 stimulation of CD4+ T cells leads to reduced ROS production in a STAT3-dependent manner¹⁰². Together, these data suggest that STAT3 leads to the suppression of ROS

production. In contrast, a recent study using a mass-spectrometry- based metabolomics profiling found that the increase in the production of ROS was a consequence of mitochondrial STAT3-augmented ETC activity¹¹⁹. Therefore, whilst it is clear that mSTAT3 alters mitochondrial ROS production and cellular ROS concentrations, the exact role of mSTAT3 in the regulation of ROS and the biological consequences still remain unclear.

The mitochondria have their own unique, 16.6 kb, circular genome encoding 13 genes, 2 RNAs and 22 tRNAs. Transcription of *mitochondrial DNA* (mtDNA) is driven by a specific transcription factor, the *transcription factor A, mitochondrial* (TFAM)⁶⁹. mSTAT3 has been physically associated with TFAM, and chromatin immunoprecipitation experiments showed that mSTAT3 binds the mitochondrial genome at the D-loop, as well as consensus STAT binding sites along the mitochondrial genome. Moreover, STAT3 deletion in keratinocytes resulted in an increased expression of mitochondrial genes indicating that STAT3 suppresses mitochondrial transcription¹²⁰. However, all of the mitochondrial proteins are crucial components of the ETC and other studies have reported that STAT3 increases the activity of the ETC⁶⁹, therefore, these two observations are inconsistent.

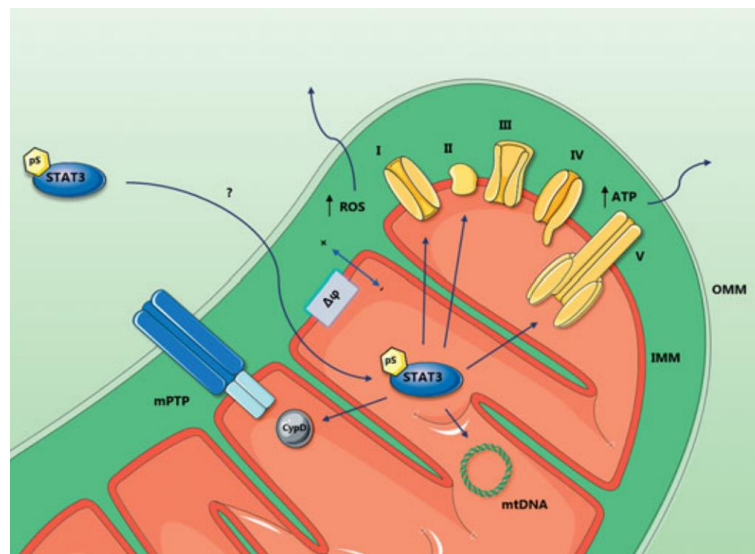


Figure 13. The non-canonical activity of STAT3 within the mitochondria. The activity of mSTAT3 primarily depends on Ser727 phosphorylation to modulate critical mitochondrial processes, including the ETC, the *mitochondrial permeability transition pore* (MPTP) opening and the transcription of mtDNA. Altogether, these mSTAT3 activities, result in elevated ATP production and mitochondrial membrane potential, as well as altered levels of ROS.

Endoplasmic reticulum: To date, the well-known anti-apoptotic STAT3 functions were based on the transcriptional activation of anti-apoptotic genes in the nucleus and on the maintenance of ETC activity in the mitochondrion. However, a recent study has demonstrated that STAT3 modulates Ca^{2+} fluxes via IP3R3 degradation at the *endoplasmic reticulum* (ER) and *mitochondria-associated membranes* (MAMs), thus regulating the sensitivity of cells to apoptotic stimuli and inhibiting Ca^{2+} - mediated cell death¹²¹.

Calcium homeostasis and the regulation of its flux between different subcellular compartments are fundamental for the control of many cellular functions, including

apoptosis¹²². The ER is the major intracellular Ca^{2+} storage compartment¹²³. The regulation of Ca^{2+} content in the ER is under control of Ca^{2+} pumps, such as the SERCAs, and of Ca^{2+} channels activated by *inositol 1,4,5-triphosphate* (IP3) and its receptor (IP3R)¹²⁴. As the membranes of the mitochondria and the ER are nearby, the excessive release of Ca^{2+} , can lead to mitochondrial Ca^{2+} overload, triggering the opening of the *mitochondrial permeability transition pore* (MPTP) and the initiation of the intrinsic apoptotic program¹²⁵. This process is mediated by the abundance and activity of the IP3Rs and in particular of IP3R3, which preferentially transmits apoptotic Ca^{2+} signals from ER to mitochondria¹²⁶. Therefore, the ER-mitochondria interface acts as a signaling hub for the activity of growth factors, oncogenes and tumor suppressors that regulate IP3R3 activity⁷³. The silencing of STAT3 in breast cancer cells significantly increases Ca^{2+} content and release, correlating with apoptotic cell death. Since both pTyr705- and pSer727-STAT3 localizes to the ER and MAMs, phosphoablative mutants (Y705F and S727A) were used to evaluate their effect on IP3R3-mediated Ca^{2+} release. It was found that pSer727-STAT3 inhibits Ca^{2+} release by interacting with IP3R3 and facilitating its degradation via the proteasome. These observations explain why tumors displaying STAT3 constitutive activation exhibit an inverse correlation between STAT3 and IP3R3 expression¹²¹.

4.6. Cancer (the paradox)

The aberrant and constitutive STAT3 activity in tumors has been related with proliferation, resistance to apoptosis, down-modulation of immune responses, promoting angiogenesis, enhancing invasion and metastasis by inducing *epithelial to mesenchymal transition* (EMT), altering the extracellular matrix inducing *matrix metalloproteinases* (MMP), promoting collagen cross-linking and tissue tension, regulating energy metabolism and mitochondrial activity, and conferring cancer stem cell features in a number of liquid and solid tumors⁷³. Furthermore, aberrant STAT3 activation is also crucial to determine the pro-tumorigenic features of most tumor-stromal cells¹²⁷. However, according to the complexity of its functions, recent evidence points to STAT3 may also act as a tumor suppressor under specific conditions, even in tumors where it was previously shown to play pro-oncogenic functions. Thus, it appears that the STAT3 functions in cancer can vary according to context, genetic background, and phase of the tumor.

STAT3 as an oncogenic driver: Since the first report of constitutively activated STAT3 in v-Src-transformed cells¹²⁸, a large number of subsequent studies have shown STAT3 to be a key protein in oncogenesis. Current estimates suggest that persistent pTyr705 is detected in more than 50% of human cancers, including both solid and hematological tumors⁶⁹. Evidence for the tumoral properties of STAT3 was originated in studies overexpressing a constitutive dimerizing STAT3 mutant (STAT3C). STAT3C acts as an activated STAT3 without the requirement for pTyr705 by disulfide bridges between 2 inserted cysteines in the SH2 domain. STAT3C exhibits transforming capacity in immortalized fibroblast and epithelial cells¹²⁹. Whilst this is an artificial mutation, several rare STAT3 activating mutations have been reported in lymphoid malignancies⁶⁹.

Typically, the aberrant activity of STAT3 in oncogenesis arises from mutations and/or persistent activation of upstream regulators, such as cytokine and growth factor receptors, as well as non-receptor tyrosine kinases.

IL6 is a potent and well-described driver of STAT3 activation in many tumors. IL6 signaling is associated with tumor progression and correlates with poor prognosis in patients with solid tumors, including breast, lung, prostate cancer and renal cell carcinoma^{130–133}. Furthermore, IL6 signaling, along with other IL6 family cytokines, modulates a variety of inflammatory processes, including inflammatory-associated tumorigenesis. For instance, IL6- and IL11-mediated STAT3 activation induces intestinal chronic inflammation leading to increased susceptibility to gastric cancer¹³⁴. Another IL6 family cytokine, the *leukemia inhibitory factor* (LIF), also activates STAT3 signaling in numerous cancer types, such as glioblastoma, nasopharyngeal carcinoma, and pancreatic ductal adenocarcinoma⁶⁹. For instance, high serum levels of LIF in nasopharyngeal carcinoma correlate with disease recurrence and resistance to radiotherapy¹³⁵. Moreover, LIF regulates the self-renewal capacity of *glioma-initiating cells* (GICs) by activating STAT3 signaling pathway¹³⁶.

Cytokines and growth factors receptors lack intrinsic tyrosine kinase activity; therefore, they rely on kinases associated with receptor cytoplasmic tails, primarily the JAK proteins. The JAK/STAT3 signaling axis is the classic example of STAT3-mediated tumorigenesis. Constitutive JAK activation, as a result of chromosomal translocations and somatic point mutations, are usual in hematological malignancies⁶⁹. Since JAKs are potent activators of STAT3, JAK tyrosine kinase inhibitors have been attractive therapeutic targets for both hematological malignancies and inflammation-associated cancers. Though these agents are clinically available, they do not have had the effect that it had been predicted.

Upregulated expression of *receptor tyrosine kinases* (RTKs) also results in enhanced STAT3 activation and is common in many tumors. For example, the oncogenic variant form of *epidermal growth factor receptor III* (EGFRvIII) forms a physical complex with STAT3 in the nucleus and promotes glial cell transformation¹³⁷. EGFRvIII has also been shown to act as a substrate for *wildtype* (WT) EGFR, and phosphorylation of both receptors is required for full STAT3 activation contributing to glioma progression¹³⁸. EGFR and STAT3 also coordinate in the upregulation of inducible *nitric oxide synthase* (iNOS) gene expression associated with tumor growth and malignancy¹³⁹. In disease models of *acute myelogenous leukemia* (AML), STAT3 inhibition abolishes RTK-mediated cellular transformation suggesting that STAT3 activation is required for tumorigenesis¹⁴⁰. Similarly, *vascular endothelial growth factor receptor 2* (VEGFR2) also facilitates STAT3 and MYC expression resulting in tumor-initiating self-renewal cellular processes in breast cancer¹⁴¹.

GPCRs have also been described to activate STAT3 and contribute to cancer progression. GPCRs activated by hormones and neurotransmitters, such as *angiotensin II* (AT1), have been reported to activate STATs 1, 2 and 3¹⁴², and besides ligand-induced activation of GPCRs, several studies have identified mutations that result in constitutively activated receptor associated with increased cellular proliferation and transformation¹⁴³. Moreover, members of GPCR family, Ga0 and Ga1, mediate cellular transformation via STAT3 activation potentially by direct interaction with and activating Src tyrosine kinase. Ectopic expression of Ga0 mutant (Q205L) leads to upregulated endogenous c-Src activity and phosphorylation of Tyr705-STAT3¹⁴⁴, and more recently, GPCRs have been also found to cross-talk with IL6 signaling via JAK/STAT3 activation. *Sphingosine-1-phosphate* (S1P), a lipid metabolite, and its receptor S1PR1 activate STAT3 via GPCRs which in turn upregulates S1PR1 expression causing a feed-forward loop in tumor cells¹⁴⁵. Alternatively, S1P may indirectly activate STAT3 via NFκB pathway and IL6 production

related to *colitis-associated cancer* (CAC) incidence¹⁴⁶. Furthermore, S1PR1–STAT3 signaling also plays a critical role in modulating immune cell behavior in the tumor microenvironment, including promoting cell migration and the formation of a pre-metastatic niche in myeloid cells¹⁴⁷. The S1PR1–STAT3 complex also facilitates the accumulation of Treg cells resulting in inhibition of cytotoxic CD8+ T cell and its anti-tumor effects¹⁴⁸.

Another vital upstream regulator of STAT3 signaling is the *Toll-like receptors* (TLR), which is a family of immune pattern recognition receptors that are activated by *pathogen-associated molecular patterns* (PAMPs)¹⁴⁹. Like cytokine receptor and GPCRs, TLRs also rely on tyrosine kinases to transmit signals from exogenous ligands and engage STAT3 to elicit a transformed state in mouse and human cells. It has been reported that increased TLR4 expression induces STAT3 activation promoting colon tumor growth *in vivo*¹⁵⁰. Furthermore, STAT3 directly upregulates TLR2 expression which drives gastric tumorigenesis¹⁵¹. Besides TLR4 and TLR2, TLR7 activation results in enhanced STAT3 activation which promotes pancreatic cancer progression and stromal inflammation¹⁵². Recent evidence shows that activated STAT3 can induce TLR9 expression in *glioma stem cells* (GSCs) which in turn recruits JAK2 and further amplifies STAT3 signaling¹⁵³. The ability of TLRs to activate STAT3 in tumors, in addition to paracrine feed-back via cytokine release, provides a direct mechanism by which inflammation promotes oncogenesis.

The role of STAT3 in tumorigenesis has been largely associated with its ability to regulate gene expression that provides a survival benefit, including the oncogene MYC. Since MYC is a downstream effector of STAT3 signaling, it has been presumed that STAT3 is irrelevant in tumors with MYC amplification¹²⁹. However, recently, STAT3 has been reported to promote the progression of MYC-driven pediatric cancer. The loss of STAT3 in these patients leads to impaired cellular proliferation, tumor reduction, and prolonged survival in xenograft models¹⁵⁴. Accordingly, treatment with a STAT3 dimerization inhibitor reduces tumor burden in mice, underlining the importance of STAT3 in MYC-mediated oncogenesis. Although previous studies show that MYC expression is regulated by STAT3, it seems that MYC amplification may influence and required STAT3 activity for its oncogenic functions.

Targeting STAT3 for cancer therapy has proved to be challenging since it lacks intrinsic enzymatic activity, and although many STAT3 inhibitors have been developed, no candidate compound has shown sufficient therapeutic effects for cancer patients to be clinically approved.

STAT3 as a tumor suppressor: The most prominent and well-studied role for STAT3 in cancer is as a proto-oncogene, however, recent evidence of tumor-suppressive roles for STAT3 entails re-evaluation of this dogma. The dual role of STAT3 became visible in glioblastoma where STAT3 exerts both tumor enhancer and suppressor activities depending on the genomic mutational profile. As mentioned before, the association between STAT3 and EGFRvIII induces glial transformation, but it has also been observed that STAT3 concomitantly suppresses malignant transformation in the absence of PTEN tumor suppressor¹³⁷. However, other reports using STAT3 inhibitors show suppression of glioma growth. Thus, whether STAT3 acts as a glioma tumor suppressor in clones without PTEN expression remains unclear.

Other studies have shown the importance of STAT3 in Ras-dependent tumorigenesis. Moreover, inhibition of STAT3 impairs the ability of Ras to drive cellular transformation⁸² and promotes tumor formation in *hepatocellular carcinoma* (HCC) harboring Ras mutations, which can be negatively regulated by NFκB signaling¹⁵⁵. However, other studies have shown an anti-tumor effect of STAT3 in the context of the tumor suppressor p14ARF (p19ARF in mouse). Constitutively activated STAT3 represses tumor growth in p19ARF-negative hepatocytes, whereas it exhibits tumor-promoting activity in cells expressing p19ARF. Consistently, knockdown of p14ARF expression in human HCC cell lines results in reduced pTyr705-STAT3 levels in xenograft models, highlighting the functional interaction between p14ARF and nuclear STAT3 activity in these tumors¹⁵⁶.

These findings in both glioblastoma and HCC, suggest that the expression of specific tumor suppressors influences STAT3 tumor-suppressive functions.

Aberrant STAT3 activation has been reported in ~50% of *non-small cell lung cancer* (NSCLC) primary tumors and cell lines, showing that STAT3 drives tumor development in this context⁶⁹. Increased STAT3 expression correlates with poorer patient outcomes, suggesting that STAT3 is clearly a pro-tumorigenic molecule, however, genetic mouse models have shown that STAT3 acts as a potent tumor suppressor in the context of KRAS (a proto-oncogene) mutant in NSCLC¹⁵⁷. In KRas mutant lung tumors, as well as in xenograft models, STAT3 loss results in increased tumor growth, higher tumor grade and enhanced vascularization leading to reduced survival. In this context, STAT3 suppresses tumor progression by sequestering NFκB within the cytoplasm thereby impairing IL8-mediated tumor myeloid infiltrating and vascularization. Therefore, low STAT3 expression is associated with poor prognosis and advanced malignancy in lung adenocarcinoma patients susceptible to KRAS mutation¹⁵⁸. Furthermore, a similar study shows that lung-specific Stat3 deletion in lung cancer promotes KRas oncogenic mutations and tumorigenesis. Accordingly, specific deletion of Stat3 in KRas-induced lung cancer also results in significantly increased tumorigenesis with pulmonary injury and inflammation¹⁵⁹.

As described previously, STAT3 promotes tumorigenesis driven by cytokine signaling, particularly IL6 and IL11. However, in a mouse model of intestinal cancer, STAT3 ablation delays the onset of early adenomas but promotes cancer progression during the late stages of the disease. This phenomenon occurs due to the downregulation of the tumor suppressor cell adhesion molecule CEACAM1, which is a target of STAT3¹⁶⁰. In a separate study, STAT3 mediates carcinoma transition of colorectal cancer cells by negative regulation of *glycogen synthase kinase 3b* (GSK3b) phosphorylation, leading to degradation of *Snail-1* (SNAIL) a crucial driver of *epithelial-mesenchymal transition* (EMT) and inhibiting cellular invasion¹⁶¹. The IL6/STAT3 signaling also participates in *prostate cancer* (PCa) development⁶⁹. However, recent studies show that absence of IL6/STAT3 signaling accelerates tumor progression in Pten mutant animal models of PCa. STAT3 loss reduced p14ARF expression accompanied by loss of senescence by downregulation of ARF-Mdm2-p53 tumor suppressor pathway and associated with increased disease recurrence in PCa patients¹⁶². In addition to p14ARF-mediated STAT3 activity in HCC (mentioned before), these findings support that STAT3 exerts tumor suppressor functions by directly targeting proteins, such as p14ARF.

Anti-cancer STAT3 activity is also observed in human *papillary thyroid carcinoma* (PTC). STAT3 knockdown in thyroid cancer-derived cell lines leads to increased tumor growth and proliferation. Based on gene expression profiling, STAT3 loss is linked to the downregulated expression of *insulin-like growth factor-binding protein 7* (IGFBP7), a tumor suppressor that promotes apoptosis and senescence, thus inhibiting proliferation. In addition, IGFBP7 expression positively correlates with pTyr705-STAT3 levels in primary PTC specimens and apart from the STAT3-mediated transcriptional activation of IGFBP7, STAT3 loss in thyroid cancer cells also results in increase HIF1 α protein level¹⁶³. Altogether, these findings show that STAT3 controls several downstream effector proteins which ultimately inhibit cellular proliferation, EMT-mediated invasion, and hypoxia-induced metabolic growth.

Typically, constitutive STAT3 activation is implicated in breast cancer progression¹⁶⁴, and many studies have also shown the central role of STAT3 in stimulating tumor growth and invasiveness *in vitro*¹⁶⁵. However, in mouse models, STAT3 ablation does not alter tumor initiation, but significantly reduces metastatic progression in breast cancer with spontaneous activation of Erb2 oncogene¹⁶⁶. Recent findings suggest that STAT3 acts also as a tumor suppressor in breast cancer. In the context of Myc, animals with genetic Stat3 deletion develop early tumor onset and EMT-like properties. However, Stat3-deficient, Myc positive tumor also develop decrease angiogenesis and partially reduced metastasis¹⁶⁷. Therefore, the biological consequence of STAT3 activation in cancer depends on the oncogenic driver event and the tumor microenvironment.

Overall, the dual role of STAT3 in cancer may be partially explained by its ability to control a wide range of target genes according to cancer type, cell of origin, and tumor microenvironment. All these observations should be taken into account regarding therapeutics benefits of STAT3 inhibition because it may result in tumor progression. More efforts in understanding the underlying mechanisms of the double-edge functions of STAT3 in cancer are still needed to successfully predict therapeutic response.

As mentioned before, previous studies in our lab demonstrated that ccRCC tumors exhibit increased KIM1 levels, which in turn mediates the expression of IL6/STAT3/HIF1 α signaling pathway. Since HIF1 α is a target gene of STAT3 and a well-established driving event for ccRCC development, the following logical step was to study the relevance of STAT3 activation in ccRCC patients. Therefore, our group analyzed the expression levels of both pTyr705- and pSer727-STAT3 in a TMA of 98 ccRCC tumors (previously used to determine KIM1 expression)^{65,66}, showing positive staining for both phosphorylated residues present in the cytoplasm but mainly located in the nuclear compartment. However, when clinical outcome parameters were correlated, only pSer727 nuclear expression levels showed statistical significance in overall survival and disease progression (see Figure 14)⁶⁶.

These results indicated that pSer727-STAT3 expression levels represent an independent prognostic factor for ccRCC patients, and suggest that STAT3 exerts a pro-oncogenic role in ccRCC mainly through Ser727 phosphorylation. Moreover, this observation raised the question if the elevated expression levels of pSer727-STAT3 might be related to enhanced transcriptional activation of a distinct subset of target genes especially relevant in ccRCC progression.

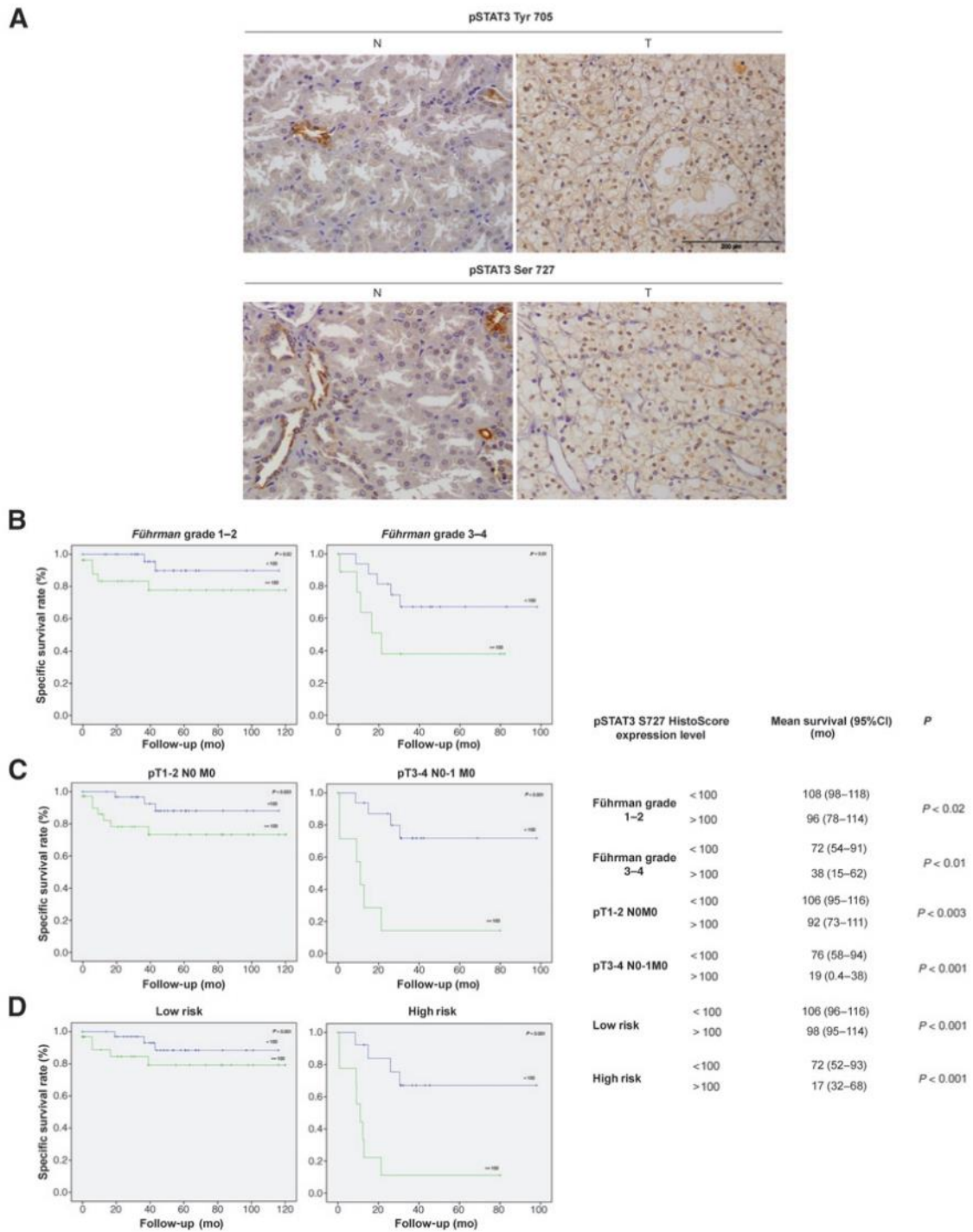


Figure 14. pTyr705- and pSer727-STAT3 expression in tumor samples from ccRCC patients and correlation with clinical outcome. a) Representative examples of pTyr705- and pSer727-STAT3 expression patterns in ccRCC tumors (T) and normal counterparts (N). Kaplan–Meier estimates of 100 months overall survival of b) Fuhrman grade 1 and 2 (left) and 3 and 4 (right), c) pT1-2 N0 M0 (left) and pT3-4 N0-1 M0-1 (right), and d) low risk (left) and high risk (right) according to pSer727-STAT3 levels. Correlation between pSer727-STAT3 HistoScore expression level (blue line, HS above 100; green line, HS below 100)⁶⁶.

RATIONALE

As mentioned throughout the introduction, our group identified for the first time the overexpression of KIM1 in tissue samples of ccRCC patients and showed that its expression regulates the activation of the IL6/STAT3/HIF1 α signaling pathway in human-derived ccRCC cell lines 769-P and 786-O. Moreover, our group also demonstrated that pSer727-STAT3 expression levels correlate with poor prognosis and low overall survival rate in ccRCC patients^{63,65,66}. Based on these results, our group proposed the following mechanism of action: upon shedding by metalloproteases, KIM1 ectodomain binds to putative specific receptors on the surface of ccRCC cells, triggers IL6 production, and activates the IL6/STAT3 signaling pathway. The activation of STAT3 in turn, besides inducing HIF1 α expression, promotes the expression of a subset of genes that would help tumor growth and metastasis (see Figure 15).

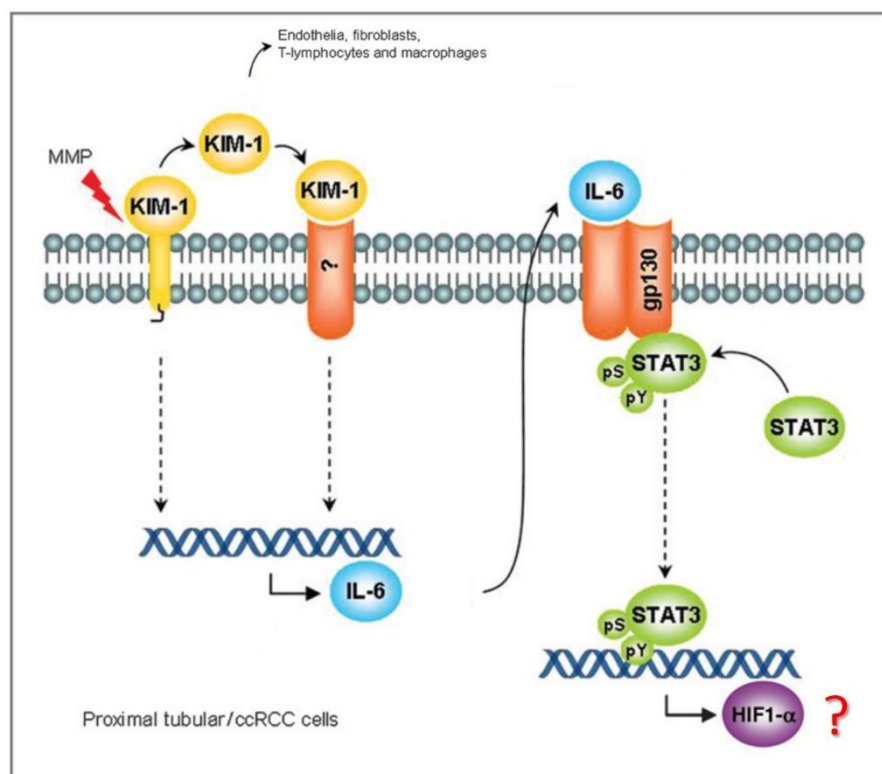


Figure 15. Proposed mechanism of action for KIM1 in ccRCC cells. Upon shedding, KIM1 promotes IL6 expression either by binding to putative specific receptors on tumor cells or by a conformational change in the cytoplasmic tail. Secreted IL6 binds to its ligand-binding receptor gp80 and thereupon to the signal transducer receptor gp130. Activated gp130 forms docking sites for STAT3, which become activated through phosphorylation. Activated STAT3 translocates to the nucleus, binds to DNA and promotes the expression of hundreds of genes, including HIF1 α . Modified from ⁶⁶.

Therefore, this study aimed to explore the contribution of pSer727-STAT3 on the genetic signature in ccRCC.

OBJECTIVES

The main objective of this study was to identify the impact of overall STAT3 phosphorylation state in gene transcription, as well as to identify the specific genes regulated by pSer727 and their associated signaling pathways.

Therefore, the specific aims were:

- To confirm in a different cohort of ccRCC patients, the prognostic value of pSer727-STAT3.
- To generate STAT3 phosphomutants including all possible combinations between Tyr705 and Ser727 in the human-derived ccRCC cell lines 769-P and 786-O. Simple mutants SA and SD where Tyr705 phosphorylation is induced by IL6 stimulation, and double mutants YF/SA and YF/SD.
- To characterize the effect of STAT3 phosphomutants in the human-derived ccRCC cell line 769-P.
- To identify the genes regulated by endogenous STAT3 in the human-derived ccRCC cell line 769-P.
- To identify the genes regulated by the overall STAT3 phosphorylation state, as well as their associated signaling pathways.
- To identify the genes regulated specifically by pSer727 as potential therapeutic targets for ccRCC treatment.
- To identify putative and novel prognostic biomarkers for ccRCC patients.

METHODOLOGY

1. CELL CULTURE

1.1. Cell lines

All cell lines used in this study were obtained from the American Type Culture Collection (ATCC® Rockville, USA) and derived from renal human tissue.

769-P (ATCC® CRL-1933) cell line: 769-P cells were isolated in 1975 from a primary clear cell adenocarcinoma of a 63-years-old Caucasian female. 769-P cells have a globular morphology with diffuse borders, have a high nucleus to cytoplasm ratio and exhibit both microvilli and desmosomes. Since they are epithelial type cells, their adherent properties allow them to grow in monolayer and also in soft agar.

786-O (ATCC® CRL-1932) cell line: 786-O cells were isolated in 1976 from a primary clear cell adenocarcinoma of a 58-years-old Caucasian male. These cells have similar morphology to 769-P cells; however, they are slightly bigger with well-delimited borders. 786-O cells are also epithelial type cells with adherent properties and can grow in monolayer and soft agar. This cell line produces a *parathyroid hormone* (PTH) like peptides, identical to peptides produced by other tumoral cell lines derived from breast and lung.

Both, 769-P and 786-O cell lines, have many characteristics of ccRCC and are the most commonly used in RCC focused research. The expression of surface receptors such as CD10 and vimentin also confirm the ccRCC phenotype. In addition, they have also mutated *vhl* or defective VHL expression, and produce high levels of VEGF which is characteristic of ccRCC.

HEK293T/17 (ATCC® CRL-11268) cell line: HEK293T/17 cells are a clone derived from *human embryonic kidney 293 cells* (HEK293) and it was generated in 1999 at the Rockefeller University. These cells were transformed to constitutively express the *simian virus 40* (SV40) large T antigen. This modification allows the replication of transfected plasmids containing the SV40 replication origin resulting in high amplification and expression of the incorporated transgenes. Clone 17 was selected specifically for its high transfectability. HEK293T cells are very easy to handle and culture because of their high rate growth and they are commonly used in molecular biology and biotechnology industries for protein expression and production of recombinant retroviruses.

1.2. Authentication

Before starting experiments, cell lines were authenticated by *short tandem repeats* (STR) analysis in the Genomics Core Facility of the Instituto de Investigaciones Biomédicas “Alberto Sols” CSIC-UAM (Madrid, Spain). The followed protocol allows co-amplification and four-color detection of ten human loci, including all ASN-0002-2011 loci (TH01, TPOX, vWA, CSF1PO, D16S539, D7S820, D13S317, D5S818) plus Amelogenin and D21S11. These loci collectively provide a genetic profile with a random match probability of 1 in 2.92×10^9 and are used for human cell lines and tissue authentication. This protocol also allows the identification of human cell line cross-contamination.

DNA from cultured cells pellet was extracted following the instructions of the DNeasy® blood and tissue kit (Qiagen #69506) and quantified with the Qubit® 2.0 fluorometer (Life Technologies). To perform STR detection, 4 ng of DNA were prepared with the GenePrint® 10 System (Promega #B9510) and amplification was performed in the ABI 3130XL Genetic Analyzer (Applied Biosystems). The STR profile was then analyzed with the GeneMapper® v3.7 software (Life Technologies) and compared against the cell line description in the ATCC database. Cell lines with ≥80% match were considered to be related, therefore reliable.

1.3. Culture

All cell lines cultured in this study (769-P, 786-O, and HEK293T) were maintained in DMEM (Dulbecco's Modified Eagle Medium, Gibco™ #42430082) supplemented with 10% FBS (Fetal Bovine Serum, Gibco™ #10270098), 1% sodium pyruvate [100 mM] (Gibco™ #11360039), 1% antibiotic/antimycotic (Gibco™ #15240-062) and 0.2% plasmocin (Invivogen #ant-mpp) at 37°C with 5% CO₂.

If 769-P cell line was transduced with pLKO.1 vector, the medium was supplemented with selection antibiotic puromycin [4 mg/ml] (Invivogen #ant-pr-1), and if it was transduced with pLX304 vector, the medium was supplemented with selection antibiotic blasticidin [35 mg/ml] (Invivogen #ant-bl-1). If 786-O cell line was transduced with pLKO.1 vector, the medium was supplemented with selection antibiotic puromycin [2 mg/ml], and if it was transduced with pLX304 vector, the medium was supplemented with selection antibiotic blasticidin [2 mg/ml].

Since all cell lines in this study own adherent properties and grow in monolayer, tissue culture treated flasks (CytoOne® #CC7682-4875 and #CC7682-4825), dishes (Nunc™ #168381, #150326 and #150318,) and well plates (Nunc™ #140675, #150628, #142475, #150687 and #167008,) were used to culture them.

All cell lines were always manipulated into a laminar flow hood.

1.4. Trypsinization

To perform cell dissociation and passage of cell lines, 0.05% trypsin-EDTA (Gibco™ #25300062) was used. Once cells reached at least 80% confluence, the medium was removed and cells were carefully washed with sterile PBS consisting of 137 mM NaCl, 2.7 mM KCl, 10 mM Na₂HPO₄, and 1.8 mM KH₂PO₄. Pre-warmed (37°C) trypsin was added (volume/area: 1 ml/75 cm²) and distributed over the monolayer. Cells were then incubated for 5 min at 37°C with 5% CO₂. Immediately after, cells were detached with gentle bumps and trypsin was inactivated with 3 times the volume of medium with 10% FBS. Afterward, cells were mechanically disaggregated with up and down pipette movements. Cells were then collected in a 15 ml Falcon tube and centrifuged at 2500 rpm for 5 min. The supernatant was discarded and the cellular pellet was resuspended in the desired volume of fresh medium depending on passage or subsequent steps.

1.5. Counting

In order to seed the appropriate number of cells for upcoming experiments, cellular concentration was determined. At this point it was important to discriminate between live and dead cells, thus once cells were trypsinized and resuspended in fresh medium, a 1:1 dilution with Trypan Blue (Sigma Aldrich #T8154) was prepared. Trypan Blue is a dye that stains cells with damaged cell membrane and provides a way to identify pro- or apoptotic cells (blue colored). To count living cells, 10 μ l of the dilution were added into a disposable chamber slide and then inserted in the Countess II Automated Cell Counter (Invitrogen #AMQAX1000). Counting was performed according to the supplier instructions.

1.6. Cryopreservation

When storage of cell lines was needed, the following freezing protocol was performed. Once cells reached 100% confluence in a T75 flask, cells were trypsinized and centrifuged at 2500 rpm for 5 min. The supernatant was discarded and the cellular pellet was resuspended in freezing medium: 3.6 ml of fresh medium and 400 μ l of sterile-filtered dimethyl sulfoxide (Sigma Aldrich #D2650). *Dimethyl sulfoxide* (DMSO) is a polar aprotic solvent that protects cells from ice crystal-induced mechanical injury. Cell suspension in freezing medium was then immediately mixed with up and down pipette movements, and 1 ml was added in a cryotube. Cryotubes were quickly placed in a freezing container (Mr. Frosty™, Thermo Scientific™ #5100-0001) and stored at -80°C overnight (O/N) to allow gradual freezing of cells. The next day, cryotubes were finally transferred to a liquid nitrogen container for long storage.

1.7. Thawing

In cases where cryopreserved cells needed to be cultured, the cells were defrosted. Thawing is a stressful process for frozen cells; hence it is important to quickly manipulate them to ensure that a high proportion of cells survive the procedure. To thawing, cryotubes containing the frozen cells were removed from liquid nitrogen and placed on dry ice, then they were rapidly placed into a 37°C water bath (<1 min) until there was a small bit of ice left in the vial. Cryotube was transferred into a laminar flow hood, opened carefully (cryovials stored in liquid-phase present a risk of explosion when thawed) and 1 ml of pre-warmed (37°C) medium was added. Defrosted cells were then rapidly transferred to a 15 ml Falcon tube containing 3 ml extra of the warm medium. The cell suspension was centrifuged at 2500 rpm for 5 min. After centrifugation, the supernatant was discarded (to remove cell debris and medium containing DMSO) and the cellular pellet was resuspended with the appropriate volume of fresh medium depending on subsequent culture surface.

1.8. Treatments

For functional assays, cells were treated with IL6 (Peprotech #200-06) [10 ng/ml] diluted in the corresponding culture medium, for at least 30 min.

2. GENE SILENCING

Gene silencing also considered as gene knockdown consists in to prevent the expression of a particular gene. When genes are silenced, their expression is reduced but not abolished as in gene knockout. Furthermore, gene silencing is often considered better than gene knockout since they allow the study of essential genes required for cell survival that cannot be completely removed, as STAT3. There are different types of gene silencing, however, one of the most used in research is the *RNA interference* (RNAi) pathway.

Currently, there are three primary categories of RNAi tools: *small interfering RNA* (siRNA), *microRNA* (miRNA) mimics, and *short hairpin RNA* (shRNA).

- siRNA: Are the most commonly used for inducing short-term gene silencing. They are usually transfected into cells and through perfect complementarity, targets for degradation a specific *messenger RNA* (mRNA).
- miRNA: Synthetic or expressed miRNAs mimics are valuable for studying gain-of-function assays. Expressed miRNAs mimics may be placed under an inducible promoter for temporal studies. miRNAs act through mRNA degradation or translational repression.
- shRNA: Delivered via plasmid transfection or viral transduction is useful for long-term gene silencing. They have a stem-loop structure that is processed by the cell into siRNAs.

The activation of the RNAi pathway is an endogenous process used by cells to regulate gene expression. The process begins with the entrance of a *double-stranded RNA* (dsRNA) molecule into the cell which activates the pathway. The dsRNA is then cleaved into small double-stranded fragments by an RNase enzyme called Dicer. These fragments are now siRNAs or miRNAs of approximately 21-23 nucleotides in length. Next, these small fragments integrate into a multi-subunit protein called *RNA-induced silencing complex* (RISC) that unwinds the double strand into two strands called “sense” and “anti-sense”. The “sense” strand is degraded, while the “anti-sense” strand remains bound to RISC and targets the homologous mRNA for cleavage and subsequent degradation (siRNA), or suppression of translation (miRNA). The reduction in transcription or translation leads to lower levels of target protein, resulting in phenotypic changes. Gene silencing can be assessed at mRNA level using methods such as RT-qPCR or at protein level via Western Blot.

2.1. Short hairpin RNA (shRNA)-mediated silencing

shRNAs sequences are usually encoded in a DNA vector that can be introduced into cells via plasmid transfection or viral transduction. shRNA molecules are divided into two main categories based on their designs: simple stem-loop and microRNA-adapted shRNA.

In this study, there were used 5 different simple stem-loop shRNAs (MISSION™ Sigma Aldrich #TRCN0000329888, #TRCN0000329886, #TRCN0000329887, #TRCN0000020840 and #TRCN0000353630) cloned into pLKO.1-puro vector (see Figure 16). The constructs purchased have a 5' *long terminal repeat* (LTR), SIN/LTR (3' LTR), and Psi packaging signal that permit lentiviral packaging using a third-generation lentiviral system. Therefore, 769-P and 786-O cell lines were transduced with the shRNAs by generation and infection of

lentiviral particles (see 7. Generation of stable transduced cell lines) and selected via puromycin resistance conferred by the vector.

The hairpin structure of shRNAs used includes an intramolecular 20-21 *base pairs* (bp) homologous to 5 different regions into the *coding sequence* (CDS) of STAT3 mRNA (see Figure 16). The bridge region (the loop) consists of 6 bp that is recognized and cleaved by Dicer upon expression via the U6 (polymerase III) promoter in the host cell. The resulting siRNAs associated with RISC continues the RNAi pathway.

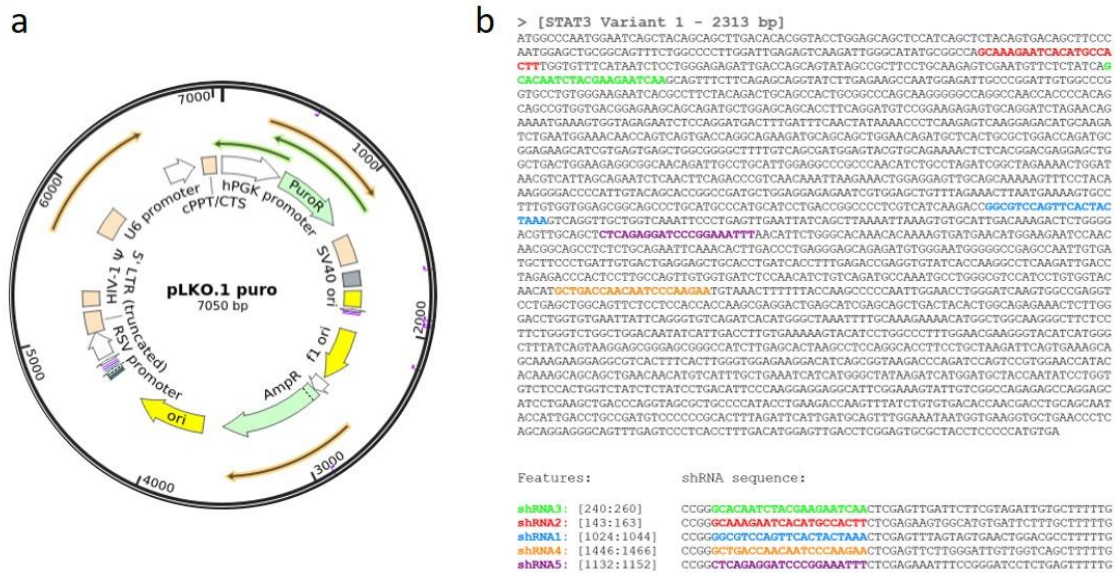


Figure 16. pLKO.1-puro vector and shRNAs sequences. a) Full sequence map of pLKO.1-puro vector carrying the different shRNAs against STAT3. b) shRNAs sequences along STAT3 CDS.

3. MUTANTS GENERATION

3.1. Primers design

Throughout this work, several primers were designed. All pairs of primers were complementary to the template region of DNA desired to mutate, however, they carried nucleotide changes in their central region.

STAT3 “rescue” mutant: A “rescue” mutant was created as a strategy to allow the gene of interest (STAT3) could be reintroduced in the cell and escape from the silencing mechanism previously incorporated. The generation of the “rescue” mutant consisted of 7 synonymous mutations upon the sequence recognized by shRNA, in this case shRNA2 (see Figure 16). Synonymous mutations changed the sequence but did not change the encoded amino acid, thus the original protein structure remained uncompromised (see Figure 17).

STAT3 WT	K	E	S	H	A	T		
RESCUE STAT3	K	E	S	H	A	T		
TEMPLATE	GC	AAA	GAA	TCA	CAT	GCC	ACT	T
RESCUE	GT	AAG	GAG	TCC	CAC	GCT	ACC	T
PRIMERS (5' - 3')								
FORWARD	GTCAAGATTGGGCATATGCGGCCAGTAAAGAGTCCCACGCTACCTTGGTGTTTCATAATCTCCTGGGAG							
REVERSE	CTCCCAGGAGATTATGAAACACCAAGGTAGCGTGGGACTCCTTACTGGCCGCATATGCCCAATCTTGAC							

Figure 17. Primer design for STAT3 "rescue" mutant. Pair of primers designed (forward and reverse) to perform 7 synonymous mutations upon the sequence recognized by shRNA2. Base pairs changed are shown in red.

STAT3 phosphomutants: Phosphorylation (the addition of a phosphate group (-PO₄²⁻) to an -OH group) is a post-translational modification catalyzed by kinases and is a usual mode of activating or deactivate a protein as a form of regulation. Even so, only three amino acids are most commonly recognized as phosphorylatable: serine, tyrosine, and threonine.

To analyze the dynamics of STAT3 phosphorylation, specifically, the effect of Tyr705 and Ser727 phosphorylation on STAT3-mediated gene expression, simple and double STAT3 phosphoablative or phosphomimetic mutants were generated: p.Tyr705Phe, p.Ser727Ala, p.Ser727Asp, p.Tyr705Phe/Ser727Ala, and p.Tyr705Phe/Ser727Asp. The strategy employed consisted of structurally similar-amino acid substitutions that prevent or mimic phosphorylation. For, phosphoablative mutations, alanine (Ala, A) or phenylalanine (Phe, F) were used, and for phosphomimetic mutation, aspartic acid (Asp, D) was the amino acid of choice (see Figure 18).

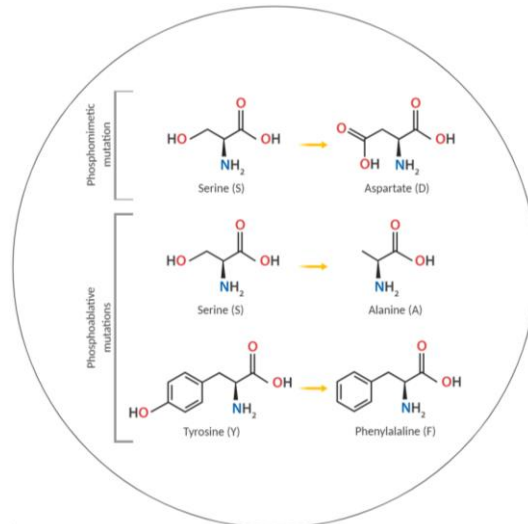


Figure 18. Amino acid substitutions in STAT3 phosphomutants. Scheme depicting structural similarities between amino acids substituted. Phosphomimetic mutation (Ser727Asp) and phosphoablative mutations (Ser727Ala, Tyr705Phe).

To generate STAT3 phosphoablative mutants, Ser727 was changed for Ala (S727A), and Tyr705 for Phe (Y705F) (see Figure 19). These substitutions abrogated the possibility of phosphorylation at these sites because besides being structurally similar, they lack the -OH group eliminating the possibility of adding a phosphate group.

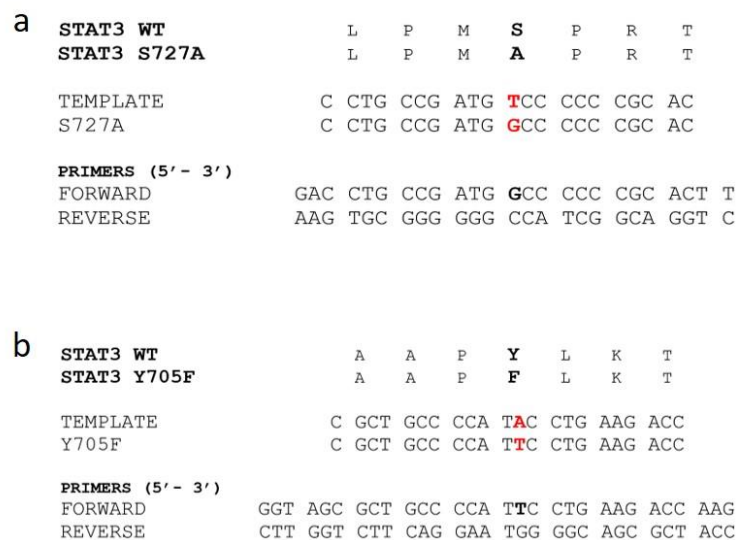


Figure 19. Primer design for STAT3 phosphoablative mutants. Pair of primers designed (forward and reverse) to create a) phosphoablative mutation of Ser727 (S727A) and b) phosphoablative mutation of Tyr705 (Y705F). Base pairs changed are shown in red.

For phosphomimetic substitution of Ser727, it was used Asp (S727D) (see Figure 20). The aspartic acid is an amino acid structurally alike to serine with a negative lateral chain, thus simulate the addition of a phosphate group (negatively charged) at this position.

STAT3 WT	L	P	M	S	P	R	T						
STAT3 S727D	L	P	M	D	P	R	T						
TEMPLATE	C	CTG	CCG	ATG	TCC	CCC	CGC	ACT					
S727D	C	CTG	CCG	ATG	GAC	CCC	CGC	ACT					
PRIMERS (5' - 3')													
FORWARD	CC	ATT	GAC	CTG	CCG	ATG	GAC	CCC	CGC	ACT	TTA	GAT	T
REVERSE	AA	TCT	AAA	GTG	CGG	GGG	TCC	ATC	GGC	AGG	TCA	ATG	G

Figure 20. Primer design for STAT3 phosphomimetic mutant. Pair of primers designed (forward and reverse) to create phosphomimetic mutation of Ser727 (S727D). Base pairs changed are shown in red.

In the case of phosphomimetic substitution of Tyr705, no amino acid was selected. Tyrosine is an aromatic amino acid and neither Asp nor Glu (phosphomimetic amino acids of choice) resembles this feature. There is a controversy in this matter and literature is full of examples, however, we decided not to mutate this amino acid and instead stimulates its phosphorylation with IL6 (a classical activator of the JAK/STAT3 pathway through Tyr705 phosphorylation).

Sequencing primers: To confirm site-direct mutagenesis and to verify that no other unintentional mutations occurred during the process, sequencing primers were designed along the STAT3 CDS (see Figure 21), as well as over the entire sequence of the pLX304 vector (see Table 1). Primers were separated between 500-700 bp to ensure sequence overlap.

```
> [STAT3 Variant 1 - 2313 bp]
ATGGCCCAATGGAATCAGCTACAGCAGCTTGACACAGGTACCTGGAGCAGCTCCATCAGCTCTACAGTGACAGCTTCCC
AATGGAGCTGGCCAGTTTCTGGCCCTTGGATTGAGAGTCAAGATTGGCCATATGGCCAGCAAGAAATCACATGCCA
CTTTGGTCTTCATAATCTCTGGGAGAGATTGACCAGCAGTATAGCCGCTTCTTGCAGAGTGCAGATTGTTCTCTATCAG
CACAACTACAGAGATCAAGCAGTTTCTCAGAGCAGGATCTTGGAGAGCCATGGAGATTGCCCGGATTTGGCCCG
CAGCCTTGGGAGAAATCAAGCCTTCTACAGACTGCAGCCACTGGCCCCAGCAAGGGCCAGGCCAACCCCCACAG
CAGCCGTGTGACGGAGAAGCAGCAGATGCTGGAGCAGCCTTTCAGGATGTCCGGAAGAGATGCGAGGATCTAGAACA
AAATGAAAGTGTAGAGAAATCTCAGGATGACTTTGATTTCAACTATAAAACCTCAAGAGTCAAGGAGACATGCAACA
TCTGAATGGAAACACCACTCAGTACAGCCAGGCAAGATGACAGCAGCTGGAACAGATGCTCACTGCCTGGACCAATGC
GGAGAACATCCTGAGTGAGCTGGCCGGGCTTTTGTACGGATGGAGTACCTGCAGAAAATCTCAGCCGACGAGGAGCTG
GCTGACTGGAGAGGGCCCAACAGATTGCTGCAATGGAGGCCCGCCCAACTTGCCTAGATCGGCTAGAAAATGGAT
AACGCTATAGCAGAATCTCAACTTCAGACCCGCTCAACAATTAAGAACTGGAGGAGTTGCAGCAAAAAGTTTCTTACA
AAGGGACCCCATTTCCAGCAGCCGCGATCTGGAGGAGAAATCTGGAGCTTTTGAAGACTTATGAAAGTGGC
TTTGTGTGGAGGGCAGCCCTGCATGCCATGATCTGCAGCCGCCCTCTCATCAAGACCCGGGTCCAGTTCACTAC
TAAAGTCAGGTTGCTGCTCAAATCCCTGAGTGAATATCAGCTTAAATTAAGTGTGCATTGACAAAAGACTCTGGGG
ACGTTGCAGCTCTCAGAGGATCCCGGAAATTAACATTTGGGCACAAACAAAAGTATGAACATGGAAGAAATCCAAC
AACGGCAGCCTCTCTGAGAAATCAAACTTGACCTGAGGGAGCAGAGATGTGGGAATGGGGCCGAGCAATTTGTA
TGCTTCCCTGATTGTACTGAGGAGCTGCACCTGATCACCTTTGAGACCGAGGTGTATCAACCAAGGCTCAAGATTGACC
TAGAGACCACTCTTGGCCAGTTGGTGATCTCCAACATCTGTGAGATGCCAAATGCCTGGGGTCCATCTGTGGTAC
AACATGCTGACCAACAAATCCCAAGAAATGAACTTTTTACCAAGCCCAATGGAACTGGATCAAGTGGCCGAGGT
CCTGGCTGGCAGTTCTCCCTCACACACAGGAGGACTGAGCAGTCCGCGAGCTACTACTGGCAGAACTCTTGG
GACCTGCTGAATATTACGGGTCTCAGATCACATGGCTAAATTTGCAAGAAACATGCCTGGCAAGGGCTTCTGG
TTCTGGTCTGCTGGCAATATCATTGACCTTGTGAAAGATACATCTGGCCCTTTGGAACGAAGGTACATCATGG
TTCTATCAGTAAGGAGCGGGAGCCGCACTTGGAGCACTAAGCCTCCAGGCACCTTCTGCTAAGATTGAGTAAAGCA
GCAAGAGGAGGGCCTCACTTCACTTGGGTGGAGAGGACATCAGCCGTAAGACCCAGATCCAGTCCGTGGAAACATAC
ACAAGCAGCAGCTGAACAACATGTCAATTTGCTGAAATCATCATGGGCTATAAGATCATGGATGCTACCAATATCCTGGT
GCTCCAGTGTCTATCTCTATCTGACATTTCCCAAGGAGGAGCATTCCGAAAGTATTGTCCGGCCAGAGAGCCAGGAGC
ATCTGAAAGTGCAGGATAGCCCTGGCCCACTGAAAGCAATTTATCTGTGTGACACCAAGACCTCCAGCAAT
ACCATTGCTGGCCAGTCCCGCCGACTTTAGATTATTGATGGCTTTGGAAATATGCTGAAGTGTCTGACCCCTC
ACCAGGAGGGCAGTTTGAATCCCTCACCTTTGACATGGAGTTGACCTGGAGTGGGCTACTCCCCCATGTGA
```

Features:	Primers (5' - 3'):
PFwd_STAT3_1	GGCCCAATGGAATCAGCTAC
PFwd_STAT3_2	GCCTGGACCAATGCGGAG
PFwd_STAT3_3	GCACCTGATCACCTTTGAG
PFwd_STAT3_4	GATGCTACCAATATCCTGGT

Figure 21. Primer design for STAT3 phosphomutants sequencing. Primers designed (forward) along the STAT3 CDS for sequencing before lentiviral transduction.

Table 1. Primers designed for pLX304 vector sequencing.

Primers (pLX304 vector)	Sequence (5' - 3')
PFwd_pLX304_1	CAAATGTCGTAACAACTCCG
PFwd_pLX304_2	GGCGACAAGGTGCTGATGCC
PFwd_pLX304_3	GTTGGTAAGCCTATCCCTAAC
PFwd_pLX304_4	GA CTGGAAGGGCTAATTCAC
PFwd_pLX304_5	CAGCTGGCGTAATAGCGAAG
PFwd_pLX304_6	GATGCTGAAGATCAGTTGGG
PFwd_pLX304_7	GACAGATCGCTGAGATAGGTG
PFwd_pLX304_8	GTCCTGTCGGGTTTCGCCAC
PFwd_pLX304_9	CTGAATTGCCGCATTGCAGAG
PFwd_pLX304_10	GTAAGACCACCGCACAGCAAG
PFwd_pLX304_11	CTGTACTTTCTATAGTAATAG
PFwd_pLX304_12	CTACAGCGTCGCCAGCGCAGC

3.2. Site-directed mutagenesis

In vitro site-directed mutagenesis is a PCR-based technique used to generate specific and intentional changes in the sequence of a gene, and it is employed to study the structure-function relationship of DNA, RNA, and proteins.

To introduce punctual mutations in a *double-stranded DNA* (dsDNA) vector, the QuikChange Lightning Site-Directed Mutagenesis Kit (Agilent Technologies #210518) was employed following the manufacturer instructions. The general procedure consisted of a dsDNA vector (pLX304) with an insert of interest (STAT3) and a pair of synthetic primers (see 3.1 Primers design), each complementary to opposite strands of the vector and both containing the desired mutation. After denaturalization of dsDNA and annealing of primers to homologous sequences, primers were extended during temperature cycling by PfuUltra HF DNA polymerase. Extension of the primers generated a mutated plasmid containing staggered nicks. After the elongation step, the product was treated with Dpn I endonuclease which recognized and digested specifically methylated and hemimethylated DNA (parental DNA template). The DNA nicked vector containing the desired mutation was then transformed into XL10-Gold ultracompetent cells.

In this work, the pLX304 vector carrying STAT3 gene and blasticidin resistance was used. This vector also contains a Psi packaging signal for lentiviral packaging (see Figure 22).

The mutagenesis reactions were prepared at a final volume of 50 μ l in a 0.2 ml thin-walled tube suitable for thermocycling, as follows:

Table 2. Components for site-directed mutagenesis

Component	Volume (per Rx)
10x reaction buffer	5 μ l
75 ng of dsDNA template	X
125 ng of primer forward	X
125 ng of primer reverse	X
dTNP mix	1 μ l
QuikSolution reagent	1.5 μ l
QuikChange Lightning Enzyme	1 μ l
MQ H ₂ O	up to 50 μ l

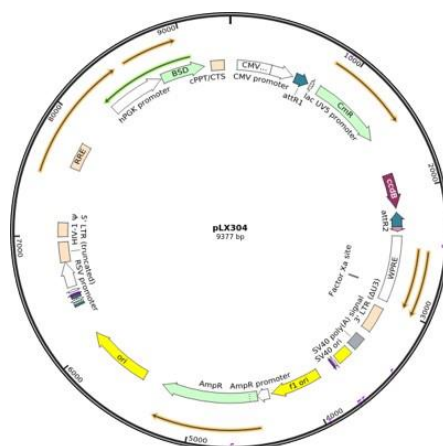


Figure 22. *pLX304* vector. Full sequence map of pLX304 vector carrying the different STAT3 phosphomutants.

Reactions were then placed in the thermal cycler and the following cycling program was executed:

Table 3. Thermal cycling program for site-directed mutagenesis

Step	Cycles	Temperature (°C)	Time
Lid	-	110	-
1	1	95	2 minutes
2 Denaturalization	18	95	30 seconds
Annealing		60	1 minute
Elongation		68	6 minutes*
3	1	68	5 minutes
Hold	-	4	-

* 30 seconds/kb of plasmid length.
pLX304 vector and STAT3 insert have ~12 kb

Once finished the temperature cycling program, 2 μ l of Dpn I restriction enzyme were added to each mutagenesis reaction and gently mixed by pipetting up and down several times. A briefly spin down was performed and then the reaction was incubated at 37°C for 5 minutes to digest the parental (the nonmutated) supercoiled dsDNA. Finally, the resultant vector containing the desired mutation was stored at -20°C or immediately transformed into XL10-Gold ultracompetent bacteria (see 4.1 Bacterial transformation).

To generate double STAT3 mutants (Tyr705Phe/Ser727Ala, Tyr705Phe/Ser727Asp), second site-directed mutations were performed once the first one was sequenced.

4. BACTERIAL MANIPULATION

4.1. Bacterial transformation

Transformation is a process of horizontal gene transfer by which some bacteria take up and incorporate foreign genetic material from the environment. Bacteria that exhibit this ability are termed as competent cells. To introduce diverse DNA vectors into bacteria for subsequent amplification, artificial competence was induced by the heat shock method.

To perform transformation, first, ultracompetent cells (in case of recently mutated DNA, XL10-Gold cells provided in the QuikChange Lightning Site-Directed Mutagenesis Kit) were gently thawed on ice. Then, 25 μl of cells were placed into a pre-chilled 1.5 ml tube and 1 μl of β -mercaptoethanol (β -ME, Agilent Technologies #200314) was added. Cells were incubated on ice for 2 min. Subsequently, 0.5-2 μl of DNA (depending on concentration or application) were transferred and incubated on ice for 30 min. Next, a 42°C heat pulse for 30 seconds was applied to cells and immediately after, cells were placed again on ice for 2 min. After heat shock, 250 μl of pre-heated (42°C) SOC medium (Invitrogen™ #15544034) were added and cells were incubated at 250 rpm and 37°C for at least 1 h. Finally, 50-200 μl of transformation reaction (depending on the vector) were plated on LB-agar (Invitrogen #30391023) plates containing ampicillin [50 $\mu\text{g}/\text{ml}$] (Roche #10835242001). Plates were incubated O/N (~16 h) at 37°C. All this procedure was performed near to a lit Bunsen burner.

4.2. Bacterial growth

Bacteria reproduce through a process called binary fission which consists of the division of a single entity into two or more entities resembling the original. The result is daughter cells genetically identical to the original cell. Furthermore, bacteria undergo exponential growth. These properties besides transformation, make bacteria the perfect vehicle for genetic material amplification.

For amplification of bacteria carrying the DNA of interest, a liquid pre-culture (5 ml) or culture (100 ml) of growth media called *Luria-Bertani* (LB) broth (Invitrogen #12795084) was utilized. If bacteria came from colonies grown in agar, only round well-defined and completely isolated colonies were picked up to avoid clonal contamination. Bacteria could also come from previously-stored glycerol. Either means, a colony or scrape, bacteria were placed on a 50 ml tube previously filled with 5 ml of LB broth and supplemented with ampicillin [50 $\mu\text{g}/\text{ml}$]. Bacteria were then incubated at 250 rpm and 37°C for at least 5 h. If further amplification was needed from pre-culture, 1 ml of bacterial pre-culture was placed on a 250 ml glass flask previously filled with 100 ml of LB broth supplemented with ampicillin [50 $\mu\text{g}/\text{ml}$] and incubated O/N (~16 h) at 250 rpm and 37°C. Bacterial handling was always performed near to a lit Bunsen burner.

4.3. Bacterial storage

For long-term storage, bacteria carrying DNA of interest were saved in glycerol. Glycerol stabilizes the frozen bacteria, preventing damage to the cell membranes and keeping the cells alive. Once bacteria had grown in a 100 ml LB culture, 800 μ l of bacterial culture were placed on a 1.5 ml tube and 200 μ l of 50% glycerol (Sigma Aldrich #G7757) were added. Bacteria and glycerol were then thoroughly mixed and freeze immediately in liquid nitrogen. Bacterial stocks were then stored at -80°C .

5. NUCLEIC ACIDS MANIPULATION

5.1. Plasmid DNA isolation

To isolate and purify plasmid DNA contained in bacteria, two different column-based kits were used depending on the size of bacterial culture. The Illustra™ plasmid Prep Mini Spin Kit (GE Healthcare #28-9042-70) was used to perform Minipreps from bacterial pre-culture (5 ml), and the NucleoBond® PC100 – Plasmid DNA Purification Kit (Macherey-Nagel #740573) was used to perform Midipreps from bacterial culture (100 ml). In both cases, protocols were carried out according to supplier instructions.

The basic principle of DNA purification consisted of a harvested previous bacterial culture by centrifugation at 6000 rpm and 4°C for 15 min. The supernatant was discarded and bacterial pellet was then lysed with an alkaline/SDS solution and RNase treatment to remove RNA molecules. Both chromosomal and plasmid DNA were denatured under these alkaline conditions. For clarification of the lysate, potassium acetate was added to form a precipitate containing chromosomal DNA and other cellular compounds. The potassium acetate buffer also neutralizes the lysate. At this point, plasmid DNA reverted to its native supercoiled structure and remained in solution. After equilibrating columns with appropriate buffer and several centrifugations steps, plasmid DNA was bound to the anion-exchange resin/silica and finally eluted after efficient washing of the column. After precipitation with isopropanol (VWR #20839.291), eluted DNA could be easily dissolved in MQ H₂O water. Isolated plasmid DNA was then stored at -20°C for downstream applications.

5.2. RNA isolation

The extraction of high-quality RNA from biological samples is a complicated process because of the ubiquitous and hardy presence of *ribonuclease enzymes* (RNases) in cells and in the environment, which can rapidly degrade RNA. To date, there are several methods to isolate RNA, however, the most common is guanidinium thiocyanate-phenol-chloroform extraction (commonly named by the brand TRIzol). In this study, this method was employed to extract total RNA from cultured cells.

Once cells reached 100% confluence in a P6-well plate, 1 ml of TRIzol (Invitrogen #15596026) was added. Lysed cells were then placed in a 1.5 ml tube and incubated for 5 min at *room temperature* (RT) to allow complete dissociation of nucleoprotein complexes. After incubation, 200 µl of chloroform (Panreac #A3691) were added and samples were vigorously agitated for 15 seconds and incubated at RT for 3 min. Samples were centrifuged at 12,000 x *g* and 4°C for 15 min. At this point, samples were separated into 3 phases: the lower organic phase corresponding to phenol-chloroform, the interphase, and a clear aqueous phase where RNA remains. Carefully, the aqueous phase was removed and placed in a new 1.5 ml tube. This step is critical because it is important to avoid dragging other phases. Then, to isolate the RNA, 500 µl of isopropanol were added and samples were incubated at RT for 10 min before centrifuged them at 12,000 x *g* and 4°C for 10 min. To wash RNA after centrifugation, the supernatant was discarded and the RNA pellet (visible or not) washed with 1 ml 75% ethanol. Samples were

thoroughly mixed and centrifuged at 12,000 $\times g$ and 4°C for 5 min. Again, the supernatant was discarded and RNA pellet air-dried for ~10 min. Once there were no traces of ethanol, pellet was resuspended with 50 μ l of RNase free H₂O. Diluted RNA was then incubated in a heat block at 60°C for 10 min to increase solubility. Finally, RNA samples were stored at -80°C until future applications.

5.3. Nucleic acids quantification

To know the concentration and purity of nucleic acids obtained from prior processes, the Nanodrop™ 2000 (Thermo Scientific™ #ND-2000) was used. The purity of nucleic acids was determined by the 260 nm/280 nm absorbance ratio. A ratio of ~1.8 is generally accepted as “pure” DNA and ~2.0 for “pure” RNA. Lower ratio to these values indicates the presence of proteins, phenol or other contaminants.

To measure nucleic acids, 1 μ l of the sample was directly placed onto the optical measuring surface of Nanodrop™ 2000. Concentration values were obtained as ng/ μ l.

5.4. Agarose-gel electrophoresis

This method is used to separate and visualize a mixed population of macromolecules such as DNA or RNA by applying an electric field to move the negatively charged molecules through a matrix of agarose. Agarose is a polysaccharide composed of helical molecules in supercoiled bundles that form channels and pores through which biomolecules can pass. Therefore, this method separates nucleic acids by charge and size (length).

To prepare 1% agarose gels, 0.5 gr of agarose (Ecogen #AG0220) were dissolved in 50 ml of TAE 1X buffer (40 mM Tris-acetate and 1 mM EDTA) and heated until the solution was crystal clear. Agarose solution was allowed to cool down, then 1.5 μ l of SYBR®Safe (Invitrogen #S33102) were added, mixed and poured in a cast with its corresponding comb. SYBR®Safe is a highly sensitive dye used to stain and visualize nucleic acids. Once agarose gel was solidified, the comb was removed and nucleic acid samples were charged in wells as well as the HyperLadder I (Ecogen #BIO-33026) molecular weight marker. Samples were prepared as follows: 5 μ l of sample plus 3 μ l of MQ H₂O and 2 μ l of 5X loading buffer (Ecogen #BIO-37045). Electrophoresis was held at 120 Volts (V) for 45 min. Agarose gel was visualized on the Odyssey® Fc Imaging System (Li-cor®) with 30-seconds exposure in the 600 channel.

5.5. Sequencing

Prior lentiviral transduction, plasmid DNAs (vector + corresponding insert) were sequenced to confirm that proper mutations were generated and no other random mutation has occurred along the sequence during mutagenesis. Sequencing was carried out by the MacroGen Sequencing Service (Madrid, Spain).

For each sequencing reaction, 2 μ g of plasmid DNA [100 ng/ml] diluted in MQ H₂O, and 20 μ l of previously designed primers [60 ng/ml] (see 3.1 Primers design) were sent to

MacroGen facilities at RT. After obtaining the results, sequences were aligned and analyzed with the Serial Cloner 2.6.1 software (Serial Basics).

5.6. RT-PCR

The *reverse transcription-PCR* (RT-PCR) is a variation of the classic *polymerase chain reaction* (PCR) technique that converts and amplifies RNA into *complementary DNA* (cDNA), hence the name: reverse transcription. The RT-PCR consists of two steps: i) RNA template is converted into cDNA using a *reverse transcriptase* (RT) enzyme, and then ii) cDNA is used as a template for exponential amplification. RT-PCR is currently the most sensitive method for detecting practically any gene.

In this study, one-step RT-PCR was performed with the High Capacity RNA-to-cDNA™ kit (Applied Biosystems #4387406), meaning that cDNA synthesis and amplification occurred in a single tube. The protocol was performed following the supplier instructions. First, 2 µg of RNA samples were diluted in nuclease-free H₂O to a final volume of 9 µl and then, reactions were set in a 0.2 ml thin-walled tube suitable for thermocycling, as follows:

Table 4. Components for RT-PCR

Component	Volume (per Rx)
2x RT buffer	10 µl
20x enzyme mix	1 µl
2 µg of RNA sample	9 µl
Final volume of 20 µl	

Reactions were then placed in the GS1 thermal cycler (G-STORM) and the following program was executed:

Table 5. Thermal cycling program for RT-PCR

Temperature (°C)	Time
37	60 minutes
95	5 minutes
4	Hold

Once finished the RT-PCR, the cDNA was stored at -20°C for future applications.

5.7. RT-qPCR

The *reverse transcription-qPCR* (RT-qPCR) is the method of choice for quantification of gene expression and the gold standard for validating results obtained from array analyses. The RT-qPCR is a combination of two variations of conventional PCR: the RT-PCR (previously described) and the quantitative real-time PCR (qPCR). In this method, RNA is first transcribed into cDNA by RT-PCR and then, the resulting cDNA is used as a template for the qPCR reaction in which a sequence of interest is amplified and quantified in each cycle. In general, qPCR uses sequence-specific DNA probes (oligonucleotide

primers) labeled with a fluorescent reporter and requires to be performed in a thermal cycler with the capacity to detect the fluorescence.

Currently, there are different fluorescent DNA probes available, however, in this work, we used TaqMan® probes (Applied Biosystems). TaqMan® probes are hydrolysis probes consisting of a fluorophore (in this case FAM) attached to the 5'-end and a quencher at the 3'-end. The principle of this probes relies on the exonuclease activity of Taq polymerase to cleave the dual-labeled probe during hybridization. As the Taq polymerase extends the primer, its exonuclease activity degrades it, releasing the fluorophore and breaking the proximity to the quencher, thus allowing fluorescence. Hence, fluorescence detected is directly proportional to the fluorophore release and the amount of DNA template present. Moreover, TaqMan® probes used are designed to span exon-exon junctions of the genes of interest to reduce the risk of false positives (see Table 2).

Table 6. List of TaqMan® probes for RT-qPCR

Gene	Name	TaqMan® probe ID
STAT3	Signal transducer and activator of transcription 3	Hs00374280_m1
TBP	TATA box binding protein	Hs00427620_m1
KRT20	Keratin 20	Hs00300643_m1
FN1	Fibronectin 1	Hs01549976_m1
WNT7A	WNT family member 7A	Hs01114990_m1
ANKS4B	Ankyrin repeat and sterile alpha motif domain containing 4B	Hs00540939_m1
ALPK2	Alpha kinase 2	Hs01085414_m1
IL6	Interleukin 6	Hs00985639_m1

To carry out the RT-qPCR, samples were prepared as follow:

Table 7. Components for RT-qPCR

Component	Volume (per Rx/well)
20 ng cDNA	4.5 µl
TaqMan® probe	0.5 µl
Master Mix 2X	5 µl
Final volume of 20 µl	

TaqMan Gene Expression Master Mix 2X (Applied Biosystems #4369016), contains all the components (AmpliTaq Gold DNA polymerase, a blend of dNTPs and a passive internal ROX dye) required to perform gene detection.

In all experiments conducted, each sample was set in triplicate, both for the gene of interest and for the internal control. Additionally, in each experiment, probes were tested in the absence of cDNA to verify that they were free from contamination. In these cases, the 4.5 µl of cDNA sample were substituted for MQ H₂O. Finally, the 10 µl of each reaction were added in a PCR 96 or 384-well plate (Thermo Scientific™ #AB0600, # AB2384) and covered with an adhesive seal. Plates were then placed in the ABI7500 Real-Time PCR System (Applied Biosystems) and the following program was run:

Table 8. Thermal cycling program for RT-qPCR

Step	Cycles	Temperature (°C)	Time
1	1	50	2 minutes
2	1	95	10 minutes
3	40	95	15 seconds
		60	1 minute
4	-	4	Hold

The RT-qPCR technique allows for absolute quantification or relative quantification. In this work, relative quantification was used based on the comparison of the *threshold cycle* (Ct) values. For that purpose, simultaneously co-amplification of an internal control besides the gene or genes of interest was performed. To analyze results, the internal control (*tata box protein*, TBP) was used to normalize samples due to its constant expression levels. Once normalized, a direct comparison of relative abundance across samples was made. The result was expressed as the ratio of gene signal relative to internal control signal.

$$2^{-\Delta\Delta Ct}$$

where:

$$\Delta Ct = \text{gene of interest Ct} - \text{internal control Ct}$$

$$\Delta\Delta Ct = \text{gen of interest } \Delta Ct - \text{internal control } \Delta Ct$$

6. TRANSIENT TRANSFECTION

The transient transfection is a technique for introducing genetic material into host cells for a limited period of time. The transiently-transfected material does not integrate into the genome, therefore it is not passed from generation to generation and it is lost by dilution during cell division. However, a high copy number of the transfected genetic material leads to high levels of protein expression within the period they exist in the cell.

For transient transfections, previously seeded cells were treated with a mix of plasmid DNA(s) of interest and transfection reagents such as *polyethyleneimine* (PEI) or Lipofectamine, diluted in DMEM w/o supplements. PEI is a polymer used to pack and deliver DNA into cells via endocytosis, while Lipofectamine is formed by vesicles (liposomes) that can easily merge with the cell membrane since they are both made of a phospholipid bilayer. The cell density as well as the concentration of each component in the transfection mix were determined by the nature of each experiment (see 7.1 Transient co-transfection for lentivirus production and 10.1 Transient co-transfection of luciferase-reporter constructs).

The overall protocol for transient transfection was carried out as follows: all the components of transfection mix were added in a 1.5 ml tube leaving, at last, the PEI (Polysciences #23966) or Lipofectamine 3000 (Thermo Fisher #L3000008). The mix was incubated at RT for 20 min. During incubation, the culture medium of cells was replaced with fresh medium w/o supplements. Finally, the mix was carefully added to cells by dripping to avoid disruption of DNA-PEI/liposome complexes and cells were incubated O/N (~16 h) at 37°C with 5% CO₂. As PEI and Lipofectamine are toxic to cells, it was important not to exceed the time of transfection. Finally, transiently transfected cells followed different courses according to their corresponding experiments.

7. GENERATION OF STABLE TRANSDUCED CELL LINES

Lentiviral transduction is an efficient method to insert genes or other types of molecules (like shRNAs) into mammalian cells unifying the ease and speed of transient transfection with the robust expression of stable cell lines. In general terms, transduction is the process by which foreign DNA (contained in a virus or viral vector) can be stably introduced into a host cell's genome. Lentiviruses, which belong to the retrovirus genus, use the host cellular machinery to amplify and package their genetic material into viral particles, hence the packaged viral vector is delivered to the target cell via membrane fusion. Therefore, this process does not require physical contact between the donor cell and the cell receiving the DNA, providing a rapid manner to establish stable genome integration of genes with high efficiency.

The general procedure to transduce cell lines consisted of a lentivirus producer cell line transiently co-transfected with second- or third-generation lentiviral plasmids. The components of both systems are: i) the transfer plasmid encoding the gene of interest flanked by *long terminal repeat* (LTR) sequences which allow the integration into the host genome, ii) the packaging plasmid contains the minimally necessary HIV genes required for virus production, and iii) the envelope plasmid encoding for *the vesicular stomatitis virus G* (VSV-G) used to ensure the formation of a highly infectious lentiviral particles. Once particles were formed and released in the supernatant by the lentivirus producer cell line, they were collected and, without determining the concentration, used to transduce the target cell lines. After genomic integration of the transfer vector, infected cells were selected, expanded and characterized.

The protocol described here leads to the generation of stable polyclonal cell lines.

7.1. Transient co-transfection for lentivirus production

In this study, HEK293T cells were used as a lentivirus producer cell line because they are easily transfectable and express high levels of proteins.

For STAT3 silencing, lentiviral particles bearing shRNAs were generated using third-generation lentiviral plasmids: pLKO.1 (transfer), VSVG (envelope), pRSV-Rev (Rev-packaging) and PKGPIR (Gag/Pol-packaging). Furthermore, lentiviral particles carrying STAT3 mutants were produced with second-generation lentiviral plasmids: pLX304 (transfer), pMD2.G (envelope) and psPAX2 (packaging).

To transiently transfect HEK293T cells, 1.5×10^6 cells/ml were seeded in TC-treated dishes and incubated at 37°C with 5% CO₂. After 6 h, the following transfection mix was prepared:

Table 9. Components for second-generation lentiviral system

Component	Concentration per Transfection
DMEM w/o supplements	20 µl/cm ²
Envelope vector	20 ng/cm ²
Packaging vector	60 ng/cm ²
Transfer vector	80 ng/cm ²
PEI [1 mg/ml]	1 µg/cm ²

Table 10. Components for third-generation lentiviral system

Component	Concentration per Transfection
DMEM w/o supplements	20 $\mu\text{l}/\text{cm}^2$
Envelope vector	20 ng/cm^2
Rev-packaging vector*	20 ng/cm^2
Gal/Pol-packaging vector*	40 ng/cm^2
Transfer vector	80 ng/cm^2
PEI [1 mg/ml]	1 $\mu\text{g}/\text{cm}^2$

* In this system, the packaging is divided into two vectors.

For second-generation system, a 1:3:4 (envelope:packaging:transfer) proportion was used. For third-generation system, a 1:1:2:4 (envelope:Rev-packaging:Gag/Pol-packaging:transfer) proportion was used.

After HEK293T transfection (see 6. Transient transfection), the culture medium was gently replaced with fresh medium and lentiviral production was induced by incubation of cells at 33°C with 5% CO₂. This temperature is ideal to stabilize the lentivirus, even though, they can also be produced at 37°C. The production of lentiviral particles began at 24 h post-transfection, however, they reached their maximum peak at 48 h, stable until 72 h.

7.2. Lentiviral transduction

Since the most accurate way to evaluate the role STAT3 in ccRCC is in their native cellular environment, the human-derived ccRCC cell lines 769-P and 786-O were chosen to be transduced. Both cell lines contain the necessary cellular machinery for synthesis, folding and quality control of STAT3, as well as the correct subcellular targeting. Moreover, PTMs were expected to be near-native.

To transduce 769-P cells, 5 x 10⁵ cells/ml were seeded in TC-treated flasks and incubated at 37°C with 5% CO₂. As cells have to grow on the same culture surface during infection, a low-density seeding was settled to avoid cells reached 100% confluence during the process. An additional flask was seeded as a negative control of infection. After 6 h of seeding, polybrene (Sigma Aldrich #TR-1003) [8 $\mu\text{g}/\text{ml}$] was added to cells to increase the efficiency of transduction by neutralizing the charge repulsion between lentiviral particles and the cell surface. Cells were incubated for 2 h at 37°C with 5% CO₂.

Afterward, the 48 h supernatant from HEK293T cells was collected and replaced with fresh medium. Then, the viral supernatant was filtered with a 0.22 mm filter (Millipore #SLGS033SS) and supplemented with 10% FBS, polybrene [8 $\mu\text{g}/\text{ml}$], and 1% non-essential amino acids (Biological Industries #01-340-1B). This enrichment of supernatant compensates the depletion of the medium produced by HEK293T cells. Finally, the medium of 769-P and 786-O cells was removed and the filtered and supplemented viral supernatant added. Cells were then incubated at 33°C with 5% CO₂. This process was repeated at 72 h without removing 24 h viral supernatant, however, at this point, the HEK293T cells were properly discarded.

After 24 h of the 72 h-transduction, the viral supernatant in 786-O and 769-P cells was removed, and fresh medium supplemented with selection antibiotics (see 1.3 Culture) was added. 769-P and 786-O cells were now incubated at 37°C with 5% CO₂ until the selection of transduced cells was completed. This step was validated with the complete death of negative control cells (non-transduced cells).

The 769-P and 786-O transduced cells were ready to be characterized.

8. PROTEIN MANIPULATION

8.1. Protein purification

Proteins are essential macromolecules consisting of one or more long chains of amino acid residues that participate in virtually every process within organisms, thus, they represent a wide field of study that provides crucial information about the cells functioning or even the whole organism. At present, proteins may be purified from cells using a variety of techniques, however, a detergent-based lysis method was preferred to isolate total proteins from cells.

In this work, the *radioimmunoprecipitation assay* (RIPA) lysis buffer was used, and prepared as follows: 150 mM NaCl (Panreac #1469941214), 5mM EDTA (Sigma Aldrich #ED255) pH 8.0, 50 mM Tris-HCl pH 8.0, 1% NP-40 (Sigma Aldrich #74385), 0.5% sodium deoxycholate (Millipore #106504), 0.1% SDS (Panreac #A0675), and supplemented with *protease inhibitor cocktail* (PIC) (Sigma Aldrich #S8820) (1:200), Na_3VO_4 (Sigma Aldrich #S6508) (1:200) and NaF (Sigma Aldrich #S7920) (1:1000). Each component of RIPA lysis buffer undertakes different purposes, for example, NaCl keeps the osmotic pressure near-physiological conditions, while NP-40 prevent non-specific interactions between proteins. SDS and sodium deoxycholate are anionic detergents that disrupt cellular membranes, and NaF works as a preservative. Importantly, to prevent the effect of endogenous proteases and phosphatases on proteins, the presence of the phosphatase inhibitor (Na_3VO_4) and the PIC was essential. Once prepared, RIPA lysis buffer was stored at -20°C until use.

The protein purification from cultured cells was carried out as follows: once cells reached 100% confluence or corresponding treatment was over, the medium was removed and the cells were washed with cold PBS. Cells were then placed on ice and, depending on the culture surface, the appropriate amount of RIPA lysis buffer was added. Cells were incubated on ice for 30 min. After this time, cells were mechanically lysed with a cell scraper and collected in a 1.5 ml tube. Samples were centrifuged at 13,000 and 4°C for 10 min. Finally, the supernatant was collected without dragging the pellet (white-colored) in a new 1.5 ml tube and stored at -20°C .

8.2. Protein quantification

Accurate protein quantification is essential to all experiments related to protein studies. A wide range of different methods have been developed for total protein quantification, yet we used the *bicinchoninic acid* (BCA) assay. This colorimetric method determines protein concentration by a color change in proportion to a known protein concentration (albumin standard).

The Pierce™ BCA protein assay (Thermo Scientific™ #23225) was carried out following the manufacturer instructions. First, the albumin standard was prepared as follows:

Table 11. Albumin standard curve

BSA ($\mu\text{g}/\mu\text{l}$)	BSA Stock (2 $\mu\text{g}/\mu\text{l}$)	RIPA lysis buffer ($V_f = 10 \mu\text{l}$)
0	-	10 μl
0.4	2 μl	8 μl
0.8	4 μl	6 μl
1.2	6 μl	4 μl
1.6	8 μl	2 μl
2.0	10 μl	-

Then, depending on the number of samples to be quantified, a BCA mix was set up: 50 μl of reactive A + 10 μl of reactive B.

Protein samples were diluted in a 1:10 proportion with RIPA lysis buffer.

Finally, 10 μl of albumin standard and diluted protein samples + 200 μl of the BCA mix (per well) were added in triplicate in a clear 96 well-plate. Samples were incubated in the dark at 37°C and the absorbance was read at 562 nm. Protein concentration was determined to subtract the average absorbance of the blank standard from the absorbance of samples and plotting the average blank-corrected values for each albumin standard vs its concentration in $\mu\text{g}/\mu\text{l}$, and multiplied by the dilution factor of samples.

8.3. Western blot

Western blot refers to *sodium dodecyl sulfate-polyacrylamide gel electrophoresis* (SDS-PAGE) and is an extensively used analytical technique to detect a specific single protein within a complex mixture of proteins. This technique also allows a semi-quantitative estimation of proteins derived from the size and intensity of their corresponding band on the blot membrane. The basic principle of this technique consists of protein sample denaturation followed by gel-electrophoresis to separate proteins by its size and transfer onto a membrane for immunostaining and visualization.

Sample preparation: Considering that an important part of this work lies in the study of proteins susceptible to phosphorylation, proper handling of them was sought. Consequently, if western blot was the upcoming technique after protein purification, samples were immediately set in Laemmli buffer to stabilize phospho-proteins.

Laemmli buffer is a *sodium dodecyl sulfate* (SDS)-containing buffer used to prepare (denature) samples for SDS-PAGE. This buffer was prepared with 300 mM Tris-HCl pH 6.8, 50% SDS, 25% glycerol, 10% β -mercaptoethanol, and 0.05% bromophenol blue (Sigma Aldrich #B5525). β -mercaptoethanol and SDS are reducing agents that denature proteins and gives them a uniform negative charge. Glycerol increases samples density, and bromophenol blue serves as a dye front that runs ahead of proteins to visualize samples during loading.

Thus, protein samples were diluted with Laemmli buffer 1X and stored at -20°C. When the next immediate step was SDS-PAGE, samples were heated at 95°C for 5 min to ensure complete denaturation.

Polyacrylamide-gel electrophoresis: To perform electrophoresis, polyacrylamide (Panreac #A1672) gels at different resolutions (depending on proteins of interest) were made as follows:

Table 12. Components for separating gel

Component	7.5%	10%	12%	15%
30% acryl/0.8% bis-	3.75 ml	5.00 ml	6.00 ml	7.00 ml
4X Tris-HCl/SDS pH 8.8	3.75 ml	3.75 ml	3.75 ml	3.75 ml
MQ H ₂ O	7.50 ml	6.25 ml	5.25 ml	3.75 ml
10% PA	100 µl	100 µl	100 µl	100 µl
TEMED	10 µl	10 µl	10 µl	10 µl

Table 13. Components for stacking gel

Component	
30% acryl/0.8% bis-	0.78 ml
4X Tris-HCl/SDS pH 6.8	1.50 ml
MQ H ₂ O	3.66 ml
10% PA	60 µl
TEMED	12 µl

Polyacrylamide gels are formed by the reaction of acrylamide and bis-acrylamide that results in a highly cross-linked gel matrix, thus acting as a sieve through which proteins move in response to the electric field applied.

For each gel, pre-cleaned glass plates were filled with 7 ml of separating gel solution. To maintain an even and horizontal resolving gel, the surface was overlaid with isopropanol. Gels were allowed to sit for 10 min at RT. Then, isopropanol was removed and the stacking gel solution was added until it overflows. Immediately after, the adequate comb (according number of samples) was inserted ensuring no air bubbles were trapped near the wells.

Once polymerized, gels were placed on a vertical electrophoresis system (Biorad #1658004) and the chamber filled with running buffer (25 mM Tris-HCl, 200 mM glycine (Sigma Aldrich #G8898), and 0.1% SDS). Hence, 20 µg of Laemmli-prepared samples were loaded in each well along with 5 µl of the Precision Plus Protein™ Dual Color (Biorad #610374) molecular weight marker. The electrophoresis was performed at 100 V until the bromophenol blue front left the gel.

Transfer: To make proteins accessible to antibody detection, they were moved from within the polyacrylamide gel onto a 0.2 µm *polyvinylidene difluoride* (PVDF) membrane. PVDF membranes (Millipore #ISEK00010) were previously activated with methanol (Panreac #A3493) for 15 seconds, hydrated with MQ H₂O for 2 min, and sited on transfer buffer (25 mM Tris-HCl, 200 mM glycine, 0.1% SDS, and 20% methanol).

After the electrophoresis is over, gels were removed from glasses and immersed in transfer buffer. Then, the transfer stack was mounted in a cassette holder as follows: foam, filter paper, polyacrylamide gel, PVDF membrane, filter paper, and foam. To ensure an even transfer, all air bubbles between layers were carefully removed with a stirring rod. The cassette holder was therefore placed in the transfer tank and transfer buffer was

added until cover it. A cooling unit was also set up in the tank. The transfer was performed at 100 V for 60 min.

Immunodetection: Once the transfer finished and before immunodetection, the membrane was blocked with 25 ml of 5% NFDM (Biorad #1706404) diluted in TBS-Tween 1X (50 mM Tris-HCl, 150 mM NaCl and 1% Tween-20) for 1 h at RT and moderate shaking. This process promotes that blank spaces in the membrane (where there are no proteins) occupying to reduce background and unspecific interactions of antibodies.

For immunodetection of the proteins of interest, membranes were incubated O/N with 4 ml of specific primary antibodies at 4°C. After incubation, membranes were washed three times in agitation with 10 ml TBS-Tween 1X to remove unbound antibody and then, incubated again with the corresponding secondary antibodies for 1 h at RT. Secondary antibodies recognize and bind to the species-specific portion of the primary antibodies and allow the detection of target proteins since they are linked to a reporter enzyme, such as *horseradish peroxidase* (HRP). Finally, membranes were washed three times in agitation with 10 ml TBS-Tween 1X and proceeded with the chemiluminescent detection.

For protein detection, membranes were soaked with 1 ml of the Immobilon Forte HRP substrate (Merck™ #WBLUF0100) for 5 min at RT, and placed on the Odyssey® Fc Imaging System (Li-cor®). Membranes were exposed during 5 min for chemiluminescent protein-detection, and 30 seconds in the 600 channel to visualize the molecular weight marker.

Throughout this work, the following antibodies were used:

Table 14. List of primary antibodies for western blot

Primary Antibody	Host	Dilution	Concentration
STAT3	Rabbit	5% BSA in TBS-Tween 1%	1:1000
pTyr705-STAT3	Mouse	5% NFDM in TBS-Tween 1%	1:1000
pSer727-STAT3	Rabbit	5% BSA in TBS-Tween 1%	1:1000
β-Tubulin	Mouse	5% NFDM in TBS-Tween 1%	1:5000

Table 15. List of secondary antibodies for western blot

Secondary Antibody	Host	Dilution	Concentration
Mouse	Rabbit	5% NFDM in TBS-Tween 1%	1:5000
Rabbit	Goat	5% NFDM in TBS-Tween 1%	1:5000

8.4. Immunocytochemistry

The *immunocytochemistry* (ICC) is a technique used to anatomically visualize the localization of a specific protein within whole cells. The detection of proteins is usually done by fluorescence under the confocal microscope using fluorophore-conjugate antibodies. Confocal microscopy allows the reconstruction of three-dimensional structures within an object by capturing multiple images at different depths, hence allowing to determine in which sub-cellular compartment the specific protein is expressing.

To carry out the ICC, 0.5×10^6 cells per well were seeded and grew on coverslips (SG #LAB550012C) until they reached the desired confluence or corresponding treatment was over. Cells were washed with PBS and fixed with 500 μ l of 4% paraformaldehyde (PFA) (Electron Microscopy Science #15714) for 30 min at RT. The PFA was removed and then, 1 ml of 50 mM NH_4Cl was added. The NH_4Cl prevents the unspecific binding of antibodies to free aldehyde groups formed as a result of PFA fixation. Cells were incubated for 30 min at RT. After incubation, cells were washed with PBS and permeabilized with 1 ml of 0.1% Triton X-100 (Millipore #1.2298.0101) for 15 min at RT. Then, cells were washed again with PBS and blocked with 1 ml of a 5% BSA/5% FBS (Gibco #1027-106) solution for 1 h at RT. For detection of proteins of interest, 25 μ l of primary of a 1:250 dilution of primary antibody α -STAT3 were deposited on parafilm and coverslips were carefully placed face down on the antibody drop taking care not to form bubbles. Coverslips were incubated O/N at 4°C in the dark.

After incubation with the primary antibody, coverslips were washed by submersion in PBS, and carefully dried with a paper towel. It was important to always be aware of the side where the cells were. The incubation with secondary antibody and stain of the nuclei was performed at the same time. Therefore, coverslips were placed face down on a 25 μ l drop of a 1:500 dilution of secondary antibody α -Rabbit Alexa Fluor 488 diluted in a solution 1:2000 of Hoescht 33342 (Invitrogen #H1399) with 5% BSA. Coverslips were incubated for 1 h at RT in the dark.

Finally, coverslips were washed by submersion in PBS, carefully dried with a paper towel and mounted face down in glass slides with 5 μ l of ProLong™ Diamond Antifade Mountant (Invitrogen #P36961). ICC preparations were then visualized and photographed with the FluoView confocal microscope (Olympus #FV100) or stored at 4°C in the dark until analysis.

8.5. Immunohistochemistry

The *immunohistochemistry* (IHC) technique is based on the same principle of ICC (detection of specific protein), nevertheless, it is performed in tissue sections rather than whole cells. Unlike the ICC, this technique allows correlating the location of proteins with their expression levels and morphologic parameters thus increasing the specificity and sensitivity of the study. Since immunohistochemical samples are surrounded by tissue architecture and other cells normally found in the intact tissue, preparation of samples is critical to maintaining cell morphology, tissue structure and mostly, the antigenicity of target proteins.

Once samples were fixed in formalin, embedded in paraffin and the corresponding sections were obtained using a microtome, the IHC protocol was performed as follows:

To remove the excess of paraffin, tissue samples were incubated O/N at 55°C. Subsequently, tissue samples were completely deparaffinized in three sequential steps: i) 15 min in xylene (Panreac #131769.1612), three times; ii) 10 min in 100% ethanol (VWR #20821.330), and iii) 5 min in 100% ethanol. Consecutively, tissue samples were hydrated in seven sequential steps of 45 seconds each: i) 100% ethanol, ii) 95% ethanol, iii) 85% ethanol, iv) 70% ethanol, v) 50% ethanol, vi) 30% ethanol and, vii) MQ H_2O ; then, tissue samples were washed with PBS-Tween 1% for 5 min, twice.

The subsequent steps were carried out with the EnVision® + Dual Link System-HRP (DAB+) kit (Dako #K4065), with mild modifications.

For antigen retrieval (epitope exposure), tissue samples were treated with 200 ml of the target retrieval solution citrate pH 6 1X (Dako #S2031). Samples were heated in the microwave for 5 min, then waited to cool to 70°C and heated again for 15 min without letting the tampon boil. Samples were allowed to cool (~35°C) at RT.

From now on, between each step of the protocol, samples were washed with PBS-Tween 1% for 5 min and carefully dried with a paper towel without touching the tissue sample. Furthermore, all the following steps were performed in the dark.

To block the endogenous peroxidase, the water-repelling DakoPen (Dako #S2002) was used to draw the tissue sample outline and 100 µl of dual endogenous enzyme block (provided in the kit) were applied. Samples were incubated at RT for 5 min.

To avoid unspecific binding, 100 µl of 5% normal horse serum diluted in PBS-Tween 1% were added to samples and incubated for 1 h at RT.

For the detection of epitopes (proteins of interest), 100 µl of a 1:250 dilution of primary antibody α -STAT3 were added and samples were incubated O/N at 4°C. It was important to keep the samples in a moist environment to prevent them from drying out during incubation. The following primary antibodies were used:

After incubation with the primary antibody, 100 µl of labeled polymer-HRP mouse/rabbit (provided in the kit) were added to samples and incubated for 1 h at RT.

For enzymatic detection of HRP, 100 µl of a 1:20 dilution of DAB + chromogen (provided in the kit) were added to samples and incubated for 20 min at RT.

To stain the nuclei, samples were submerged in Harris hematoxylin (Sigma Aldrich #GH5316) for 1 min and then washed with MQ H₂O as necessary to remove all traces of hematoxylin.

Once finished the immunostaining, tissue samples were dehydrated in six sequential steps of 45 seconds each: i) 30% ethanol, ii) 50% ethanol, iii) 70% ethanol, iv) 85% ethanol, v) 95% ethanol and, vi) 100% ethanol. Afterward, samples were submerged in xylene for 3 min, twice.

Finally, the slides were mounted with 1 drop of DPX mountant (BDH #36029), taking care not to form bubbles. Mounted slides were stored at 4°C in the dark until analysis in the microscope.

9. FUNCTIONAL ASSAYS

All functional assays were performed in the presence of IL6 [10 ng/ml].

9.1. Cell proliferation (XTT assay)

Cell proliferation or cell growth is the process by which the number of cells increases, and is defined by the balance between cell divisions and cell loss through cell death or differentiation. Furthermore, proliferation is also one of the hallmarks in cancer development and progression due to the constitutive activation of many signal transduction pathways that stimulates cell growth.

To measure cell proliferation, the same principle of the colorimetric XTT assay (previously used to determine cell viability) was used. Therefore, 2.5×10^3 (769-P) cells per well were seeded in a TC 96-well plate and incubated for 24, 48 and 72 h at 37°C with 5% CO₂. After each time point, the medium was replaced with 100 µl of fresh medium and 50 µl of XTT mix, prepared with a 1:50 dilution of labeling reagent and electron-coupling reagent (provided in the kit), were added. Cells were then incubated for 4 h at 37°C with 5% CO₂ in the dark. Once incubation with XTT finished, the absorbance was read at 490 nm and 630 nm as the reference wavelength (background). The results were calculated subtracting the absorbance at 630 nm to 490 nm, and a time-curve was constructed plotting absorbance values at each time point. Three independent experiments were carried out in triplicate.

9.2. Cell aggregation

Cell aggregation is the phenomenon by which dissociated cells *in vitro* tend to group themselves with cells of their own type. This phenomenon, not yet well-studied, may have a correlation with cell-cell interactions.

To analyze cell aggregation, cells were dissociated by trypsinization (see 1.4 Trypsinization) and vortexed at full speed for 1 min. To observe whether or not the formation of cell aggregates took place, photographs were taken immediately after the vortex step. Three independent experiments were carried out in triplicate.

9.3. Adhesion assay

Cell adhesion is the capacity of cells to bind to the *extracellular matrix* (ECM), other cells or a specific surface, and is an essential feature for the growth and survival of cells. Cancer cells, especially the highly metastatic types, are believed to have enhanced adhesion ability that often facilitates migration to a new site to establish new tumors in different locations. Cell adhesion assay is therefore often used to evaluate the metastatic ability of cancer cells.

To evaluate adhesion capacity, 500 µl of a dilution 1:50 of collagen I (Corning #354236) in PBS was used to coat each well of a TC P12-well plate and incubated O/N at 4°C. Collagen I was used as an ECM protein to facilitate cell adhesion. After coating, wells were

washed with PBS and air-dry at RT inside the hood. Afterward, 2×10^4 cells per well were seeded and incubated for 30 min at 37°C with 5% CO₂ to allow the cells to adhere to the surface. After incubation, cells were carefully washed with PBS to remove any non-adherent cells. Then, cells were fixed with 500 µl of 4% PFA for 30 min at RT. Subsequently, PFA was removed and 500 µl of 0.1% crystal violet (Sigma Aldrich #V5265) were added to stain cells. Cells were incubated for 15 min at RT. Finally, cells were washed three times with PBS and lysed with 500 µl of 1% SDS at 100 rpm for 15 min. Absorbance was measured at 590 nm on a spectrophotometer. Three independent experiments were carried out in triplicate.

9.4. Clonogenic assay

The clonogenic capacity is defined as the ability of a single cell to grow into a colony. Since cancer cells undergo unlimited division, they usually exhibit greater clonogenic capacity that correlates with the aggressiveness of tumors.

The clonogenic assay or colony formation assay assesses the differences in reproductive viability (capacity of cells to produce progeny) where only a fraction of seeded cells retain the capacity to produce colonies consisting of at least 50 cells. The clonogenic assay is the method of choice to test cell reproductive after treatment, but can also be used to determine the effect of genetic manipulation. In this assay, cells are seeded at very low density to form colonies in 1-3 weeks. The appropriate cell dilution isolates cells and avoids cell-cell contact influencing growth. Once the assay has finished, colonies are fixed, stained and counted.

To evaluate clonogenic capacity, 1.0×10^3 (769-P) cells per well were seeded in a TC P6-well plate and incubated for 7 days at 37°C with 5% CO₂. After incubation, the medium was removed and cells were fixed with 500 µl of 4% PFA for 15 min at RT. Cells were then washed with PBS and stained with 500 µl of 0.1% crystal violet for 15 min at RT. Cells were washed three times with PBS and photographed. Finally, the cells were lysed with 500 µl of 1% SDS at 100 rpm for 15 min. Absorbance was measured at 590 nm on a spectrophotometer. Three independent experiments were carried out in triplicate.

9.5. Migration (wound-healing assay)

Cell migration or cell motility is a highly dynamic multistep process which relies on membranous protrusions to assemble, extend, disassemble and retract, and plays a key role in many physiological and pathological (i.e. tumor metastasis) processes. Moreover, tumor cells display a high migration rate that often results in the poor prognosis of patients' survival.

Currently, the two most widely used migration assays are the scratch (wound-healing) assay and the transmembrane (transwell) assay. In this work, the wound-healing assay was employed. This method typically consists of a “wound” gap in a cell monolayer and the “healing” by cell migration towards the center of the gap and allows to study the migration of pharmacologically and genetically manipulated cells. To properly analyze migration, various motility parameters including velocity, straightness and leading-edge dynamics should be taken into account.

To evaluate cell migration, the culture-inserts 2 wells (Ibidi #81176) were used instead of scratching the surface of the cell monolayer. These inserts are 2-well structures divided by a gap of 500 μm that were placed in wells of a TC P12-well plate. Twenty-four hours before the experiment, 3.5×10^4 (769-P) cells per well-insert were seeded and incubated at 37°C with 5% CO_2 . Once cells reached 100% confluence as a monolayer (~ 24 h at this density), the culture-insert was removed and the cells were washed with PBS. Then, 2 ml of culture medium without FBS were added to inhibit proliferation and promote only migration. Cells were incubated in the Cell R live cell microscope (Olympus #TIRFM) for 24 h and photographs were taken every 30 min. Cell migration was calculated as the percentage of the total wound area and values were plotted at each time point. Three independent experiments were carried out in triplicate.

9.6. Transwell invasion assay

Invasion is the direct extension and penetration of cells into neighboring tissues and is characteristic of cancer cells. Invasion is different from metastasis, in which tumoral cells spread through the circulatory or the lymphatic system to more distant locations.

Cell invasion assay is used to study the interactions between cells and the ECM, which not only provides a structural scaffold for cells but also contains various biological factors for cell survival and growth. Cancer cells can secrete enzymes that degrade certain components of the ECM to move towards chemoattractants or to simply establish niches for growth. Metastatic tumor cells often show more invasiveness to the ECM due to their higher motility and/or enzymatic activity for degrading ECM components. Matrigel is often used as ECM in invasion assays because it resembles the complex ECM found in many tissues.

In this work, the transwell invasion assay was employed. This assay consisted of a permeable membrane of support positioned between two compartments that mimic two different sets of microenvironments. Cells on the upper side of the membrane sensed the chemoattractant placed on the lower side and migrated through the pores towards the source of the chemoattractant. Cells that invaded across the membrane were quantified by fixing and counting.

Before the experiment was carried out, cells were deprived of FBS O/N and the 8 μm membrane of the transwells (Thermo Fisher #140629) was covered with 100 μl of a 1:10 dilution of Matrigel (Corning #354248) in medium without FBS. The Matrigel coating was performed on ice (Matrigel solidifies at RT) and afterward incubated for 30 min at RT.

To evaluate invasion, transwells were placed in wells of a P24-well plate and 5×10^4 (769-P) cells per well were seeded in the upper side of the transwell filled with medium without FBS. In the lower side of the membrane, 500 μl of medium with 10% FBS as chemoattractant were added. Cells were then incubated for 48 h at 37°C with 5% CO_2 . Once incubation was finished, transwells were placed in a new P24-well plate and cells that had invaded to the lower side of the membrane were fixed with 500 μl of 4% PFA for 15 min at RT. After fixation, transwells were washed with PBS and the cells in the upper side of the membrane were gently removed with a cotton swab. Once removed all non-invasive cells, nuclei of cells in the lower side of the membrane were stained with 500 μl of a dilution 1:2000 of Hoechst 33342 in PBS for 15 min at RT and in the dark. Transwells

were then washed with PBS and air-dried in the dark. Finally, four representative photographs of invasive cells were taken and counted with the software ImageJ (NIH). Three independent experiments were carried out in triplicate.

9.7. Anchorage-independent growth (soft agar assay)

The anchorage-independent growth is the ability of cells to grow independently of a solid surface and is a hallmark of carcinogenesis. Moreover, the anchorage-independent growth phenotype predicts tumor aggressiveness and metastatic potential.

The anchorage-independent growth assay, also known as soft agar colony formation assay, is a well-established *in vitro* method for characterizing the ability of cells to grow in a semi-solid surface. This assay can be thought of as a combination of the clonogenic assay and the cell invasion assay since it evaluates the ability of cells to degrade the surrounding environment besides their capability to create cell niches or colonies. Hence, it is considered one of the most stringent tests for malignant transformation in cells.

Before the experiment was performed, the bottom of the wells of a TC P24-well plate was coated with 500 μ l of 0.6% Noble Agar (Affymetrix #J10907) diluted in culture medium (bottom layer) and left to solidify for 30 min at RT. This coating was performed to avoid cell attachment from the plate.

To evaluate the anchorage-independent growth, 2.0×10^4 cells per well diluted in 500 μ l of 0.3% Noble Agar (upper layer) were seeded onto the bottom layer and incubated for 30 min at RT to solidify. Cells were incubated for 28 days at 37°C with 5% CO₂ and fed with 100 μ l of culture medium every three days. Once colonies were formed and grown, cells were stained with 100 μ l of nitro blue tetrazolium chloride [1 mg/ml] (Abcam #AB146262) O/N at 37°C with 5% CO₂. *Nitro blue tetrazolium chloride* (NBT) uses the same principle of XTT to evaluate cell viability and produces a deep-blue-colored precipitate as a result of redox potential. After cell staining, photographs were taken and the colonies formed counted with the software OpenCFU (Quentin Geissmann). Three independent experiments were carried out in triplicate.

9.8. Tumorspheres formation assay

Tumorspheres are solid, spherical structures developed from the proliferation of *cancer stem cells* (CSCs). CSCs are defined as a subpopulation of cells within a tumor with the ability to self-renew, drive tumor progression, drug resistance and metastatic properties. Tumorspheres are easily distinguished from single or aggregated cells as these cells appear to fuse together (with a characteristic dark center) and individual cells do not.

Tumorspheres formation refers to the cultivation of cancer cells onto an ultralow attachment surface in serum-free media supplemented with growth factors. Tumorspheres formation is widely used to analyze the self-renewal ability of CSCs and to enrich these cells from bulk cancer cells. This method also provides a reliable platform for screening potential anti-tumoral agents on CSCs, which are more translatable into *in vivo* compared with general monolayer culture.

In this study, the tumorspheres formation assay was employed to determine if genetic modifications in our cell lines resulted in a more CSC-like phenotype.

For tumorspheres formation assay, a special culture medium was prepared as follows: Dulbecco's Modified Eagle Medium/F12 (Gibco #31331093) supplemented with EGF (Peprotech #AF-100-15) [20 ng/ml], *basic fibroblast growth factor* (bFGF) (Peprotech #100-18B) [20 ng/ml], and 1X B27 supplement (Gibco #17504044).

To cultivate tumorspheres, 2.0×10^4 (769-P) cells per well were seeded in an ultralow attachment plates TC P24-well plate and incubated for 10 days at 37°C with 5% CO₂. Every two days, 100 µl of fresh medium were added without removing the previous medium. To record tumorsphere growth, photographs were taken at the end of the experiment. Three independent experiments were carried out in triplicate.

10. LUCIFERASE-REPORTER ASSAY

The reporter assay is a strategy for studying the regulation of gene expression by using reporter genes. A reporter gene is a gene whose product can be readily measured after transfection and ideally should be absent from the cells used in the study and not affect the normal physiology, such as firefly luciferase. Luciferase is an enzyme that catalyzes a reaction with its substrate (luciferin) to produce bioluminescence. Reporter genes are usually fused with the gene or DNA region of interest and cloned into an expression vector that is transiently transfected into cells and assayed quantitatively after 1-3 days through a luminometer. Therefore, the expression of the reporter gene expressed as luminescence is proportional to the activity of the gene or DNA region of interest.

In this study, a dual-luciferase reporter assay was performed with the Signal Reporter Assay (Qiagen #CCS-9028). This system is composed of three main components: i) the reporter which is an inducible reporter construct encoding for firefly luciferase joined to tandem repeats of STAT3 *transcriptional response element* (TRE) mixed with a constitutively expressing renilla luciferase construct under the control of a CMV immediate early promoter (40:1); ii) the negative control which is a non-inducible reporter construct mixed with a constitutively expressing renilla luciferase construct (40:1); and iii) the positive control which is a constitutively expressing GFP construct, mixed with a constitutively expressing firefly luciferase and a constitutively expressing renilla luciferase (40:1:1). The utilization of a constitutively expressing renilla luciferase construct as an internal control (housekeeping) enhances experimental accuracy and minimizes variability in terms of the number and viability of the transfected cells. Furthermore, both, the negative and the positive controls are critical to identifying specific effects thus determining background reporter activity, and for visual confirmation of transfection, respectively (see Figure 23).

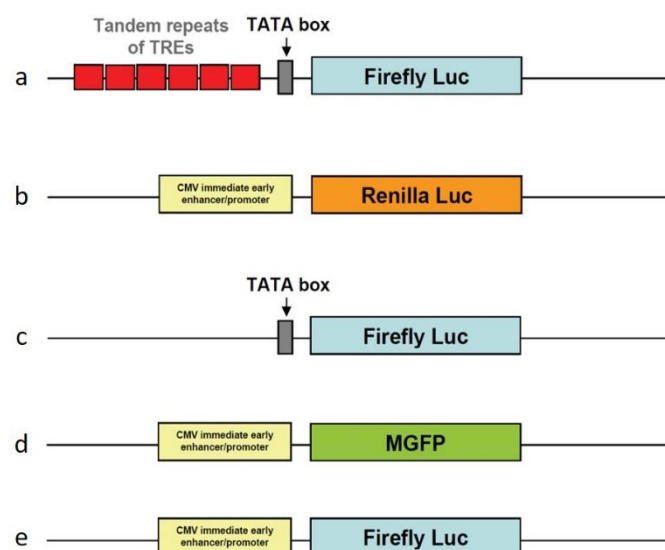


Figure 23. Constructs of STAT3 luciferase-reporter assay. a) Reporter joined to tandem repeats of STAT3 *transcriptional response element* (TRE) and firefly luciferase. b) Constitutively expressing renilla under the control of CMV promoter. c) Negative control of the reporter joined to firefly luciferase. d) Positive control of transfection expressing GFP construct under the control of CMV promoter. e) Positive control of the reporter expressing firefly luciferase under the control of CMV promoter.

10.1. Transient co-transfection of luciferase-reporter constructs

In this study, we aim to analyze the transcription capacity of STAT3 phosphomutants on the STAT3 consensus promoter in the presence and absence of IL6, therefore, stable transduced cell lines carrying the different STAT3 phosphomutants were transiently transfected with the luciferase-reporter constructs.

To transiently transfect cell lines, 1.25×10^5 cells per well were seeded in a TC P24-well plate and incubated at 37°C with 5% CO₂. Once cells reached 50-70% confluence (~24 h at this density), the following transfection mixes were prepared:

Table 16. Components of STAT3 luciferase-reporter

Component	Volumes per Transfection
DMEM w/o supplements	36.5 µl
Reporter mix [100 ng/ml]*	10 µl
Negative control [100 ng/ml]*	
Positive control [100 ng/ml] *	
Lipo-Reagent 3000	2 µl
Lipofectamine 3000	1.5 µl
* Each component was added in their corresponding mix	

After transfection (see 6. Transient transfection), cells were incubated O/N at 37°C with 5% CO₂. After incubation, the transfection medium was replaced with 500 µl of fresh medium and cells were incubated for 48 h at 37°C with 5% CO₂. Therefore, treatment with IL6 [10 ng/ml] was added to the corresponding wells and cells were incubated O/N at 37°C with 5% CO₂.

10.2. Quantitative determination of gene expression

To measure luciferase activity in the transiently transfected STAT3 mutants, the Dual-Luciferase Reporter Assay (Promega #E1910) was used following the supplier instructions. This assay consists of measurement of both, luciferase and renilla activities, sequentially. In the first reaction, luciferin is used as a substrate to assess the activity of luciferase followed by renilla luciferin to assess the activity of renilla with a parallel signal quenching of luciferase.

First, to cell lysis, the culture medium was removed and cells were washed with PBS. Then, 100 µl of passive lysis buffer 1X (provided in the kit) were added and cells were mechanically lysed with a cell scraper, collected in a 1.5 ml tube and place on ice. At this point, samples can be stored at -80°C or continued with the protocol.

For quantitative measure of luminescence, 25 µl of samples per well were placed in an opaque P96-well plate (Nirco #900093) and detection of luciferase and renilla was performed in the Synergy Mx luminometer (BioTek) as follows: 25 µl of luciferase assay reagent (provided in the kit) were dispensed followed by a delay of 3 seconds and reading of luciferase for 10 seconds. Therefore, 25 µl of Stop & Glo reagent (provided in the kit) were dispensed followed by a delay of 3 seconds and reading of renilla for 10 seconds.

All the previous steps were automatically performed in the luminometer for each of the wells.

Finally, gene expression was measured as luciferase activity normalized by internal renilla activity and expressed as *relative light units* (RLU). Three independent experiments were carried out in triplicate.

11. TISSUE MICROARRAY (TMA)

The tissue microarrays (TMAs) consists of separate tissue cores from paraffin blocks and assembled in array fashion to allow multiplex histological analysis commonly by IHC or fluorescent in situ hybridization. TMAs are particularly useful in the analysis of cancer patients' samples since they are assembled into the same block and can be stained with the same protocol to avoid experimental variability, thus the use of TMAs in combination with IHC is the method of choice to study and validate diagnostic, prognostic and treatment predictive cancer biomarkers. Moreover, the possibility to correlate protein expression patterns obtained from TMAs with clinical parameters within a defined patient cohort represents a powerful resource of information.

In this study, a TMA comprising 82 ccRCC patient's cohort was constructed to evaluate the expression of pSer727-STAT3 as a validation of a previous cohort of 98 ccRCC patients.

11.1. Case selection

For case selection, clinical and pathologic information from 82 ccRCC patients treated with radical or partial nephrectomy for ccRCC between 2008 and 2010 and clinically followed up to 2017 at the Vall d'Hebron Hospital were retrospectively reviewed. Standard tumor data were collected including the date of diagnostic, demographic information, stage, Fuhrman grade, nodal and metastasis spread, initial therapy, subsequent therapy, and outcome information.

Primary tumor histology was recorded from surgical resections and pathologic information was based on a re-review of all surgical samples to determine histologic subtype. The anatomic extent of the tumor was classified using the tumor-node-metastasis (TNM) system, and clinical and follow-up information was based on physician reports. Prognostic stratification of patients affected by ccRCC was scored using the University of California Los Angeles (UCLA) Integrated Staging System–Union Internationale Contre le Cancer (UICC) nomogram.

11.2. TMA construction

The TMA of the 82 ccRCC patients previously selected was constructed from paraffin-embedded ccRCC tissues provided by the Department of Pathology at the Vall d'Hebron Hospital. Sections of paraffin-embedded tissues were stained with hematoxylin and eosin and reviewed for selection of representative areas. For each sample, 1 mm diameter cores of 3 different areas of the carcinoma were obtained using a semi-automated tissue arrayer (Chemicon International). As controls for pSer727 staining, 3 cores of benign areas far from the tumor were included. Finally, tissue cores were embedded in a paraffin block in a precisely spaced array pattern. Sections from this block were cut using a microtome, mounted and analyzed by IHC.

11.3. TMA immunohistochemistry

Nuclear and cytosolic pSer727-STAT3 expression was assessed by IHC following the previously described protocol (see 8.5 Immunohistochemistry).

11.4. TMA analysis

Once samples were stained by IHC, pSer727-STAT3 staining was scored by an expert pathologist, blinded to clinicopathologic variables. pSer727-STAT3 expression was evaluated in a semi-quantitative manner by immune-histo-score (H-score) based on the percentage and intensity of stained cells. Nuclear and cytosolic pSer727-STAT3 staining was scored as: 0 = no appreciable staining; 1 = weak staining; 2 = moderate staining; and 3 = strong staining. Therefore, the H-score was calculated as $1 \times (\% \text{ weak}) + 2 \times (\% \text{ moderate}) + 3 \times (\% \text{ intense})$ ranging from 0 to 300. For each ccRCC sample, 3 independent tissue cores were evaluated and the H-score was expressed as the mean.

Associations between pSer727-STAT3 expression and clinicopathologic parameters were evaluated with the nonparametric Mann–Whitney U test. Disease-free survival was calculated as the date of surgery to the date of loco-regional or distant recurrence. Kaplan-Meier survival curves were compared using the log-rank test. Multivariate analysis was performed using a Cox regression model to estimate the independent prognostic importance of clinicopathologic parameters. All the statistical analysis was performed with the Statistical Package for Social Sciences software (IBM).

12. MICROARRAY

A microarray is a collection of DNA spots attached to a solid surface used to measure the expression levels of a large number of genes simultaneously, thus giving a global gene expression profiling. The principle behind microarrays rests on the ability to test many (tens of thousands) different cDNA sequences (targets) by hybridization with complementary DNA sequence (probes) contained in spots. Hybridization between two strands occurs under high-stringency conditions by forming hydrogen bonds. The more complementarity between strands, the tighter non-covalent bonding. Thus, after washing of non-specific sequences, only strongly paired strands will remain hybridized. Detection occurs through fluorescence attached to target sequences and relative quantification depends on the fluorescent signal strength from a spot. The identity of each probe is known by its location on the array.

In this work, a Clariom S array (Applied Biosystems #902926) was used for gene-level expression profiling of STAT3 phosphomutants. The Clariom S array covers all known well-annotated genes (>20,000) thus providing a robust study of differential gene expression between samples. Since the microarray study aims to analyze the transcriptome, cDNA resulting from reverse transcription of total RNA was used.

12.1. Experimental design

The main objective for microarray analysis was to identify the genes (and their associated pathways) that are regulated by the overall STAT3 phosphorylation state, as well as by pSer727-STAT3. For that purpose, the following experimental conditions were considered:

Table 17. Experimental conditions for microarray analysis

# Samples	Experimental Condition	Description
5	pLKO	Control of silencing: normal expression of endogenous STAT3
5	shRNA2	Absence (reduction) of STAT3
5	pLX304	Control of overexpression: absence (reduction) of STAT3
5	WT	Normal activity of STAT3
5	YF	Tyr705 unphosphorylated, free Ser727
5	SA	Ser727 unphosphorylated, free Tyr705
5	SD	Ser727 phosphorylated, free Tyr705
5	YF/SA	Both Tyr705 and Ser727 unphosphorylated
5	YF/SD	Tyr705 unphosphorylated, Ser727 phosphorylated

There were 9 experimental conditions with 5 replicates each, therefore this study was based on 45 samples.

All experimental conditions for microarray samples were carried out in the presence of IL6.

12.2. Sample preparation and hybridization

To prepare samples for microarray analysis, 1.5×10^5 cells per well were seeded in a TC P6-well plate and incubated for 24 h at 37°C with 5% CO₂. Therefore, cells were treated with IL6 [10 ng/ml] for 48 h to induce the expression of early- and late genes. Once treatment was over, RNA isolation was carried out as previously described (see 5.2 RNA isolation).

RNA quantification was performed in the BioAnalyzer 2100 (Agilent Technologies #G2939BA) in a nano-chip format. The BioAnalyzer is a chip-based capillary electrophoresis machine for assessment of sizing, quantitation, integrity, and purity of RNA, DNA and protein samples. Bioanalyzer assigns an *RNA integrity number* (RIN) from 0-10 to RNA samples, labeling it as “good”, “medium” or “bad” quality. To measure RNA, 1 µl of sample was placed on the Bioanalyzer chip. Concentration values were obtained as ng/µl and the corresponding integrity label assigned.

Hybridization of the Clariom S array was performed with the GeneTitan MC System (Affymetrix #00-0373) in the *Unitat d'Alta Tecnologia* (UAT) of the Vall d'Hebron Institute of Research (VHIR). The followed protocol consisted of reverse transcription of 200 ng of total RNA into cDNA using the WT pico HT kit (Thermo Fisher #902622). The resulting cDNA was fragmented, labeled and hybridized using the GeneAtlas Hybridization, Wash, and Stain Kit for WT Array Strips (Thermo Fisher #901667), and finally, the Clariom S array was placed in the GeneTitan MC System for scanning.

12.3. Quality control

After hybridization, the unprocessed data underwent a *quality control* (QC) to verify the performance of the entire previous process, and to identify if the data obtained were suitable for the normalization process and appropriate for differential gene expression analysis.

Different types of QC were performed on microarray samples, including i) *principal components analysis* (PCA) to identify the presence of technical problems based on the distribution of samples; ii) heatmap to determine the distance between samples based on biological, experimental or technical effects; and iii) hierarchical clustering to assess how samples were grouped among them based on their similarity.

Once the different outlier-detection approaches were performed, they were compared to decide whether or not a sample should be removed. In this study, only samples that were identified as an outlier by more than one criterion were considered to rule out.

12.4. Preprocessing: normalization and filtering

In order to make the samples comparable, as well as to remove technical biases, the samples were preprocessed using the *robust microarray analysis* (RMA) method. In addition, the exon level values were averaged to yield one expression value per gene. Some QC checks were performed again once the samples were normalized.

To correct for batch effects, a batch factor was included in the linear model used for differential expression analysis.

To increase statistical power and reduce unnecessary noise, some genes that cannot be considered to be either expressed or differentially expressed were removed. Therefore, the standard deviations of all genes were calculated, ordered and plotted, and those genes whose standard deviations were below the 65 percentile of all standard deviations were removed.

12.5. Selection of differentially expressed genes

To select differentially expressed genes, an analysis based on adjusting a linear model with empirical Bayes moderation of the variance was used. This analysis is similar to ANOVA albeit specifically developed for microarray data analysis. The empirical Bayes analysis implemented yielded several performance measures to decide which genes were differentially expressed:

- logFC or M is the estimated fold change (in log 2 scale) between the conditions considered
- AveExpr is the average expression (in log 2 scale) of genes across all samples
- T is a “moderate-t”, statistically similar to the usual Student’s t
- P.Value is the p-Value corresponding to t
- adj.P.Value is the p-Value adjusted for multiple testing by the Benjamini and Hochberg method
- B is the B-statistic and roughly indicates the logarithm of the odds that a gene is differentially expressed vs is not

Each comparison yielded a list of genes sorted from most to least differentially expressed, called a top table.

In this study, the selection of the differentially expressed genes was based on an adj.P.Value <0.25 and a logFC > 0.5.

12.6. Multiple comparisons

To find the degree of overlapped genes among different experimental conditions, simple ad multiple comparisons analysis was performed and plotted as Venn Diagrams.

To evaluate differential gene expression among samples, each experimental condition was compared against its corresponding control based on the plasmids they contained. These comparisons also served to remove the IL6 effects unrelated to the activation of the STAT3 pathway. The following comparisons were considered:

Table 18. Initial comparisons of STAT3 phosphomutants against their corresponding controls

Comparison	Description
pLKO vs shRNA2	To identify the genes regulated by endogenous STAT3
WT vs pLX304	To identify the genes regulated by STAT3 normal activity
YF vs pLX304	To identify the genes regulated by STAT3 when only Ser727 is phosphorylated
SA vs pLX304	To identify the genes regulated by STAT3 when only Tyr705 is phosphorylated
SD vs pLX304	To identify the genes regulated by STAT3 when both Tyr705 and Ser727 are phosphorylated
YF/SA vs pLX304	To identify the genes regulated by STAT3 when both Tyr705 and Ser727 are unphosphorylated
YF/SD vs pLX304	To identify the genes regulated by STAT3 when only Ser727 is phosphorylated

Based on simple comparisons previously performed, an initial multiple comparison was carried out as proof of concept to validate that Ser727Asp mutation indeed mimics Ser727 phosphorylation at gene expression level.

Table 19. Multiple comparison to validate phosphomimetic Ser727Asp mutation

Multiple Comparison	Description
YFvspLX304 vs YFSDvspLX304	To validate whether Ser727Asp mutation mimics native pSer727 at gene expression level

One last multiple comparison was performed to identify common genes between each experimental condition, as well as to identify pSer727-dependent genes.

Table 20. Multiple comparison between all STAT3 phosphomutants

Multiple Comparison	Description
SAvspLX304 vs SDvspLX304 vs YFSAvspLX304 vs YFSDvspLX304	To identify common genes among all STAT3 phosphomutants, as well as genes dependent on Ser727 phosphorylation

Finally, to visualize common patterns of differentially expressed genes (expression profiles), they were clustered and represented as heatmaps.

12.7. Analysis of biological significance

To identify the signaling pathways associated to differential expression, an analysis of biological significance was performed in the web server g:Profiler (<https://biit.cs.ut.ee/gprofiler/gost>) using filtered (adj.P.Value <0.25, logFC >0.5) and ranked lists (according to adj.P.Value). Overrepresented *molecular functions* (MC), *cellular components* (CC), and *biological functions* (BF) were determined by using the *Gene Ontology* (GO) database, which is the most commonly used resource for pathway enrichment analysis. Since electronic GO annotations are not manually curated, they were discarded from this study to avoid less reliable results. It was considered statistically significant when adj.P.Value <0.05. The protocol followed is thoroughly described in ¹⁶⁸.

RESULTS

1. pSer727-STAT3 EXPRESSION LEVELS IN ccRCC PATIENTS (VALIDATION)

In 2014, our group described the expression of pSer727-STAT3 as an independent prognostic factor of survival in a study with 98 ccRCC patients⁶⁶, therefore, in this work, we aimed to validate this finding in a different cohort of 82 ccRCC patients.

The present study included 56 men (68.3%) and 26 women (31.7%) median age: 72 years range: 38–92, with ccRCC. The tumor was on the right side in 43 cases (52.4%) and left in 39 cases (47.6%). A total of 77 (93.9%) presented with localized tumors and 5 (6.1%) with metastasis. Sixty-eight patients (82.9%) underwent radical nephrectomy, while 14 underwent nephron-sparing surgery (tumorectomy or partial nephrectomy). Fuhrman grade grouped I-II consisted of 42 cases (51.2%), and III-IV consisted of 40 cases (48.8%). The most frequently observed tumor size (pT) stages were pT1a in 45.1% and pT1b in 23.2%. Lymphovascular invasion was present in only 3.6% of patients. Finally, the risk group was low in 43.9%, intermediate in 34.1% and high in 22% of patients studied (see Table 21). Because of the availability of novel targeted therapies since 2008, patients who recidivated (n=15) were treated with adjuvant therapy. All patients were considered for statistical analysis.

Immunostaining for pSer727-STAT3 was assessed in a TMA comprising the 82 ccRCC patients and 3 cores of benign areas far from the tumor were included as controls in each slide. Representative images of ccRCC tumors and normal tissue counterparts stained with a specific antibody against pSer727-STAT3 shown that unaffected normal tissue was negative for staining, whereas ccRCC tumors showed positive staining in nucleus and cytosol (see Figure 24). The presence of pSer727-STAT3 in the cytosol might be explained by recent reports indicating that pSer727-STAT3 locates and functions in mitochondria and endoplasmic reticulum. Moreover, some ccRCC tumors exhibited different localization patterns between nucleus and cytoplasm, suggesting that perhaps the degree of pSer727-STAT3 expression in one compartment or another determines different STAT3 functions at certain stages of tumor development.

Different from the previous TMA analysis, in this study, pSer727-STAT3 expression levels were analyzed both in the nucleus and the cytosol. Upon signal intensity evaluation using H-score, results were correlated with clinical outcome. H-score values of 80 and 40 (nucleus and cytosol, respectively) were arbitrarily determined as the threshold to distinguish patients with high or low pSer727-STAT3 staining. Kaplan-Meier estimates of mortality showed statistically significant differences in overall survival rates between patients with high versus low pSer727-STAT3 H-score. We found that both nucleus and cytosol correlate significantly with patient survival, however, the cytosolic levels were not statistically as relevant as those in the nucleus (see Figure 25). Multivariate analysis for nuclear (P= 0.008; 95% CI, 1.004–1.026) and cytosolic (P= 0.022; 95% CI, 1.003–1.042) pSer727-STAT3, indicates that its expression levels, indeed, correlates with classical clinicopathologic features. These results strongly validate the value of pSer727-STAT3 as an independent factor clinically relevant in ccRCC.

Table 21. Patients and tumor characteristics

Variable	No. (%) or variable unit
Patient age (years)	
Median	72.17
Mean (range)	70.56 (38-92)
Sex, No. (%)	
Male	56 (68.3)
Female	26 (31.7)
Tumor side	
Right	43 (52.4)
Left	39 (47.6)
Clinical presentation, No. (%)	
Radical	68 (82.9)
Neph. sparing	14 (17.1)
Adjuvant Treatment, No. (%)	15 (18.3)
Führman grade, No. (%)	
I-II	42 (51.2)
III-IV	40 (48.8)
Primary tumor size, No. (%)	
pT1a	37 (45.1)
pT1b	19 (23.2)
pT2	4 (4.9)
pT3a	13 (15.9)
pT3b	8 (9.8)
pT4	1 (1.2)
Lymphovascular invasion, No. (%)	
pNx	20 (24.4)
pN0	59 (72.0)
pN1	2 (2.4)
pN2	1 (1.2)
Metastasis, No. (%)	
pM0	77 (93.9)
pM1	5 (6.1)
Risk group, No. (%)	
Low	36 (43.9)
Intermediate	28 (34.1)
High	18 (22.0)
Follow-up (months)	
Median for all patients	79.57
Mean for all patients	72.15 (2-112)
Neph. sparing: nephron-sparing surgery, pT: tumor size, pN: nodal involvement, pM: metastasis	

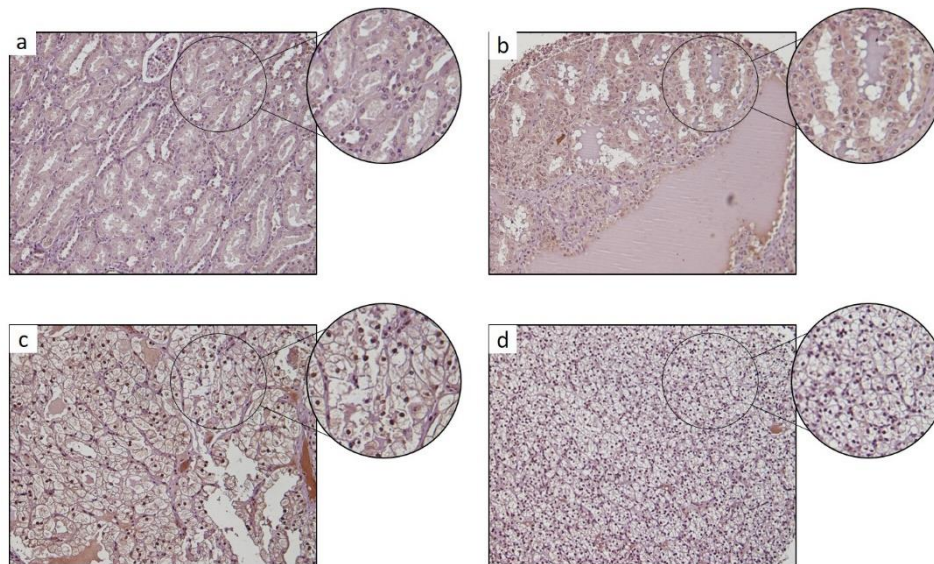


Figure 24. *pSer727-STAT3* expression in tumor samples from ccRCC patients. Representative images of a) normal counterparts and tumor samples displaying b) only cytosolic *pSer727-STAT3*; c) nuclear and cytosolic *pSer727-STAT3*; d) only nuclear *pSer727-STAT3*.

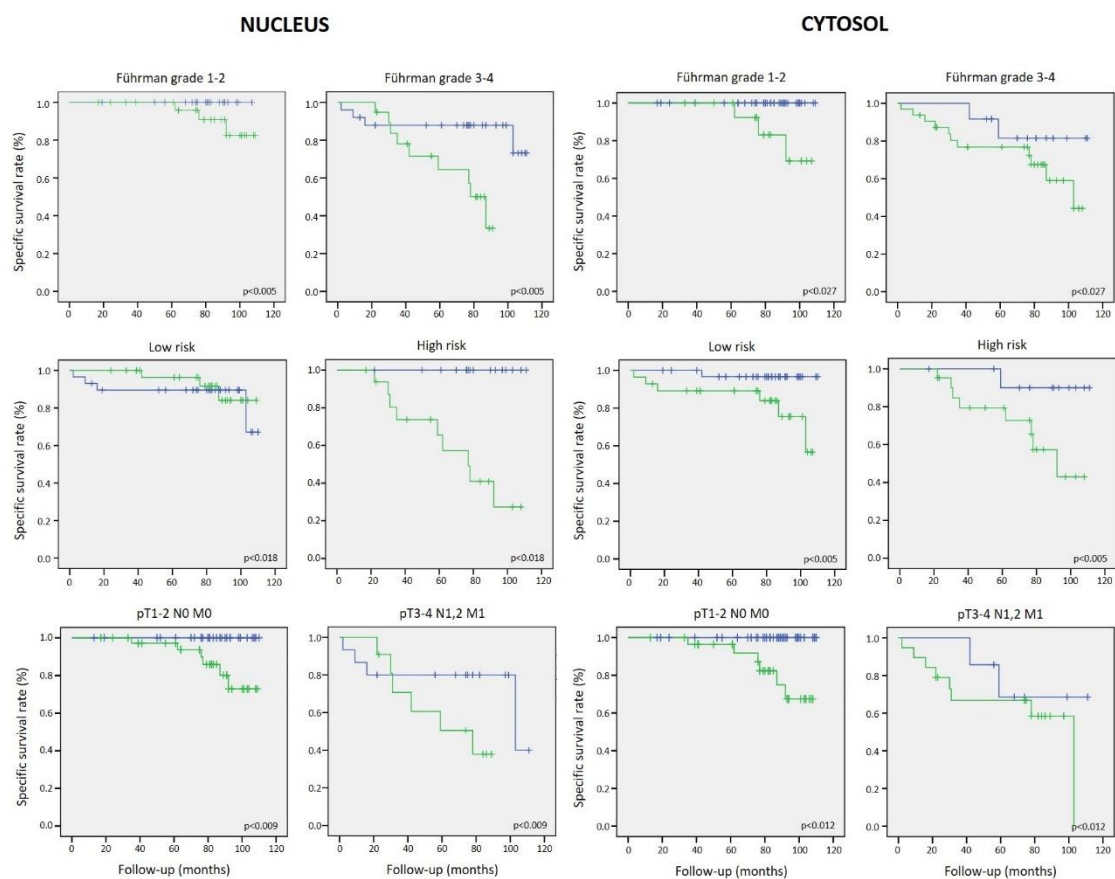


Figure 25. Correlation of *pSer727-STAT3* H-score with clinical outcome. Kaplan–Meier estimates of 120 months overall survival according to *pSer727-STAT3* H-score. Nuclear and cytosolic *pSer727-STAT3* staining was scored as: 0 = no appreciable staining; 1 = weak staining; 2 = moderate staining; and 3 = strong staining and calculated as 1 x (% weak) + 2 x (% moderate) + 3 x (% intense) ranging from 0 to 300. Correlation between nuclear *pSer727-STAT3* H-score expression levels (blue line, HS below 80; green line, HS above 80) (left panel) and cytosolic *pSer727-STAT3* H-score expression levels (blue line, HS below 40; green line, HS above 40) (right panel), and mean survival of ccRCC patients according to Fuhrman grade (1-2, 3-4), risk group (low, high), and clinical stage (pT1-2 N0 M0, pT3-4 N1,2 M1).

2. GENERATION AND CHARACTERIZATION OF STAT3 PHOSPHOMUTANTS

STAT3 and specially pTyr705-STAT3 has been largely related to oncogenic processes in several human cancers, however, our studies in ccRCC have demonstrated that pSer727 expression levels rather than pTyr705, correlates with a poor outcome of ccRCC patients. Therefore, we aim to elucidate the role of overall STAT3 phosphorylation state and especially the contribution of pSer727, on the genetic signature in ccRCC, in order to identify specific target genes of each STAT3 phosphorylation state. For that purpose, we created STAT3 phosphomutants (phosphoablative or phosphomimetic) and analyzed their effects on human-derived ccRCC cell lines: 769-P and 786-O.

2.1. STAT3 silencing

STAT3 is an essential molecule for cell survival and cannot be completely removed from cells, therefore, in order to be able to introduce STAT3 phosphomutants and analyze their effects, we first silenced endogenous STAT3 by using shRNAs that specifically target STAT3 mRNA for degradation. In this study, we tested 5 different shRNAs stably transduced in both ccRCC cell lines (769-P and 786-O) and evaluated their efficiency by western blot and RT-qPCR (see Figure 26). Our results showed that shRNA2 and shRNA3 were the most efficient in knockdown STAT3. According to the RT-qPCR, the efficiency of shRNAs in the 769-P cell line was: shRNA1 70.6%, shRNA2 80.6%, shRNA3 75.9%, shRNA4 62%, and shRNA5 had no effect; in turn, the efficiency in the 786-O cell line was: shRNA1 69.9%, shRNA2 79.3%, shRNA3 84%, shRNA4 67.2%, and shRNA5 14.2%. For both cell lines, the percentage of silencing was referred to pLKO, which corresponds to the parental cell line transduced with empty lentiviral vector (negative control of silencing).

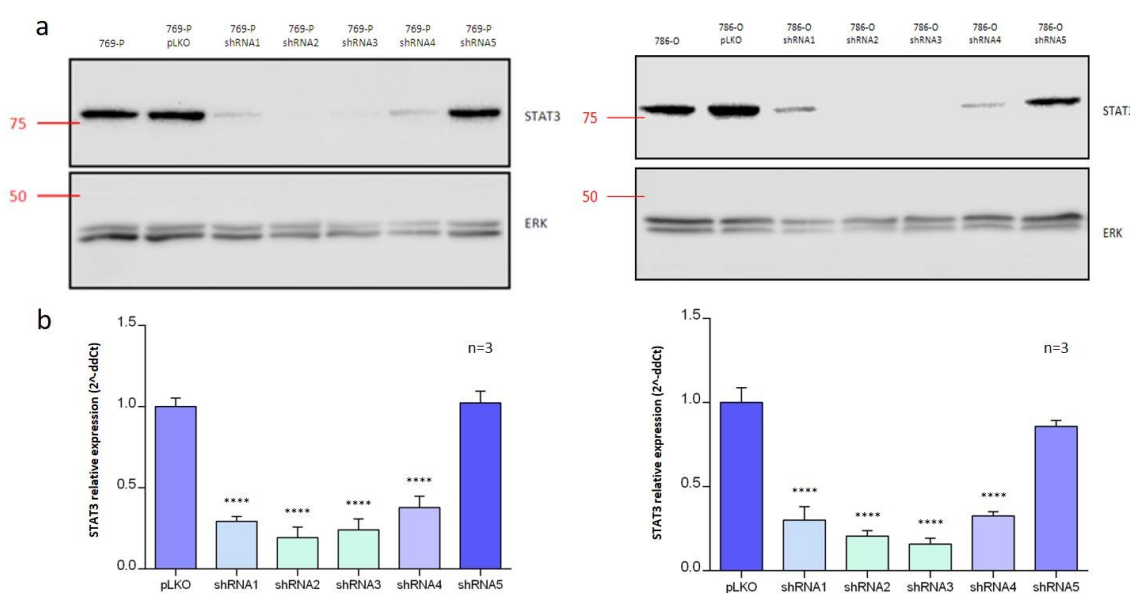


Figure 26. Silencing of endogenous STAT3 in the ccRCC cell lines 769-P and 786-O. a) Representative western blots showing shRNAs efficiency after lentiviral transduction in 769-P (left panel) and 786-O (right panel) cell lines. b) RT-qPCR of STAT3 expression after silencing in 769-P (left panel) and 786-O (right panel) cell lines. shRNA2 and shRNA3 were the most efficient in silencing STAT3 in both cell lines. pLKO (parental cell lines transduced with empty lentiviral vector) represents the negative control of silencing. Error bars represent means \pm SD. * Comparisons vs pLKO, $p < 0.05$.

Based on these results, we selected the cell lines transduced with shRNA2, who have similar and robust effect (~80% silencing) on both cell lines.

2.2. Generation of STAT3 phosphomutants

Once we have silenced endogenous STAT3, we created a “rescue” mutant. This strategy consisted of synonymous mutations upon the sequence recognized by shRNA2 to allow the reintroduction of STAT3 gene without being susceptible to degradation. Subsequently, we generated 5 different STAT3 simple and double phosphomutants: Tyr705Phe (YF), Ser727Ala (SA), Ser727Asp (SD), Tyr705Phe/Ser727Ala (YF/SA), and Tyr705Phe/Ser727Asp (YF/SD) over the “rescue” mutant. Phosphoablative mutants consisted of changes for phenylalanine or alanine (Tyr705Phe, Ser727Ala), whereas phosphomimetic mutant changed serine for aspartic acid (Ser727Asp). We did not generate a phosphomimetic mutant of Tyr705, because tyrosine substitutions that mimic phosphorylation are controversial. Many studies, indeed use aspartic or glutamic acid to simulate tyrosine phosphorylation, however, none of these amino acids actually have a tyrosine-like structure (due to its aromatic ring). Thus, the results of these studies should be taken with caution. A different approximation to analyze the effect of pTyr705 relies on its native activation after stimulation with IL6, which is a classic activator of STAT3 through Tyr705 phosphorylation.

Analysis of IL6 stimulation: To determine the effect of IL6 on STAT3 in our cell lines, 769-P and 786-O cells were stimulated with different concentrations of IL6 (0, 10, 30, 50, 100 and 200 ng/ml) at different times (15 min, 24 and 48 h) (see Figure 27). The results were analyzed by western blot showing that IL6 induces Tyr705 phosphorylation from 10 ng/ml (upper panel, second lane) and has a maximum effect at 15 min (lower panel, second lane), which is reduced but sustained until 48 h (lower panel). Moreover, Ser727 was found constitutively phosphorylated in both cell lines (upper and lower panels, first lanes) and stimulation with IL6 at any concentration and time had no effect on it.

These results demonstrate that stimulation with IL6 induces Tyr705 phosphorylation while it has no effect on Ser727, which is constitutively phosphorylated in both cell lines (769-P and 786-O).

Based on the previous results, we decided not to mutate Tyr705 and instead stimulate its native phosphorylation with IL6 [10 ng/ml]. Moreover, augmented IL6 circulating levels in plasma of ccRCC patients has been described¹³³, thereby, the use of IL6 in our cellular models resembles the actual scenario in patients.

Sequencing of STAT3 phosphomutants: Before lentiviral transduction of STAT3 phosphomutants, plasmids DNAs (vector and their corresponding inserts) were sequenced and aligned using STAT3 WT CDS as template. Our results confirmed that proper mutations were generated and no other random mutation occurred during site-directed mutagenesis (see Figure 28).

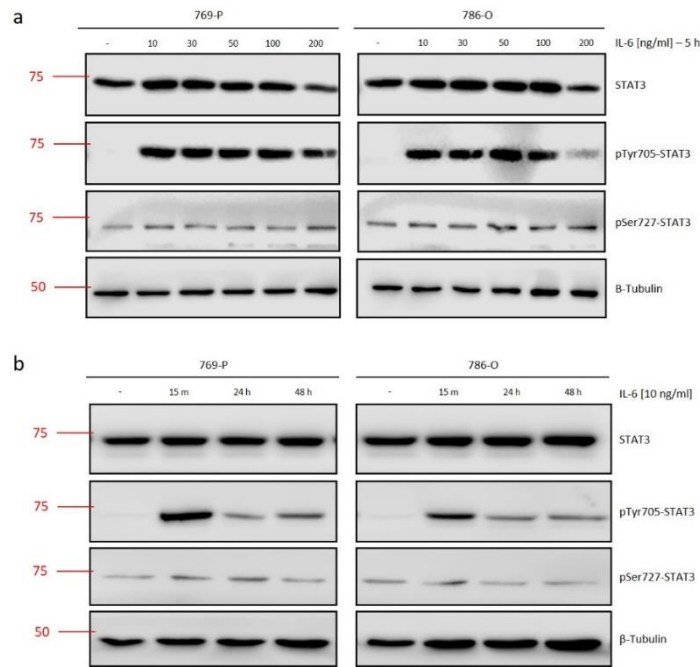


Figure 27. The effect of IL6 on STAT3 in 769-P and 786-O cell lines. a) Representative western blots of IL6 stimulation at different concentrations (0, 10, 30, 50, 100 and 200 ng/ml) showing that IL6 induces Tyr705 phosphorylation from 10 ng/ml and has no effect on Ser727, which is constitutively phosphorylated in both cell lines: 769-P (left panel) and 786-O (right panel). b) Representative western blots of IL6 stimulation [10 ng/ml] at different times (15 min, 24 and 48 h) showing that IL6 has a maximum effect on Tyr705 phosphorylation at 15 min and maintained until 48 h in 769-P (left panel) and 786-O (right panel) cell lines. Once more, IL6 has no effect on Ser727 phosphorylation at any time.

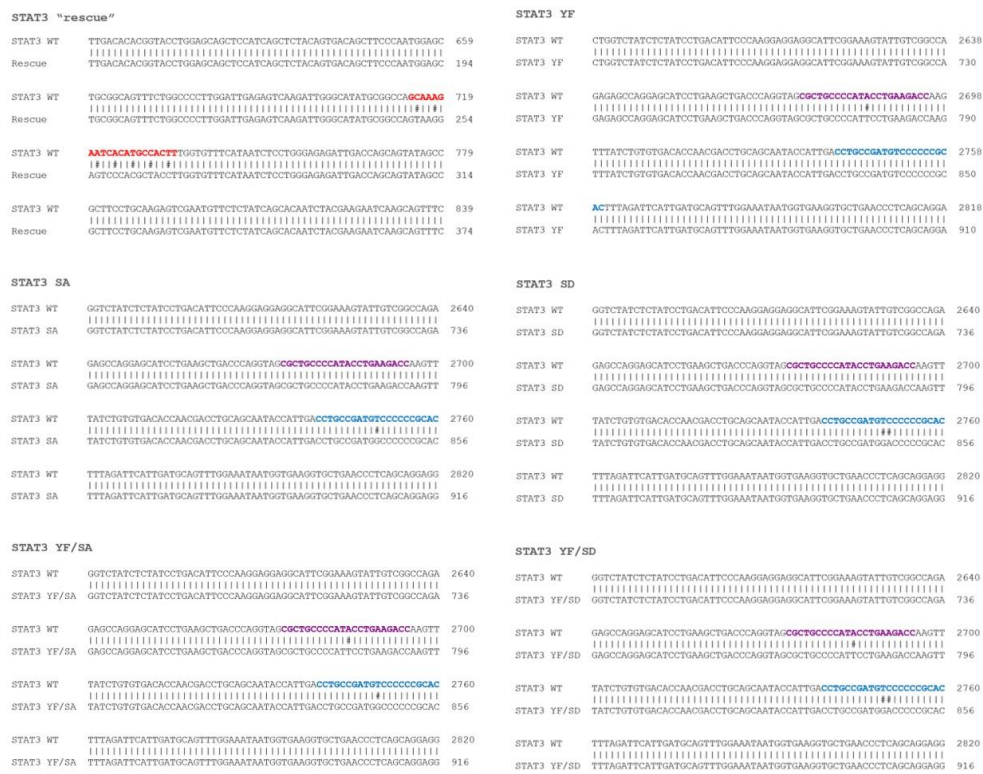


Figure 28. Sequencing and alignment of STAT3 phosphomutants. Partial sequences of STAT3 phosphomutants alignment after sequencing showing that appropriate mutations were placed. Base pairs in red correspond to "rescue" mutant, in purple to Tyr705 mutations, and in blue to Ser727 mutations. The # represents differences from template (STAT3 WT).

2.3. Overexpression and characterization of STAT3 phosphomutants

Once lentiviral transduction of STAT3 phosphomutants was performed, in previously silenced 769-P and 786-O cell lines (shRNA2), we characterized them by western blot and assessed their relative expression by RT-qPCR (see Figure 29). The banding pattern in the western blots showed the correct and uniform protein expression of STAT3 phosphomutants (upper panel). It can be also observed that specific antibodies against pTyr705 and pSer727 do not recognize these residues when they were mutated (lanes 3-7 of both blots), indicating that proper substitutions were placed in these sites. Moreover, stimulation with IL6 [10 ng/ml] for 30 min, induced the phosphorylation of Tyr705 in simple STAT3 mutants where Tyr705 remained native (lanes 4 and 5 of both blots). It is interesting to note that STAT3 WT has both residues phosphorylated, Tyr705 by stimulation with IL6 and Ser727 by the inherent mechanism in both ccRCC cell lines (lane 2 of both blots). The pLX304 cell line was transduced with empty overexpression lentiviral vector on previous silenced cell line, thus, it represents the negative control of overexpression in previously silenced cell lines (lane 1 of both blots). Furthermore, RT-qPCRs in both cell lines showed that STAT3 expression levels were similar among all mutants (lower panel), which represents a crucial feature to compare their phenotypic effects and transcriptional activity without biases.

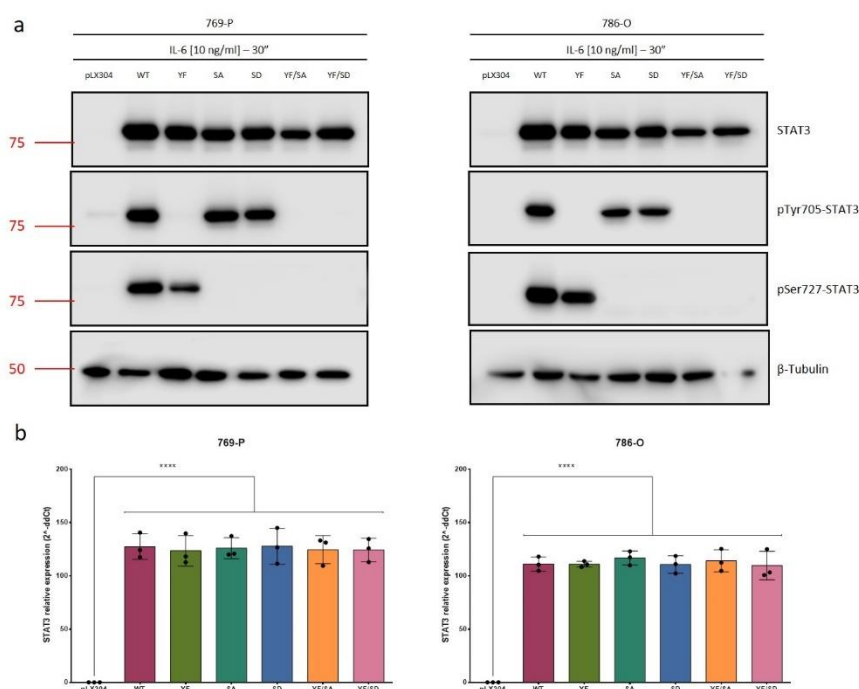


Figure 29. Overexpression of STAT3 phosphomutants in the ccRCC cell lines 769-P and 786-O. a) Representative western blots showing overexpression of STAT3 phosphomutants in 769-P (left panel) and 786-O (right panel) cell lines. Specific antibodies against pTyr705 and pSer727 do not recognize mutations at these sites as an indirect validation of proper mutations. Stimulation with IL6 induces pTyr705 in mutants where Tyr705 remained native. b) RT-qPCR of STAT3 expression in 769-P (left panel) and 786-O (right panel) cell lines. All mutants present similar relative expressions making them suitable for comparison. pLX304 (cell lines transduced with empty lentiviral vector of overexpression) represents STAT3 silencing. Error bars represent means \pm SD. * Comparisons vs pLX304, $p < 0.05$.

By generating these mutants, we ended up with a collection of different forms of phosphorylated STAT3. Although the main objective of this work was to determine the pSer727-dependent genes, we did not exclude the possibility of a dynamic phosphorylation process in STAT3, thus we covered all possible combinations between Tyr705 and Ser727. Since we decided to induce Tyr705 phosphorylation by stimulation with IL6 in all the experiments, the phosphomutants generated represent the following STAT3 phosphorylation states:

Table 22. STAT3 phosphomutants

STAT3 phosphomutant	Description
WT	Native STAT3 phosphorylation in ccRCC cell lines
YF	Unphosphorylated Tyr705, native Ser727 phosphorylation (YF/S ^p)
SA	Tyr705 phosphorylated by IL6, unphosphorylated Ser727 (Y ^p /SA)
SD	Tyr705 phosphorylated by IL6, phosphomimetic Ser727 (Y ^p /SD)
YF/SA	Both unphosphorylated Tyr705 and Ser727
YF/SD	Unphosphorylated Tyr705, phosphomimetic Ser727

It is important to highlight that YF and YF/SD represents the same STAT3 phosphorylation state. The YF mutant has a free Ser727, which in our cellular models is constitutively phosphorylated (see Figure 29). Therefore, the YF mutant was added to our collection, as a proof-of-concept to validate phosphomimetic mutation of Ser727 (SD).

The canonical STAT3 activation signaling pathway indicates that STAT3 is mainly found in the nucleus after Tyr705 phosphorylation, however, the non-canonical mechanisms of STAT3 activation have demonstrated that STAT3 can be also found in the cytosol, mitochondria, and endoplasmic reticulum. Moreover, it has been shown that STAT3 shuttles between the cytosol and the nucleus without the requirement of pTyr705. Therefore, we aimed to determine the cellular localization of our STAT3 phosphomutants. ICC experiments were performed in the presence of IL6 [10 ng/ml] showing that **all STAT3 phosphomutants localize at both compartments, cytosol, and nucleus** (see Figure 30). This result suggests that indeed, STAT3 shuttles between nucleus and cytosol in any of its phosphorylated forms, which could explain the transcriptional activity previously reported in the absence of the canonical pTyr705. Another possibility that cannot be dismissed is that overexpression by itself produces this localization pattern.

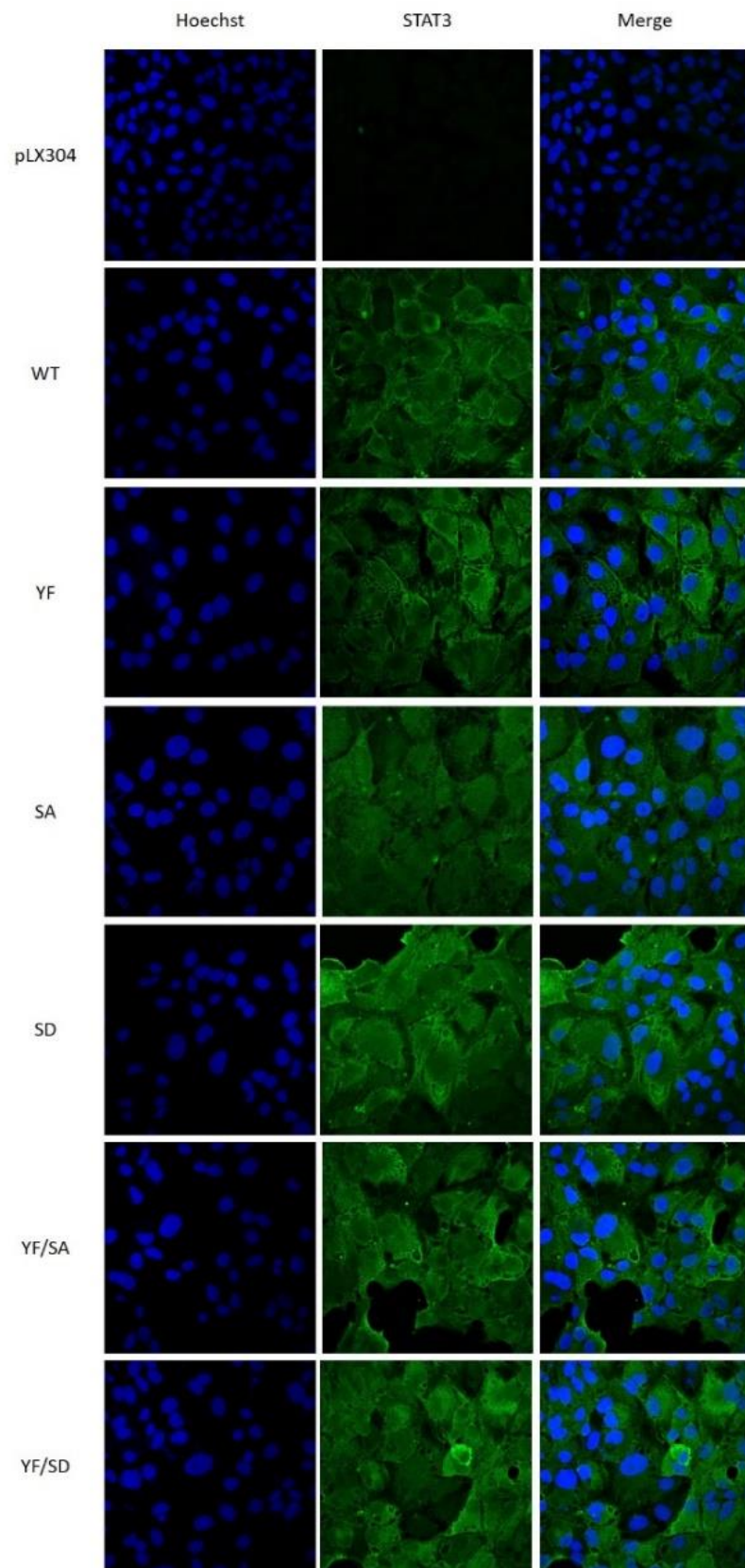


Figure 30. Localization of STAT3 phosphomutants by immunocytochemistry. Representative images of ICC showing that overexpressed STAT3 phosphomutants are located both in nucleus and in cytosol.

Our results showed that **phosphomimetic mutants of Ser727 (SD and YF/SD) exhibited the highest proliferation rates** compared with STAT3 WT. Moreover, no significant differences were found between these two mutants, suggesting that the effect observed is independent of the Tyr705 phosphorylation state. In addition, phosphoablative mutants of Ser727 (SA and YF/SA) displayed the lowest rates of proliferation. However, in this particular case, there were significant differences between them, indicating that in the absence of pSer727, pTyr705 contributes to cell growth. Finally, YF and YF/SD, representing the same STAT3 phosphorylation state, did not exhibit significant differences between them, as expected.

3.2. Phosphorylation at Ser727-STAT3 promotes migration

Cell migration or cell motility is an important feature for maintaining physiological processes within cells, however, under oncogenic conditions, tumor cells tend to display higher migration rates that often result in metastasis.

We evaluated the migration capacity of our STAT3 phosphomutants by using the wound-healing assay. Cells were incubated for 24 h in the absence of FBS to inhibit proliferation and promote only cellular migration, and migration was recorded by taking photographs every 30 min (see Figure 32).

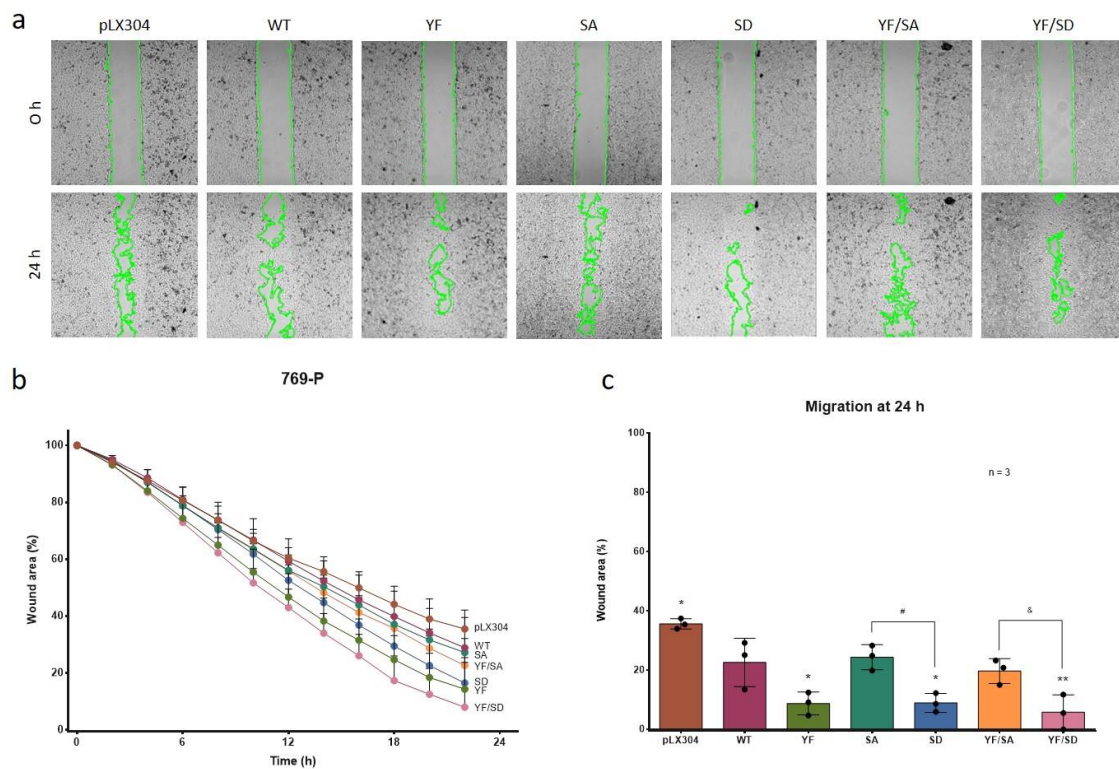


Figure 32. Migration capacity of STAT3 phosphomutants. a) Representative images of wound closure at 0 and 24 h. b) Migration rates plotted every 30 min showing that pSer727-STAT3 induces higher cell migration independently of Tyr705 (YF/SD, YF, and SD). c) Wound area to be closed at 24 h. Both graphs (a, b) indicate cell migration rates expressed as the percentage of the total wound area. Error bars represent means \pm SD. * Comparisons vs WT, $p < 0.05$; # Comparison between SA and SD, $p < 0.05$; & Comparison between YF/SA and YF/SD, $p < 0.05$.

These experiments showed that **phosphomimetic mutants of Ser727 (SD and YF/SD) exhibited higher motility rates** compared with STAT3 WT. Since no significant differences were found between these two mutants, we propose that the effect of pSer727 on migration is independent of Tyr705, as seen in proliferation. Furthermore, phosphoablative mutants of Ser727 (SA and YF/SA) did not show significant differences when compared to STAT3 WT.

3.3. Phosphorylation at Ser727-STAT3 favors colony formation

The clonogenic capacity is the ability of a single cell to produce colonies consisting of at least 50 cells. Since cancer cells undergo unlimited replicative division, the positive evaluation of this feature is often related to more aggressive phenotypes.

To assess the capacity of STAT3 phosphomutants to form colonies, cells were seeded at very low density, to avoid that cell-cell contact influenced proliferation, and incubated for 7 days. The resulting colonies were stained with crystal violet and counted by measuring the absorbance (see Figure 33).

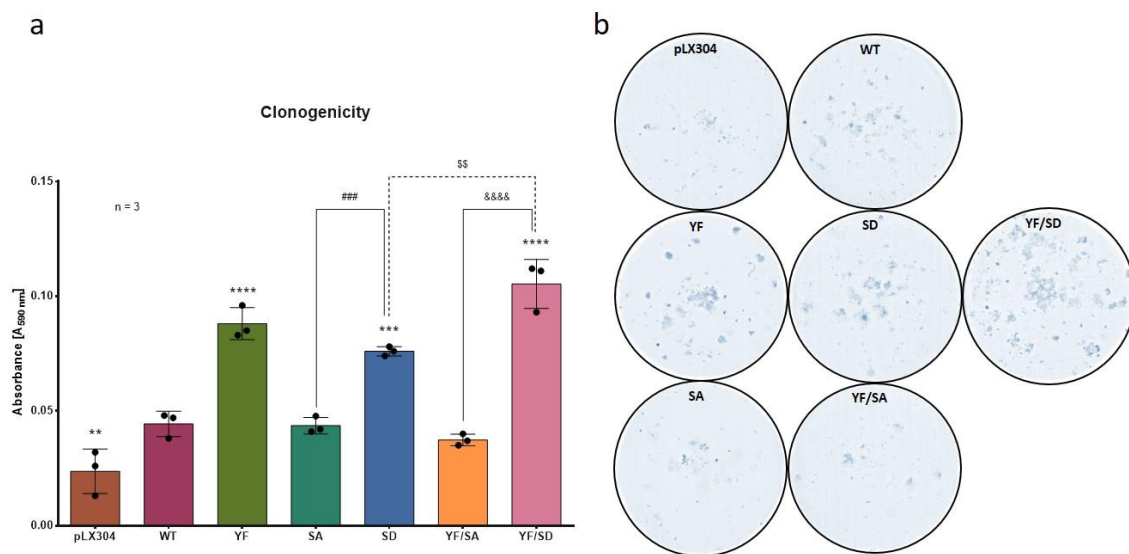


Figure 33. Clonogenic capacity of STAT3 phosphomutants. a) Clonogenic capacity expressed as absorbance of colonies formed and stained with crystal violet after 7 days of growth. b) Representative images of colony formation showing that the YF/SD mutant produces the highest number of colonies and STAT3 silencing (pLX304) the lowest. Error bars represent means \pm SD. * Comparisons vs WT, $p < 0.05$; # Comparison between SA and SD, $p < 0.05$; & Comparison between YF/SA and YF/SD, $p < 0.05$; \$ Comparison between SD and YF/SD, $p < 0.05$.

Our results showed, once more, that **phosphorylation of Ser727 induces augmented colony formation (SD and YF/SD)** compared to STAT3 WT. However, in this particular case, we did find significant differences between these two mutants, being YF/SD more clonogenic than SD. This result indicates that in the absence of cell-cell interactions, cellular division is mainly promoted when only Ser727 is phosphorylated (YF/SD). This observation suggests that pSer727 by itself promotes the expression of certain subset of genes involved in the development of more aggressive phenotypes, and moreover, that the overall STAT3 phosphorylation state leads to different cellular outcomes. No significant changes between phosphoablative mutants of Ser727 (SA and YF/SA) in comparison to STAT3 WT, were observed. The lack of significative differences between SA and YF/SA indicates that the contribution of pTyr705 in clonogenic capacity is substantially lower than pSer727.

3.4. Phosphorylation at Ser727-STAT3 increases anchorage-independent growth

The anchorage-independent growth is the ability of cells to grow independently of a solid surface and is a hallmark of carcinogenesis. The evaluation of this oncogenic characteristic represents one of the most stringent assays to predict aggressiveness and metastatic potential *in vitro* since it evaluates the capacity of cells to degrade the surrounding environment as well as their ability to create cell niches or colonies.

To evaluate anchorage-independent growth of STAT3 phosphomutants, cells were diluted and seeded in Noble Agar, left to grow for 28 days, and stained with NBT (which relies on the same principle that XTT). Colonies were photographed and counted (see Figure 34).

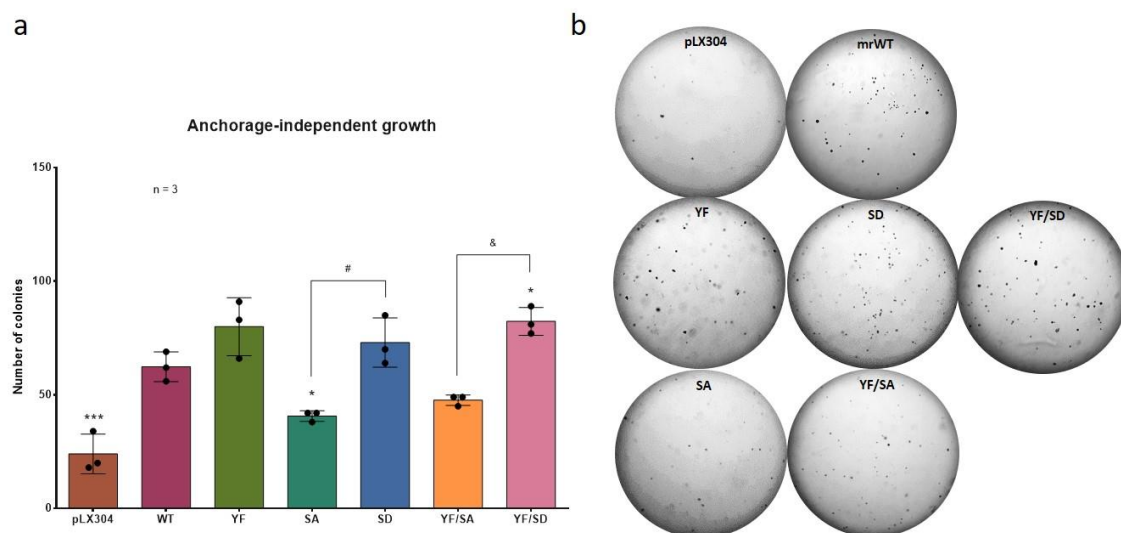


Figure 34. Anchorage-independent growth capacity of STAT3 phosphomutants. a) Anchorage-independent growth expressed as the number of colonies grown after 28 days, showing that only YF/SD mutant had a significantly higher effect compared to STAT3 WT. b) Representative images of soft-agar colony formation. Error bars represent means \pm SD. * Comparisons vs WT, $p < 0.05$; # Comparison between SA and SD, $p < 0.05$; & Comparison between YF/SA and YF/SD, $p < 0.05$.

In this experiment, although simple mutant SD showed a tendency to promote anchorage-independent growth, only the YF/SD mutant exhibit a significant increase compared to STAT3 WT. This result indicates that a **STAT3 phosphorylated at Ser727, in the absence of pTyr705, has a major effect on anchorage-independent growth than when both residues are phosphorylated.** Moreover, the phosphorylation of Tyr705 alone (SA), had a negative effect on anchorage-independent capacity and behaved similarly to STAT3 silencing (pLX304). Since this experiment is more restrictive than the previous ones, it was not surprising that only YF/SD mutant, which has exhibited more dominant effects in all the assays, was the only one that stands out showing a more oncogenic phenotype.

3.5. Phosphorylation at Ser727-STAT3 promotes cell aggregation

Cell aggregation is a phenomenon by which dissociated cells *in vitro* tend to group themselves. Although this phenomenon is not yet well-studied, it is thought to be related to cell-cell interactions.

This particular phenomenon was largely observed on some of the STAT3 phosphomutants, therefore we decided to record it in a proper way. To do so, we designed a simple protocol that consisted of dissociating the cells, vortexing them at full speed for 1 min and taking photographs as visual evidence of cell aggregation capacity (see Figure 35). It was observed that **STAT3 phosphomutants where Ser727 was phosphorylated either constitutively or by phosphomimetic mutation (YF, SD, and YF/SD) formed cellular aggregates**. This phenomenon could be related to the pSer727-induced expression of surface proteins that favor cell-cell interactions in suspension.

769-P

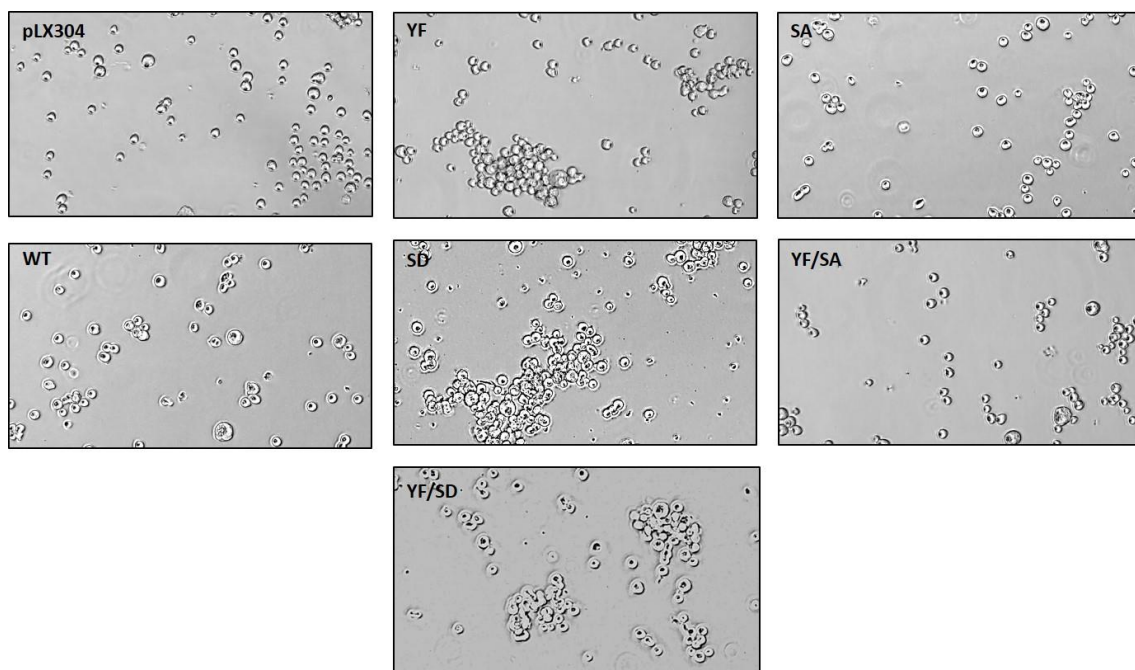


Figure 35. Cellular aggregation capacity of STAT3 phosphomutants. Representative images of dissociated cells after 1 min vortexing. It can be observed that STAT3 phosphomutants with native or phosphomimetic mutations for pSer727 (YF, SD, and YF/SD) form cellular aggregates. STAT3 phosphomutants where Ser727 phosphorylation was not induced, remain as single cells in suspension.

To this point, it is important to mention that **in all functional experiments previously described, STAT3 phosphomutants including STAT3 WT, were significantly more active compared to STAT3 silencing (pLX304)**. As pLX304 constitutes the absence of STAT3 within the cellular context, and STAT3 has been widely described in tumor development, these results were expected. Furthermore, **YF and YF/SD mutants exhibited the same behavior in each experiment, demonstrating that indeed, phosphomimetic mutation SD functions as a constitutively phosphorylated Ser727**.

3.6. None of the STAT3 phosphomutants induces cell adhesion

Cell adhesion is the capacity of cells to bind to the ECM, other cells or a specific surface, and is an essential feature for the growth and survival of cells. Cancer cells, especially the highly metastatic types, are believed to have enhanced adhesion ability that often facilitates migration to a new site to establish new tumors in different locations. Cell adhesion assay is therefore often used to evaluate the metastatic ability of cancer cells.

To evaluate cell adhesion capacity in STAT3 phosphomutants, we used collagen I as an ECM. Cells were seeded and allowed to adhere for 30 min. Cell adhesion was evaluated by staining cells with crystal violet and measured as absorbance at 590 nm (see Figure 36). Our results showed that **none of the STAT3 phosphomutants were significantly different, not even when compared to STAT3 silencing (pLX304) or STAT3 WT, suggesting that STAT3 is not involved in adhesion capacity.**

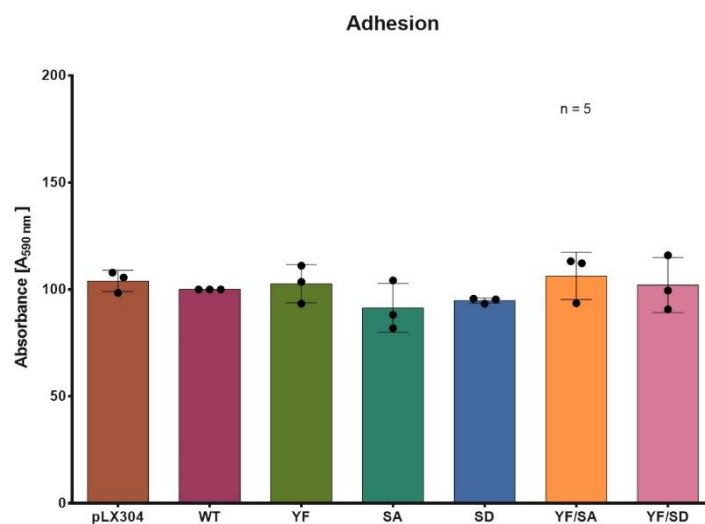


Figure 36. Cell adhesion capacity of STAT3 phosphomutants. No significant differences in adhesion capacity were found among STAT3 phosphomutants, suggesting that STAT3 is not involved in this process.

3.7. The absence of phosphorylation at Ser727-STAT3 promotes invasion

Invasion is defined as the direct extension and penetration of cells into neighboring tissues and is characteristic of cancer cells. During invasion, cancer cells secrete enzymes that degrade the ECM to move towards chemoattractants or to simply establish niches for growth. Metastatic cells often show more invasiveness due to their higher motility and/or enzymatic activity.

To evaluate the invasion capacity of STAT3 phosphomutants, we used the transwell assay consisting of a permeable membrane coated with Matrigel as ECM. The permeable membrane divides the transwell into two compartments that mimic two different sets of microenvironments: the upper side containing the cells and the lower side as the source of FBS as chemoattractant. Cells that invaded across the membrane after 48 h were fixed, stained with Hoechst and counted (see Figure 37). Surprisingly, it was observed that **phosphoablative mutants of Ser727 (SA and YF/SA) were the only ones with a significant increase in invasiveness** compared to STAT3 WT. Moreover, phosphomimetic mutants of Ser727 (SD and YF/SD) significantly exhibited lower invasive capacity. These results display a completely opposite behavior to the phenotype observed in previous experiments, however, it could be partially explained by the observation that STAT3 phosphomutants with native or induced pSer727 (YF, SD, and YF/SD) tended to cluster on the Matrigel layer (data not shown) as seen in suspension (see Figure 35). Therefore, this result suggests that pSer727 favors the formation of cell niches rather than invasion.

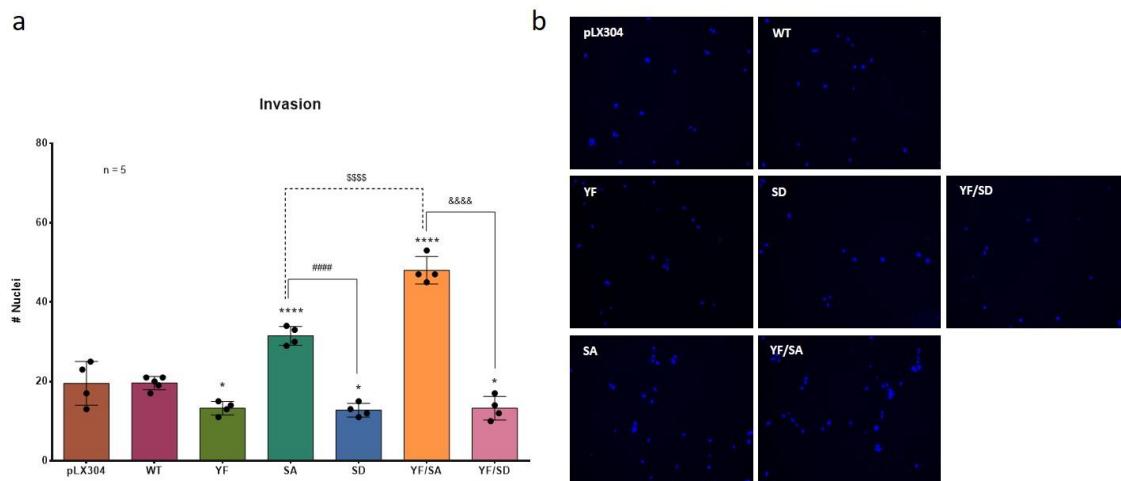


Figure 37. Invasion capacity of STAT3 phosphomutants. a) Invasion capacity expressed as the number of stained nuclei corresponding with invading cells. It can be observed that only phosphoablative mutants of Ser727 (SA and YF/SA) exhibited a significant higher invasion capacity compared to STAT3 WT. b) Representative images of stained nuclei found in the lower side of the permeable membrane after 48 h. Error bars represent means \pm SD. * Comparisons vs WT, $p < 0.05$; # Comparison between SA and SD, $p < 0.05$; & Comparison between YF/SA and YF/SD, $p < 0.05$; & Comparison between SA and YF/SA, $p < 0.05$.

Since the previous two assays evaluating adhesion and invasion capacity are highly related to the metastatic capacity of cells, the results obtained on both experiments, may be partially explained as a lack of metastatic properties in our cell lines.

3.8. All STAT3 phosphomutants form tumorspheres

Tumorspheres are solid, spherical structures developed from the proliferation of CSCs and represent a subpopulation of cells within a tumor with the ability to self-renew, drive tumor progression, drug resistance and metastatic properties. Tumorspheres are easily distinguishable from single or aggregated cells as these cells appear to fuse together (with a characteristic dark center) and individual cells do not.

In this study, the tumorspheres formation capacity was assessed to determine whether a certain STAT3 phosphorylation state results in a more CSC-like phenotype. Cells were seeded in an ultralow attachment surface (to maintain cells in suspension) and cultured for 10 days in a serum-free media supplemented with growth factors (see Figure 38). It was observed that **all STAT3 phosphomutants, including STAT3 WT and even STAT3 silenced (pLX304) were able to form tumorspheres**. This result could indicate that STAT3 is not involved in driving the CSC phenotype. Nevertheless, we also observed that phosphoablative mutants of Ser727 (SA and YF/SA) exhibited a higher number of dead cells around the tumorspheres. Moreover, the core of tumorspheres formed by SA and YF/SA seemed lighter and less compact than the ones formed by the other mutants. Based on these results, whether STAT3 and its phosphorylation state contribute to CSC phenotype remains unclear and more experiments should be carried out in order to solve this question.

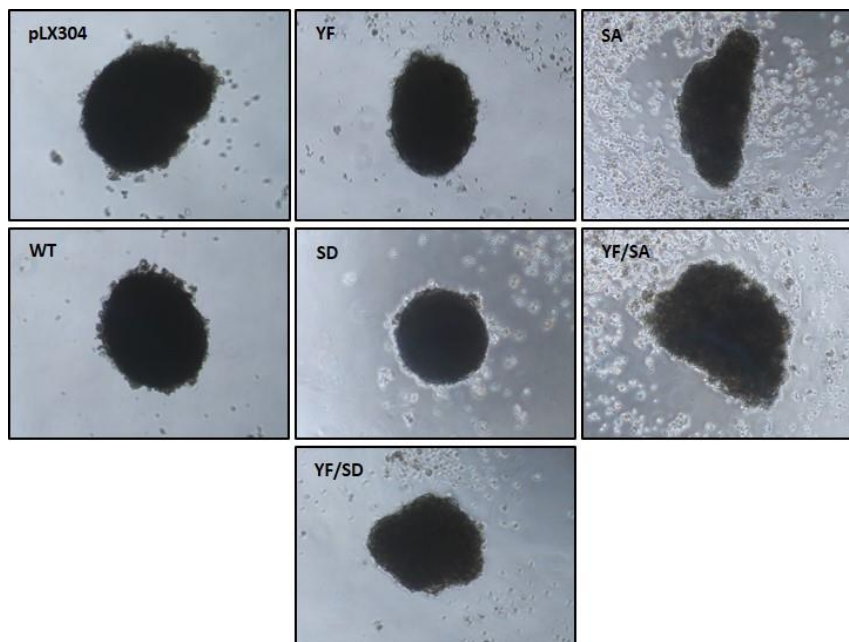


Figure 38. Tumorspheres formation capacity of STAT3 phosphomutants. Representative images of tumorspheres formed after 10 days of culture in a serum-free media supplemented with growth factors. It can be observed that all STAT3 phosphomutants including STAT3 and STAT3 silencing (pLX304) formed tumorspheres. SA and YF/SA mutants exhibited high cell mortality and their tumorspheres cores were lighter in comparison with the other mutants.

Since the functional characterization of STAT3 phosphomutants clearly showed phenotypic differences between Tyr705 and Ser727 phosphorylation, we decided to evaluate their effects on gene transcription through microarray analysis.

4. VALIDATION OF GENE EXPRESSION PROFILES FROM MICROARRAY

The main objective for microarray analysis was to identify the genes and their associated pathways regulated by the overall STAT3 phosphorylation state, as well as by Ser727-STAT3. Therefore, we used a Clariom S array that covers all known well-annotated genes (>20,000). 769-P cell lines transduced with STAT3 phosphomutants were stimulated with IL6 [10 ng/ml] to induce phosphorylation of Tyr705 in mutants where it was unchanged, and for maintaining homogeneity among samples. After 48 h, total RNA from 45 samples (9 experimental conditions with 5 replicates each) was extracted and reverse transcribed to cDNA to analyze transcriptome.

Microarray quality control: Before analyzing differential expression, raw data from microarray underwent quality control to identify potential outliers and was corrected for batch effect. In this study, all samples were distributed appropriately and passed quality control, thus they were accepted for normalization and further analysis. Furthermore, to increase statistical power and reduce unnecessary noise, genes that were not considered to be differentially expressed were removed based on their standard deviations (see Figure 39). Hence, the differential expression analysis was performed with 6485 genes.

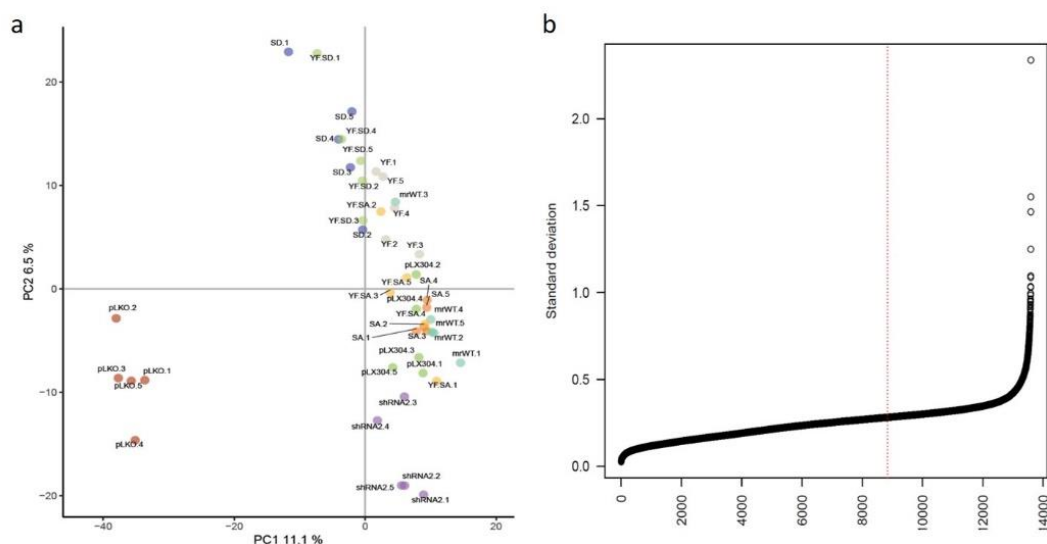


Figure 39. Quality control of microarray raw data. a) Principal component analysis (PCA) for normalized batch-corrected data showing clustering of samples according to their group. b) Standard deviations of all probesets in the microarray. The red line indicates the cut-off corresponding to probesets below the 65 percentile.

Initial observations: Initial comparisons between samples were carried out against its corresponding controls as follows: pLKO vs shRNA2, WT vs pLX304, YF vs pLX304, SA vs pLX304, SD vs pLX304, YF/SA vs pLX304, and YF/SD vs pLX304. STAT3 expression levels among phosphomutants showed similar fold change (logFC) values, corroborating the previous results obtained by RT-qPCR (see Figure 29) and indicating that there was no variability between samples to be concerned (see Table 23).

Table 23. STAT3 logFC values

Comparison	STAT3 expression	
	logFC	adj.P.Val
WT vs pLX304	5.13916	3.40E-40
YF vs pLX304	5.07374	6.08E-40
SA vs pLX304	5.05620	7.12E-40
SD vs pLX304	5.14054	3.35E-40
YF/SA vs pLX304	4.93790	2.09E-39
YF/SD vs pLX304	5.09523	5.02E-40

The selection of differentially expressed genes was based on an adj.P.Value <0.25 and a logFC >0.5, and yielded a list of genes sorted from most to least differentially expressed (see Table 24). The largest number of differentially expressed genes was obtained from pLKO vs shRNA2 (representing the genes regulated by endogenous STAT3 expression) and from SD vs pLX304 (representing the genes regulated by both pTyr705- and pSer727-STAT3), whereas SA vs pLX304 and YF/SA vs pLX304 comparisons (both carrying phosphoablative mutations for Ser727-STAT3) yielded the fewest differentially expressed genes.

Table 24. Differentially expressed genes (adj.P.value <0.25, logFC >0.5)

Comparison	Upregulated	Downregulated	Total
pLKO vs shRNA2	438	380	818
WT vs pLX304	123	126	249
YF vs pLX304	59	99	158
SA vs pLX304	74	58	132
SD vs pLX304	250	205	455
YF/SA vs pLX304	77	67	144
YF/SD vs pLX304	153	189	342

Microarray validation: To validate the results obtained from the microarray, an arbitrary selection of 5 of the most differentially expressed genes (see Table 25) among initial comparisons were selected and their expression was evaluated by RT-qPCR in both human-derived ccRCC cell lines 769-P and 786-O (see Figure 40). The results showed that the expression pattern of the genes selected (KRT20, FN1, WNT7A, ANKS4B, ALPK2, and IL6) corresponds with the differential expression analysis in both cell lines, thus the results obtained from microarray were considered reliable.

Table 25. Expression values from microarray

Gene Symbol	WT vs pLX304		YF vs pLX304		SA vs pLX304		SD vs pLX304		YF/SA vs pLX304		YF/SD vs pLX304	
	logFC	adj.P.Val	logFC	adj.P.Val	logFC	adj.P.Val	logFC	adj.P.Val	logFC	adj.P.Val	logFC	adj.P.Val
KRT20	-11.551	4.56E-07	-0.5899	9.61E-02	0.5083	9.03E-01	0.5337	7.73E-01	-0.5778	1.20E-01	0.8143	1.95E-04
FN1	-0.5273	1.14E-01	-15.816	1.75E-11	-0.5595	6.12E-01	-0.8035	1.08E-04	-0.5067	7.79E-01	-13.356	1.89E-09
WNT7A	0.5994	3.44E-01	0.7359	2.55E-02	0.6567	6.63E-02	-0.5354	8.34E-01	11.641	4.44E-05	0.5207	2.71E-01
ANKS4B	-0.7174	9.61E-02	0.7018	1.46E-01	-11.794	2.17E-03	11.861	4.17E-04	0.5608	8.73E-01	14.402	2.25E-05
ALPK2	0.5378	7.41E-02	-0.6964	1.29E-02	0.6766	1.86E-02	-10.268	2.30E-05	0.5225	9.34E-01	-12.216	7.18E-07
IL6	-10.021	8.10E-02	-10.912	6.06E-02	-0.5848	7.92E-01	-0.6899	2.45E-01	0.5076	9.84E-01	-10.403	4.27E-02

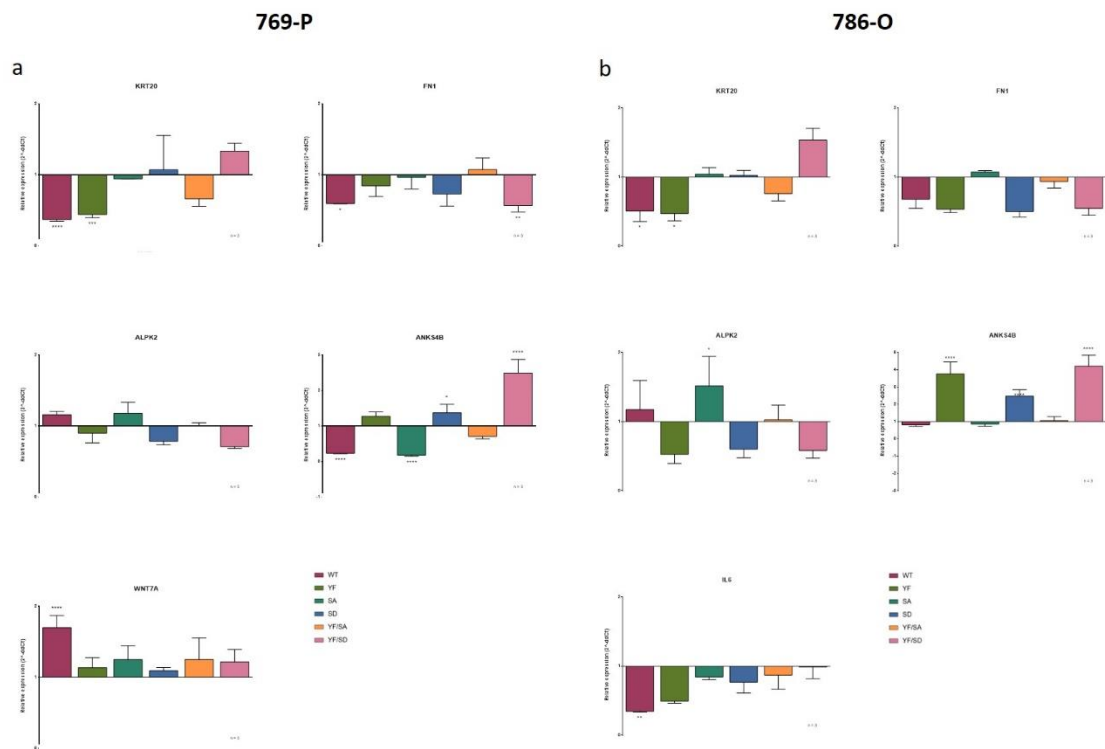


Figure 40. Validation of microarray results in ccRCC cell lines 769-P and 786-O by RT-qPCR. Relative expression of KRT20, FN1, WNT7A, ANKS4B, ALPK2 and IL6 in a) 769-P and b) 786-O cell lines. The expression pattern of the selected genes agrees with differential gene expression found in microarrays. The black line (y=1) represents pLX304 normalized values. Error bars represent means \pm SD. * Comparisons vs pLX304, $p < 0.05$.

5. TRANSCRIPTIONAL ACTIVITY OF STAT3 PHOSPHOMUTANTS

5.1. Endogenous STAT3 regulates the expression of 818 genes

To identify the genes regulated by endogenous STAT3 expression as well as the signaling pathways related to its native activation in the ccRCC cell line 769-P, gene expression between pLKO (empty vector of silencing: endogenous STAT3 expression) and shRNA2 (STAT3 silencing) was compared. This comparison yielded a total of 818 genes specifically regulated by endogenous STAT3 of which 438 were found upregulated and 380 downregulated (see table 26). The visualization of common patterns (heatmap) showed a clear opposite pattern and appropriate hierarchical clustering of groups, indicating that the differentially expressed genes founded are clearly regulated by endogenous STAT3 (see Figure 41).

Table 26. 30 most differentially expressed genes in pLKO vs shRNA2

Upregulated genes			Downregulated genes		
Gene Symbol	logFC	adj.P.Val	Gene Symbol	logFC	adj.P.Val
NTS	6.21531	2.53386E-32	TAGLN	-2.95926	2.65882E-11
AKR1B10	4.98557	7.38022E-28	LCP1	-2.42205	4.63559E-13
AKR1B15	4.71663	1.63865E-30	ADAMTS6	-2.29149	1.65336E-11
KRT20	3.78887	1.10211E-25	GFRA1	-2.21133	1.28977E-13
HABP2	3.34242	1.42805E-19	CGB2	-2.17622	1.94587E-13
TM4SF4	3.05886	2.71985E-18	MYL9	-2.14600	2.25049E-13
CLTRN	2.81502	1.38544E-15	CGB7	-2.14356	1.94587E-13
CPVL	2.76388	2.61058E-14	CLEC4E	-2.13043	4.55841E-09
LRP2	2.72827	3.00177E-12	INHBA	-2.12498	1.85537E-09
AKR1C2	2.64893	3.49950E-18	SNAI2	-2.10270	9.10034E-08
ACE2	2.50257	4.73629E-13	STX11	-1.94363	4.55841E-09
CFH	2.49010	5.14360E-14	ABCA1	-1.93293	2.62157E-16
LRRC19	2.36132	2.00409E-10	RNF182	-1.85063	1.47171E-13
SPRY1	2.32570	7.57390E-10	CCL2	-1.72628	1.23031E-06
MMP7	2.25922	2.78332E-13	ACTA2	-1.71191	3.28136E-12

The analysis of biological significance of the 818 differentially expressed genes in pLKO vs shRNA2 showed that they are mainly implicated in 20 *molecular functions* (MC) which include: NADP+ 1-oxidoreductase activity, steroid dehydrogenase activity, oxidoreductase activity, growth factor binding, actin-binding, extracellular matrix structural constituent, and monocarboxylic acid-binding, among others. These genes were also related to 20 *cellular components* (CC) which include: plasma membrane, extracellular space, endoplasmic reticulum, extracellular matrix, and cell projection, among others. Finally, 36 *biological processes* (BP) were found associated to endogenous STAT3 activity, including: cell adhesion, anaerobic alcohol metabolism processes, glycoside metabolism processes, regulation of cell population proliferation, response to wounding, lipid metabolic processes, circulatory system development, extrinsic apoptotic

signaling pathway, cell differentiation, cellular and tissue development, and extracellular structure organization, among others. To simplify overview, only the 15 most significant MF, CC and BP are shown (see Figure 42).

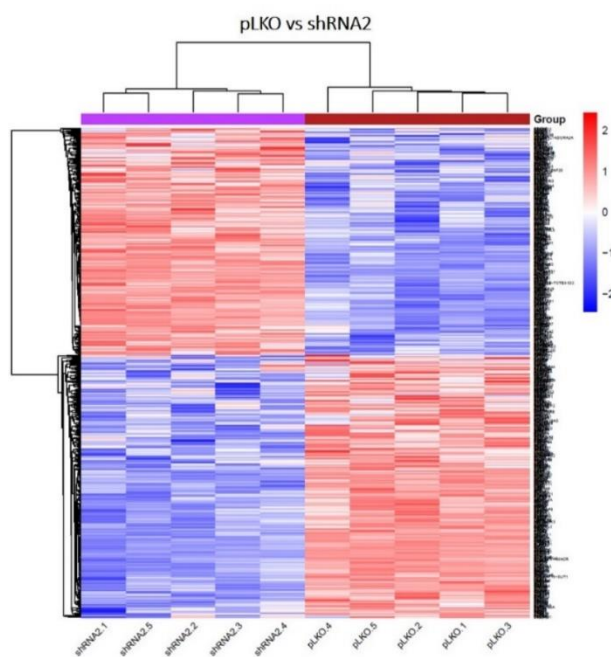
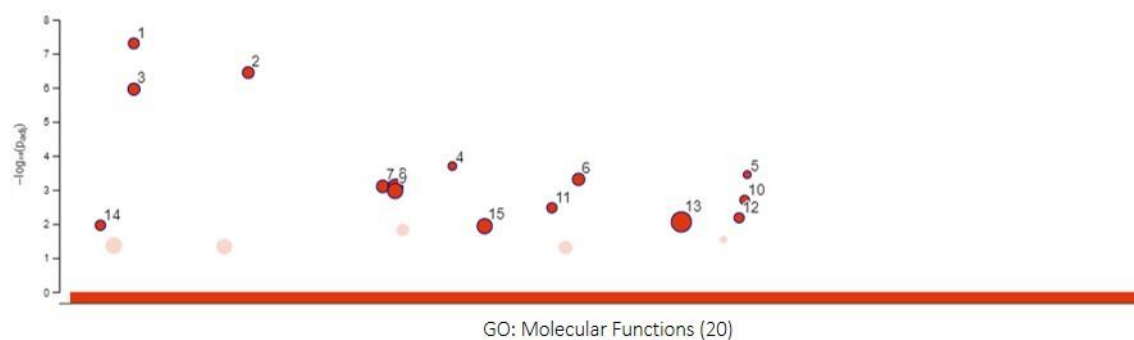
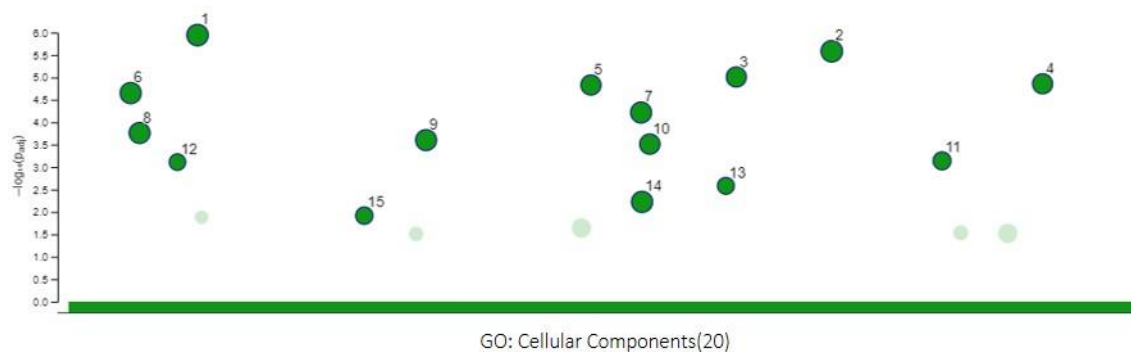


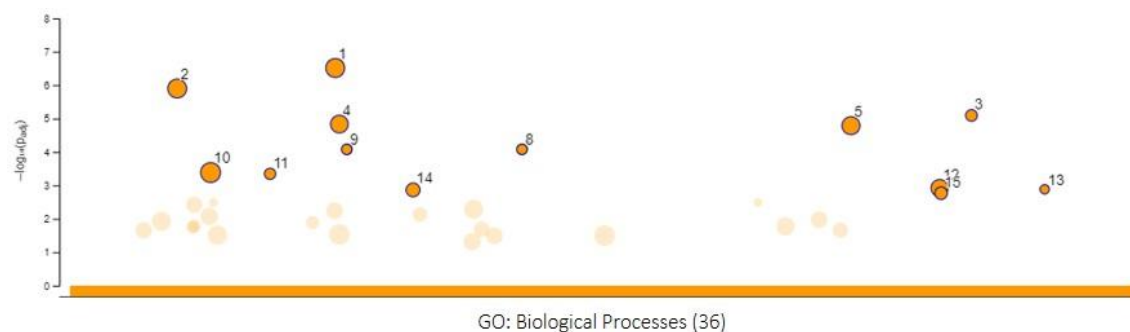
Figure 41. Heatmap: comparison between pLKO and shRNA2. Expression patterns of endogenous STAT3 (pLKO) vs STAT3 silencing (shRNA2). adj.P.Value <0.25 and logFC >0.5.



ID	Term Name	Term ID	adj.P.Val
1	alditol: NADP+ 1-oxidoreductase activity	GO:0004032	5.0E-08
2	alcohol dehydrogenase (NADP+) activity	GO:0008106	3.6E-07
3	aldo-keto reductase (NADP) activity	GO:0004033	1.1E-06
4	phenanthrene 9,10-monooxygenase activity	GO:0018636	2.0E-04
5	trans-1,2-dihydrobenzene-1,2-diol dehydrogenase activity	GO:0047115	3.6E-04
6	steroid dehydrogenase activity, acting on the CH-OH group of donors, NAD or NADP as acceptor	GO:0033764	4.9E-04
7	steroid dehydrogenase activity	GO:0016229	7.9E-04
8	oxidoreductase activity, acting on the CH-OH group of donors, NAD or NADP as acceptor	GO:0016616	8.1E-04
9	oxidoreductase activity, acting on CH-OH group of donors	GO:0016614	1.1E-03
10	ketosteroid monooxygenase activity	GO:0047086	2.0E-03
11	bile acid binding	GO:0032052	3.4E-03
12	androsterone dehydrogenase activity	GO:0047023	6.6E-03
13	ion binding	GO:0043167	8.7E-03
14	retinal dehydrogenase activity	GO:0001758	1.1E-02
15	growth factor binding	GO:0019838	1.2E-02



ID	Term Name	Term ID	adj.P.Val
1	plasma membrane	GO:0005886	1.1E-06
2	cell periphery	GO:0071944	2.6E-06
3	extracellular exosome	GO:0070062	9.8E-06
4	extracellular vesicle	GO:1903561	1.4E-05
5	extracellular organelle	GO:0043230	1.5E-05
6	extracellular region	GO:0005576	2.2E-05
7	extracellular region part	GO:0044421	6.1E-05
8	extracellular space	GO:0005615	1.7E-04
9	vesicle	GO:0031982	2.5E-04
10	plasma membrane part	GO:0044459	3.1E-04
11	plasma membrane region	GO:0098590	7.2E-04
12	endoplasmic reticulum lumen	GO:0005788	7.7E-04
13	collagen-containing extracellular matrix	GO:0062023	2.6E-03
14	membrane part	GO:0044425	6.0E-03
15	extracellular matrix	GO:0031012	1.2E-02



ID	Term Name	Term ID	adj.P.Val
1	biological adhesion	GO:0022610	3.1E-07
2	cell adhesion	GO:0007155	1.3E-06
3	tertiary alcohol metabolic process	GO:1902644	8.1E-06
4	regulation of cell adhesion	GO:0030155	1.5E-05
5	cell-cell adhesion	GO:0098609	1.6E-05
6	aminoglycoside antibiotic metabolic process	GO:0030647	8.3E-05
7	daunorubicin metabolic process	GO:0044597	8.3E-05
8	polyketide metabolic process	GO:0030638	8.3E-05
9	doxorubicin metabolic process	GO:0044598	8.3E-05
10	anatomical structure morphogenesis	GO:0009653	4.1E-04
11	glycoside metabolic process	GO:0016137	4.5E-04
12	organic hydroxy compound metabolic process	GO:1901615	1.2E-03
13	brush border assembly	GO:1904970	1.3E-03
14	primary alcohol metabolic process	GO:0034308	1.4E-03
15	quinone metabolic process	GO:1901661	1.7E-03

Figure 42. Dot plots of significant MF, CC, and BP found in pLKO vs shRNA2. g:Profiler analysis yielded 20 MF, 20 CC and 36 BP related to endogenous STAT3 expression (pLKO vs shRNA2) according to Gene Ontology (GO) database. The top 15 enriched terms are shown on the lists. adj.P.Value <0.05.

These results obtained from the differential expression analysis as well as from the biological significance analysis in pLKO vs shRNA2 are valuable because they represent the first molecular characterization of STAT3 role in ccRCC. We identified that **endogenous STAT3 regulates the expression of 818 genes implicated in important biological processes related to oncogenesis** such as cell adhesion, proliferation, cell motility, and apoptosis. Furthermore, some of the overrepresented MF found in our study **correlate with the ccRCC phenotype, such as an increased lipid and glycogen metabolism.**

5.2. STAT3 WT overexpression recovers the expression of 249 genes

To identify the genes regulated by STAT3 WT overexpression, we compared the gene expression between STAT3 WT (STAT3 overexpression) and pLX304 (empty vector of overexpression: STAT3 silencing). There were found **249 differentially expressed genes regulated by STAT3 WT overexpression of which 123 were found upregulated and 126 downregulated** (see table 27). The hierarchical clustering observed in the heatmap shows an opposite pattern as observed in pLKO vs shRNA2 (see Figure 43). Although the pattern of differentially expressed genes clearly indicates that they are regulated by STAT3 WT overexpression, it was expected that WT vs pLX304 comparison yielded a similar number of genes as pLKO vs shRNA2, however, technically, pLKO and WT cannot be compared because both contain different plasmids and possibly carrying different effects on cells.

Table 27. 30 most differentially expressed genes in STAT3 WT vs pLX304

Upregulated genes			Downregulated genes		
Gene Symbol	logFC	adj.P.Val	Gene Symbol	logFC	adj.P.Val
CNTN6	1.7767	1.63E-10	LCP1	-2.1329	2.86E-10
COL6A3	1.4310	5.42E-08	IL36B	-1.7864	1.15E-05
KCNIP1	1.3922	3.89E-09	SLCO1B3	-1.4607	4.62E-06
FLG	1.2653	1.15E-05	EHD2	-1.4496	1.11E-09
FGB	1.2098	6.64E-09	GALM	-1.4020	7.64E-06
AGT	1.1005	1.94E-04	CLTRN	-1.2649	3.42E-05
NNMT	1.0921	2.81E-05	KRT20	-1.1551	4.56E-07
CGB2	1.0798	8.02E-05	ST8SIA4	-1.1478	6.98E-05
VSTM4	1.0786	1.68E-06	SLC22A3	-1.1204	7.64E-06
EPHA7	1.0748	2.03E-07	IL18	-1.1175	4.07E-07
SLCO4C1	1.0425	1.06E-03	SLC6A20	-1.0948	1.40E-04
CGB7	0.9868	2.57E-04	ACE2	-1.0370	1.72E-03
FOLR1	0.9762	1.81E-04	IL6	-1.0021	8.10E-02
TRMT9B	0.9432	9.61E-04	PTX3	-1.0017	9.14E-02
SCN9A	0.9180	1.37E-04	SORBS2	-0.9568	8.85E-04

Based on the number of differentially expressed genes (249) from WT vs pLX304 comparison, the analysis of biological significance showed few overrepresented categories. There were found 5 MF consisting of sodium-independent organic anion transmembrane transporter activity, protein tyrosine kinase activator activity, receptor regulator activity, signaling receptor activator activity, and receptor-ligand activity. Nine CC were found overrepresented in STAT3 WT overexpression, all of them related to the cell membrane. Lastly, 8 BP were found including regulation of cell adhesion, extracellular matrix organization, and syncytium formation. (see Figure 44).

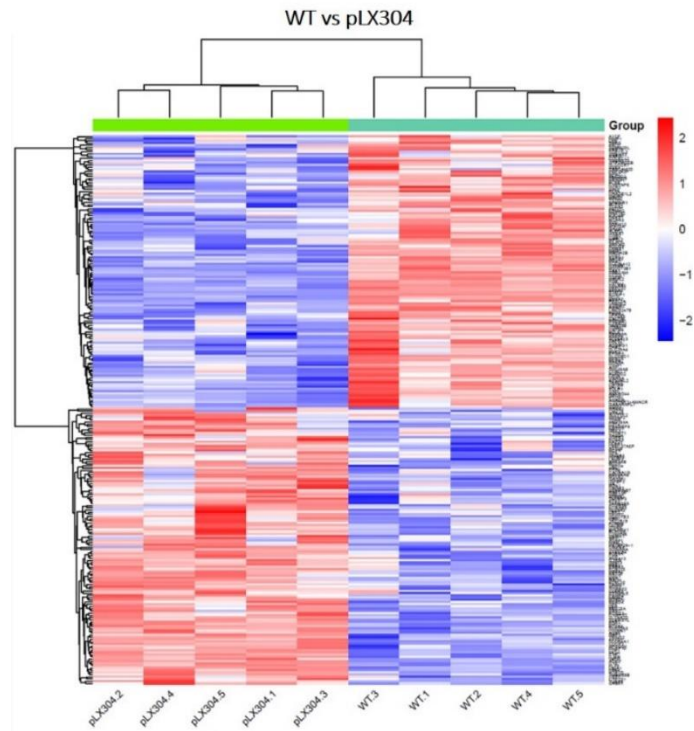
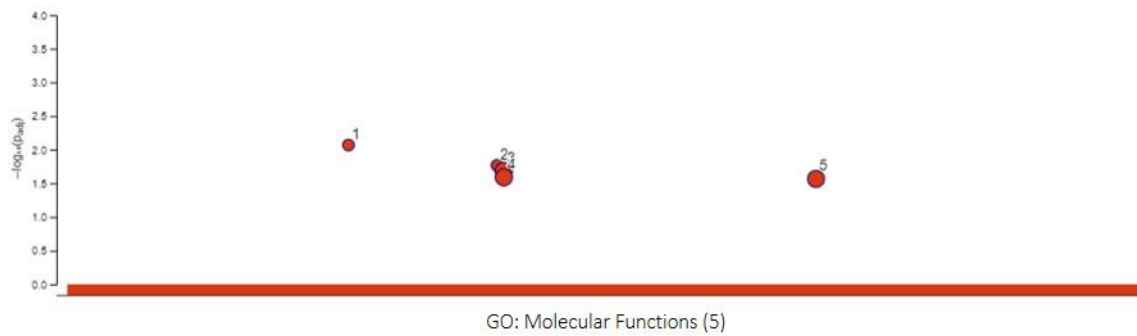
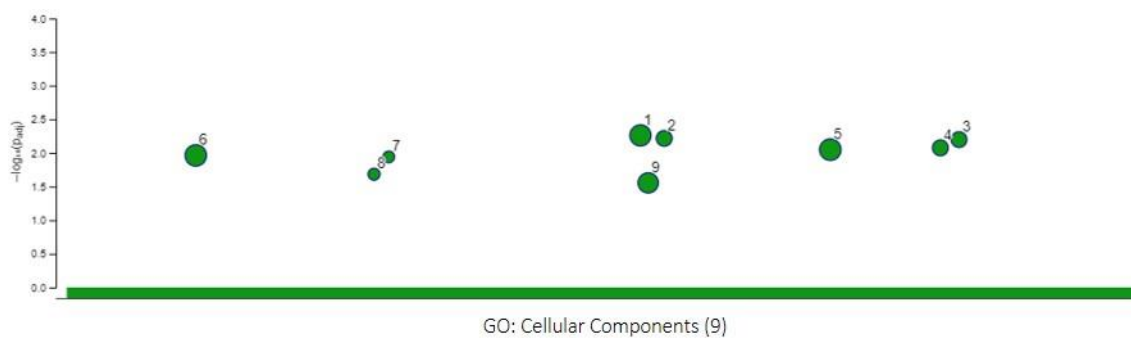


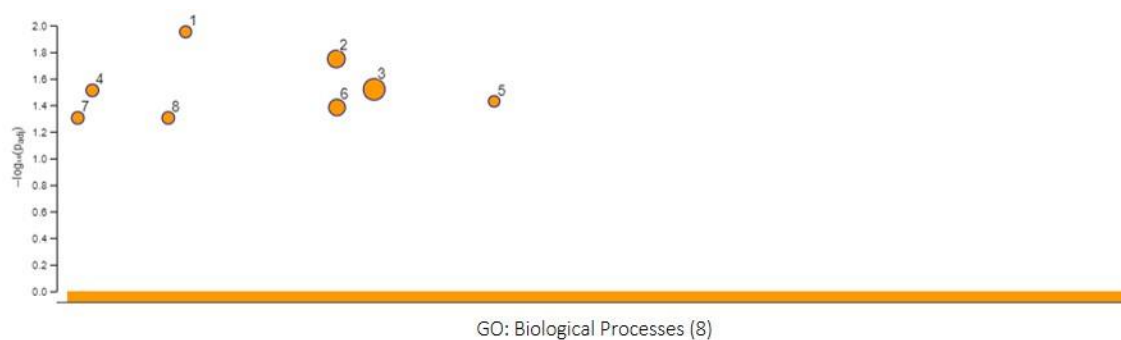
Figure 43. Heatmap: comparison between STAT3 WT and pLX304. Expression patterns of STAT3 WT overexpression (WT) vs STAT3 silencing (pLX304). adj.P.Value <0.25 and logFC >0.5.



ID	Term Name	Term ID	adj.P.Val
1	sodium-independent organic anion transmembrane transporter activity	GO:0015347	8.5E-03
2	protein tyrosine kinase activator activity	GO:0030296	1.7E-02
3	receptor regulator activity	GO:0030545	2.1E-02
4	signaling receptor activator activity	GO:0030546	2.6E-02
5	receptor ligand activity	GO:0048018	2.7E-02



ID	Term Name	Term ID	adj.P.Val
1	membrane part	GO:0044425	5.5E-03
2	membrane raft	GO:0045121	6.1E-03
3	membrane microdomain	GO:0098857	6.3E-03
4	membrane region	GO:0098589	8.4E-03
5	cell periphery	GO:0071944	8.9E-03
6	plasma membrane	GO:0005886	1.1E-02
7	anchored component of external side of plasma membrane	GO:0031362	1.1E-02
8	intrinsic component of external side of plasma membrane	GO:0031233	2.1E-02
9	plasma membrane part	GO:0044459	2.8E-02



ID	Term Name	Term ID	adj.P.Val
1	myoblast fusion	GO:0007520	1.1E-02
2	regulation of cell adhesion	GO:0030155	1.8E-02
3	multicellular organismal process	GO:0032501	3.0E-02
4	regulation of systemic arterial blood pressure by hormone	GO:0001990	3.1E-02
5	sodium-independent organic anion transport	GO:0043252	3.7E-02
6	extracellular matrix organization	GO:0030198	4.1E-02
7	syncytium formation	GO:0006949	5.0E-02
8	syncytium formation by plasma membrane fusion	GO:0000768	5.0E-02

Figure 44. Dot plots of significant MF, CC, and BP found in STAT3 WT vs pLX304. g:Profiler analysis yielded 5 MF, 9 CC and 8 BP related to STAT3 WT overexpression (WT vs pLX304) according to Gene Ontology (GO) database. The top enriched terms are shown on the lists. adj.P.Value <0.05

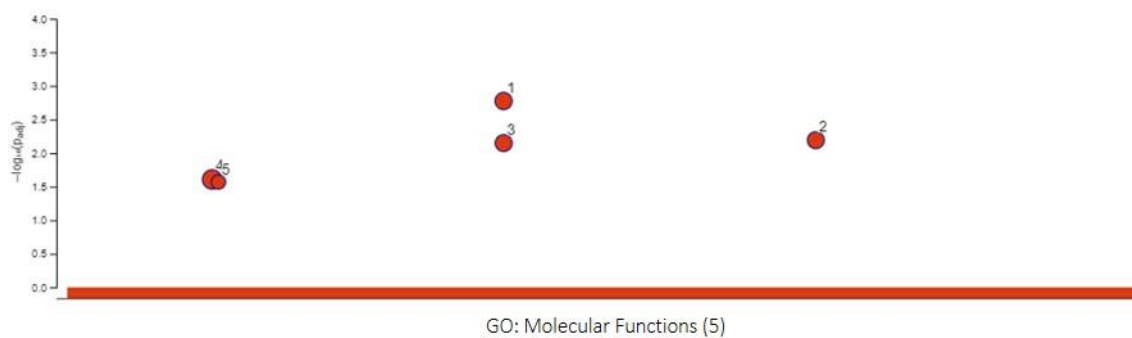
5.3. Phosphorylation of Tyr705-STAT3 (SA mutant) induces the expression of 132 genes.

To identify the genes regulated by pTyr705, we compared the gene expression between SA (Tyr705 phosphorylated by IL6, unphosphorylated Ser727) and pLX304 (empty vector of overexpression: STAT3 silencing). We found **132 differentially expressed genes regulated by pTyr705 (SA) overexpression of which 74 were upregulated and 58 downregulated** (see Table 28). This mutant exhibited the lowest number of differentially expressed genes to the other mutants, suggesting that the effect of pTyr705-STAT3 in the ccRCC cell lines 769-P is subtle.

Table 28. 30 most differentially expressed genes in SA vs pLX304

Upregulated genes			Downregulated genes		
Gene Symbol	logFC	adj.P.Val	Gene Symbol	logFC	adj.P.Val
NNMT	1.3285	1.06E-06	LCP1	-2.0427	1.73E-09
SAA1	1.0696	1.50E-03	ANKS4B	-1.1794	2.17E-03
FGB	1.0432	9.21E-07	IL36B	-1.1120	1.82E-02
KCNIP1	1.0005	2.51E-05	IL18	-1.0888	1.46E-06
AGT	0.9857	2.50E-03	UBD	-0.9863	1.50E-03
CNTN6	0.9215	8.74E-04	GPR34	-0.9197	1.54E-02
SCN9A	0.9091	5.39E-04	GALM	-0.9078	1.02E-02
TRMT9B	0.8953	4.44E-03	PDE9A	-0.8935	5.39E-04
CGB2	0.8951	2.81E-03	NOS3	-0.8700	4.63E-03
PTGDS	0.8490	1.80E-02	SLC6A20	-0.8328	1.09E-02
TCP11L2	0.8231	4.14E-02	TRIM31	-0.8317	2.19E-02
CDH6	0.8186	8.74E-04	C1S	-0.8236	7.74E-03
EFCAB13	0.8172	4.14E-02	GUCA2A	-0.8108	1.38E-02
CGB7	0.8121	7.74E-03	SLCO1B3	-0.7957	3.62E-02
TOMM20L	0.7907	2.30E-02	GFPT2	-0.7916	1.54E-02

The low number of differentially expressed genes (132) from SA vs pLX304 comparison produced a restricted analysis of biological significance, thus we only found 5 MF overrepresented: receptor regulator activity, receptor-ligand activity, signaling receptor activator activity, signaling receptor binding, and hormone activity. Moreover, there were no significant CC and only 3 significant BP: regulation of muscle adaptation, muscle adaptation, and tissue remodeling (see Figure 45).



ID	Term Name	Term ID	adj.P.Val
1	receptor regulator activity	GO:0030545	1.7E-03
2	receptor ligand activity	GO:0048018	6.4E-03
3	signaling receptor activator activity	GO:0030546	7.1E-03
4	signaling receptor binding	GO:0005102	2.5E-02
5	hormone activity	GO:0005179	2.7E-02



ID	Term Name	Term ID	adj.P.Val
1	regulation of muscle adaptation	GO:0043502	4.7E-03
2	muscle adaptation	GO:0043500	9.1E-03
3	tissue remodeling	GO:0048771	2.8E-02

Figure 45. Dot plots of significant MF, CC, and BP found in SA vs pLX304. g:Profiler analysis yielded 5 MF and 3 BP related to pTyr705-STAT3 (SA vs pLX304) according to Gene Ontology (GO) database. The top enriched terms are shown on the lists. adj.P.Value <0.05

5.4. Complete STAT3 phosphorylation (SD mutant) regulates the expression of 455 genes.

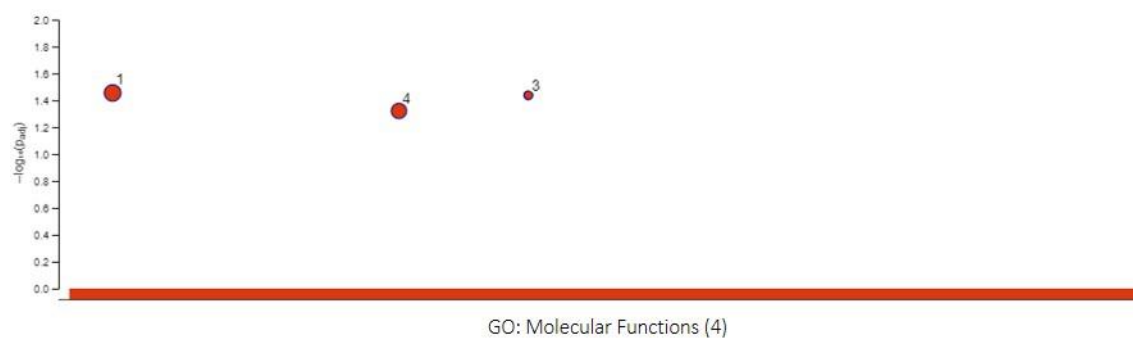
To identify the genes regulated by the complete phosphorylation state of STAT3 (pTyr705 and pSer727), we compared the gene expression between SD (Tyr705 phosphorylated by IL6, phosphomimetic pSer727) and pLX304 (empty vector of overexpression: STAT3 silencing). We found **455 differentially expressed genes regulated by SD overexpression of which 250 were upregulated and 205 downregulated** (see Table 29). This mutant showed **the highest number of differentially expressed genes**, which correlates with previous reports indicating that phosphorylation at both sites produced an optimal activation of STAT3.

Table 29. 30 most differentially expressed genes in SD vs pLX304

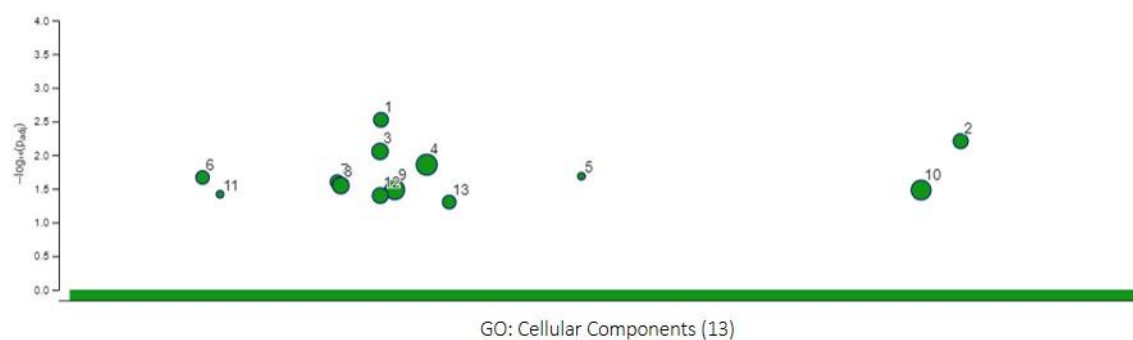
Upregulated genes			Downregulated genes		
Gene Symbol	logFC	adj.P.Val	Gene Symbol	logFC	adj.P.Val
CNTN6	2.7715	1.22E-17	LCP1	-3.1181	3.36E-16
PLPPR5	1.6484	6.19E-09	PTX3	-1.7359	1.83E-04
SLC6A13	1.4414	3.33E-05	GBP1	-1.6894	1.57E-08
A1CF	1.3771	5.03E-07	EDN2	-1.6772	1.01E-06
SLCO4C1	1.2966	2.25E-05	TRIM22	-1.5995	6.17E-09
FGB	1.2790	1.80E-09	CLEC4E	-1.5649	2.41E-05
DDIT4	1.2570	5.03E-07	CTSS	-1.4597	2.57E-06
C1QTNF3-AMACR	1.2482	3.06E-06	UBD	-1.3528	1.85E-06
TEAD2	1.2189	1.85E-05	TNFAIP3	-1.3526	3.40E-04
AMACR	1.2057	1.42E-05	ROR1	-1.3444	3.44E-07
PLXDC2	1.1949	2.71E-07	TAGLN	-1.3269	1.70E-03
KCNJ13	1.1894	1.49E-03	ANKRD1	-1.3062	1.34E-03
ANKS4B	1.1861	4.17E-04	MYL9	-1.2977	1.71E-06
METTL7A	1.1761	2.62E-03	C1S	-1.2825	2.38E-06
CFI	1.0827	6.11E-04	SNAI2	-1.2576	2.38E-03

The analysis of biological significance of the 455 differentially expressed genes in SD vs pLX304 comparison showed that they are mainly implicated in 4 MF consisting of actin-binding, endothelin B receptor binding, bombesin receptor binding, and oxidoreductase activity, acting on paired donors, with incorporation or reduction of molecular oxygen. These genes were also found significant in 13 CC, most of them related to cell motility processes which include: cell leading edge membrane, actin-based cell projection, filopodium, cell projection membrane, and ruffle membrane, among others. Moreover, 31 BP were found significant, which include: response to external stimulus, ERK1 and ERK2 cascade, cell adhesion, immune system processes, response to interferon-gamma, positive regulation of cell migration, chemotaxis, positive regulation of cell motility, and cellular response to interleukin 1, among others. To simplify overview, only the 15 most significant BP are shown (see Figure 46).

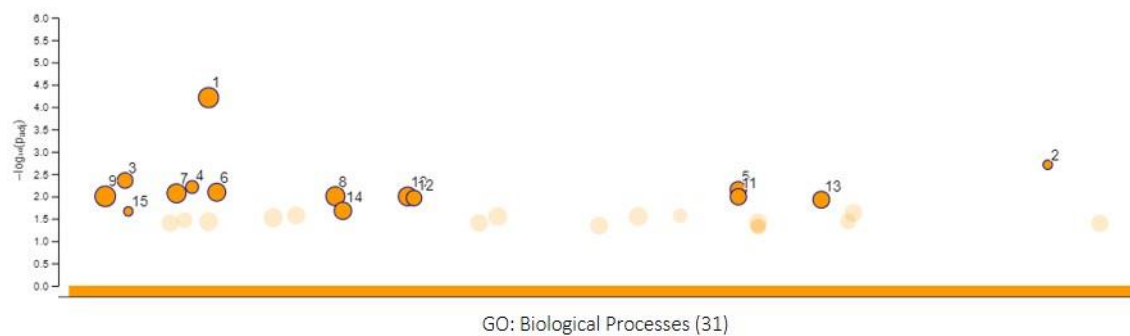
If we compare the effect of SA mutant (Tyr705 phosphorylated by IL6), where only 132 genes were differentially expressed, with SD (both pTyr705 and pSer727), the result clearly suggests that **phosphorylation at Ser727 substantially increases STAT3 activity**. Moreover, the sets of genes induced when both residues are phosphorylated are mainly related to cell motility, which is a hallmark of carcinogenesis. Our functional experiments also support this observation, i.e. experiments to evaluate migration capacity showed that migration rates in SD mutant were significantly higher than SA mutant (see Figure 32).



ID	Term Name	Term ID	adj.P.Val
1	actin binding	GO:0003779	3.5E-02
2	endothelin B receptor binding	GO:0031708	3.6E-02
3	bombesin receptor binding	GO:0031705	3.6E-02
4	oxidoreductase activity, acting on paired donors, with incorporation or reduction of molecular oxygen	GO:0016705	4.8E-02



ID	Term Name	Term ID	adj.P.Val
1	leading edge membrane	GO:0031256	3.0E-03
2	actin-based cell projection	GO:0098858	6.2E-03
3	cell leading edge	GO:0031252	8.8E-03
4	vesicle	GO:0031982	1.4E-02
5	TAP complex	GO:0042825	2.1E-02
6	brush border	GO:0005903	2.1E-02
7	filopodium	GO:0030175	2.5E-02
8	axon	GO:0030424	2.8E-02
9	cytoplasmic vesicle	GO:0031410	3.3E-02
10	intracellular vesicle	GO:0097708	3.3E-02
11	guanylate cyclase complex, soluble	GO:0008074	3.8E-02
12	cell projection membrane	GO:0031253	4.0E-02
13	ruffle membrane	GO:0032587	5.0E-02



ID	Term Name	Term ID	adj.P.Val
1	response to external stimulus	GO:0009605	6.2E-05
2	brush border assembly	GO:1904970	2.0E-03
3	heart morphogenesis	GO:0003007	4.4E-03
4	neuron recognition	GO:0008038	6.2E-03
5	ERK1 and ERK2 cascade	GO:0070371	7.1E-03
6	animal organ morphogenesis	GO:0009887	8.1E-03
7	cell adhesion	GO:0007155	8.5E-03
8	biological adhesion	GO:0022610	9.9E-03
9	immune system process	GO:0002376	1.0E-02
10	response to cytokine	GO:0034097	1.0E-02
11	regulation of ERK1 and ERK2 cascade	GO:0070372	1.0E-02
12	response to interferon-gamma	GO:0034341	1.1E-02
13	regulation of anatomical structure size	GO:0090066	1.2E-02
14	positive regulation of cell migration	GO:0030335	2.1E-02
15	regulation of systemic arterial blood pressure by endothelin	GO:0003100	2.2E-02

Figure 46. Dot plots of significant MF, CC, and BP found in SD vs pLX304. g:Profiler analysis yielded 4 MF, 13 CC, and 31 BP related to complete STAT3 phosphorylation (SD vs pLX304) according to Gene Ontology (GO) database. The top 15 enriched terms are shown on the lists. adj.P.Value <0.05

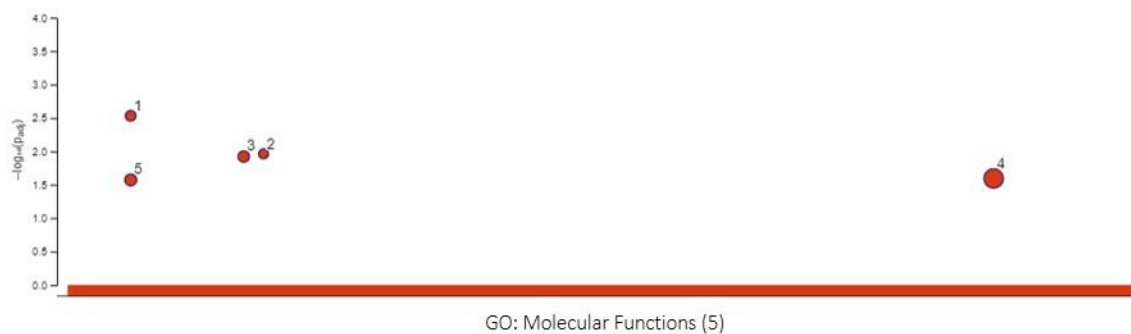
5.5. Unphosphorylated STAT3 (YF/SA mutant) induced the expression of 144 genes.

To identify the genes regulated by the absence of phosphorylation in STAT3 (neither pTyr705 nor pSer727), the gene expression between YF/SA (both unphosphorylated Tyr705 and Ser727) and pLX304 (empty vector of overexpression: STAT3 silencing) was compared. We found **144 differentially expressed regulated by YF/SA overexpression of which 77 were upregulated and 67 downregulated** (see Table 30). Interestingly, this mutant showed a slight increase in differential gene expression compared to the lowest gene expression in SA mutant. It could be reasonable to think that unphosphorylated STAT3 should behave as the absence of STAT3 (pLX304), however, some studies have pointed out that unphosphorylated STAT3 can regulate gene transcription of a subclass of target genes and that also it can form a complex with NFκB, as a non-canonical STAT3 activation.

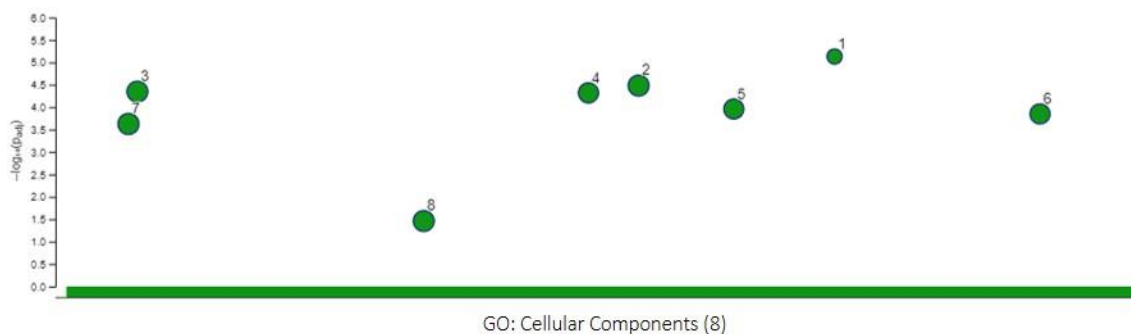
Table 30. 30 most differentially expressed genes in YF/SA vs pLX304

Upregulated genes			Downregulated genes		
Gene Symbol	logFC	adj.P.Val	Gene Symbol	logFC	adj.P.Val
CNTN6	1.6522	8.67E-10	C1S	-2.4756	1.80E-14
WNT7A	1.1641	4.44E-05	CFH	-2.4062	9.42E-13
PLPPR5	1.0606	1.35E-04	TRIM22	-1.6938	1.04E-09
RENBP	0.9980	3.80E-04	CFB	-1.6682	5.38E-09
EPHA7	0.9218	8.41E-06	CFI	-1.3759	3.56E-05
HS3ST3B1	0.9094	8.97E-06	CP	-1.3139	5.38E-09
NPNT	0.8948	2.72E-03	LCP1	-1.1433	3.80E-04
HS3ST3A1	0.8687	4.35E-05	GBP1	-0.9470	2.40E-03
DOCK2	0.8625	3.77E-03	IRF9	-0.9241	2.17E-05
SLC6A13	0.8311	7.48E-02	TGM2	-0.9141	8.97E-06
PSG8	0.8226	4.64E-03	GBP2	-0.9089	2.10E-06
PSG1	0.8208	3.58E-04	EPAS1	-0.8568	2.45E-06
AKR1B10	0.8163	4.64E-03	APOL1	-0.8358	8.97E-06
PSG3	0.8143	2.64E-03	CST2	-0.8335	2.24E-03
AKR1B15	0.8124	2.43E-04	RAB27B	-0.8082	5.48E-05

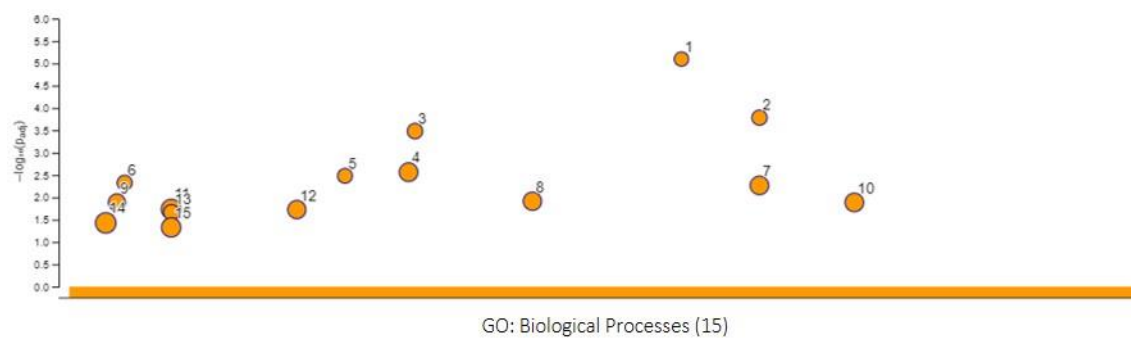
The analysis of biological significance of the 144 differentially expressed genes from YF/SA vs pLX304, showed few overrepresented categories. There were found 5 MF consisting of alditol NADP+ 1-oxidoreductase activity, heparan sulfate glucosamine 3-sulfotransferase 1 activity, alcohol dehydrogenase (NADP+) activity, molecular function regulator, and aldo-keto reductase (NADP) activity. Eight CC were found overrepresented of which 6 are related to extracellular processes. Lastly, 15 BP were found to be significant (see Figure 47). Once more, it is interesting that the 3 most significant biological processes founded were related to interferon-gamma because it is one of the main activators of the NFκB signaling pathway.



ID	Term Name	Term ID	adj.P.Val
1	alditol: NADP+ 1-oxidoreductase activity	GO:0004032	2.9E-03
2	[heparan sulfate]-glucosamine 3-sulfotransferase 1 activity	GO:0008467	1.1E-02
3	alcohol dehydrogenase (NADP+) activity	GO:0008106	1.2E-02
4	molecular function regulator	GO:0098772	2.5E-02
5	aldo-keto reductase (NADP) activity	GO:0004033	2.7E-02



ID	Term Name	Term ID	adj.P.Val
1	blood microparticle	GO:0072562	7.4E-06
2	extracellular region part	GO:0044421	3.3E-05
3	extracellular space	GO:0005615	4.5E-05
4	extracellular organelle	GO:0043230	4.8E-05
5	extracellular exosome	GO:0070062	1.1E-04
6	extracellular vesicle	GO:1903561	1.4E-04
7	extracellular region	GO:0005576	2.4E-04
8	vesicle	GO:0031982	3.5E-02



ID	Term Name	Term ID	adj.P.Val
1	interferon-gamma-mediated signaling pathway	GO:0060333	8.0E-06
2	cellular response to interferon-gamma	GO:0071346	1.6E-04
3	response to interferon-gamma	GO:0034341	3.3E-04
4	response to cytokine	GO:0034097	2.7E-03
5	regulation of complement activation	GO:0030449	3.3E-03
6	regulation of humoral immune response	GO:0002920	4.7E-03
7	cellular response to cytokine stimulus	GO:0071345	5.4E-03
8	innate immune response	GO:0045087	1.2E-02
9	regulation of immune effector process	GO:0002697	1.3E-02
10	defense response to other organism	GO:0098542	1.3E-02
11	immune response	GO:0006955	1.8E-02
12	cytokine-mediated signaling pathway	GO:0019221	1.9E-02
13	complement activation	GO:0006956	2.2E-02
14	immune system process	GO:0002376	3.7E-02
15	defense response	GO:0006952	4.7E-02

Figure 47. Dot plots of significant MF, CC, and BP found in YF/SA vs pLX304. g:Profiler analysis yielded 5 MF, 8 CC, and 15 BP related unphosphorylated STAT3 (YF/SA vs pLX304) according to Gene Ontology (GO) database. The top enriched terms are shown on the lists. adj.P.Value <0.05

5.6. Phosphorylation of Ser727-STAT3 (YF/SD mutant) regulates 342 genes.

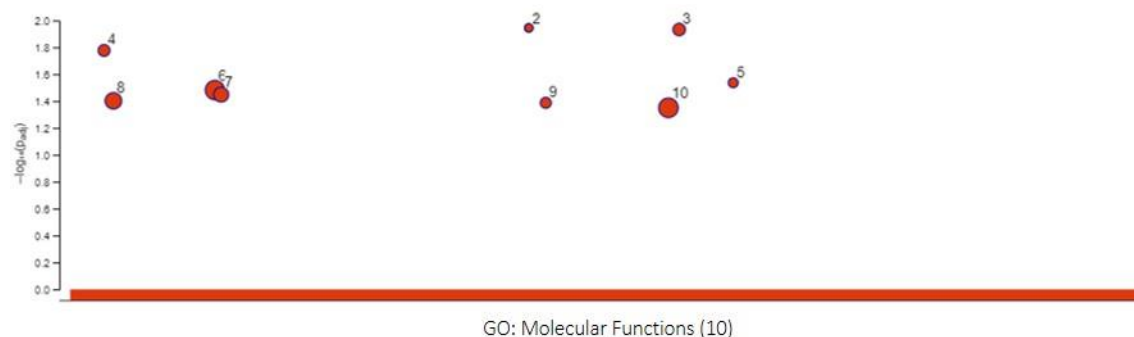
To identify the genes regulated by pSer727, we compared the gene expression between YF/SD (unphosphorylated Tyr705, phosphomimetic Ser727) and pLX304 (empty vector of overexpression: STAT3 silencing). There were found **342 differentially expressed genes regulated by YF/SD overexpression of which 153 were upregulated and 189 downregulated** (see Table 31). This mutant was the second to have the highest number of differentially expressed genes after SD. This observation suggests that **phosphorylation at Ser727 indeed increases gene transcription regardless of the Tyr705 phosphorylation state.**

Table 31. 30 most differentially expressed genes in YF/SD vs pLX304

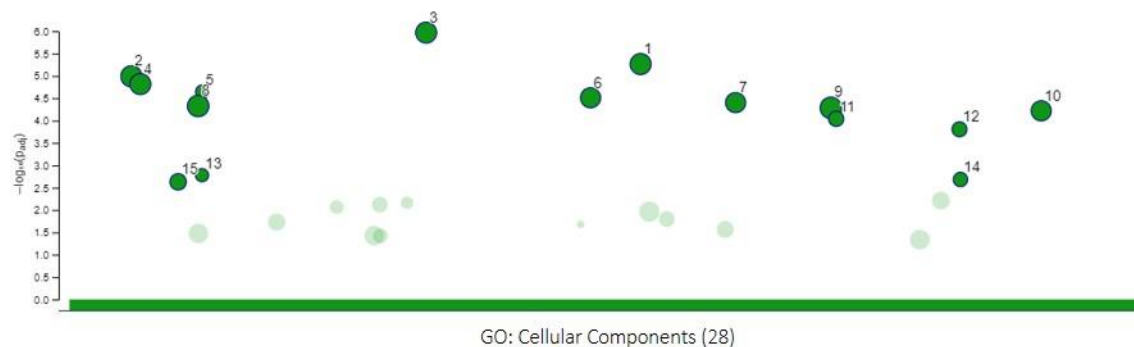
Upregulated genes			Downregulated genes		
Gene Symbol	logFC	adj.P.Val	Gene Symbol	logFC	adj.P.Val
CNTN6	1.8954	5.22E-12	LCP1	-3.1203	4.90E-16
PLPPR5	1.6667	2.66E-09	CFH	-2.6428	2.31E-14
A1CF	1.5088	4.13E-08	C1S	-2.5312	5.19E-15
ANKS4B	1.4402	2.25E-05	TRIM22	-2.1121	6.18E-13
CLRN3	1.3499	1.26E-04	CFB	-1.8762	1.04E-10
CLTRN	1.3159	9.60E-06	IGFBP3	-1.7921	3.47E-12
ERBB3	1.2305	7.23E-04	SLCO1B3	-1.4707	2.13E-06
NROB2	1.2278	1.97E-07	GBP1	-1.4539	3.99E-07
CIDEB	1.2200	2.79E-05	TNFAIP3	-1.3545	3.46E-04
MYO7B	1.2044	3.63E-05	CLEC4E	-1.3444	2.80E-04
GLUL	1.1894	7.71E-09	EDN1	-1.3386	8.50E-05
ACE2	1.1766	1.82E-04	FN1	-1.3356	1.89E-09
METTL7A	1.1744	3.23E-03	MYL9	-1.2956	1.25E-06
KCNJ3	1.0780	5.91E-04	SNAI2	-1.2905	2.12E-03
UGT2A3	1.0604	8.98E-06	EDN2	-1.2812	1.16E-04

The results from the analysis of biological significance of the 342 differentially expressed genes in YF/SD vs pLX304 were surprising. Even when YF/SD presented a lower number of differentially expressed genes than SD, it yielded **the highest number of overrepresented molecular functions, cellular components, and biological functions.** There were found 10 MF consisting of endothelin B receptor binding, bombesin receptor binding, proteoglycan binding, fibronectin-binding, androsterone dehydrogenase activity, signaling receptor binding, integrin binding, actin-binding, insulin-like growth factor I binding, and identical protein binding. The genes regulated by YF/SD were founded related to 28 CC which include: extracellular spaces, plasma membrane, actin-based cell projection, endoplasmic reticulum, collagen-containing extracellular matrix, leading-edge membrane, and intracellular vesicle, among others. Moreover, 97 BF were founded to be significant, including response to cytokine, response to interferon-gamma, immune system processes, response to external stimulus, cell motility and migration, locomotion, cell population proliferation, defense response, regulation of cell adhesion, cell differentiation, tissue development, chemotaxis, response to stress, ERK1 and ERK2

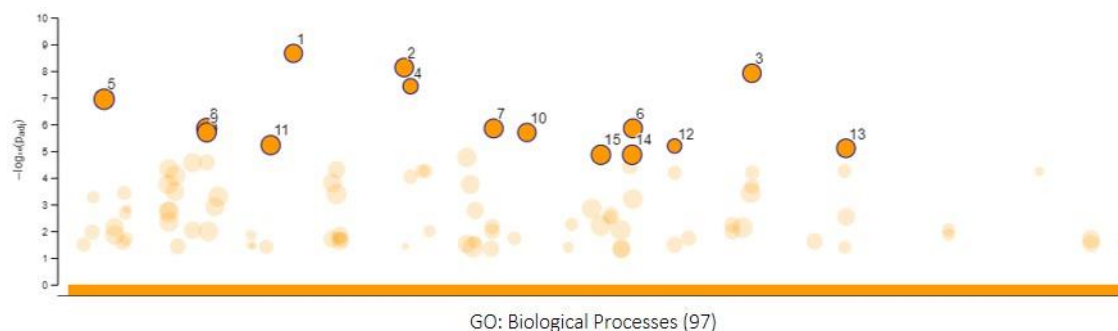
cascade, positive regulation of NFκB signaling, negative regulation of extrinsic apoptotic signaling pathway, positive regulation of cell migration, regulation of cell-cell adhesion, negative regulation of toll-like receptor 3 signaling pathway, and extracellular structure organization, among others. To simplify overview, only the 15 most significant biological processes are shown (see Figure 48).



ID	Term Name	Term ID	adj.P.Val
1	endothelin B receptor binding	GO:0031708	1.1E-02
2	bombesin receptor binding	GO:0031705	1.1E-02
3	proteoglycan binding	GO:0043394	1.2E-02
4	fibronectin binding	GO:0001968	1.7E-02
5	androsterone dehydrogenase activity	GO:0047023	2.9E-02
6	signaling receptor binding	GO:0005102	3.3E-02
7	integrin binding	GO:0005178	3.6E-02
8	actin binding	GO:0003779	4.0E-02
9	insulin-like growth factor I binding	GO:0031994	4.1E-02
10	identical protein binding	GO:0042802	4.5E-02



ID	Term Name	Term ID	adj.P.Val
1	vesicle	GO:0031982	1.1E-06
2	extracellular region part	GO:0044421	5.4E-06
3	extracellular region	GO:0005576	1.0E-05
4	extracellular space	GO:0005615	1.5E-05
5	brush border	GO:0005903	2.3E-05
6	extracellular organelle	GO:0043230	3.1E-05
7	extracellular exosome	GO:0070062	4.0E-05
8	plasma membrane	GO:0005886	4.7E-05
9	cell periphery	GO:0071944	5.2E-05
10	extracellular vesicle	GO:1903561	6.0E-05
11	blood microparticle	GO:0072562	9.1E-05
12	actin-based cell projection	GO:0098858	1.6E-04
13	microvillus	GO:0005902	1.7E-03
14	cluster of actin-based cell projections	GO:0098862	2.1E-03
15	endoplasmic reticulum lumen	GO:0005788	2.3E-03



ID	Term Name	Term ID	adj.P.Val
1	cytokine-mediated signaling pathway	GO:0019221	2.2E-09
2	response to cytokine	GO:0034097	7.4E-09
3	cellular response to cytokine stimulus	GO:0071345	1.2E-08
4	response to interferon-gamma	GO:0034341	3.7E-08
5	immune system process	GO:0002376	1.1E-07
6	response to external biotic stimulus	GO:0043207	1.4E-06
7	response to other organism	GO:0051707	1.4E-06
8	response to external stimulus	GO:0009605	1.4E-06
9	response to biotic stimulus	GO:0009607	2.0E-06
10	innate immune response	GO:0045087	2.0E-06
11	cell migration	GO:0016477	6.0E-06
12	interferon-gamma-mediated signaling pathway	GO:0060333	6.4E-06
13	defense response to other organism	GO:0098542	7.9E-06
14	cell motility	GO:0048870	1.4E-05
15	localization of cell	GO:0051674	1.4E-05

Figure 48. Dot plots of significant MF, CC, and BP found in YF/SD vs pLX304. g:Profiler analysis yielded 10 MF, 28 CC, and 97 BP related pSer727-STAT3 (YF/SD vs pLX304) according to Gene Ontology (GO) database. The top 15 enriched terms are shown on the lists. adj.P.Value <0.05

The striking effect of Ser727 phosphorylation on biological significance, suggests that the subset of genes regulated by pSer727 is associated with a broad of processes within cells. Moreover, most of them are hallmarks of oncogenesis and correlate with the results obtained from functional experiments, where YF/SD was the most significant mutant to induce cell proliferation, migration, clonogenicity, and anchorage-independent growth.

6. YF AND YF/SD MUTANTS REPRESENT THE SAME STAT3 PHOSPHORYLATION STATE

We observed in functional experiments that YF and YF/SD mutants behave similarly with no significant differences between them, suggesting that, as we thought initially, they represent the same STAT3 phosphorylation state. To corroborate this at gene transcription level, we performed a multiple comparison analysis between YF vs pLX304 and YF/SD vs pLX304 (see Figure 49). We found that they share 134 differentially expressed genes corresponding to 84.8% (YF) and 39.2% (YF/SD) of their total expression (158 and 342 genes, respectively). The visualization of common expression patterns (heatmap) showed that indeed, the hierarchical clustering of differentially expressed genes in both mutants are similar, being YF/SD more distant to pLX304 (see Figure 50).

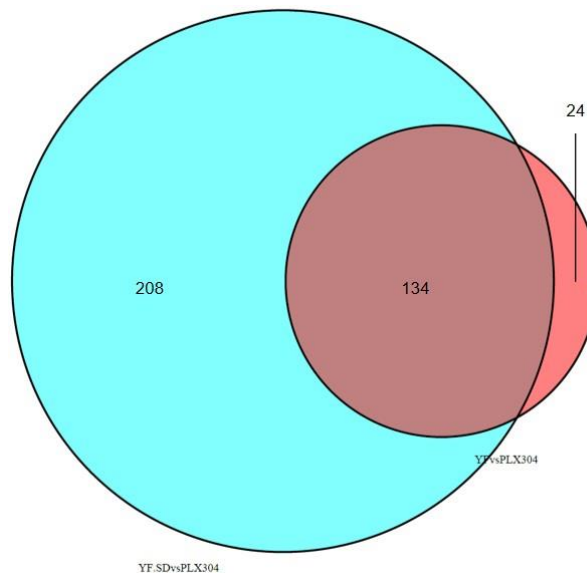


Figure 49. Venn diagram of multiple comparisons between YF vs pLX304 and YF/SD vs pLX304. Upregulated and downregulated genes were analyzed together. Genes at the intersection correspond to common genes, while genes at the outer sets correspond to specific genes of each comparison. adj.P.Value <0.25 and logFC >0.5.

These results suggest that native phosphorylation of Ser727 in YF mutant does not reach the same transcriptional strength than Ser727 phosphomimetic mutation in YF/SD, however, it maintains the necessary gene expression to exhibit the same phenotypic outcome. This observation results reasonably if we consider that when performing this kind of mutations, either phosphomimetic or phosphoablative, we are pushing the phenotype to see exacerbated changes.

Based on the phenotypic and genetic similarities between YF and YF/SD mutants, we conclude that phosphomimetic mutation SD, indeed mimics native Ser727 phosphorylation, thus, both represent the same STAT3 phosphorylation state (unphosphorylated Tyr705, pSer727).

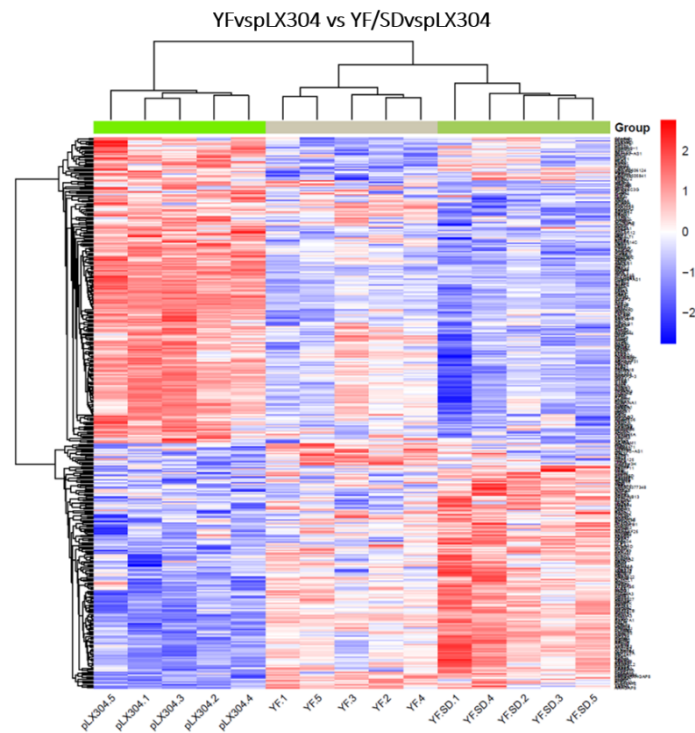


Figure 50. Heatmap: multiple comparisons between YF vs pLX304 and YF/SD vs pLX304. Expression patterns of native Ser727 phosphorylation (YF vs pLX304) vs phosphomimetic mutation at Ser727 (YF/SD vs pLX304). adj.P.Value <0.25 and logFC >0.5.

For experimental clarity and based on the transcriptional activity of YF and YF/SD, we decided that the YF/SD mutant constitutes the best approach to evaluate the effect of pSer727-STAT3 on gene transcription. Therefore, multiple comparisons to identify the specific subsets of genes depending on pSer727 were performed only with YF/SD mutant.

7. STAT3 WT EXPRESSES GENES ASSOCIATED WITH DIFFERENT PHOSPHORYLATION STATES

To analyze the transcriptional behavior of STAT3 WT within the context of our cellular model of ccRCC (769-P cell line), we performed a multiple comparison between WT vs pLX304, SA vs pLX304, SD vs pLX304, YF/SA vs pLX304 and YF/SD vs pLX304. The analysis was carried out with upregulated and downregulated genes separately to be sure that genes were in the same direction (see Table 32). We observed that **overexpression of STAT3 WT regulates the expression of common genes among all STAT3 phosphomutants**, being more similar to SD mutant (both residues phosphorylated), followed by SA (only Tyr705 phosphorylated), YF/SD (only Ser727 phosphorylated) and YF/SA (unphosphorylated STAT3).

Table 32. Common genes with WT vs pLX304

Comparison	Upregulated	Downregulated	Total
SD vs pLX304	50 (40.7%)	38 (30.2%)	88 (35.4%)
SA vs pLX304	43 (35.0%)	33 (26.2%)	76 (30.6%)
YF/SD vs pLX304	16 (13.0%)	34 (27.0%)	50 (20.0%)
YF/SA vs pLX304	21 (17.1%)	18 (14.3%)	39 (15.7%)

Although the maximum transcriptional similarity founded was 35.4% with SD mutant, this result suggests that **native activation of STAT3 within 769-P cells is mainly driven by phosphorylation at both sites**. However, this observation can be also interpreted as a highly dynamic process of STAT3 activation where STAT3 shuttle between one phosphorylation state or another depending on the cellular context and different intrinsic regulatory mechanisms at a given time.

8. THE STAT3 EXPRESSION PATTERN CHANGES AS Tyr705 AND Ser727 BECOME PHOSPHORYLATED

To visualize the differential expression pattern among all STAT3 phosphomutants, we constructed a heatmap including SA vs pLX304, SD vs pLX304, YF/SA vs pLX304 and YF/SD vs pLX304. The resultant heatmap beautifully shows the gradual transition of transcriptional activity as both residues become phosphorylated (left to right) (see Figure 51). Unphosphorylated STAT3 (YF/SA) is the closest mutant to STAT3 silencing (pLX304), followed by Tyr705 phosphorylation (SA). The expression pattern clearly begins to seem opposite to pLX304 when Ser727 becomes phosphorylated (YF/SD) and finally, complete transition ends with the phosphorylation of both residues (SD) representing the complete activation of STAT3.

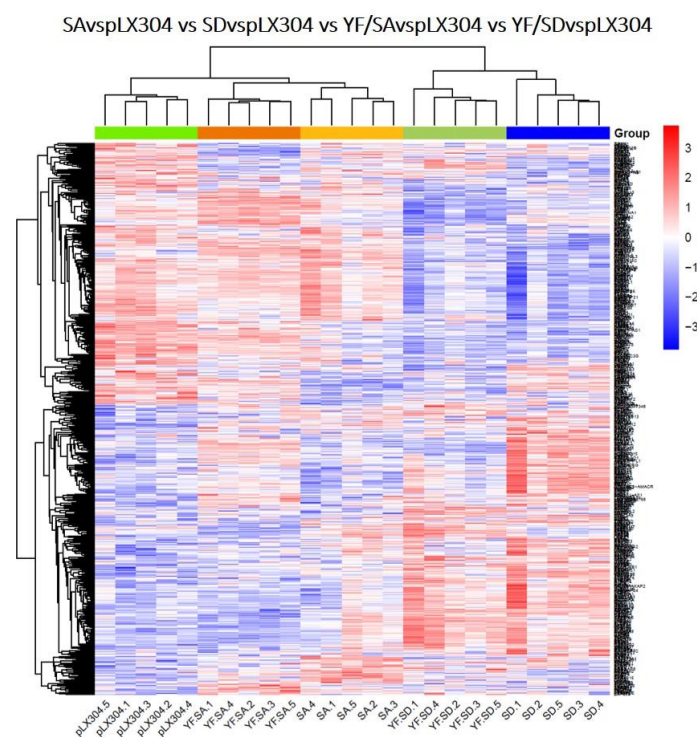


Figure 51. Heatmap: multiple comparisons between all STAT3 phosphomutants. Expression patterns of SA vs pLX304, SD vs pLX304, YF/SA vs pLX304 and YF/SD vs pLX304. adj.P.Value <0.25 and logFC >0.5.

This result indicates that pSer727 has a more striking effect on STAT3 activation than pTyr705.

9. STAT3 REGULATES THE EXPRESSION OF 265 GENES REGARDLESS OF ITS PHOSPHORYLATION STATE

Until now, we have analyzed the overall effect of each STAT3 phosphomutant on gene transcription and determined their associated signaling pathways, however, as the main objective of this work was to identify the genes regulated specifically by pSer727, we performed multiple comparisons including all mutants (SA vs pLX304, SD vs pLX304, YF/SA vs pLX304 and YF/SD vs pLX304). This approach allowed us to identify 265 genes scattered among all STAT3 phosphomutants, of which 131 were upregulated and 134 downregulated (see Figure 52). These genes were expressed without following a clear pattern regarding Tyr705 or Ser727 phosphorylation state (located at the intersections of the Venn diagrams), and moreover, none of them was found to be inversely expressed in any of the STAT3 phosphomutants. **This result indicates that there are genes regulated by STAT3 regardless of its phosphorylation state and possibly dependent on the cellular context.**

Additionally, we also found 12 common genes (4 upregulated and 8 downregulated), located at the inner intersection of all STAT3 phosphomutants, indicating that these genes are regulated by STAT3 in any of its phosphorylation states (see Table 33).

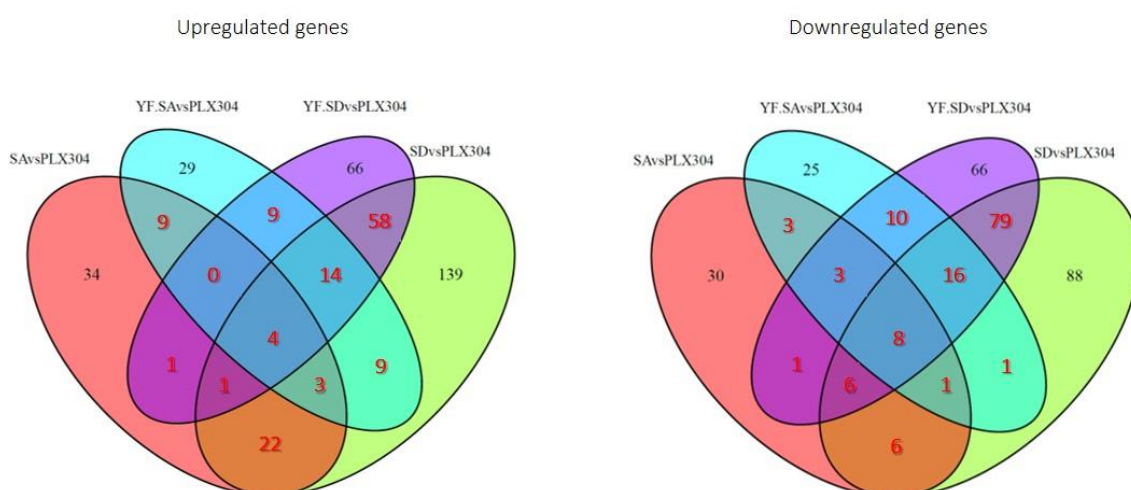


Figure 52. Venn diagrams of multiple comparisons between all STAT3 phosphomutants and common genes. Upregulated and downregulated genes were analyzed separately. Genes at the intersections correspond to common genes expressed regardless of STAT3 phosphorylation state (red numbers), while genes at the outer sets correspond to specific genes of each comparison. adj.P.Value <0.25 and logFC >0.5.

The genes located at the outer sets of the Venn diagrams, constitute those specifically regulated by the different STAT3 phosphorylation states.

Table 33. Common genes regulated by STAT3

Upregulated genes		Downregulated genes	
<i>Gene Symbol</i>	<i>Name</i>	<i>Gene Symbol</i>	<i>Name</i>
EPHA7	EPH receptor A7	UBD	ubiquitin D
NUPR1	nuclear protein 1, transcriptional regulator	FCGR3B	Fc fragment of IgG receptor IIIb
CNTN6	contactin 6	GBP1	guanylate binding protein 1
TOMM20L	translocase of outer mitochondrial membrane 20 like	LCP1	lymphocyte cytosolic protein 1
		NOS3	nitric oxide synthase 3
		C1S	complement C1s
		BHLHE41	basic helix-loop-helix family member e41
		GFPT2	glutamine-fructose-6-phosphate transaminase 2

10. PHOSPHORYLATION OF Ser727 ACTS BY A DIFFERENT PATHWAY FROM CANONICAL STAT3 ACTIVATION

To determine whether the different STAT3 phosphomutants act through the canonical STAT3 activation pathway or not, we performed a luciferase-reporter assay with the STAT3 consensus promoter. All cells were assessed in the absence or the presence of IL6, to induce Tyr705 phosphorylation in mutants where it was unchanged (STAT3 WT, SA, and SD). Transcriptional activity was measured as luciferase expression and expressed as relative light units (see Figure 53). We observed that there was no significant transcriptional activity in any of the STAT3 phosphomutants in the absence of IL6 (left panel), however, when cells were stimulated with IL6, transcriptional activity raised only in mutants where Tyr705 was not manipulated (SA and SD), including STAT3 WT. This result indicates that **phosphorylation of Tyr705 is an indispensable feature for STAT3 activity through its canonical pathway regardless of Ser727 phosphorylation state.**

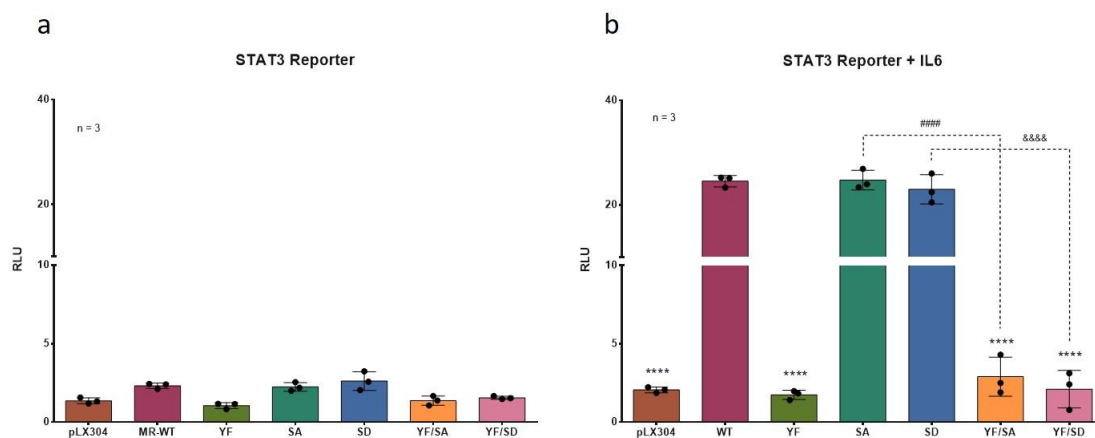


Figure 53. Luciferase-reporter assay of STAT3 phosphomutants. Transcriptional activity of STAT3 phosphomutants was assessed on the STAT3 consensus promoter and measured as luciferase expression in the a) absence and b) the presence of IL6 [10 ng/ml]. It can be observed that stimulation with IL6 (which induces Tyr705 phosphorylation) increases transcriptional activity only in STAT3 WT, SA, and SD mutants. Error bars represent means \pm SD. * Comparisons vs WT, $p < 0.05$; # Comparison between SA and YF/SA, $p < 0.05$; & Comparison between SD and YF/SD, $p < 0.05$.

Based on the differential expression analysis, it is clear that mutants carrying phosphomimetic mutation for Ser727 (SD) exhibited higher transcriptional activity, therefore, and **according to the luciferase-reporter assay, we hypothesize that the activity of pSer727-STAT3 is mediated by a non-canonical pathway.**

11. PHOSPHORYLATION OF Ser727-STAT3 SPECIFICALLY REGULATES THE EXPRESSION OF 132 GENES

To identify the genes specifically regulated by pSer727, we used a very conservative approach to select expressed genes only when Ser727 was phosphorylated. These genes were located at the outer set of YF/SD vs pLX304 and not expressed in any other STAT3 phosphomutant (see Figure 54). We found **132 pSer727-STAT3 dependent genes** of which **66 were upregulated** and **66 were downregulated** (see Table 34).

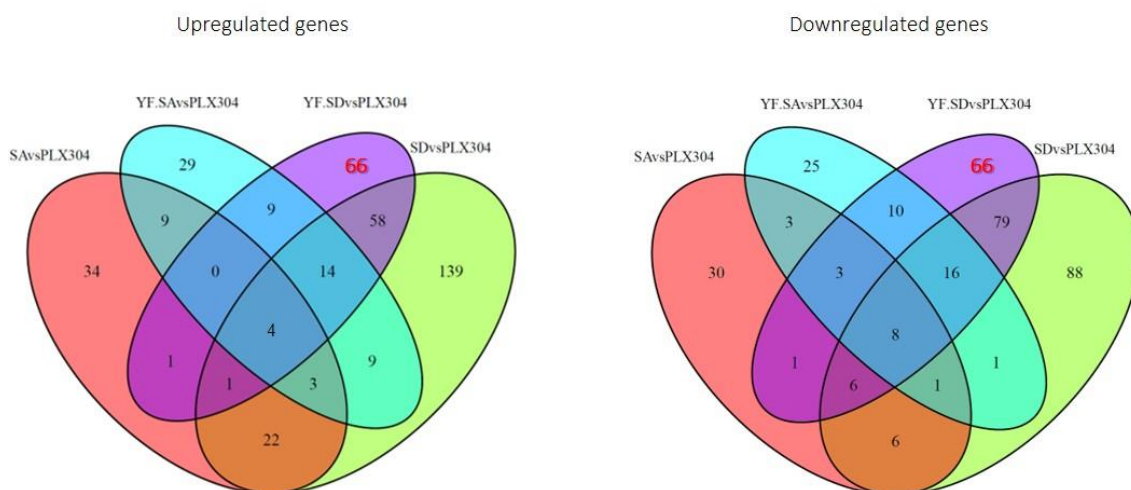


Figure 54. Venn diagrams of multiple comparisons between all STAT3 phosphomutants and pSer727-dependent genes. Upregulated and downregulated genes were analyzed separately. Genes at the intersections correspond to common genes, while genes at the outer sets of YF/SD vs pLX304 correspond to specific genes regulated by pSer727-STAT3 (red numbers). adj.P.Value <0.25 and logFC >0.5.

Table 34. Subset of genes regulated by pSer727-STAT3

Upregulated genes		Downregulated genes	
Gene Symbol	Name	Gene Symbol	Name
TSTD1	thiosulfate sulfurtransferase like domain 1	NNMT	nicotinamide N-methyltransferase
CTDSPL	CTD small phosphatase like	GPC6	glypican 6
GNPMB	glycoprotein nmb	CITED2	Cbp/p300 interacting transactivator carboxy-terminal 2
ZBTB18	zinc finger and BTB domain containing 18	IFITM3	interferon induced transmembrane protein 3
NEBL	nebulette	IFITM2	interferon induced transmembrane protein 2
HHLA2	HERV-H LTR-associating 2	LYPD1	LY6/PLAUR domain containing 1
FBXO27	F-box protein 27	ADH1C	alcohol dehydrogenase 1C (class I), gamma polypeptide
ADH6	alcohol dehydrogenase 6 (class V)	COL4A1	collagen type IV alpha 1 chain
ACMSD	aminocarboxymuconate decarboxylase	VSTM2L	V-set and transmembrane domain containing 2 like
SLC9B2	solute carrier family 9 member B2	ODAPH	odontogenesis associated phosphoprotein
SMCR5	Smith-Magenis syndrome chromosome region, 5	ABCA1	ATP binding cassette subfamily A member 1
METTL27	methyltransferase like 27	EPHB1	EPH receptor B1
RDH10	retinol dehydrogenase 10	SLC16A9	solute carrier family 16 member 9
DNASE2	deoxyribonuclease 2, lysosomal	ABCA5	ATP binding cassette subfamily A member 5
CRYBG1	crystallin beta-gamma domain containing 1	MSRB3	methionine sulfoxide reductase B3
STK32A	serine/threonine kinase 32A	CLUL1	clusterin like 1
F2RL1	F2R like trypsin receptor 1	MUC19	mucin 19, oligomeric

Upregulated genes		Downregulated genes	
<i>Gene Symbol</i>	<i>Name</i>	<i>Gene Symbol</i>	<i>Name</i>
STOX1	storkhead box 1	HPGD	15-hydroxyprostaglandin dehydrogenase
FGR	FGR proto-oncogene, Src family tyrosine kinase	ICAM1	intercellular adhesion molecule 1
TFEC	transcription factor EC	OR52B6	olfactory receptor family 52 subfamily B member 6
PLCH1	phospholipase C eta 1	IFIT3	interferon induced protein with tetratricopeptide 3
ZNF683	zinc finger protein 683	IGFBP5	insulin like growth factor binding protein 5
STEAP2	STEAP2 metalloreductase	C6orf58	chromosome 6 open reading frame 58
TOX3	TOX high mobility group box family member 3	IRS1	insulin receptor substrate 1
CDH20	cadherin 20	JUNB	JunB proto-oncogene, AP-1 transcription factor subunit
HLA-DPB1	major histocompatibility complex, class II, DP 1	KCNH1	potassium voltage-gated channel subfamily H member 1
FOXA1	forkhead box A1	MCC	MCC, WNT signaling pathway regulator
HNF4A	hepatocyte nuclear factor 4 alpha	MRC1	mannose receptor C-type 1
HTR1D	5-hydroxytryptamine receptor 1D	MYBL1	MYB proto-oncogene like 1
ZC3H6	zinc finger CCCH-type containing 6	NGF	nerve growth factor
SLC6A17	solute carrier family 6 member 17	SERPINA1	serpin family A member 1
LGALS2	galectin 2	GPR85	G protein-coupled receptor 85
LGALS4	galectin 4	TMEM45A	transmembrane protein 45A
CASC10	cancer susceptibility 10	P3H2	prolyl 3-hydroxylase 2
LRP2	LDL receptor related protein 2	MCOLN3	mucoilin 3
MAL	mal, T cell differentiation protein	TBC1D2	TBC1 domain family member 2
ARSF	arylsulfatase F	MBNL3	muscleblind like splicing regulator 3
NEB	nebulin	SULF2	sulfatase 2
OVGP1	oviductal glycoprotein 1	SLC44A2	solute carrier family 44 member 2
PDE9A	phosphodiesterase 9A	PTPRO	protein tyrosine phosphatase, receptor type O
PADI3	peptidyl arginine deiminase 3	MOK	MOK protein kinase
SERPIN13	serpin family B member 13	RELB	RELB proto-oncogene, NF-kB subunit
KRT20	keratin 20	RRAD	RRAD, Ras related glycolysis inhibitor and calcium
PPL	periplakin	SAA1	serum amyloid A1
PRSS8	serine protease 8	CEACAM1	carcinoembryonic antigen related cell adhesion 1
VANGL2	VANGL planar cell polarity protein 2	SDC2	syndecan 2
SCNN1D	sodium channel epithelial 1 delta subunit	SDC4	syndecan 4
LRRC19	leucine rich repeat containing 19	SGK1	serum/glucocorticoid regulated kinase 1
SLC3A1	solute carrier family 3 member 1	CDKL5	cyclin dependent kinase like 5
SLC7A2	solute carrier family 7 member 2	SULT1C2	sulfotransferase family 1C member 2
SLC17A1	solute carrier family 17 member 1	TGFBI	transforming growth factor beta induced
ABCC8	ATP binding cassette subfamily C member 8	THBS1	thrombospondin 1
TGFBR3	transforming growth factor beta receptor 3	WNT2B	Wnt family member 2B
TM4SF4	transmembrane 4 L six family member 4	PREX2	phosphatidylinositol-3,4,5-trisphosphate dependent 2
WAS	Wiskott-Aldrich syndrome	ADAM12	ADAM metalloproteinase domain 12
CLIP4	CAP-Gly domain containing linker protein family 4	TTC29	tetratricopeptide repeat domain 29
ZNF385D	zinc finger protein 385D	SOX14	SRY-box 14
BAIAP2L2	BAI1 associated protein 2 like 2	ANTXR1	ANTXR cell adhesion molecule 1
CUBN	cubilin	SLC9A7	solute carrier family 9 member A7
SYNC	syncollin, intermediate filament protein	IFITM1	interferon induced transmembrane protein 1
NROB2	nuclear receptor subfamily 0 group B member 2	B3GALT1	beta-1,3-galactosyltransferase 1
ABHD1	abhydrolase domain containing 1	CBR1	carbonyl reductase 1
TNFSF11	TNF superfamily member 11	TNFSF10	TNF superfamily member 10
KCNK5	potassium two pore domain channel subfamily K 5	ENDOU	endonuclease, poly(U) specific
PROZ	protein Z, vitamin K dependent plasma glycoprotein	MSC	musculin
CREB5	cAMP responsive element binding protein 5	CD33	CD33 molecule

Considering that pSer727-STAT3 expression levels indicate poor prognosis and low overall survival in patients with ccRCC, these 132 genes specifically regulated by pSer727-STAT3 represent new potential therapeutic targets to improve patient's outcome.

Since all differentially expressed genes in YF/SD (342) contribute to overall biological significance, the analysis of overrepresented processes only related to those 132 genes would give a biased result. Therefore, we decided to correlate these specific genes with the whole biological context of YF/SD previously determined (see Figure 48). We identified that **genes specifically regulated by pSer727 significantly contribute to 45 biological processes of the total of 97 found in YF/SD** (see Table 35).

Table 35. Biological processes (BP) associated to pSer727-dependent genes

Term ID	Term Name	adj.P.Value
GO:0019221	cytokine-mediated signaling pathway	2.2E-09
GO:0034097	response to interferon-gamma	7.4E-09
GO:0071345	response to other organism	1.2E-08
GO:0034341	response to external stimulus	3.7E-08
GO:0002376	innate immune response	1.1E-07
GO:0043207	defense response to other organism	1.4E-06
GO:0051707	localization of cell	1.4E-06
GO:0009605	Locomotion	1.4E-06
GO:0009607	defense response to virus	2.0E-06
GO:0045087	regulation of cell adhesion	2.0E-06
GO:0016477	cell surface receptor signaling pathway	6.0E-06
GO:0060333	response to type I interferon	6.4E-06
GO:0098542	biological adhesion	7.9E-06
GO:0048870	movement of cell or subcellular component	1.4E-05
GO:0051674	regulation of cell population proliferation	1.4E-05
GO:0040011	cell differentiation	1.7E-05
GO:0009615	multi-organism process	2.6E-05
GO:0008283	tissue development	2.7E-05
GO:0051607	positive regulation of response to stimulus	3.9E-05
GO:0006952	Taxis	4.6E-05
GO:0030155	response to stress	5.0E-05
GO:0035150	leukocyte migration	5.6E-05
GO:0097746	endocrine process	5.6E-05
GO:0035296	viral entry into host cell	5.6E-05
GO:1904970	cellular developmental process	5.9E-05
GO:0071357	anatomical structure morphogenesis	6.4E-05
GO:0060337	response to interferon-beta	6.4E-05
GO:0007166	regulation of I-kappaB kinase/NF-kappaB signaling	8.4E-05
GO:0034340	regulation of ERK1 and ERK2 cascade	9.1E-05
GO:0022610	positive regulation of cell migration	1.5E-04
GO:0006928	regulation of immune system process	1.8E-04
GO:0042127	regulation of response to cytokine stimulus	1.8E-04
GO:0071346	regulation of systemic arterial blood pressure	2.1E-04
GO:0007155	regulation of cell-cell adhesion	3.3E-04
GO:0071310	negative regulation of extrinsic apoptotic signaling pathway	3.7E-04
GO:0030154	regulation of cell migration	4.1E-04
GO:0010033	regulation of anatomical structure size	5.0E-04
GO:0001990	positive regulation of cell motility	5.3E-04
GO:0009888	retinoid metabolic process	1.2E-03
GO:0048584	cell chemotaxis	1.5E-03
GO:0003100	negative regulation of toll-like receptor 3 signaling pathway	1.5E-03
GO:0042330	regulation of cellular component movement	1.7E-03
GO:0006950	extracellular structure organization	1.9E-03
GO:0003044	positive regulation of cellular component movement	2.1E-03

In summary, the results obtained from microarray analysis demonstrated that **different subsets of genes are regulated depending on the overall STAT3 phosphorylation state**, and more importantly, that **phosphorylation at Ser727 has a more powerful effect on STAT3 activation than pTyr705**.

12. IDENTIFICATION OF PUTATIVE AND NOVEL BIOMARKERS FOR ccRCC

The determination of pSer727-STAT3 expression levels relies on the immunohistochemical evaluation of tumor tissue samples obtained from biopsy or after nephrectomy. Thus, in order to explore alternatives to pSer727, we analyze their specific target genes as potential and novel prognostic biomarkers.

From the previous list of specifically pSer727-STAT3-regulated genes, we evaluated genes based on the following criteria: i) inclusion of only upregulated genes, ii) genes whose have been previously associated to the development and progression of human cancers (manually analyzed based on the literature), iii) genes which have not been previously associated to other types of renal cell carcinoma (see Table 36).

Based on the established criteria, we selected 10 genes as potential and novel biomarkers for ccRCC patients of which 2 of them: the *glycoprotein nonmetastatic melanoma protein B* (GPNMB) and the *cytokeratin 20* (KRT20), represent better non-invasive alternatives to pSer727-STAT3 because both can be detected in blood and urine samples of ccRCC patients. However, further studies should be performed in order to validate these candidates.

Table 36. Putative and novel biomarkers for ccRCC

Gene Symbol	Types of cancer where the gene has been reported	Reference	Observations
GPNMB	Osteosarcoma, ovarian cancer, breast cancer, bladder cancer, head and neck squamous cell carcinoma, glioma, lung cancer, oral squamous cell carcinoma, pancreatic cancer, prostate cancer, melanoma, and hepatocellular carcinoma.	169–180	Transmembrane glycoprotein, which undergoes shedding and ectodomain release.
HHLA2	Colorectal carcinoma, lung cancer, osteosarcoma, and oral squamous cell carcinoma,	181–183	Newly identified member of the B7 immune checkpoint family.
F2RL1	Hepatocellular carcinoma, ovarian clear cell carcinoma, hepatocellular carcinoma, oral squamous cell carcinoma, glioblastoma, lung cancer, gastric cancer, bile duct cancer, breast cancer, and endometrial cancer.	184–193	Cell surface receptor, immunomodulator.
FGR	Acute myelogenous leukemia, ovarian carcinoma, lung cancer, and B-cell lymphoma.	194–197	Proto-oncogene.
STEAP2	Prostate cancer	198	Six-transmembrane protein.
TOX	Cutaneous T-cell lymphoma, lung cancer, and breast cancer.	199,200	Immunomodulator, nuclear factor.
FOXA1	Prostate cancer, colorectal cancer, breast cancer, nasopharyngeal carcinoma, gastric cancer, thyroid cancer, epithelial ovarian cancer, and glioma.	201–208	Transcription factor.
HTR1D	Pancreatic cancer.	209	Serotonin receptor.
LGALS4	Pancreatic cancer, urothelial carcinoma, colorectal carcinoma, hepatocellular carcinoma, and lung carcinoma.	210–214	Modulates cell-cell and cell-matrix interactions.
KRT20	Gastric carcinoma, colorectal cancer, breast cancer, hepatocellular carcinoma, colon cancer, gastrointestinal carcinoma, bladder cancer, head and neck cancer.	215–222	Can be detected in blood samples and urine.

In this study, the selection parameters were set to delimit the candidates according to our capacity for data analysis at the time of the study. The exclusion of the other genes does not mean in any way that they are not biologically important or that they cannot represent possible biomarkers for the same purpose.

DISCUSSION

1. NUCLEAR AND CYTOSOLIC pSer727-STAT3 EXPRESSION LEVELS IN ccRCC PATIENTS

Previous studies in our lab analyzed the nuclear expression of pTyr705- and pSer727-STAT3 in tissue samples of ccRCC patients and demonstrated that only pSer727 levels correlated with a poorer outcome and lower overall survival (Patent No. WO 2014/041064 A1, granted in Europe and USA in 2016)⁶⁶. This is, pSer727 expression levels constitute an independent prognostic factor that divides ccRCC patients into two groups: those with low pSer727 levels and better prognosis, and those with high pSer727 expression prone to die faster over time. Although it is true that pSer727 expression was also detected in cytosol, it was not evaluated at that time.

In the present work, the expression of pSer727 both in the nucleus and cytosol was evaluated in a different cohort of 82 ccRCC patients. We decided to include the analysis of cytosolic pSer727 expression due to recent reports indicating that pSer727 has an important role in the regulation of mitochondrial activity and modulation of Ca²⁺ release from the endoplasmic reticulum^{110,121}. Both processes in line with the pro-oncogenic role of STAT3. We thought that pSer727 may exhibit a dual role in ccRCC by controlling gene transcription in the nucleus while regulating energy metabolism in the mitochondria and apoptosis through the endoplasmic reticulum.

Our results showed positive staining for pSer727 in the nucleus and cytosol and completely negative in normal tissue. Both nuclear and cytosolic pSer727 were found to be significant when correlated with patient overall survival, validating the previous finding. According to our results, other studies evaluating the expression of pSer727-STAT3 in tissue samples of *cervical intraepithelial neoplasia* (CIN) and prostate cancer, have also reported a significant correlation of pSer727 expression levels to clinicopathologic outcome^{223,224}.

Furthermore, different pSer727 expression patterns were found among ccRCC samples. Some samples were found to be positive for pSer727 staining only in the nucleus or in the cytosol, while others were positive in both compartments. These results suggest that possibly pSer727 expression in one compartment or another determines different STAT3 functions at certain stages of tumor development. It might be possible that localization of pSer727 in the cytosol and specifically in the mitochondria, responds to a shift in cellular energy metabolism driving the initial stages of transformation. Otherwise, the presence of pSer727 in the endoplasmic reticulum could represent a well-established anti-apoptotic mechanism in late stages of tumor development. Nevertheless, to confirm this hypothesis, more experiments should be carried out to determine if indeed, pSer727 expression pattern changes over time and under different stages of ccRCC development. In line with our data, the analysis of pSer727-STAT3 expression in CIN has also identified nuclear and cytosolic expression patterns of pSer727, both correlating with nuclear expression of the cellular marker of proliferation Ki67²²³.

Whether in the nucleus or cytosol, the expression of pSer727-STAT3 certainly determines a poor prognosis for ccRCC patients.

2. STAT3 PHOSPHOMUTANTS (EXPERIMENTAL DESIGN)

In this work, a collection of different forms of phosphorylated STAT3 was generated covering all possible combinations between Tyr705 and Ser727. Although the main objective was to determine the genes dependent on Ser727 phosphorylation, we could not exclude the possibility of a dynamic phosphorylation modulation in STAT3, implying that phosphorylation state at one site could impact the phosphorylation state in the other. This idea arose from previous studies showing that phosphorylation of Ser727 by ERK family of *mitogen-activated protein* (MAP) kinases, negatively modulates Tyr705 phosphorylation^{80,225}. If STAT3 has an intrinsic modulation mechanism, our mutants represent all the possible phosphorylation states between these two residues.

The experimental design of the different STAT3 phosphomutants was thoroughly meditated. Initially, phosphomimetic mutants for Tyr705 were considered. In fact, a first collection of double STAT3 phosphomutants was generated including Tyr705Asp (YD/SA, YD/SD, YF/SA, and YF/SD). Several studies have reported the use of aspartic acid or glutamic acid to mimic Tyr705 phosphorylation, however, all of them indirectly assessed their influence on specific targets genes by RT-qPCR and none of them show transcriptional activity on a reporter assay^{226–229}. When we first evaluated the transcriptional activity of those initial double STAT3 mutants by luciferase-reporter assay, we observed that none of them exhibited transcriptional activity even in the presence of IL6 (data not shown). Based on the literature, we expected that mutants carrying phosphoablative mutations for Tyr705 (YF) did not respond to STAT3 canonical activation pathway, however, it resulted shocking that phosphomimetic mutations (YD) did not either. Since one of the main objectives of this work was to compare transcriptional activity, this result was considered unacceptable to continue. For that reason, we pursue for another approach to induce endogenous Tyr705 phosphorylation. Stimulation with IL6 seemed to be the best option since it is a well-known activator of STAT3 through phosphorylation of this residue. We analyze the effect of IL6 in our cell lines (769-P and 786-O) and found that IL6 induced only Tyr705 phosphorylation and having no effect on Ser727. Moreover, our cell lines were constitutively phosphorylated at Ser727. Interestingly, there are several studies showing that IL6 also stimulates Ser727 phosphorylation by an ERK-independent process^{80,230–233}. However, in our ccRCC cellular models we have not observed this effect, maybe due to the fact that Ser727 is already phosphorylated at basal conditions and probably through other mechanisms different to those induced by IL6. Therefore, we were confident to use IL6 to induce Tyr705 phosphorylation without affecting Ser727.

Regarding phosphomimetic mutation for Ser727 (SD), we used aspartic acid which structurally resembles serine and it is usually the amino acid of choice for this type of substitutions. Since we have observed that Ser727 is phosphorylated at basal conditions, we added the simple mutant YF (phosphoablative mutation for Tyr705, free Ser727) to validate the effect of phosphomimetic mutation SD. As both represent the same STAT3 phosphorylation state, we thought that functional experiments, as well as differential gene expression, should yield similar results. Indeed, we found that both mutants behave similarly, thus we concluded that phosphomimetic mutation SD was biologically functional and the results obtained from it were reliable.

3. STAT3 LOCALIZES AT NUCLEUS AND CYTOSOL REGARDLESS ITS PHOSPHORYLATION STATE

The classic model of STAT3 signaling indicates that STAT3 is a cytoplasmic transcription factor that requires nuclear entry to activate transcription. At present, it is known that STAT3 shuttles between nuclear and cytosolic compartments independent of pTyr705¹⁰¹. We examined the localization of our STAT3 phosphomutants and found that STAT3 was located at both compartments in any of its forms. In agreement with our data, nuclear translocation of STAT3 has been showed to be independent of Tyr705 phosphorylation and mediated by the nuclear import domain of STAT3 (importin- α 3) in some tumors and primary cells²³⁴. Moreover, it has been reported that STAT3 dimerization is independent of cytokine stimulation, thus existing preformed complexes ready to enter the nucleus and further mediate gene transcription of downstream genes related to tumorigenesis^{234,235}.

It is also possible that overexpression by itself produced this localization pattern, where only part of the molecules is properly localized and the rest is dispersed within the cells. According to our results, if this happens in our cellular models, it is clear that it does not negatively modify the activity of STAT3 phosphomutants.

4. PHOSPHORYLATION AT Ser727-STAT3 PROMOTES A PRO-TUMORAL PHENOTYPE *IN VITRO*

To date, there are more than 11,000 scientific articles relating STAT3 with cancer. Most of them, attributing the oncogenic properties of STAT3 to Tyr705 phosphorylation. Recently, Ser727 phosphorylation has emerged as an event that enhances STAT3 transcriptional activity in addition to non-genomic roles that promote cancer development. Nevertheless, many studies on the role of pSer727 have been done under the presumption that Tyr705 phosphorylation occurs prior to Ser727 phosphorylation, thus, underestimating the role of pSer727 by itself. Recent studies have shown that STAT3 can be activated by pSer727 in the absence of pTyr705 in non-cancerous and cancerous cells^{224,236}. For example, immunohistochemical studies on melanoma specimens of primary lesions revealed that Ser727 phosphorylation precedes pTyr705 in early stages of melanoma progression, indicating that pSer727 is not necessarily a secondary event after pTyr705 and suggesting that pSer727 has a role in the regulation of cell survival activity in melanocytic cells²³⁷.

In this work, we functionally characterized different STAT3 mutants representing different phosphorylation states in a ccRCC cellular model (769-P cell line) by analyzing proliferation capacity, cell motility, colony formation ability, anchorage-independent growth, cell aggregation, cell adhesion, invasion capacity and the ability to form tumorspheres.

Our experiments demonstrated that mutants carrying phosphomimetic substitutions for Ser727 (SD and YF/SD) exhibited a significantly higher rate of proliferation, migration, clonogenic capacity, anchorage-independent growth on soft agar and tended to form cell aggregates. Moreover, no significant differences were found between SD and YF/SD in

these experiments, indicating that their effects are clearly independent of Tyr705 phosphorylation state.

According to our results, it has been demonstrated that in the absence of pTyr705, pSer727 activates STAT3 signaling and promotes enhancing survival in macrophages, neuronal stem cells, and prostate cancer cells^{224,236,238}. Furthermore, a previous study using a constitutively active form of STAT3 (STAT3C), consisting of a dimerizing STAT3 without the requirement of pTyr705, showed that after transfection into HEK293T cells, STAT3 was phosphorylated at Ser727 but not at Tyr705. They further showed that overexpressed STAT3C was capable of driving transcription, inducing transformation and enhancing tumorigenicity in immortalized fibroblast and epithelial cells, suggesting that pSer727 was indispensable for STAT3C-mediated oncogenic events¹²⁹. Similarly, a study using a double STAT3 phosphomutant (YF/SE) resulted in STAT3 activation that enhanced anchorage-independent growth *in vitro* and tumorigenesis *in vivo*, whereas YF/SA phosphomutant impaired the oncogenic capacity of STAT3 in models of prostate cancer²²⁷.

At present, several studies have pointed out the oncogenic role of Ser727 phosphorylation. Electrophoretic mobility shift assay and western blot analysis of phosphorylated STAT3 in macrophages demonstrated that STAT3 was constitutively activated in a pSer727-dependent manner. This study found that Mcl-1, which is a member of the family Bcl-2 and an essential molecule for macrophage survival, was regulated by pSer727-STAT3. Expression of a dominant-negative STAT3 resulted in inhibition of Mcl-1 and consequently cell death²³⁶. Moreover, another study demonstrated that expression of Mcl-1L via Ser727 phosphorylation through the MEK-ERK pathway protects melanocytes and melanoma cells from UVB-induced apoptosis²³⁹. Another study demonstrated that *glycochenodeoxycholate* (GCDCA), which is a bile salt formed in the liver, enhances survival of liver cancer cells through the activation of STAT3 by phosphorylation at Ser727 via mitogen-activated protein kinase/ERK1/2 pathway, contributing to the progression of human liver cancer and chemoresistance²⁴⁰. Furthermore, a report in the role of apoptosis-induced by paclitaxel demonstrated that, after treatment with this drug, apoptosis was induced in *esophageal squamous cell carcinoma* (ESCC) cell lines by increasing the release of cytochrome c via downregulation of pSer727-STAT3 levels²⁴¹. STAT3 expression was also analyzed in 18 human endometrial cancer cell lines showing that pTyr705 was not expressed in any of the cell lines tested, while pSer727 was highly expressed. Moreover, in the same study, the effect of a novel STAT3 inhibitor (HO-3867) was tested showing a substantial decrease of pSer727 levels which in turn induced cell cycle arrest and apoptosis, suggesting that pSer727 independently of Tyr705 phosphorylation state, has an important role on oncogenesis of endometrial cancer²⁴². Another group reported that progestins induced Ser727 phosphorylation via activation of c-Src/p42/p44 MAPK pathways in murine progestin-dependent breast cancer cells. Expression of a phosphoablative mutation of Ser727 (SA) showed that pSer727 is required for full transcriptional activation of cyclin D1, whose activity is required for cell cycle G1/S transition, inducing *in vivo* and *in vitro* growth, and indicating that pSer727 is necessary to promote breast cancer growth²⁴³. Different isoforms of *protein kinases C* (PKC) has also been related to pSer727-STAT3 and cell growth, i.e. *protein kinase C epsilon* (PKCε), which is a novel calcium-dependent PKC isoform that acts as a transforming oncogene by promoting cell survival, has been

demonstrated as a protein partner of STAT3 α (which has Tyr705 and Ser727 sites) and not of STAT3 β (which lacks Ser727 site). PKC ϵ -STAT3 interaction and Ser727 phosphorylation have been observed in squamous cell, prostate, skin melanoma, glioma, bladder, colon, pancreatic, and breast cancers *in vitro*. Inhibition of PKC ϵ by specific siRNA inhibits pSer727, STAT3 DNA binding, and gene expression, as well as cell migration in all the tested cell lines²⁴⁴. Furthermore, it has also been described that, after insulin stimulation, a different isoform of PKC (PKC δ) interacts with STAT3 inducing proliferation and cell migration in keratinocytes. Overexpression of a phosphoablative mutation of Ser727 (SA) eliminates insulin-induced PKC δ -STAT3 interaction, thus proliferation. These results indicate that PKC δ acts through pSer727-STAT3 and both are essential for inducing cell growth in keratinocytes²⁴⁵.

Altogether, these studies demonstrate that pSer727 has an independent role from Tyr705 in driving tumor development by different mechanisms, thus reinforcing the results obtained in this work where pSer727 has demonstrated to exert a potent tumoral phenotype on ccRCC.

During the performance of functional experiments was noticed that, when cells were in suspension, cell aggregates tended to be formed only in mutants carrying phosphomimetic mutation of Ser727 (SD and YF/SD) as well as in YF mutant (where Ser727 was natively phosphorylated). Thus, we conceived a simple experiment to record that phenomenon. Cells were detached by treatment with trypsin, vortexed for 1 min and visualized under the microscope. Our results showed that native or phosphomimetic pSer727 formed cell clusters that cannot be explained in terms of random aggregation because this behavior was consistent in all experiments. Recently, it has been demonstrated that homotypic aggregation of tumor cells is an important feature in the development of breast cancer as it might prevent anoikis²⁴⁶. However, the molecular fingerprint of this phenotype is not well defined yet and is thought to be partially overlapped with innate abilities of epithelial cells^{247,248}.

Invasion capacity is an important feature presented by cancer cells and especially metastatic cells which confer the ability to establish niches for growth into neighboring tissues. EMT is often considered a prerequisite for cancer cell invasion and some studies have shown that oncostatin M induces Ser727 phosphorylation and promotes EMT in breast cancer cells MCF-7, whereas inhibition of Ser727 phosphorylation decreased invasion in prostate cancer cell line DU145^{244,249}. Expression of EMT markers such as E-cadherin or vimentin has been also reported in prostate cancer cell lines as a result of Ser727 phosphorylation²²⁴. These findings suggest that Ser727 phosphorylation is sufficient to mediate EMT and tumor cell invasion regardless of Tyr705 phosphorylation state. However, in this study we have not been able to find such correlation. Our results showed that surprisingly and in an opposite manner to the other functional experiments performed, SA and YF/SA mutants displayed the highest invasive capacity. This result may be partially explained by the observation of cell aggregates on the Matrigel layer only in mutants carrying phosphomimetic mutations of Ser727 (SD and YF/SD). In our experiments, cells were seeded at adequate density, and uniformly distributed at the beginning of the assay, however after 24 h, the formation of cellular aggregates began to be observed (data not shown). This experiment was repeated at different cell densities with same outcome. Therefore, we established that the formation of cell aggregates on Matrigel was a clear phenotypic feature of SD and YF/SD mutants, which possibly

prevented the migration and invasion of cells towards the chemoattractant, suggesting that pSer727 favors the formation of cell niches rather than invasion in our ccRCC cellular model.

The formation of cell aggregates and the result obtained from the invasion assay led us to hypothesize that invasion might rather occur by aggregates that migrate collectively and do not lose completely the epithelial phenotype, than by isolated mesenchymal cells. Accordingly, it has been reported that collective migration of cells eventually leads to aggregation in large clusters^{247,250,251}, indicating that cancer invasion by collective migration might not require the complete loss of epithelial markers. This alternative mechanism of invasion could explain our results. It is still unknown if collective migration can confer a selective advantage as opposed to pure isolated mesenchymal cell migration. In principle, aggregation of cells into clusters might represent a selective advantage over single cells due to the ability to escape certain facets of the immune response and to be advantageous after extravasation, where adhesion-dependent signaling is no longer present^{252,253}. To solve whether our cell lines SD and YF/SD indeed invade as collective clusters, a different type of invasion assay should be performed following a novel model of chemotaxis-driven cell aggregation²⁵⁴.

STAT3 is an important molecule in tumor biology for its ability to promote cancer through a plethora of different mechanisms, including the regulation of cancer stem cell activities. It is widely accepted that tumors contain a subpopulation of cells called *cancer stem cells* (CSCs) with the capacity of self-renew, drive tumor progression, drug resistance and metastatic properties^{255,256}. STAT3 has been reported to have an essential role in maintaining the expression of genes that are important for stem cell phenotype and are used as markers of CSCs. The most common are CD24, CD34, CD38, CD44, CD90, and CD133, together with *aldehyde dehydrogenase* (ALDH), and the ability to form spheroids in suspension *in vitro*²⁵⁷. It has been described that STAT3 pathway is preferentially active in subpopulations of cells enriched for CSC markers and its inhibition decreases cell viability and tumorspheres formation. STAT3 has been found to physically interact with CD44 and NFκB and activates the catalytic subunit of telomerase to prolong proliferative potential²⁵⁸. Moreover, STAT3 can increase CD133 expression through functional cooperation with NFκB and HIF1α²⁵⁹. Other studies have reported a direct link between EMT and gain of CSC properties²⁶⁰ and STAT3 activation plays an important role in EMT induction in different types of tumors. Induction of EMT after STAT3 activation and expansion of the CSC population has been observed^{261,262}. STAT3 activation has been also observed in HER2 negative breast cancer, where it also correlates with CSC properties²⁵⁷. Furthermore, STAT3 is a critical transcription factor in angiogenesis, participating in the expression and protein stability of HIF1α and regulating or being itself regulated by VEGF. This involvement was also shown to play a role in maintaining the self-renewal properties of CSCs¹⁴¹. STAT3 can be activated and thereby contribute to CSCs properties by the BMX and Ras homolog family member C and it can be activated also epigenetically by the histone-lysine N-methyltransferase *Enhancer of Zeste Homolog 2* (EZH2)^{88,263,264}. Taking all these observations together, the role of STAT3 in promoting and maintaining CSC properties are highly complex. Nevertheless, and despite all evidence pointing to STAT3 as a master regulator of stemness, we could not find this relationship. Our results showed that all our STAT3 phosphomutants were able to form tumorspheres, even the cell line where STAT3 was silenced (pLX304), which results contradictory to previous findings.

Moreover, we could only observe the formation of a single tumorsphere containing all or almost all of the cells seeded. When we tried to disaggregate these single tumorspheres for following enrichment experiments of CSCs, all cells died. Therefore, we are not positive if this result was due to a technical issue or indeed represents the behavior of our mutants. What we are sure of is that the spheres formed possessed the characteristics of a tumorsphere, containing a compact core that darkens and grows as time passed, indicating proliferation. Based on this result, we cannot conclude whether STAT3 and its phosphorylation state contributes to the CSC phenotype in our ccRCC model and more experiments should be carried on.

Regardless of invasion and tumorspheres formation assays, the rest of the functional experiments demonstrate that phosphorylation at Ser727-STAT3 clearly promotes an oncogenic phenotype *in vitro*.

Until now, the characterization of STAT3 phosphomutants has been carried out on the human-derived ccRCC cell line 769-P, however, future perspectives include their analysis and characterization *in vivo*. Since it has been reported that 769-P cell line does not form tumors *in vivo*, besides having a second cellular model to validate our results, 786-O cell lines were also transduced with all STAT3 phosphomutants to produce xenografts in immunosuppressed mice. We are looking forward to performing these experiments.

5. THE EFFECT OF ENDOGENOUS STAT3 ACTIVATION IN ccRCC

One of the specific aims to accomplish by doing microarray analysis was to identify the genes regulated by STAT3 under basal conditions in our cellular model of ccRCC (769-P), thus, we compared the gene expression between pLKO (empty vector of silencing: endogenous STAT3 silencing) and shRNA2 (STAT3 silencing). We found 818 differentially expressed genes significantly involved in 20 molecular functions, 20 cellular compartments, and 36 biological processes according to g:Profiler analysis and the gene ontology (GO) database.

According to the Warburg effect, ccRCC is one of the cancers considered as a role model because it is driven by metabolic shift to aerobic glycolysis followed by lactic acid fermentation as the major form of energy production during normoxia⁴⁸. Moreover, transcriptomic studies have demonstrated that expression levels of genes involved in the suppression of oxidative phosphorylation and glycolysis pathways are usually increased in ccRCC^{34,50}. Upregulation of the pentose phosphate pathway and fatty acid synthesis are also common, which agrees with ccRCC phenotype where cells are rich in lipids and glycogen. In that regard, our analysis showed that genes regulated by STAT3 significantly contribute to the activation of several of these molecular functions, such as aldo-keto reductase family 1 members (AKR1B15, AKR1B10, AKR1C2, AKR1C1, and AKR1C3), ATP-binding cassette ABC transporters (ABCA1), cytochrome P450 family members (CYP4F11), aldehyde dehydrogenase family members (ALDH1A1), phosphatidic acid phosphatase family members (PLPP3 and PLPP2), lysophosphatidic acid acyltransferase protein family members (GPAT3), fatty acid elongases (ELOVL6), and solute carrier family members (SLC44A2, SLC44A3, and SLC27A2), to mention a few.

The activation of endogenous STAT3 was also found to be significantly related to biological processes considered hallmarks of cancer. Cell adhesion, positive regulation of cell population and proliferation, response to wounding, negative regulation of extrinsic apoptotic signaling, extracellular structure organization, and cell differentiation are some of them. Even though pLKO and shRNA2 were not included in the functional assays, it is important to notice that pLKO cell line was also observed to form cell aggregates (data not shown) as phosphomimetic mutants of Ser727 (SD and YF/SD). This phenotype correlates with the results obtained from microarray analysis, where biological processes related to cell adhesion and cell-cell adhesion were significantly overrepresented.

Furthermore, the gene EPAS1, codifying for HIF2 α , was found upregulated by endogenous STAT3 expression. As mentioned before, the inactivation of VHL constitutes the earliest oncogenic driving event for ccRCC²¹ and leads to upregulated expression of oncogenic HIF1 α and HIF2 α . The aberrant accumulation of HIF proteins results in uncontrolled activation of HIF target genes that regulate angiogenesis, glycolysis, cell migration, dedifferentiation, and apoptosis¹⁵. Moreover, HIF1 α was previously found overexpressed in 769-P cells as a result of IL6/STAT3 pathway activation by KIM1. These results indicate that STAT3 contributes to dysregulated response to hypoxia in ccRCC by upregulation of both HIF1 α and HIF2 α .

So far, STAT3 has been largely studied in several human cancers but not in ccRCC. Moreover, most of the studies on ccRCC have focused on its genomic and molecular characterization, but none of them has described the relationship between STAT3 and ccRCC. Therefore, our data from the differential expression as well as from the analysis of biologic significance constitutes the first study on the role of STAT3 in ccRCC.

6. THE EFFECT OF STAT3 PHOSPHORYLATION STATE IN ccRCC

Once we identified the genes and signaling pathways associated with STAT3 in basal conditions, we analyzed the differential expression among the different STAT3 phosphomutants. This analysis showed that overexpression of STAT3 WT recovered ~30% (249 genes) of STAT3 activity compared to endogenous STAT3 activation (pLKO). While it is true that these two cell lines cannot be technically compared, it gives us an idea of the general behavior of STAT3 overexpression. Nevertheless, the transcriptional activity of STAT3 WT was sufficient to induce a different phenotype from pLX304 (STAT3 silencing), as observed in functional experiments. According to our initial characterization, STAT3 WT is phosphorylated at both residues: pTyr705 induced by treatment with IL6, and pSer727 by intrinsic mechanisms of 769-P cells, thus, although minor, its functional behavior was similar to SD mutant.

SA and YF/SA were the mutants with the lower number of genes differentially expressed (132 and 144 genes, respectively). Interestingly, the transcriptional activity of SA was slightly lower than the YF/SA. Since the only difference between these two mutants is the phosphorylation state of Tyr705, and SA was the mutant with the lower number of differentially expressed genes, this result suggests that the effect of pTyr705-STAT3 in our ccRCC cellular model is subtle. These results are, indeed, in accordance with those

observed in ccRCC patients, where no significant correlation was found between pTyr705 in tumors and overall survival of patients⁶⁶.

Furthermore, several studies have demonstrated that unphosphorylated STAT3, which refers to the absence of Tyr705 phosphorylation, is capable to cooperate with NFκB in the transcription of a subclass of NFκB target genes by forming a transcription factor complex^{102,103}. In order to explore this non-canonical mechanism of STAT3 activation, we performed a luciferase-reporter assay with the NFκB consensus promoter. We tested all STAT3 phosphomutants and our preliminary results showed that only the YF/SA mutant exhibited transcriptional activity (data not shown). Since YF/SD has a phosphoablative mutation for Tyr705 as YF/SA, we expected that it would have transcriptional activity as well. However, this result suggests that the phosphorylation state of Ser727 is relevant to determine whether STAT3 cooperates with NFκB or not. Confirmation of these preliminary results, might indicate that previous reports assuming that only the absence of phosphorylation at Tyr705 is sufficient for transcribing NFκB genes, are partially incorrect.

SD and YF/SD were the mutants exhibiting the higher number of differentially expressed genes (455 and 342 genes, respectively), indicating that phosphorylation at Ser727 substantially increases transcriptional activity.

SD mutant, which represents a complete STAT3 phosphorylation state, showed the most potent transcriptional activity. It has been described that phosphorylation at both residues produced an optimal activation of STAT3 and increases the number of target genes, as we observed. For instance, a study reported that RhoA can efficiently activate STAT3 transcriptional activity by both Tyr705 and Ser727 phosphorylation in HEK293T, CHO-4, and BRL-4 cell lines. Further experiments demonstrated that STAT3 cooperates with RhoA for full transcriptional STAT3 activation and oncogenic transformation observed by an increase in both the number and size of anchorage-independent colonies. The use of a phosphoablative mutations for Tyr705 (YF) and Ser727 (SA) separately, diminished the ability of cells to grow in soft agar, demonstrating that full activation of STAT3 is necessary for RhoA-mediated transformation⁸¹. The analysis of biological significance of SD target genes yielded 31 overrepresented biological processes resembling those found associated with endogenous STAT3 activation, including cell adhesion and positive regulation of cell migration. Furthermore, regulation of ERK1 and ERK2 cascade appeared overrepresented, correlating with previous findings where phosphorylation of Ser727 was reported to be induced by ERK family of mitogen-activated protein (MAP) kinases in response to growth factors⁸⁰.

Although the SD mutant yielded the higher number of differentially expressed genes, the analysis of biological significance resulted in YF/SD as the mutant with the largest number of overrepresented molecular functions, cellular components, and biological processes. The YF/SD-mediated expression of 342 genes was associated with 97 biological processes indicating that these genes dependent on Ser727 phosphorylation regulate highly specific and constrained signaling pathways. Otherwise, the biological significance analysis would yield fewer overrepresented processes than SD. Furthermore, most of the biological processes found significant in YF/SD were related to cell motility and migration, cell population and proliferation, cell adhesion, chemotaxis, and negative regulation of extrinsic apoptosis, which are hallmarks of carcinogenesis. Indeed, these

overrepresented pathways correlate to the functional experiments, where YF/SD was the most significant mutant to induce cell proliferation, migration, clonogenicity, and anchorage-independent growth. Overall, our data supports all the previous studies indicating that pSer727 has a potent effect in inducing tumorigenesis in several human cancers. Hence, the striking biological effect of Ser727 phosphorylation in the absence of pTyr705 observed in our experiments, demonstrates that this phosphorylation state is superior in promoting oncogenesis.

Additionally, and based on the marked difference in biologic significance between SD and YF/SD (31 vs 97 overrepresented processes), this finding also suggests that, somehow, phosphorylation of Tyr705 attenuates the effect of pSer727, possibly through STAT3 being shared into canonical and non-canonical activation pathways.

By multiple comparisons of all STAT3 phosphomutants and visualization through heatmap, it was possible to observe the differential expression transition as both residues became phosphorylated. From STAT3 silencing (pLX304) through unphosphorylated STAT3 (YF/SA), Tyr705 phosphorylation (SA), Ser727 phosphorylation (YF/SD) to complete STAT3 phosphorylation at both residues (SD). The changes in STAT3 transcriptional activity according to its phosphorylation state are evident and demonstrates that phosphorylation at Ser727 is clearly more forceful than phosphorylation at Tyr705.

Multiple comparisons among all STAT3 phosphomutants also allowed us to identify 265 genes expressed without following a clear pattern regarding Tyr705 or Ser727 phosphorylation state. The expression of these common genes indicates that they are regulated by STAT3 regardless of its phosphorylation state and suggests that their expression may be influenced by the cellular context.

To our knowledge, this is the first report analyzing the effect of different STAT3 phosphorylation states in the context of ccRCC, providing important insights into overall STAT3 transcriptional behavior.

7. PHOSPHORYLATION OF Ser727 ACTS BY A DIFFERENT ACTIVATION SIGNALING PATHWAY FROM CANONICAL

To date, it is acknowledged that STAT3 can be activated by two different main pathways. The canonical activation pathway relying on the phosphorylation of Tyr705 and nuclear transcription of target genes, and the non-canonical activation pathway which is phosphorylation-independent and includes genomic and non-genomic STAT3 functions. To determine if the transcriptional activity observed in our STAT3 phosphomutants was driven by the canonical activation pathway, we performed a luciferase-reporter assay with the STAT3 consensus promoter. We observed that only mutants where Tyr705 phosphorylation was induced by IL6 treatment (SA and SD), acted through the STAT3 canonical pathway regardless of the Ser727 phosphorylation state. This result agreed with the literature showing that pTyr705 is an indispensable feature for STAT3 canonical transcriptional activity, whereas suggests that the gene transcription observed in phosphomimetic mutants of Ser727 (SD) is driven by a different pathway from canonical.

To support this finding, previous studies on analyzing the non-canonical transcriptional activity of STAT3 have been carried on, however, none of them have achieved compelling conclusions. For instance, a study using a computational strategy to describe the complete repertoire of STAT3 binding sites genome-wide, irrespective of the cell type or cellular conditions, resulted in 1.35 million hits. This result represents a potential universe of STAT3-binding sites²⁶⁵. Moreover, this incredible number of putative binding sites does not account for other determining factors, such as functional partnerships with other co-activator molecules or transcription factors. In that regard, a global sequence analysis of the STAT3 promoter regions did not reveal a significant dependence on the total number of STAT3 motifs and gene transcription, whereas other studies have found that, depending on the STAT3 PTMs and phosphorylation state, it can form transcriptional enhanceosomes with other proteins, such as c-Jun, FoxP3, BRD4, and NFκB, thus influencing different transcriptional outcomes^{103,266,267}. Another study based on ChIP-seq in human Th17 cells identified 4371 STAT3-binding sites, where approximately 94% of them were located in introns or intergenic regions, suggesting that STAT3 may regulate gene expression via binding to distal regulatory elements that amplify the effect of STAT3 on gene expression. The same study also analyzed STAT3 DNA-binding in response to cytokines stimulation at different times, founding that STAT3-binding sites change over time and that at later stages of Th17 differentiation, STAT3 influences gene expression mostly through mechanisms that do not involve direct binding to promoters⁸⁵. Based on these reports, it is evident that STAT3 activation and further transcription capacity is a highly intricate and regulated process far from being completely understood.

In our particular case, it is undeniable the increase in transcriptional activity drive by pSer727-STAT3, thus, further studies are needed to solve how pSer727 promotes gene expression. A ChIP-seq analysis is in our future perspectives, in order to determine the binding dynamics between pSer727-STAT3 and the DNA. Nevertheless, we do not dismiss the possibility of cooperative interactions with other proteins either.

8. THE SUBSET OF pSer727-DEPENDENT GENES AS POTENTIAL THERAPEUTIC TARGETS FOR ccRCC TREATMENT

Based on the correlation found between pSer727-STAT3 expression levels and the poor outcome in ccRCC patients, as well as on the observation that cell lines carrying a phosphomimetic mutation for Ser727 (SD) exhibit a pro-tumoral phenotype *in vitro*, we aimed to identify the subset of pSer727-target genes as especially relevant genes in ccRCC progression. For that purpose, we used a very conservative approach to select genes only expressed in YF/SD mutant that were not expressed in any other STAT3 phosphomutant. We identified 132 pSer727-dependent genes that significantly contribute to 45 of 97 biological processes found overrepresented in YF/SD analysis, including response to extracellular stimulus, cell adhesion, cell differentiation, tissue development, taxis, response to stress, response to cytokines, and negative regulation of apoptosis. All of them associated with tumor development.

The identification of this subset of genes *per se* constitutes the first description of the transcriptional contribution of pSer727-STAT3 in ccRCC, and more importantly, it offers

the opportunity to consider all these genes as potential therapeutic targets, since they depict, at least in part, the molecular context that leads to ccRCC progression.

At present, the specific inhibition of STAT3 has been pursued, and although many STAT3 inhibitors have been developed, no candidate has shown sufficient therapeutic effects to be clinically approved. Moreover, the dual role of STAT3 in cancer should be taken into account because STAT3 inhibition may result in tumor progression.

In that regard, during the development of this study, we collaborated with the company CEAMED S.A in testing the compound CM-728 as a potential STAT3 inhibitor. The objective of this collaboration was to determine whether CM-728 inhibited Tyr705 or Ser727 phosphorylation or both in our ccRCC cellular models (769-p and 786-O). Our results demonstrated that CM-728 strongly inhibited pTyr705 at lower doses than Sunitinib, which is the current first-line treatment for metastatic ccRCC, however, it had no effect on pSer727 (data not shown). This result illustrates the complexity of inhibiting a protein such as STAT3 having several mechanisms of activation with different outcomes. Thus, the identification of pSer727-dependent genes constitutes a niche of putative and more manageable therapeutic targets.

Further studies on the determination of those genes acting as nodes of several oncogenic signaling pathways downstream pSer727-STAT3 should be performed, in order to narrow the candidates for future validation as therapeutic targets.

9. PUTATIVE AND NOVEL PROGNOSTIC BIOMARKERS FOR ccRCC (FUTURE VALIDATION)

pSer727-STAT3 has demonstrated to be a consistent and reliable biomarker that indicates low overall survival of ccRCC patients, however, its detection depends on immunohistochemical techniques performed on tissue samples obtained through invasive procedures, and its evaluation by expert pathologists is prone to human error. Moreover, the assessment of phosphorylated proteins by ICC is more complicated than regular proteins and requires more careful handling of tissue samples to preserve intact phosphorylated residues.

Hence, the identification of the pSer727-dependent genes provides the opportunity of exploring alternatives to pSer727-STAT3 that may also function as ccRCC prognostic biomarkers and may be easier to detect and measure.

To this end, and based on our capacity for data analysis at the time of the study, we set cut-off parameters to select the most appealing candidates. Thinking ahead of the development of detection kits, we only included upregulated genes that were manually curated based on the literature, to select only those who have been previously associated with the development and progression of human cancers but not to other types of RCC. The exclusion of downregulated genes, as well as those genes unrelated to tumor development, does not mean in any way that they are not biologically important or that they cannot represent possible biomarkers for the same purpose. These selection criteria were used only to narrow the list of candidates and may change in the future depending on further analysis.

Therefore, after sieving, we ended up with 10 candidates as potential and novel prognostic biomarkers for ccRCC patients, including i) transmembrane proteins (GPNMB, STEAP2, and LGALS4), ii) cell surface receptors (HHLA2, F2RL1, and HTR1D), transcription factors (TOX and FOXA1), iii) a proto-oncogene (FGR), and an intermediate filament (KRT20).

Since we attempted to find a less invasive alternative to pSer727-STAT3, we selected the glycoprotein nonmetastatic melanoma protein B (GPNMB) and the cytokeratin 20 (KRT20) as the most promising candidates, because both can be detected in blood and urine samples. In contrast to tissue biopsies, where tumoral heterogeneity could lead to biased results, the use of liquid biopsies represents the best approach to determine the general condition of tumors.

As future perspectives, an initial ICC analysis to detect the protein expression of these two genes will be performed in the same TMA used to validate the pSer727-STAT3 (82 ccRCC patients), to observe whether the results found *in vitro* do also occur *in vivo*.

Given that our group already collaborate with the Urology Department at Vall d'Hebron Hospital and we have collected tissue samples of different types of RCCs, as well as blood and urine samples of ccRCC patients before surgery to two years follow-up after surgery (collected every 3 months) and we have access to the clinical record of all patients included on both TMAs (94 and 82 ccRCC patients, respectively), we are able to pursue further validation of these candidates as promising prognostic biomarkers.

We propose to evaluate the expression of GPNMB and KRT20 in blood and urine samples of patients with different types of RCC. This analysis will allow us to determine whether their expression is restricted to ccRCC. If positive, a retrospective analysis correlating their expression levels with clinicopathological characteristics of ccRCC patients would be performed to validate their value as soluble prognostic factors.

Depending on the results, the development of a detection kit, i.e. an ELISA assay, that facilitates the assessment of these two biomarkers, would be considered.

Furthermore, if GPNMB and/or KRT20 turn out to be specific to ccRCC and not to another type of RCC, they could also be used as diagnostic biomarkers, after suspicion from imaging studies. Moreover, if we would be able to find a correlation between the expression levels and tumor stage, we could establish ELISA detection ranges that allow a fast and reliable analysis that indicates the stage of the disease.

Besides the potential of GPNMB and KRT20 as prognostic and possibly diagnostic biomarkers, they could also be thought of as indicators of response to treatment. To date, there are no clinically usable markers with whom to follow up on ccRCC patients during and after treatment. Therefore, they would represent an easily readable and non-invasive form to follow disease progression.

CONCLUSIONS

STAT3 is a latent transcription factor that regulates downstream genes involved in essential biological processes including cell differentiation, proliferation, migration, apoptosis inhibition, and survival. The aberrant activation of STAT3 has been related to the development of ~50% of all human cancers, including ccRCC. Since ccRCC is the most prevalent and lethal histological subtype of RCC, and the molecular mechanisms behind its tumorigenesis still remain unclear, in this study, we analyzed the role of STAT3 in ccRCC, and specifically the contribution of pSer727-STAT3 in tumor progression.

To conclude, the main findings of this study are:

- Nuclear and cytosolic pSer727-STAT3 expression levels correlate with poor prognosis and low overall survival in ccRCC patients.
- Phosphorylation of Ser727-STAT3 induces a pro-tumoral phenotype *in vitro* in the human-derived ccRCC cell line 769-P.
- Endogenous STAT3 regulates the expression of 818 genes associated with biological processes that correlate to ccRCC phenotype.
- There are genes regulated by STAT3 regardless of its phosphorylation state.
- Phosphorylation of Ser727-STAT3 has a more striking effect on STAT3 activation than pTyr705.
- Phosphorylation of Ser727-STAT3 mediates gene transcription by a different activation pathway from canonical.
- Phosphorylation of Ser727-STAT3 specifically regulates a subset of 132 target genes that constitute putative therapeutic targets and novel biomarkers for ccRCC.

In summary, the present study, responds to the urgent need to better understand ccRCC biology and constitute the first analysis on the role of overall STAT3 phosphorylation and pSer727-STAT3 in ccRCC. Our results demonstrate that pSer727 is capable of activating STAT3 signaling through transcription of downstream target genes that induce a pro-tumoral phenotype *in vitro*. More importantly, our findings are clinically relevant given that pSer727 is expressed in ccRCC patients and correlates with lower overall survival, leading support to the notion that pSer727-STAT3 phosphorylation alone plays an important role in ccRCC development and progression.

BIBLIOGRAPHY

1. Douglas Eaton PJ. *Vander's Renal Physiology*. 7th ed. McGraw Hill; 2009.
2. Betts JGKAY. *Anatomy and Physiology*. Vol 53. OpenStax; 2019. doi:10.1017/CBO9781107415324.004
3. Bray F, Ferlay J, Soerjomataram I, Siegel RL, Torre LA, Jemal A. Global Cancer Statistics 2018: GLOBOCAN Estimates of Incidence and Mortality Worldwide for 36 Cancers in 185 Countries. *CA Cancer J Clin*. 2018;00:1-31. doi:10.3322/caac.21492
4. Linehan WM, Ricketts CJ. The Cancer Genome Atlas of renal cell carcinoma: findings and clinical implications. *Nat Rev Urol*. 2019. doi:10.1038/s41585-019-0211-5
5. Rini, Brian I.; Campbell SC. *Renal Cell Carcinoma*. Vol 66. PMPH-USA; 2009.
6. Cheville JC, Lohse CM, Zincke H, Weaver AL, Blute ML. Comparisons of outcome and prognostic features among histologic subtypes of renal cell carcinoma. *Am J Surg Pathol*. 2003;27(5):612-624. doi:10.1097/00000478-200305000-00005
7. Cohen D, Zhou M. Molecular Genetics of Familial Renal Cell Carcinoma Syndromes. *Clin Lab Med*. 2005;25(2):259-277. doi:10.1016/j.cll.2005.01.003
8. Murphy WM, Grignon DJ, Perlman EJ, Armed Forces Institute of Pathology (U.S.), Universities Associated for Research and Education in Pathology. *Tumors of the Kidney, Bladder, and Related Urinary Structures*. Armed Forces Institute of Pathology; 2004.
9. Delahunt B, Eble JN, McCredie MR, Bethwaite PB, Stewart JH, Bilous AM. Morphologic typing of papillary renal cell carcinoma: comparison of growth kinetics and patient survival in 66 cases. *Hum Pathol*. 2001;32(6):590-595. doi:10.1053/hupa.2001.24984
10. Antonelli A, Portesi E, Cozzoli A, et al. The collecting duct carcinoma of the kidney: a cytogenetical study. *Eur Urol*. 2003;43(6):680-685. doi:10.1016/s0302-2838(03)00152-0
11. Karakiewicz PI, Trinh Q-D, Rioux-Leclercq N, et al. Collecting Duct Renal Cell Carcinoma: A Matched Analysis of 41 Cases. *Eur Urol*. 2007;52(4):1140-1146. doi:10.1016/j.eururo.2007.01.070
12. Tokuda N, Naito S, Matsuzaki O, et al. Collecting duct (Bellini duct) renal cell carcinoma: a nationwide survey in Japan. *J Urol*. 2006;176(1):40-43; discussion 43. doi:10.1016/S0022-5347(06)00502-7
13. Davis CJ, Mostofi FK, Sesterhenn IA. Renal Medullary Carcinoma The Seventh Sickle Cell Nephropathy. *Am J Surg Pathol*. 1995;19(1):1-11. doi:10.1097/00000478-199501000-00001
14. Watanabe IC, Billis A, Guimarães MS, et al. Renal medullary carcinoma: report of seven cases from Brazil. *Mod Pathol*. 2007;20(9):914-920. doi:10.1038/modpathol.3800934
15. Hsieh JJ, Purdue MP, Signoretti S, et al. Renal cell carcinoma. *Ren Cell Carcinoma Mol Featur Treat Updat*. 2017;3(March):1-19. doi:10.1007/978-4-431-55531-5_2
16. Shuch B, Vourganti S, Ricketts CJ, et al. Defining early-onset kidney cancer: implications for germline and somatic mutation testing and clinical management. *J Clin Oncol*. 2014;32(5):431-437. doi:10.1200/JCO.2013.50.8192
17. Sun M, Thuret R, Abdollah F, et al. Age-adjusted incidence, mortality, and survival rates of stage-specific renal cell carcinoma in North America: a trend analysis. *Eur Urol*. 2011;59(1):135-141. doi:10.1016/j.eururo.2010.10.029
18. McLaughlin J, Lipworth L, Tarone R, Blot W. *Cancer Epidemiology and Prevention*. (Schottenfeld D, Fraumeni JF, eds.). Oxford University Press; 2006. <http://www.oxfordscholarship.com/view/10.1093/acprof:oso/9780195149616.001.0001/acprof-9780195149616>. Accessed January 24, 2019.
19. Karami S, Schwartz K, Purdue MP, et al. Family history of cancer and renal cell cancer risk in Caucasians and African Americans. *Br J Cancer*. 2010;102(11):1676-1680.

- doi:10.1038/sj.bjc.6605680
20. Haas NB, Nathanson KL. Hereditary kidney cancer syndromes. *Adv Chronic Kidney Dis.* 2014;21(1):81-90. doi:10.1053/j.ackd.2013.10.001
 21. Kaelin WG. von Hippel-Lindau disease. *Annu Rev Pathol Mech Dis.* 2007;2(1):145-173. doi:10.1146/annurev.pathol.2.010506.092049
 22. Heng DYC, Xie W, Regan MM, et al. External validation and comparison with other models of the International Metastatic Renal-Cell Carcinoma Database Consortium prognostic model: A population-based study. *Lancet Oncol.* 2013;14(2):141-148. doi:10.1016/S1470-2045(12)70559-4
 23. Reuter VE, Tickoo SK. Differential diagnosis of renal tumours with clear cell histology. *Pathology.* 2010;42(4):374-383. doi:10.3109/00313021003785746
 24. Fuhrman SA, Lasky LC, Limas C. Prognostic significance of morphologic parameters in renal cell carcinoma. *Am J Surg Pathol.* 1982;6(7):655-663. <http://www.ncbi.nlm.nih.gov/pubmed/7180965>. Accessed September 16, 2015.
 25. Stewart-Merrill SB, Thompson RH, Boorjian SA, et al. Oncologic Surveillance After Surgical Resection for Renal Cell Carcinoma: A Novel Risk-Based Approach. *J Clin Oncol.* 2015;33(35):4151-4157. doi:10.1200/JCO.2015.61.8009
 26. Motzer RJ, Bacik J, Murphy BA, Russo P, Mazumdar M. Interferon-alfa as a comparative treatment for clinical trials of new therapies against advanced renal cell carcinoma. *J Clin Oncol.* 2002;20(1):289-296. doi:10.1200/JCO.20.1.289
 27. Bex A, Ljungberg B, van Poppel H, Powles T. The Role of Cytoreductive Nephrectomy: European Association of Urology Recommendations in 2016. *Eur Urol.* 2016;70(6):901-905. doi:10.1016/j.eururo.2016.07.005
 28. Blom JHM, van Poppel H, Maréchal JM, et al. Radical Nephrectomy with and without Lymph-Node Dissection: Final Results of European Organization for Research and Treatment of Cancer (EORTC) Randomized Phase 3 Trial 30881 Editorial by Urs E. Studer and Frédéric D. Birkhäuser on pp. x-y of this issue. *Eur Urol.* 2008;55:28-34. doi:10.1016/j.eururo.2008.09.052
 29. Van Poppel H, Da Pozzo L, Albrecht W, et al. A prospective, randomised EORTC intergroup phase 3 study comparing the oncologic outcome of elective nephron-sparing surgery and radical nephrectomy for low-stage renal cell carcinoma. *Eur Urol.* 2011;59(4):543-552. doi:10.1016/j.eururo.2010.12.013
 30. Campbell SC, Novick AC, Belldegrun A, et al. Guideline for Management of the Clinical T1 Renal Mass. *J Urol.* 2009;182(4 SUPPL.):1271-1279. doi:10.1016/j.juro.2009.07.004
 31. El Dib R, Touma NJ, Kapoor A. Cryoablation vs radiofrequency ablation for the treatment of renal cell carcinoma: a meta-analysis of case series studies. *BJU Int.* 2012;110(4):510-516. doi:10.1111/j.1464-410X.2011.10885.x
 32. Vera-Badillo FE, Templeton AJ, Duran I, et al. Systemic therapy for non-clear cell renal cell carcinomas: A systematic review and meta-analysis. *Eur Urol.* 2015;67(4):740-749. doi:10.1016/j.eururo.2014.05.010
 33. Kapitsinou PP, Haase VH. The VHL tumor suppressor and HIF: insights from genetic studies in mice. *Cell Death Differ.* 2008;15(4):650-659. doi:10.1038/sj.cdd.4402313
 34. Cancer Genome Atlas Research Network. Comprehensive molecular characterization of clear cell renal cell carcinoma. *Nature.* 2013;499(7456):43-49. doi:10.1038/nature12222
 35. Sato Y, Yoshizato T, Shiraishi Y, et al. Integrated molecular analysis of clear-cell renal cell carcinoma. *Nat Genet.* 2013;45(8):860-867. doi:10.1038/ng.2699
 36. Hakimi AA, Pham CG, Hsieh JJ. A clear picture of renal cell carcinoma. *Nat Genet.* 2013;45(8):849-850. doi:10.1038/ng.2708

37. Voss MH, Hakimi AA, Pham CG, et al. Tumor genetic analyses of patients with metastatic renal cell carcinoma and extended benefit from mTOR inhibitor therapy. *Clin Cancer Res*. 2014;20(7):1955-1964. doi:10.1158/1078-0432.CCR-13-2345
38. Li L, Shen C, Nakamura E, et al. SQSTM1 Is a Pathogenic Target of 5q Copy Number Gains in Kidney Cancer. *Cancer Cell*. 2013;24(6):738-750. doi:10.1016/j.ccr.2013.10.025
39. Mitchell TJ, Turajlic S, Rowan A, et al. Timing the Landmark Events in the Evolution of Clear Cell Renal Cell Cancer: TRACERx Renal. *Cell*. 2018;173(3):611-623.e17. doi:10.1016/j.cell.2018.02.020
40. Hakimi AA, Ostrovnaya I, Reva B, et al. Adverse outcomes in clear cell renal cell carcinoma with mutations of 3p21 epigenetic regulators BAP1 and SETD2: A report by MSKCC and the KIRC TCGA research network. *Clin Cancer Res*. 2013;19(12):3259-3267. doi:10.1158/1078-0432.CCR-12-3886
41. Kapur P, Peña-Llopis S, Christie A, et al. Effects on survival of BAP1 and PBRM1 mutations in sporadic clear-cell renal-cell carcinoma: a retrospective analysis with independent validation. *Lancet Oncol*. 2013;14(2):159-167. doi:10.1016/S1470-2045(12)70584-3
42. Nam SJ, Lee C, Park JH, Moon KC. Decreased PBRM1 expression predicts unfavorable prognosis in patients with clear cell renal cell carcinoma. *Urol Oncol Semin Orig Investig*. 2015;33(8):340.e9-340.e16. doi:10.1016/j.urolonc.2015.01.010
43. Hsieh JJ, Chen D, Wang PI, et al. Genomic Biomarkers of a Randomized Trial Comparing First-line Everolimus and Sunitinib in Patients with Metastatic Renal Cell Carcinoma. *Eur Urol*. 2017;71(3):405-414. doi:10.1016/j.eururo.2016.10.007
44. Manley BJ, Zabor EC, Casuscelli J, et al. Integration of Recurrent Somatic Mutations with Clinical Outcomes: A Pooled Analysis of 1049 Patients with Clear Cell Renal Cell Carcinoma. *Eur Urol Focus*. 2017;3(4-5):421-427. doi:10.1016/j.euf.2016.06.015
45. Gerlinger M, Endesfelder D, Math D, et al. Intratumor heterogeneity and branched evolution revealed by multiregion sequencing. 2012.
46. Gerlinger M, Horswell S, Larkin J, et al. Genomic architecture and evolution of clear cell renal cell carcinomas defined by multiregion sequencing. *Nat Genet*. 2014;46(3):225-233. doi:10.1038/ng.2891
47. Sankin A, Hakimi AA, Mikkilineni N, et al. The impact of genetic heterogeneity on biomarker development in kidney cancer assessed by multiregional sampling. *Cancer Med*. 2014;3(6):1485-1492. doi:10.1002/cam4.293
48. Warburg O. On the origin of cancer cells. *Science (80-)*. 1956;123(3191):309-314. doi:10.1126/science.123.3191.309
49. Linehan WM, Schmidt LS, Crooks DR, et al. The Metabolic Basis of Kidney Cancer. *Cancer Discov*. 2019;9(8):1006-1021. doi:10.1158/2159-8290.CD-18-1354
50. Eales KL, Hollinshead KER, Tennant DA. Hypoxia and metabolic adaptation of cancer cells. *Oncogenesis*. 2016;5:e190. doi:10.1038/oncsis.2015.50
51. Hakimi AA, Reznik E, Lee CH, et al. An Integrated Metabolic Atlas of Clear Cell Renal Cell Carcinoma. *Cancer Cell*. 2016;29(1):104-116. doi:10.1016/j.ccell.2015.12.004
52. Şenbabaoğlu Y, Gejman RS, Winer AG, et al. Tumor immune microenvironment characterization in clear cell renal cell carcinoma identifies prognostic and immunotherapeutically relevant messenger RNA signatures. *Genome Biol*. 2016;17(1):231. doi:10.1186/s13059-016-1092-z
53. Zhou L, Liu XD, Sun M, et al. Targeting MET and AXL overcomes resistance to sunitinib therapy in renal cell carcinoma. *Oncogene*. 2016;35(21):2687-2697. doi:10.1038/onc.2015.343
54. Dong Y, Manley BJ, Becerra MF, et al. Tumor Xenografts of Human Clear Cell Renal Cell Carcinoma But Not Corresponding Cell Lines Recapitulate Clinical Response to Sunitinib: Feasibility of Using Biopsy Samples. *Eur Urol Focus*. 2017;3(6):590-598. doi:10.1016/j.euf.2016.08.005

55. Wang SS, Gu YF, Wolff N, et al. Bap1 is essential for kidney function and cooperates with Vhl in renal tumorigenesis. *Proc Natl Acad Sci U S A*. 2014;111(46):16538-16543. doi:10.1073/pnas.1414789111
56. Escudier B, Cosaert J, Jethwa S. Targeted therapies in the management of renal cell carcinoma: role of bevacizumab. *Biologics*. 2008;2(3):517-530. <http://www.pubmedcentral.nih.gov/articlerender.fcgi?artid=2721410&tool=pmcentrez&rendertype=abstract>.
57. Molina AM, Feldman DR, Voss MH, et al. Phase 1 trial of everolimus plus sunitinib in patients with metastatic renal cell carcinoma. *Cancer*. 2012;118(7):1868-1876. doi:10.1002/cncr.26429
58. Motzer RJ, Escudier B, McDermott DF, et al. Nivolumab versus everolimus in advanced renal-cell carcinoma. *N Engl J Med*. 2015;373(19):1803-1813. doi:10.1056/NEJMoa1510665
59. Amin A, Dudek AZ, Logan TF, et al. Survival with AGS-003, an autologous dendritic cell-based immunotherapy, in combination with sunitinib in unfavorable risk patients with advanced renal cell carcinoma (RCC): Phase 2 study results. *J Immunother Cancer*. 2015;3(1). doi:10.1186/s40425-015-0055-3
60. Chen W, Hill H, Christie A, et al. Targeting renal cell carcinoma with a HIF-2 antagonist. *Nature*. 2016;539(7627):112-117. doi:10.1038/nature19796
61. Tran HT, Liu Y, Zurita AJ, et al. Prognostic or predictive plasma cytokines and angiogenic factors for patients treated with pazopanib for metastatic renal-cell cancer: a retrospective analysis of phase 2 and phase 3 trials. *Lancet Oncol*. 2012;13(8):827-837. doi:10.1016/S1470-2045(12)70241-3
62. Armstrong AJ, George DJ, Halabi S. Serum lactate dehydrogenase predicts for overall survival benefit in patients with metastatic renal cell carcinoma treated with inhibition of mammalian target of rapamycin. *J Clin Oncol*. 2012;30(27):3402-3407. doi:10.1200/JCO.2011.40.9631
63. Vila MR, Kaplan GG, Feigelstock D, et al. Hepatitis A virus receptor blocks cell differentiation and is overexpressed in clear cell renal cell carcinoma. *Kidney Int*. 2004;65(5):1761-1773. doi:10.1111/j.1523-1755.2004.00601.x
64. Kaplan G, Totsuka A, Thompson P, Akatsuka T, Moritsugu Y, Feinstone SM. Identification of a surface glycoprotein on African green monkey kidney cells as a receptor for hepatitis A virus. *EMBO J*. 1996;15(16):4282-4296. <http://www.ncbi.nlm.nih.gov/pubmed/8861957>. Accessed October 9, 2018.
65. Cuadros T, Trilla E, Vilà MR, et al. Hepatitis A virus cellular receptor 1/kidney injury molecule-1 is a susceptibility gene for clear cell renal cell carcinoma and hepatitis A virus cellular receptor/kidney injury molecule-1 ectodomain shedding a predictive biomarker of tumour progression. *Eur J Cancer*. 2013;49(8):2034-2047. doi:10.1016/j.ejca.2012.12.020
66. Cuadros T, Trilla E, Sarro E, et al. HAVCR/KIM-1 activates the IL-6/STAT-3 Pathway in ccRCC and Determines Tumor Progression and Patient Outcome. *Cancer Res*. 2014. doi:10.1158/0008-5472.CAN-13-1671
67. May JY, Negrier S, Combaret V, et al. Serum Level of Interleukin 6 as a Prognosis Factor in Metastatic Renal Cell Carcinoma. *Cancer Res*. 1992;52(12):3317-3322.
68. Kishimoto T. The biology of interleukin-6. *Blood*. 1989;74(1):1-10. doi:10.1159/000420758
69. Guanizo AC, Fernando CD, Garama DJ, Daniel J. STAT3 : a multifaceted oncoprotein. *Growth Factors*. 2018;0(0):1-14. doi:10.1080/08977194.2018.1473393
70. Takeda K, Noguchi K, Shi W, et al. Targeted disruption of the mouse Stat3 gene leads to early embryonic lethality. *Proc Natl Acad Sci U S A*. 1997;94(8):3801-3804. doi:10.1073/pnas.94.8.3801
71. Miklossy G, Hilliard TS, Turkson J. Therapeutic modulators of STAT signalling for human diseases. *Nat Rev Drug Discov*. 2013;12(8):611-629. doi:10.1038/nrd4088

72. Caldenhoven E, Van Dijk TB, Solari R, et al. STAT3 β , a splice variant of transcription factor STAT3, is a dominant negative regulator of transcription. *J Biol Chem*. 1996;271(22):13221-13227. doi:10.1074/jbc.271.22.13221
73. Avalle L, Poli V. Nucleus, Mitochondrion, or Reticulum? STAT3 à La Carte. *Int J Mol Sci*. 2018;19(9):2820. doi:10.3390/ijms19092820
74. Aigner P, Just V, Stoiber D. STAT3 isoforms: Alternative fates in cancer? *Cytokine*. 2018;(January). doi:10.1016/j.cyto.2018.07.014
75. Ecker A. The dark and the bright side of Stat3: proto-oncogene and tumor-suppressor. *Front Biosci*. 2009;Volume(14):2944. doi:10.2741/3425
76. Lee J, Baldwin WM, Lee CY, Desiderio S. Stat3 β mitigates development of atherosclerosis in apolipoprotein E-deficient mice. *J Mol Med*. 2013;91(8):965-976. doi:10.1007/s00109-013-1013-5
77. Marino F, Orecchia V, Regis G, et al. STAT3 β controls inflammatory responses and early tumor onset in skin and colon experimental cancer models. *Am J Cancer Res*. 2014;4(5):484-494. <http://www.ncbi.nlm.nih.gov/pubmed/25232490>. Accessed October 26, 2019.
78. Schindler C, Levy DE, Decker T. JAK-STAT signaling: from interferons to cytokines. *J Biol Chem*. 2007;282(28):20059-20063. doi:10.1074/jbc.R700016200
79. Silver DL, Naora H, Liu J, Cheng W, Montell DJ. Activated Signal Transducer and Activator of Transcription (STAT) 3 : Localization in Focal Adhesions and Function in Ovarian Cancer Cell Motility Activated Signal Transducer and Activator of Transcription (STAT) 3 : Localization in Focal Adhesions an. 2004:3550-3558. doi:10.1158/0008-5472.CAN-03-3959
80. Chung J, Uchida E, Grammer TC, Blenis J. STAT3 serine phosphorylation by ERK-dependent and -independent pathways negatively modulates its tyrosine phosphorylation. *Mol Cell Biol*. 1997;17(11):6508-6516. <http://www.pubmedcentral.nih.gov/articlerender.fcgi?artid=232504&tool=pmcentrez&rendertype=abstract>.
81. Aznar S, Valerón PF, Del Rincon S V., Pérez LF, Perona R, Lacal JC. Simultaneous tyrosine and serine phosphorylation of STAT3 transcription factor is involved in RhoA GTPase oncogenic transformation. *Mol Biol Cell*. 2001;12(10):3282-3294. doi:10.1091/mbc.12.10.3282
82. Gough DJ, Corlett A, Schlessinger K, Wegrzyn J, Larner AC, Levy DE. Mitochondrial STAT3 supports RasDependent oncogenic transformation. *Science (80-)*. 2009;324(5935):1713-1716. doi:10.1126/science.1171721
83. Waitkus MS, Chandrasekharan UM, Willard B, et al. Signal Integration and Gene Induction by a Functionally Distinct STAT3 Phosphoform. *Mol Cell Biol*. 2014;34(10):1800-1811. doi:10.1128/MCB.00034-14
84. Yuan ZL, Guan YJ, Chatterjee D, Chin YE. Stat3 dimerization regulated by reversible acetylation of a single lysine residue. *Science (80-)*. 2005;307(5707):269-273. doi:10.1126/science.1105166
85. Ray S, Boldogh I, Brasier AR. STAT3 NH2-terminal acetylation is activated by the hepatic acute-phase response and required for IL-6 induction of angiotensinogen. *Gastroenterology*. 2005;129(5):1616-1632. doi:10.1053/j.gastro.2005.07.055
86. Xu YS, Liang JJ, Wang Y, et al. STAT3 Undergoes Acetylation-dependent Mitochondrial Translocation to Regulate Pyruvate Metabolism. *Sci Rep*. 2016;6(November):39517. doi:10.1038/srep39517
87. Yang J, Huang J, Dasgupta M, et al. Reversible methylation of promoter-bound STAT3 by histone-modifying enzymes. *Proc Natl Acad Sci U S A*. 2010;107(50):21499-21504. doi:10.1073/pnas.1016147107
88. Kim E, Kim M, Woo DH, et al. Phosphorylation of EZH2 Activates STAT3 Signaling via STAT3 Methylation and Promotes Tumorigenicity of Glioblastoma Stem-like Cells. *Cancer Cell*.

- 2013;23(6):839-852. doi:10.1016/j.ccr.2013.04.008
89. Perry E, Tsuya R, Levitsky P, et al. TMF/ARA160 is a BC-box-containing protein that mediates the degradation of Stat3. *Oncogene*. 2004;23(55):8908-8919. doi:10.1038/sj.onc.1208149
 90. Ray S, Zhao Y, Jamaluddin M, Edeh CB, Lee C, Brasier AR. Inducible STAT3 NH2 terminal mono-ubiquitination promotes BRD4 complex formation to regulate apoptosis. *Cell Signal*. 2014;26(7):1445-1455. doi:10.1016/j.cellsig.2014.03.007
 91. Xie Y, Kole S, Precht P, Pazin MJ, Bernier M. S-Glutathionylation impairs signal transducer and activator of transcription 3 activation and signaling. *Endocrinology*. 2009;150(3):1122-1131. doi:10.1210/en.2008-1241
 92. Kurdi M, Booz GW. Evidence that IL-6-type cytokine signaling in cardiomyocytes is inhibited by oxidative stress: Parthenolide targets JAK1 activation by generating ROS. *J Cell Physiol*. 2007;212(2):424-431. doi:10.1002/jcp.21033
 93. Butturini E, Darra E, Chiavegato G, et al. S-glutathionylation at Cys328 and Cys542 impairs STAT3 phosphorylation. *ACS Chem Biol*. 2014;9(8):1885-1893. doi:10.1021/cb500407d
 94. Yuan J, Zhang F, Niu R. Multiple regulation pathways and pivotal biological functions of STAT3 in cancer. *Sci Rep*. 2015;5:1-10. doi:10.1038/srep17663
 95. Yu H, Lee H, Herrmann A, Buettner R, Jove R. Revisiting STAT3 signalling in cancer: new and unexpected biological functions. *Nat Rev Cancer*. 2014;14(11):736-746. doi:10.1038/nrc3818
 96. Darnell JE, Kerr IM, Stark GR. Jak-STAT pathways and transcriptional activation in response to IFNs and other extracellular signaling proteins. *Science (80-)*. 1994;264(5164):1415-1421. doi:10.1126/science.8197455
 97. Guschin D, Rogers N, Briscoe J, et al. A major role for the protein tyrosine kinase JAK1 in the JAK/STAT signal transduction pathway in response to interleukin-6. *EMBO J*. 1995;14(7):1421-1429. doi:10.1002/j.1460-2075.1995.tb07128.x
 98. Ndubuisi MI, Guo GG, Fried V a, Etlinger JD, Sehgal PB. Cellular Physiology of STAT3 : Where ' s the Cytoplasmic Monomer ?*. *Biochemistry*. 1999;274(36):25499-25509.
 99. Haan S, Kortylewski M, Behrmann I, Müller-Esterl W, Heinrich PC, Schaper F. Cytoplasmic STAT proteins associate prior to activation. *Biochem J*. 2000;345 Pt 3:417-421. <http://www.ncbi.nlm.nih.gov/pubmed/10642496>. Accessed October 25, 2019.
 100. Pranada AL, Metz S, Herrmann A, Heinrich PC, Müller-Newen G. Real time analysis of STAT3 nucleocytoplasmic shuttling. *J Biol Chem*. 2004;279(15):15114-15123. doi:10.1074/jbc.M312530200
 101. Ng IHW, Ng DCH, Jans DA, Bogoyevitch MA. Selective STAT3- α or - β expression reveals spliceform-specific phosphorylation kinetics, nuclear retention and distinct gene expression outcomes. *Biochem J*. 2012;447(1):125-136. doi:10.1042/BJ20120941
 102. Yang J, Chatterjee-Kishore M, Staugaitis SM, et al. Novel roles of unphosphorylated STAT3 in oncogenesis and transcriptional regulation. *Cancer Res*. 2005;65(3):939-947. doi:65/3/939 [pii]
 103. Yang J, Liao X, Agarwal MK, Barnes L, Auron PE, Stark GR. Unphosphorylated STAT3 accumulates in response to IL-6 and activates transcription by binding to NF κ B. *Genes Dev*. 2007;21(11):1396-1408. doi:10.1101/gad.1553707
 104. Timofeeva OA, Chasovskikh S, Lonskaya I, et al. Mechanisms of unphosphorylated STAT3 transcription factor binding to DNA. *J Biol Chem*. 2012;287(17):14192-14200. doi:10.1074/jbc.M111.323899
 105. Rodrigues BR, Queiroz-Hazarbassanov N, Lopes MH, et al. Nuclear unphosphorylated STAT3 correlates with a worse prognosis in human glioblastoma. *Pathol Res Pract*. 2016;212(6):517-523. doi:10.1016/j.prp.2016.03.001

106. Sehgal PB, Guo GG, Shah M, Kumar V, Patel K. Cytokine signaling: STATs in plasma membrane rafts. *J Biol Chem*. 2002;277(14):12067-12074. doi:10.1074/jbc.M200018200
107. Guo GG, Patel K, Kumar V, et al. Association of the chaperone glucose-regulated protein 58 (GRP58/ER-60/ERp57) with Stat3 in cytosol and plasma membrane complexes. *J Interferon Cytokine Res*. 2002;22(5):555-563. doi:10.1089/10799900252982034
108. Meier JA, Larner AC. Toward a new STATE: The role of STATs in mitochondrial function. *Semin Immunol*. 2014;26(1):20-28. doi:10.1016/j.smim.2013.12.005
109. Wegrzyn J, Potla R, Chwae Y-J, et al. Function of Mitochondrial Stat3 in Cellular Respiration. *Science*. 2009;323(February):793-798. doi:10.1126/science.1164551
110. Tammineni P, Anugula C, Mohammed F, Anjaneyulu M, Larner AC, Sepuri NBV. The import of the transcription factor STAT3 into mitochondria depends on GRIM-19, a component of the electron transport chain. *J Biol Chem*. 2013;288(7):4723-4732. doi:10.1074/jbc.M112.378984
111. Shen Y, La Perle KMD, Levy DE, Darnell JE. Reduced STAT3 activity in mice mimics clinical disease syndromes. *Biochem Biophys Res Commun*. 2005;330(1):305-309. doi:10.1016/j.bbrc.2005.02.154
112. Phillips D, Reilley MJ, Aponte AM, et al. Stoichiometry of STAT3 and mitochondrial proteins: Implications for the regulation of oxidative phosphorylation by protein-protein interactions. *J Biol Chem*. 2010;285(31):23532-23536. doi:10.1074/jbc.C110.152652
113. Wegrzyn J, Potla R, Chwae YJ, et al. Function of mitochondrial Stat3 in cellular respiration. *Science (80-)*. 2009;323(5915):793-797. doi:10.1126/science.1164551
114. Zhang Q, Raje V, Yakovlev VA, et al. Mitochondrial localized Stat3 promotes breast cancer growth via phosphorylation of serine 727. *J Biol Chem*. 2013;288(43):31280-31288. doi:10.1074/jbc.M113.505057
115. Boengler K, Hilfiker-Kleiner D, Heusch G, Schulz R. Inhibition of permeability transition pore opening by mitochondrial STAT3 and its role in myocardial ischemia/reperfusion. *Basic Res Cardiol*. 2010;105(6):771-785. doi:10.1007/s00395-010-0124-1
116. Yang R, Rincon M. Mitochondrial Stat3, the need for design thinking. *Int J Biol Sci*. 2016;12(5):532-544. doi:10.7150/ijbs.15153
117. Mantel C, Messina-Graham S, Moh A, et al. Mouse hematopoietic cell-targeted STAT3 deletion: Stem/progenitor cell defects, mitochondrial dysfunction, ROS overproduction, and a rapid aging-like phenotype. *Blood*. 2012;120(13):2589-2599. doi:10.1182/blood-2012-01-404004
118. Sarafian TA, Montes C, Imura T, et al. Disruption of astrocyte STAT3 signaling decreases mitochondrial function and increases oxidative stress in vitro. *PLoS One*. 2010;5(3). doi:10.1371/journal.pone.0009532
119. Garama DJ, Harris TJ, White CL, et al. A Synthetic Lethal Interaction between Glutathione Synthesis and Mitochondrial Reactive Oxygen Species Provides a Tumor-Specific Vulnerability Dependent on STAT3. *Mol Cell Biol*. 2015;35(21):3646-3656. doi:10.1128/mcb.00541-15
120. Macias E, Rao D, Carbajal S, Kiguchi K, Digiovanni J. Stat3 binds to mtDNA and regulates mitochondrial gene expression in keratinocytes. *J Invest Dermatol*. 2014;134(7):1971-1980. doi:10.1038/jid.2014.68
121. Avalle L, Camporeale A, Morciano G, et al. STAT3 localizes to the ER, acting as a gatekeeper for ER-mitochondrion Ca²⁺ fluxes and apoptotic responses. *Cell Death Differ*. 2018. doi:10.1038/s41418-018-0171-y
122. Danese A, Patergnani S, Bonora M, et al. Calcium regulates cell death in cancer: Roles of the mitochondria and mitochondria-associated membranes (MAMs). *Biochim Biophys Acta Bioenerg*. 2017;1858(8):615-627. doi:10.1016/j.bbabi.2017.01.003
123. Rizzuto R, Pinton P, Carrington W, et al. Close contacts with the endoplasmic reticulum as

- determinants of mitochondrial Ca²⁺ responses. *Science* (80-). 1998;280(5370):1763-1766. doi:10.1126/science.280.5370.1763
124. Mak DOD, Foskett JK. Inositol 1,4,5-trisphosphate receptors in the endoplasmic reticulum: A single-channel point of view. *Cell Calcium*. 2015;58(1):67-78. doi:10.1016/j.ceca.2014.12.008
 125. Morciano G, Giorgi C, Bonora M, et al. Molecular identity of the mitochondrial permeability transition pore and its role in ischemia-reperfusion injury. *J Mol Cell Cardiol*. 2015;78:142-153. doi:10.1016/j.yjmcc.2014.08.015
 126. Mendes CCP, Gomes DA, Thompson M, et al. The type III inositol 1,4,5-trisphosphate receptor preferentially transmits apoptotic Ca²⁺ signals into mitochondria. *J Biol Chem*. 2005;280(49):40892-40900. doi:10.1074/jbc.M506623200
 127. Avalle L, Camporeale A, Camperi A, Poli V. STAT3 in cancer: A double edged sword. *Cytokine*. 2017;98(January):42-50. doi:10.1016/j.cyto.2017.03.018
 128. Kaplan MH, Sun YL, Hoey T, Grusby MJ. Impaired IL-12 responses and enhanced development of Th2 cells in Stat4- deficient mice. *Nature*. 1996;382(6587):174-177. doi:10.1038/382174a0
 129. Bromberg J. Stat proteins and oncogenesis. *New York*. 2002;109(9):1133-1137. doi:10.1172/JCI200215644.Cytokines
 130. Nakashima J, Tachibana M, Horiguchi Y, et al. Serum interleukin 6 as a prognostic factor in patients with prostate cancer. *Clin Cancer Res*. 2000;6(7):2702-2706.
 131. Pine SR, Mechanic LE, Enewold L, et al. Increased levels of circulating interleukin 6, interleukin 8, c-reactive protein, and risk of lung cancer. *J Natl Cancer Inst*. 2011;103(14):1112-1122. doi:10.1093/jnci/djr216
 132. Sansone P, Storci G, Tavorari S, et al. IL-6 triggers malignant features in mammospheres from human ductal breast carcinoma and normal mammary gland. 2007;117(12). doi:10.1172/JCI32533DS1
 133. Wang Y, Zhang Y. Prognostic role of interleukin-6 in renal cell carcinoma: a meta-analysis. *Clin Transl Oncol*. August 2019. doi:10.1007/s12094-019-02192-x
 134. Ernst M, Najdovska M, Grail D, et al. STAT3 and STAT1 mediate IL-11-dependent and inflammation-associated gastric tumorigenesis in gp130 receptor mutant mice. *J Clin Invest*. 2008;118(5):1727-1738. doi:10.1172/JCI34944
 135. Liu SC, Tsang NM, Chiang WC, et al. Leukemia inhibitory factor promotes nasopharyngeal carcinoma progression and radioresistance. *J Clin Invest*. 2013;123(12):5269-5283. doi:10.1172/JCI63428
 136. Peñuelas S, Anido J, Prieto-Sánchez RM, et al. TGF- β Increases Glioma-Initiating Cell Self-Renewal through the Induction of LIF in Human Glioblastoma. *Cancer Cell*. 2009;15(4):315-327. doi:10.1016/j.ccr.2009.02.011
 137. De La Iglesia N, Konopka G, Puram S V., et al. Identification of a PTEN-regulated STAT3 brain tumor suppressor pathway. *Genes Dev*. 2008;22(4):449-462. doi:10.1101/gad.1606508
 138. Jahani-Asl A, Yin H, Soleimani VD, et al. Control of glioblastoma tumorigenesis by feed-forward cytokine signaling. *Nat Neurosci*. 2016;19(6):798-806. doi:10.1038/nn.4295
 139. Lo HW, Hsu SC, Ali-Seyed M, et al. Nuclear interaction of EGFR and STAT3 in the activation of the iNOS/NO pathway. *Cancer Cell*. 2005;7(6):575-589. doi:10.1016/j.ccr.2005.05.007
 140. Ning ZQ, Li J, McGuinness M, Arceci RJ. STAT3 activation is required for Asp(816) mutant c-Kit induced tumorigenicity. *Oncogene*. 2001;20(33):4528-4536. doi:10.1038/sj.onc.1204590
 141. Zhao D, Pan C, Sun J, et al. VEGF drives cancer-initiating stem cells through VEGFR-2/Stat3 signaling to upregulate Myc and Sox2. *Oncogene*. 2015;34(24):3107-3119. doi:10.1038/onc.2014.257

142. Liang H, Venema VJ, Wang X, Ju H, Venema RC, Marrero MB. Regulation of angiotensin II-induced phosphorylation of STAT3 in vascular smooth muscle cells. *J Biol Chem.* 1999;274(28):19846-19851. doi:10.1074/jbc.274.28.19846
143. Arvanitakis L, Geras-Raaka E, Varma A, Gershengorn MC, Cesarman E. Human herpesvirus KSHV encodes a constitutively active G-protein- coupled receptor linked to cell proliferation. *Nature.* 1997;385(6614):347-349. doi:10.1038/385347a0
144. Ram PT. Stat3-mediated transformation of NIH-3T3 cells by the constitutively active Q205L Gao protein. *Science (80-).* 2000;287(5450):142-144. doi:10.1126/science.287.5450.142
145. Lee H, Deng J, Kujawski M, et al. STAT3-induced S1PR1 expression is crucial for persistent STAT3 activation in tumors. *Nat Med.* 2010;16(12):1421-1428. doi:10.1038/nm.2250
146. Liang J, Nagahashi M, Kim EY, et al. Sphingosine-1-Phosphate Links Persistent STAT3 Activation, Chronic Intestinal Inflammation, and Development of Colitis-Associated Cancer. *Cancer Cell.* 2013;23(1):107-120. doi:10.1016/j.ccr.2012.11.013
147. Deng J, Liu Y, Lee H, et al. S1PR1-STAT3 Signaling Is Crucial for Myeloid Cell Colonization at Future Metastatic Sites. *Cancer Cell.* 2012;21(5):642-654. doi:10.1016/j.ccr.2012.03.039
148. Priceman SJ, Shen S, Wang L, et al. S1PR1 Is Crucial for Accumulation of Regulatory T Cells in Tumors via STAT3. *Cell Rep.* 2014;6(6):992-999. doi:10.1016/j.celrep.2014.02.016
149. Medzhitov R, Janeway CA. Innate immunity: The virtues of a nonclonal system of recognition. *Cell.* 1997;91(3):295-298. doi:10.1016/S0092-8674(00)80412-2
150. Eyking A, Ey B, Rünzi M, et al. Toll-like receptor 4 variant D299G induces features of neoplastic progression in Caco-2 intestinal cells and is associated with advanced human colon cancer. *Gastroenterology.* 2011;141(6):2154-2165. doi:10.1053/j.gastro.2011.08.043
151. Tye H, Kennedy CL, Najdovska M, et al. STAT3-driven upregulation of TLR2 promotes gastric tumorigenesis independent of tumor inflammation. *Cancer Cell.* 2012;22(4):466-478. doi:10.1016/j.ccr.2012.08.010
152. Ochi A, Graffeo CS, Zambirinis CP, et al. Toll-like receptor 7 regulates pancreatic carcinogenesis in mice and humans. *J Clin Invest.* 2012;122(11):4118-4129. doi:10.1172/JCI63606
153. Herrmann A, Cherryholmes G, Schroeder A, et al. TLR9 is critical for glioma stem cell maintenance and targeting. *Cancer Res.* 2014;74(18):5218-5228. doi:10.1158/0008-5472.CAN-14-1151
154. Garg N, Bakhshinyan D, Venugopal C, et al. CD133+ brain tumor-initiating cells are dependent on STAT3 signaling to drive medulloblastoma recurrence. *Oncogene.* 2017;36(5):606-617. doi:10.1038/onc.2016.235
155. He G, Yu GY, Temkin V, et al. Hepatocyte IKK β /NF- κ B Inhibits Tumor Promotion and Progression by Preventing Oxidative Stress-Driven STAT3 Activation. *Cancer Cell.* 2010;17(3):286-297. doi:10.1016/j.ccr.2009.12.048
156. Schneller D, Machat G, Sousek A, et al. p19ARF/p14ARF controls oncogenic functions of signal transducer and activator of transcription 3 in hepatocellular carcinoma. *Hepatology.* 2011;54(1):164-172. doi:10.1002/hep.24329
157. D'Arcangelo M, Cappuzzo F. K-Ras Mutations in Non-Small-Cell Lung Cancer: Prognostic and Predictive Value. *ISRN Mol Biol.* 2012;2012:837306. doi:10.5402/2012/837306
158. Grabner B, Schramek D, Mueller KM, et al. Disruption of STAT3 signalling promotes KRAS-induced lung tumorigenesis. *Nat Commun.* 2015;6. doi:10.1038/ncomms7285
159. Zhou J, Qu Z, Yan S, et al. Differential roles of STAT3 in the initiation and growth of lung cancer. *Oncogene.* 2015;34(29):3804-3814. doi:10.1038/onc.2014.318
160. Musteanu M, Blaas L, Mair M, et al. Stat3 Is a Negative Regulator of Intestinal Tumor Progression

- in ApcMin Mice. *Gastroenterology*. 2010;138(3). doi:10.1053/j.gastro.2009.11.049
161. Lee J, Kim JCK, Lee SE, et al. Signal transducer and activator of transcription 3 (STAT3) protein suppresses adenoma-to-carcinoma transition in Apcmin/+ mice via regulation of Snail-1 (SNAIL) protein stability. *J Biol Chem*. 2012;287(22):18182-18189. doi:10.1074/jbc.M111.328831
 162. Pencik J, Schleder M, Gruber W, et al. STAT3 regulated ARF expression suppresses prostate cancer metastasis. *Nat Commun*. 2015;6:7736. doi:10.1038/ncomms8736
 163. Couto JP, Daly L, Almeida A, et al. STAT3 negatively regulates thyroid tumorigenesis. *Proc Natl Acad Sci U S A*. 2012;109(35):E2361-E2370. doi:10.1073/pnas.1201232109
 164. Hsieh FC, Cheng G, Lin J. Evaluation of potential Stat3-regulated genes in human breast cancer. *Biochem Biophys Res Commun*. 2005;335(2):292-299. doi:10.1016/j.bbrc.2005.07.075
 165. Burke WM, Jin X, Lin HJ, et al. Inhibition of constitutively active Stat3 suppresses growth of human ovarian and breast cancer cells. *Oncogene*. 2001;20(55):7925-7934. doi:10.1038/sj.onc.1204990
 166. Ranger JJ, Levy DE, Shahalizadeh S, Hallett M, Muller WJ. Identification of a Stat3-dependent transcription regulatory network involved in metastatic progression. *Cancer Res*. 2009;69(17):6823-6830. doi:10.1158/0008-5472.CAN-09-1684
 167. Jhan JR, Andrechek ER. Stat3 accelerates Myc induced tumor formation while reducing growth rate in a mouse model of breast cancer. *Oncotarget*. 2016;7(40):65797-65807. doi:10.18632/oncotarget.11667
 168. Reimand J, Isserlin R, Voisin V, et al. Pathway enrichment analysis and visualization of omics data using g:Profiler, GSEA, Cytoscape and EnrichmentMap. *Nat Protoc*. 2019;14(2):482-517. doi:10.1038/s41596-018-0103-9
 169. Jin R, Jin YY, Tang YL, Yang HJ, Zhou XQ, Lei Z. GPNMB silencing suppresses the proliferation and metastasis of osteosarcoma cells by blocking the PI3K/Akt/mTOR signaling pathway. *Oncol Rep*. 2018;39(6):3034-3040. doi:10.3892/or.2018.6346
 170. Ma R qiong, Tang Z jian, Ye X, et al. Overexpression of GPNMB predicts an unfavorable outcome of epithelial ovarian cancer. *Arch Gynecol Obstet*. 2018;297(5):1235-1244. doi:10.1007/s00404-018-4699-3
 171. Weterman MAJ, Ajubi N, van Dinter IMR, et al. nmb, a novel gene, is expressed in low-metastatic human melanoma cell lines and xenografts. *Int J Cancer*. 1995;60(1):73-81. doi:10.1002/ijc.2910600111
 172. Tian F, Liu C, Wu Q, et al. Upregulation of glycoprotein nonmetastatic B by colony-stimulating factor-1 and epithelial cell adhesion molecule in hepatocellular carcinoma cells. *Oncol Res*. 2013;20(8):341-350. doi:10.3727/096504013X13657689382851
 173. Smuczek B, Santos E de S, Siqueira AS, Pinheiro JJV, Freitas VM, Jaeger RG. The laminin-derived peptide C16 regulates GPNMB expression and function in breast cancer. *Exp Cell Res*. 2017;358(2):323-334. doi:10.1016/j.yexcr.2017.07.005
 174. Zhang YX, Qin CP, Zhang XQ, et al. Knocking down glycoprotein nonmetastatic melanoma protein B suppresses the proliferation, migration, and invasion in bladder cancer cells. *Tumor Biol*. 2017;39(4). doi:10.1177/1010428317699119
 175. Arosarena OA, Barr EW, Thorpe R, Yankey H, Tarr JT, Safadi FF. Osteoactivin regulates head and neck squamous cell carcinoma invasion by modulating matrix metalloproteases. *J Cell Physiol*. 2018;233(1):409-421. doi:10.1002/jcp.25900
 176. Bao G, Wang N, Li R, Xu G, Liu P, He B. Glycoprotein non-metastatic melanoma protein B promotes glioma motility and angiogenesis through the Wnt/ β -catenin signaling pathway. *Exp Biol Med*. 2016;241(17):1968-1976. doi:10.1177/1535370216654224
 177. Oyewumi MO, Manickavasagam D, Novak K, et al. Osteoactivin (GPNMB) ectodomain protein

- promotes growth and invasive behavior of human lung cancer cells. *Oncotarget*. 2016;7(12):13932-13944. doi:10.18632/oncotarget.7323
178. Arosarena OA, dela Cadena RA, Denny MF, et al. Osteoactivin Promotes Migration of Oral Squamous Cell Carcinomas. *J Cell Physiol*. 2016;231(8):1761-1770. doi:10.1002/jcp.25279
 179. Torres C, Linares A, Alexandre MJ, et al. The potential role of the glycoprotein osteoactivin/glycoprotein nonmetastatic melanoma protein b in pancreatic cancer. *Pancreas*. 2015;44(2):302-310. doi:10.1097/MPA.0000000000000250
 180. Fiorentini C, Bodei S, Bedussi F, et al. GPNMB/OA protein increases the invasiveness of human metastatic prostate cancer cell lines DU145 and PC3 through MMP-2 and MMP-9 activity. *Exp Cell Res*. 2014;323(1):100-111. doi:10.1016/j.yexcr.2014.02.025
 181. Zhu Z, Dong W. Overexpression of HHLA2, a member of the B7 family, is associated with worse survival in human colorectal carcinoma. *Onco Targets Ther*. 2018;11:1563-1570. doi:10.2147/OTT.S160493
 182. Cheng H, Janakiram M, Borczuk A, et al. HHLA2, a new immune checkpoint member of the B7 family, is widely expressed in human lung cancer and associated with EGFR mutational status. *Clin Cancer Res*. 2017;23(3):825-832. doi:10.1158/1078-0432.CCR-15-3071
 183. Xiao Y, Li H, Yang LL, et al. The Expression Patterns and Associated Clinical Parameters of Human Endogenous Retrovirus-H Long Terminal Repeat-Associating Protein 2 and Transmembrane and Immunoglobulin Domain Containing 2 in Oral Squamous Cell Carcinoma. *Dis Markers*. 2019;2019:5421985. doi:10.1155/2019/5421985
 184. Sun L, Li PB, Yao YF, et al. Proteinase-activated receptor 2 promotes tumor cell proliferation and metastasis by inducing epithelial-mesenchymal transition and predicts poor prognosis in hepatocellular carcinoma. *World J Gastroenterol*. 2018;24(10):1120-1133. doi:10.3748/wjg.v24.i10.1120
 185. Aman M, Ohishi Y, Imamura H, et al. Expression of protease-activated receptor-2 (PAR-2) is related to advanced clinical stage and adverse prognosis in ovarian clear cell carcinoma. *Hum Pathol*. 2017;64:156-163. doi:10.1016/j.humpath.2017.04.008
 186. Mußbach F, Ungefroren H, Günther B, et al. Proteinase-activated receptor 2 (PAR2) in hepatic stellate cells - evidence for a role in hepatocellular carcinoma growth in vivo. *Mol Cancer*. 2016;15(1). doi:10.1186/s12943-016-0538-y
 187. Al-Eryani K, Cheng J, Abé T, et al. Protease-activated receptor 2 modulates proliferation and invasion of oral squamous cell carcinoma cells. *Hum Pathol*. 2015;46(7):991-999. doi:10.1016/j.humpath.2015.03.003
 188. Luo R, Wang X, Dong Y, Wang L, Tian C. Activation of protease-activated receptor 2 reduces glioblastoma cell apoptosis. *J Biomed Sci*. 2014;21(1). doi:10.1186/1423-0127-21-25
 189. Huang SH, Li Y, Chen HG, Rong J, Ye S. Activation of proteinase-activated receptor 2 prevents apoptosis of lung cancer cells. *Cancer Invest*. 2013;31(9):578-581. doi:10.3109/07357907.2013.845674
 190. Wang GJ, Wang Y Bin, Li DN, Deng BB. Expression of protease-activated receptor-2 in human gastric stromal tumor and its clinicopathological significance. *Hepatogastroenterology*. 2013;60(128):2125-2128. doi:10.5754/hge13467
 191. Eguchi H, Iwaki K, Shibata K, Ogawa T, Ohta M, Kitano S. Protease-activated receptor-2 regulates cyclooxygenase-2 expression in human bile duct cancer via the pathways of mitogen-activated protein kinases and nuclear factor kappa B. *J Hepatobiliary Pancreat Sci*. 2011;18(2):147-153. doi:10.1007/s00534-010-0318-9
 192. Su S, Li Y, Luo Y, et al. Proteinase-activated receptor 2 expression in breast cancer and its role in breast cancer cell migration. *Oncogene*. 2009;28(34):3047-3057. doi:10.1038/onc.2009.163

193. Expression of protease activated receptor-2 related to angiogenesis in tumor advancement of uterine endometrial cancers. - PubMed - NCBI. <https://www.ncbi.nlm.nih.gov/pubmed/17203172>. Accessed November 13, 2019.
194. Weir MC, Shu ST, Patel RK, et al. Selective Inhibition of the Myeloid Src-Family Kinase Fgr Potently Suppresses AML Cell Growth in Vitro and in Vivo. *ACS Chem Biol*. 2018;13(6):1551-1559. doi:10.1021/acscchembio.8b00154
195. Kim HS, Han HD, Armaiz-Pena GN, et al. Functional roles of Src and Fgr in ovarian carcinoma. *Clin Cancer Res*. 2011;17(7):1713-1721. doi:10.1158/1078-0432.CCR-10-2081
196. Zarn JA, Zimmermann SM, Pass MK, Waibel R, Stahel RA. Association of CD24 with the kinase c-fgr in a small cell lung cancer cell line and with the kinase lyn in an erythroleukemia cell line. *Biochem Biophys Res Commun*. 1996;225(2):384-391. doi:10.1006/bbrc.1996.1184
197. Joosten M, Ginzler S, Blex C, et al. A novel approach to detect resistance mechanisms reveals FGR as a factor mediating HDAC inhibitor SAHA resistance in B-cell lymphoma. *Mol Oncol*. 2016;10(8):1232-1244. doi:10.1016/j.molonc.2016.06.001
198. Burnell SEA, Spencer-Harty S, Howarth S, et al. STEAP2 Knockdown Reduces the Invasive Potential of Prostate Cancer Cells. *Sci Rep*. 2018;8(1). doi:10.1038/s41598-018-24655-x
199. McGirt LY, Degesys CA, Johnson VE, Zic JA, Zwerner JP, Eischen CM. TOX expression and role in CTCL. *J Eur Acad Dermatology Venereol*. 2016;30(9):1497-1502. doi:10.1111/jdv.13651
200. Tessema M, Yingling CM, Grimes MJ, et al. Differential epigenetic regulation of TOX subfamily high mobility group box genes in lung and breast cancers. *PLoS One*. 2012;7(4). doi:10.1371/journal.pone.0034850
201. Parolia A, Cieslik M, Chu SC, et al. Distinct structural classes of activating FOXA1 alterations in advanced prostate cancer. *Nature*. July 2019. doi:10.1038/s41586-019-1347-4
202. Park YL, Kim SH, Park SY, et al. Forkhead-box A1 regulates tumor cell growth and predicts prognosis in colorectal cancer. *Int J Oncol*. 2019;54(6):2169-2178. doi:10.3892/ijo.2019.4771
203. Wang S, Singh SK, Katika MR, Lopez-Aviles S, Hurtado A. High throughput chemical screening reveals multiple regulatory proteins on FOXA1 in breast cancer cell lines. *Int J Mol Sci*. 2018;19(12). doi:10.3390/ijms19124123
204. Li J, Wang W, Chen S, et al. FOXA1 reprograms the TGF- β -stimulated transcriptional program from a metastasis promoter to a tumor suppressor in nasopharyngeal carcinoma. *Cancer Lett*. 2019;442:1-14. doi:10.1016/j.canlet.2018.10.036
205. Kim JY, Kim CH, Lee Y, Lee JH, Chae YS. Tumour infiltrating lymphocytes are predictors of lymph node metastasis in early gastric cancers. *Pathology*. 2017;49(6):589-595. doi:10.1016/j.pathol.2017.06.003
206. Nonaka D. A study of FoxA1 expression in thyroid tumors. *Hum Pathol*. 2017;65:217-224. doi:10.1016/j.humpath.2017.05.007
207. Wang LL, Xiu YL, Chen X, et al. The transcription factor FOXA1 induces epithelial ovarian cancer tumorigenesis and progression. *Tumor Biol*. 2017;39(5). doi:10.1177/1010428317706210
208. Wang L, Qin H, Li L, et al. Forkhead-box A1 transcription factor is a novel adverse prognosis marker in human glioma. *J Clin Neurosci*. 2013;20(5):654-658. doi:10.1016/j.jocn.2012.03.055
209. Gurbuz N, Ashour AA, Alpay SN, Ozpolat B. Down-regulation of 5-HT1B and 5-HT1D receptors inhibits proliferation, clonogenicity and invasion of human pancreatic cancer cells. *PLoS One*. 2014;9(9):e110067. doi:10.1371/journal.pone.0110067
210. Hu D, Ansari D, Zhou Q, Sasor A, Said Hilmersson K, Andersson R. Galectin 4 is a biomarker for early recurrence and death after surgical resection for pancreatic ductal adenocarcinoma. *Scand J Gastroenterol*. 2019;54(1):95-100. doi:10.1080/00365521.2018.1561937

211. Wu MM, Li CF, Lin LF, et al. Promoter hypermethylation of LGALS4 correlates with poor prognosis in patients with urothelial carcinoma. *Oncotarget*. 2017;8(14):23787-23802. doi:10.18632/oncotarget.15865
212. Barrow H, Rhodes JM, Yu LG. Simultaneous determination of serum galectin-3 and -4 levels detects metastases in colorectal cancer patients. *Cell Oncol*. 2013;36(1):9-13. doi:10.1007/s13402-012-0109-1
213. Cai Z, Zeng Y, Xu B, et al. Galectin-4 serves as a prognostic biomarker for the early recurrence / metastasis of hepatocellular carcinoma. *Cancer Sci*. 2014;105(11):1510-1517. doi:10.1111/cas.12536
214. Hayashi T, Saito T, Fujimura T, et al. Galectin-4, a novel predictor for lymph node metastasis in lung adenocarcinoma. *PLoS One*. 2013;8(12). doi:10.1371/journal.pone.0081883
215. You X, Wang Y, Wu J, et al. Aberrant cytokeratin 20 mRNA expression in peripheral blood and lymph nodes indicates micrometastasis and poor prognosis in patients with gastric carcinoma. *Technol Cancer Res Treat*. 2019;18. doi:10.1177/1533033819832856
216. Li WX, Xiao HW, Hong XQ, Niu WX. Predictive value of CK20 in evaluating the efficacy of treatment and prognosis after surgery for colorectal cancer. *Genet Mol Res*. 2015;14(2):5823-5829. doi:10.4238/2015.May.29.14
217. Tunca B, Egeli U, Cecener G, et al. CK19, CK20, EGFR and HER2 status of circulating tumor cells in patients with breast cancer. *Tumori*. 2012;98(2):243-251. doi:10.1700/1088.11937
218. Fanni D, Nemolato S, Ganga R, et al. Cytokeratin 20-positive hepatocellular carcinoma. *Eur J Histochem*. 2009;53(4):269-274. doi:10.4081/ejh.2009.269
219. Ye X, Li Y, Hou G, Liu Z, Chen T. [Significance of cytokeratin gene (CK-20 mRNA) expression in metastatic lymph nodes in colon carcinoma patients]. *Zhonghua Zhong Liu Za Zhi*. 2002;24(3):261-263. <http://www.ncbi.nlm.nih.gov/pubmed/12515621>. Accessed November 13, 2019.
220. Moll R, Zimbelmann R, Goldschmidt MD, et al. The human gene encoding cytokeratin 20 and its expression during fetal development and in gastrointestinal carcinomas. *Differentiation*. 1993;53(2):75-93. doi:10.1111/j.1432-0436.1993.tb00648.x
221. Arias-Stella JA, Shah AB, Gupta NS, Williamson SR. CK20 and p53 immunohistochemical staining patterns in urinary bladder specimens with equivocal Atypia: Correlation with outcomes. *Arch Pathol Lab Med*. 2018;142(1):64-69. doi:10.5858/arpa.2016-0411-OA
222. Kekilli KE, Abakay CD, Tezcan G, et al. Effects of EGFR, CK19, CK20 and Survivin gene expression on radiotherapy results in patients with locally advanced head and neck cancer. *Asian Pac J Cancer Prev*. 2015;16(7):3023-3027. doi:10.7314/apjcp.2015.16.7.3023
223. Yang SF, Yuan SSF, Yeh YT, et al. The role of p-STAT3 (ser727) revealed by its association with Ki-67 in cervical intraepithelial neoplasia. *Gynecol Oncol*. 2005;98(3):446-452. doi:10.1016/j.ygyno.2005.05.032
224. Qin HR, Kim H, Kim J, et al. Activation of Stat3 through a Phosphomimetic Serine727 Promotes Prostate Tumorigenesis Independent of Tyrosine705 phosphorylation. 2010;68(19):7736-7741. doi:10.1158/0008-5472.CAN-08-1125.Activation
225. Wakahara R, Kunimoto H, Tanino K, et al. Phospho-Ser727 of STAT3 regulates STAT3 activity by enhancing dephosphorylation of phospho-Tyr705 largely through TC45. 2012:132-145. doi:10.1111/j.1365-2443.2011.01575.x
226. Yin S, Wu H, Lv J, et al. SHP-1 arrests mouse early embryo development through downregulation of Nanog by dephosphorylation of STAT3. *PLoS One*. 2014;9(1):e86330. doi:10.1371/journal.pone.0086330
227. Huang G, Yan H, Ye S, Tong C, Ying Q-L. STAT3 phosphorylation at tyrosine 705 and serine 727

- differentially regulates mouse ESC fates. *Stem Cells*. 2014;32(5):1149-1160. doi:10.1002/stem.1609
228. Jin J, Liu J, Chen C, et al. The deubiquitinase USP21 maintains the stemness of mouse embryonic stem cells via stabilization of Nanog. *Nat Commun*. 2016;7:13594. doi:10.1038/ncomms13594
229. Min T-R, Park H-J, Park MN, Kim B, Park S-H. The Root Bark of *Morus alba* L. Suppressed the Migration of Human Non-Small-Cell Lung Cancer Cells through Inhibition of Epithelial-Mesenchymal Transition Mediated by STAT3 and Src. *Int J Mol Sci*. 2019;20(9). doi:10.3390/ijms20092244
230. Kim J-H, Kim JE, Liu H-Y, Cao W, Chen J. Regulation of interleukin-6-induced hepatic insulin resistance by mammalian target of rapamycin through the STAT3-SOCS3 pathway. *J Biol Chem*. 2008;283(2):708-715. doi:10.1074/jbc.M708568200
231. Schuringa JJ, Jonk LJ, Dokter WH, Vellenga E, Kruijer W. Interleukin-6-induced STAT3 transactivation and Ser727 phosphorylation involves Vav, Rac-1 and the kinase SEK-1/MKK-4 as signal transduction components. *Biochem J*. 2000;347 Pt 1:89-96. <http://www.ncbi.nlm.nih.gov/pubmed/10727406>. Accessed November 9, 2019.
232. Kojima H, Sasaki T, Ishitani T, et al. STAT3 Regulates Nemo-Like Kinase by Mediating Its Interaction with IL-6-Stimulated TGF β -Activated Kinase 1 for STAT3 Ser-727 Phosphorylation. *Proc Natl Acad Sci U S A*. 102:4524-4529. doi:10.2307/3375015
233. Schuringa J-J, Wierenga ATJ, Kruijer W, Vellenga E. Constitutive Stat3, Tyr705, and Ser727 phosphorylation in acute myeloid leukemia cells caused by the autocrine secretion of interleukin-6. *Blood*. 2000;95(12):3765-3770. doi:10.1182/blood.V95.12.3765.012k50_3765_3770
234. Liu L, McBride KM, Reich NC. STAT3 nuclear import is independent of tyrosine phosphorylation and mediated by importin-alpha3. *Proc Natl Acad Sci U S A*. 2005;102(23):8150-8155. doi:10.1073/pnas.0501643102
235. Novak U, Ji H, Kanagasundaram V, Simpson R, Paradiso L. STAT3 forms stable homodimers in the presence of divalent cations prior to activation. *Biochem Biophys Res Commun*. 1998;247(3):558-563. doi:10.1006/bbrc.1998.8829
236. Liu H, Ma Y, Cole SM, et al. Serine phosphorylation of STAT3 is essential for Mcl-1 expression and macrophage survival. *Blood*. 2003;102(1):344-352. doi:10.1182/blood-2002-11-3396
237. Sakaguchi M, Oka M, Iwasaki T, Fukami Y, Nishigori C. Role and regulation of STAT3 phosphorylation at Ser727 in melanocytes and melanoma cells. *J Invest Dermatol*. 2012;132(7):1877-1885. doi:10.1038/jid.2012.45
238. A. A-T, R.R. L, F. S, et al. Notch signalling regulates stem cell numbers in vitro and in vivo. *Nature*. 2006;442(7104):823-826. <http://www.ncbi.nlm.nih.gov/pubmed/16799564>. Accessed November 10, 2019.
239. Fukumoto T, Iwasaki T, Okada T, et al. High expression of Mcl-1L via the MEK-ERK-phospho-STAT3 (Ser727) pathway protects melanocytes and melanoma from UVB-induced apoptosis. *Genes to Cells*. 2016;21(2):185-199. doi:10.1111/gtc.12330
240. Wang J, Zhou M, Jin X, et al. Glycochenodeoxycholate induces cell survival and chemoresistance via phosphorylation of STAT3 at Ser727 site in HCC. *J Cell Physiol*. September 2019. doi:10.1002/jcp.29159
241. Zhang X, Wu X, Zhang F, et al. Paclitaxel induces apoptosis of esophageal squamous cell carcinoma cells by downregulating STAT3 phosphorylation at Ser727. *Oncol Rep*. 2017;37(4):2237-2244. doi:10.3892/or.2017.5503
242. Tierney BJ, McCann GA, Naidu S, et al. Aberrantly activated pSTAT3-Ser727 in human endometrial cancer is suppressed by HO-3867, a novel STAT3 inhibitor. *Gynecol Oncol*. 2014;135(1):133-141. doi:10.1016/j.ygyno.2014.07.087

243. Tkach M, Roseblit C, Rivas MA, et al. P42/p44 MAPK-mediated Stat3Ser727 phosphorylation is required for progestin-induced full activation of Stat3 and breast cancer growth. *Endocr Relat Cancer*. 2013;20(2):197-212. doi:10.1530/ERC-12-0194
244. Aziz MH, Hafeez BB, Sand JM, et al. Protein kinase C mediates Stat3Ser727 phosphorylation, Stat3-regulated gene expression, and cell invasion in various human cancer cell lines through integration with MAPK cascade (RAF-1, MEK1/2, and ERK1/2). *Oncogene*. 2010;29(21):3100-3109. doi:10.1038/onc.2010.63
245. Gartsbein M, Alt A, Hashimoto K, Nakajima K, Kuroki T, Tennenbaum T. The role of protein kinase C δ activation and STAT3 Ser727 phosphorylation in insulin-induced keratinocyte proliferation. *J Cell Sci*. 2006;119(3):470-481. doi:10.1242/jcs.02744
246. Zhao Q, Barclay M, Hilkens J, et al. Interaction between circulating galectin-3 and cancer-associated MUC1 enhances tumour cell homotypic aggregation and prevents anoikis. *Mol Cancer*. 2010;9. doi:10.1186/1476-4598-9-154
247. Friedl P, Gilmour D. Collective cell migration in morphogenesis, regeneration and cancer. *Nat Rev Mol Cell Biol*. 2009;10(7):445-457. doi:10.1038/nrm2720
248. Ramel D, Wang X, Laflamme C, Montell DJ, Emery G. Rab11 regulates cell-cell communication during collective cell movements. *Nat Cell Biol*. 2013;15(3):317-324. doi:10.1038/ncb2681
249. Lufe C, Koh TH, Uchida T, Cao X. Pin1 is required for the Ser727 phosphorylation-dependent Stat3 activity. *Oncogene*. 2007;26(55):7656-7664. doi:10.1038/sj.onc.1210567
250. Friedl P, Hegerfeldt Y, Tusch M. Collective cell migration in morphogenesis and cancer. *Int J Dev Biol*. 2004;48(5-6):441-449. doi:10.1387/ijdb.041821pf
251. Friedl P, Locker J, Sahai E, Segall JE. Classifying collective cancer cell invasion. *Nat Cell Biol*. 2012;14(8):777-783. doi:10.1038/ncb2548
252. Liotta LA, Kleinerman J, Sidel GM. The Significance of Hematogenous Tumor Cell Clumps in the Metastatic Process. *Cancer Res*. 1976;36(3):889-894.
253. Friedl P, Wolf K. Tumour-cell invasion and migration: Diversity and escape mechanisms. *Nat Rev Cancer*. 2003;3(5):362-374. doi:10.1038/nrc1075
254. Puliafito A, De Simone A, Seano G, et al. Three-dimensional chemotaxis-driven aggregation of tumor cells. *Sci Rep*. 2015;5:15205. doi:10.1038/srep15205
255. Rosen JM, Jordan CT. The increasing complexity of the cancer stem cell paradigm. *Science (80-)*. 2009;324(5935):1670-1673. doi:10.1126/science.1171837
256. Nassar D, Blanpain C. Cancer Stem Cells: Basic Concepts and Therapeutic Implications. *Annu Rev Pathol Mech Dis*. 2016;11(1):47-76. doi:10.1146/annurev-pathol-012615-044438
257. Pattabiraman DR, Weinberg RA. Tackling the cancer stem cells-what challenges do they pose? *Nat Rev Drug Discov*. 2014;13(7):497-512. doi:10.1038/nrd4253
258. Chung SS, Aroh C, Vadgama J V. Constitutive activation of STAT3 signaling regulates hTERT and promotes stem cell-like traits in human breast cancer cells. *PLoS One*. 2013;8(12). doi:10.1371/journal.pone.0083971
259. Won C, Kim BH, Yi EH, et al. Signal transducer and activator of transcription 3-mediated CD133 up-regulation contributes to promotion of hepatocellular carcinoma. *Hepatology*. 2015;62(4):1160-1173. doi:10.1002/hep.27968
260. Mani SA, Guo W, Liao MJ, et al. The Epithelial-Mesenchymal Transition Generates Cells with Properties of Stem Cells. *Cell*. 2008;133(4):704-715. doi:10.1016/j.cell.2008.03.027
261. Liu WH, Chen MT, Wang ML, et al. Cisplatin-selected resistance is associated with increased motility and stem-like properties via activation of STAT3/Snail axis in atypical teratoid/rhabdoid tumor cells.

- Oncotarget*. 2015;6(3):1750-1768. doi:10.18632/oncotarget.2737
262. Chung SS, Giehl N, Wu Y, Vadgama J V. STAT3 activation in HER2-overexpressing breast cancer promotes epithelial-mesenchymal transition and cancer stem cell traits. *Int J Oncol*. 2014;44(2):403-411. doi:10.3892/ijo.2013.2195
263. Guryanova OA, Wu Q, Cheng L, et al. Nonreceptor Tyrosine Kinase BMX Maintains Self-Renewal and Tumorigenic Potential of Glioblastoma Stem Cells by Activating STAT3. *Cancer Cell*. 2011;19(4):498-511. doi:10.1016/j.ccr.2011.03.004
264. Islam M, Sharma S, Teknos TN. RhoC regulates cancer stem cells in head and neck squamous cell carcinoma by overexpressing IL-6 and phosphorylation of STAT3. *PLoS One*. 2014;9(2). doi:10.1371/journal.pone.0088527
265. Vallania F, Schiavone D, Dewilde S, et al. Genome-wide discovery of functional transcription factor binding sites by comparative genomics: The case of Stat3. *Proc Natl Acad Sci U S A*. 2009;106(13):5117-5122. doi:10.1073/pnas.0900473106
266. Zhang X, Darnell JE. Functional importance of Stat3 tetramerization in activation of the alpha 2-macroglobulin gene. *J Biol Chem*. 2001;276(36):33576-33581. doi:10.1074/jbc.M104978200
267. Hossain DMS, Panda AK, Manna A, et al. FoxP3 acts as a cotranscription factor with STAT3 in tumor-induced regulatory T cells. *Immunity*. 2013;39(6):1057-1069. doi:10.1016/j.immuni.2013.11.005

